

Dr. Ing. G. HERRMANN  
Berlin

Dr. Phil S. WAGENER  
London

---

# THE OXIDE-COATED CATHODE

*Translated by*

Dr. Phil. S. WAGENER

*Post Office Research Station  
Dollis Hill, London*

VOLUME TWO  
PHYSICS  
INCLUDING THERMAL EMISSION FROM  
METALS AND SEMI-CONDUCTORS



LONDON  
CHAPMAN & HALL LTD.  
36 ESSEX STREET, W.C.2

1951

*First published in Great Britain 1951*

Catalogue No. 452/4

*Printed and bound in Great Britain by William Clowes and Sons, Limited  
London and Beccles*

## PREFACE

### VOLUME Two

THE physics of the oxide-coated cathode must of necessity be based on foundations which are much wider in scope than those for cathodes consisting simply of metals. This is due to the fact that the oxide cathode is an ionic solid and that for investigating the mechanism of its electron emission it is necessary also to take into account the phenomena of electrical conduction and diffusion in such solids. A separate review of the physics of the oxide cathode seems therefore justified.

When work on such a review was started, it was thought that it could be confined to a discussion of experimental work and its theoretical interpretation on oxide cathodes alone. It was soon realized, however, that an adequate knowledge of some of the fundamentals which had to be used could not be assumed in the case of every reader. There were few up-to-date reviews of such fundamentals which could be relied upon and many controversial points requiring clarification. The subject matter of the book had therefore to be extended to the discussion of these fundamentals, which are presented under the main headings of "Thermal Emission" and "Phenomena in Ionic Solids." In addition to these two subjects a special chapter has been devoted to a critical discussion of the methods for measuring the work function of electron emitters. As these basic ideas make up about one-half of the present volume, the sub-title "Thermal Emission from Metals and Semi-Conductors" has been chosen for it.

When discussing thermal emission in general a choice had to be made between two possible ways of attacking this problem, namely, by thermodynamical or by statistical methods. It was felt to be impracticable to use both methods simultaneously or even alternately in different sections. The statistical method was chosen because it allows a clear visualization of the behaviour of the emitting electrons. No inference, however, should be drawn from this choice on the suitability of the thermodynamical method, which, as is well known, has the advantage of giving more universal results.

When dealing with the physics of the oxide cathode itself, a

## PREFACE

model of its fundamental mechanism had to be adopted. The so-called semi-conductor model, which has come into the foreground during the last fifteen years, seemed to be the most suitable for this purpose, and it has been attempted to prove that this model gives a reliable basis for further investigations. A special chapter has been devoted to this end where all secondary phenomena such as effects of core metals and residual gases have been deliberately neglected. The use of the term "secondary" for these phenomena only refers to their connection with the mechanism of emission and bears no relation to their practical importance. It is fully recognized that it is in fact these phenomena which inhibit the application of oxide cathodes in practice, and a detailed discussion of them has therefore been given in the two concluding chapters.

Naturally, the treatment of the subject matter had to be rather broad owing to the large number of investigations and to the inconsistencies of some of the results. It was thought to be necessary to discuss, or at least to mention, every work on oxide cathodes which has been published, and it is hoped that such a treatment will be of advantage not only to the newcomer on the field but also to those who have been working on it for many years. The literature has been covered up to the beginning of 1950.

The units generally used in this book are Giorgi's rationalized M.K.S. units (meter, kilogram, and second and the appropriate electrical units, volt, ampere, etc.). Only in a few cases was the application of these units felt to be unsuitable, as, for instance, when using densities. Densities (of mass) have been given as usual in g./cm.<sup>3</sup>, current densities in amp./cm.<sup>2</sup>, and electron densities have generally been referred to 1 cm.<sup>3</sup> as the unit volume. However, wherever units other than the rationalized ones have been employed, this has been explicitly stated.

The translator again wishes to express his appreciation to all those mentioned in the first volume who assisted in preparing the translation. He is also much indebted to Messrs. Chapman and Hall, Ltd. for the willingness with which they have met all his wishes concerning the publication of this work.

G. HERRMANN  
S. WAGENER

*January, 1951*

# CONTENTS OF VOLUME II

<i>Chapter</i>		<i>Page</i>
<b>1. THE THERMAL EMISSION OF ELECTRONS FROM METALS</b>		<b>1</b>
1. The Fermi-Dirac Distribution of Energy of the Electrons in a Metal		1
2. The Potential Barrier at the Surface of a Metal		13
3. The Passage of the Electrons across the Metal-Vacuum Boundary		21
4. The Characteristics of a Diode		28
4.1. Galvani and contact potential		29
4.2. Equation for the retarding field current		31
4.3. Equation for the space-charge current		35
4.4. Equation for the saturated current		44
5. The Influence of Adsorbed Foreign Materials on Electron Emission from Metals		47
5.1. Influence of foreign materials on the work function		47
5.2. Adsorption of caesium (W-Cs)		50
5.3. Adsorption of barium (W-Ba)		53
5.4. Adsorption of thorium (W-Th)		54
5.5. Adsorption of oxygen (W-O)		55
5.6. Adsorption of several materials		56
6. The Surface Fields and their Influence on the Work Function		58
<b>2. METHODS OF MEASURING THE WORK FUNCTION OF METALS</b>		<b>70</b>
7. Importance and Fundamentals of the Measurement of the Work Function		70
8. Richardson Line Method		72
9. Calorimetric Measurement of the Work Function		78
10. Measurement of the Work Function by Means of the Contact Potential		82
10.1. Kelvin's method		83
10.2. Zisman's method		84
10.3. Intersection method		84
10.4. Displacement of the characteristic		87
10.5. Magnetic method		89
11. Application of Photo- or Field-Emission		89
11.1. Measurement of the frequency limit of photo-electrons		91
11.2. Measurement of the stopping potential		93
11.3. The photo-electric line		93
11.4. Application of field emission		94
12. Experimental Values of the Work Function and Dependence on Temperature		96
<b>3. PHENOMENA IN IONIC SOLIDS</b>		<b>108</b>
13. Formation of Ionic Solids and Lattice Defects in such Solids		108
14. Diffusion		113

## CONTENTS

<i>Chapter</i>	<i>Page</i>
15. Ionic Conduction	117
16. Electronic Conduction	121
17. The Energy Distribution of Electrons in an Excess Semi-Conductor and the Relation between Conductivity and Temperature	129
 <b>4. THE MECHANISM OF THE EMISSION FROM AN ACTIVATED OXIDE COATING IN EQUILIBRIUM</b>	 <b>150</b>
18. Experimental Details and Physical Constants of the Oxide Coating	150
19. The Oxide Coating as an Excess Semi-Conductor	156
19.1. Proof of the existence of excess barium	156
19.2. Proof of the development of oxygen during the activation	159
19.3. Location of the excess barium	160
20. The Emission Equation of an Excess Semi-Conductor	165
21. Application of the Methods of Measuring the Work Function to the Oxide Cathode	174
21.1. Experimental details	174
21.2. Richardson line	178
21.3. Calorimetric measurement	184
21.4. Photo-electric methods	185
21.5. Contact potential measurements	187
21.6. Temperature dependence of the work function	191
22. Electronic Conduction and Internal Work Function of the Oxide Coating.	193
23. The Potential Barrier at the Surface of the Oxide Cathode (External Work Function)	203
24. Allied Phenomena	206
24.1. Photo-electric emission	207
24.2. Secondary emission	208
24.3. Luminescence	209
 <b>5. OXIDE COATINGS OF DIFFERENT COMPOSITION</b>	 <b>214</b>
25. Emission from Pure Metal Oxides	214
26. Emission from Mixed Oxide Coatings	218
26.1. Mixtures of alkaline earth oxides	218
26.2. Mixtures with other metal oxides	228
27. Multilayer Cathodes and Foreign-Activated Cathodes	230
27.1. Multilayer cathodes	230
27.2. Foreign-activated cathodes	231
27.3. Conclusions for the composite cathodes	235
28. The Influence of Heterogeneity in the Composition of the Oxide Coating on the Emission	238
 <b>6. VARIATIONS IN THE EQUILIBRIUM OF THE OXIDE COATING</b>	 <b>245</b>
29. The Activation	245
29.1. Activation by reduction	246

## CONTENTS

<i>Chapter</i>	<i>Page</i>
29.2. Activation by drawing current	252
29.3. Activation by electron and ion bombardment	254
30. Experimental Details of Variations in the Equilibrium of the Fully Activated Oxide Coating	254
30.1. Influence of variations in temperature	255
30.2. Influence of variations in anode voltage	256
30.3. The processes producing the variations in equilibrium	259
31. Processes at the Surface of the Oxide Coating	261
31.1. Evaporation of excess barium	261
31.2. Emission of ions	263
31.3. Poisoning of the cathode	264
32. Processes at the Interface between Oxide Coating and Core Metal	276
33. Processes in the Interior of the Oxide Coating	286
33.1. Ionic conduction	287
33.2. Diffusion	289
34. The Combination of the Various Processes and their Influence on Emission and Life	291
 APPENDIX: FLUCTUATIONS OF THE EMISSION CURRENT OF THE OXIDE CATHODE (FLICKER EFFECT)	299
 BIBLIOGRAPHY	303
 INDEX TO AUTHORS	305
 SUBJECT INDEX	309

## SYMBOLS AND VALUES OF CONSTANTS

$A, A_0$	constant of the emission equation
$A_w$	atomic weight
$B$	a constant
$C$	universal constant, $C = \frac{2\pi mk}{h^2}$
$D$	diffusion coefficient
$D_e$	coefficient of transmissivity for electrons
$E$	energy
$E$	electrical field strength
$F$	denoting a function
$F$	force
$G$	occupancy of an energy level for electrons
$H$	Hall constant
$H$	magnetic field strength
$I$	electrical current
$I_e$	emission current in general
$I_{ph}$	photo-electric current
$I_r$	retarding field current
$I_s$	saturated current
$I_{sp}$	space-charge current
$I^*$	peak current
$J$	integral
$K$	a constant
$L$	Avogadro's number
$M$	molecular weight
$\mathbf{M}$	dipole moment
$N$	number of electrons per unit volume
$P$	power
$P_H$	heater power
$P_{cool}$	cooling power
$Q$	quantity of heat
$R$	resistance
$R_c$	coating resistance
$S$	surface area
$S_t$	total surface of a cathode
$S_c$	coating surface
$S_e$	emitting surface

## SYMBOLS

<i>T</i>	temperature ( $^{\circ}$ K.)
<i>T<sub>a</sub></i>	actual temperature
<i>T<sub>b</sub></i>	brightness temperature
<i>U</i>	contact potential
<i>V</i>	potential, voltage
<i>W</i>	efficiency of a cathode
<i>X, Y</i>	points in space
<i>Z</i>	atomic number
<i>a</i>	constant of the conductivity formula
<i>b</i>	acceleration
<i>c</i>	concentration
<i>c</i>	velocity of light
<i>d</i>	cathode-anode spacing or lattice constant
<i>d<sub>c</sub></i>	thickness of oxide coating
<i>e</i>	electronic charge
<i>e<sub>t</sub></i>	total radiant emissivity
<i>e<sub>λ</sub></i>	spectral radiant emissivity
<i>f</i>	a function
<i>h</i>	coefficient of heat expansion
<i>h</i>	Planck's constant
<i>j</i>	current density
<i>k</i>	a constant
<i>k</i>	Boltzmann's constant
<i>l</i>	length
<i>m</i>	mass
<i>m</i>	mass of electron
<i>n</i>	number of atoms, ions, etc.
<i>n<sub>e</sub></i>	coefficient of refraction for electrons
<i>p</i>	pressure
<i>p<sub>i</sub></i>	momentum co-ordinate
<i>q</i>	cross-section
<i>q<sub>i</sub></i>	position co-ordinate
<i>r</i>	radius of atoms or ions
<i>s</i>	number of atoms or ions per unit of area
<i>t</i>	time
<i>u</i>	mobility
<i>u<sub>i</sub></i>	ionic mobility
<i>v</i>	velocity
<i>x</i> } <i>y</i> }	special position co-ordinates
<i>z</i>	

## SYMBOLS

$\alpha$	polarization constant
$\beta$	experimental value found for the index of exponential emission and conductivity formulæ
$\gamma$	degree of disorder
$\delta$	density
$\epsilon$	dielectric constant
$\epsilon_0$	dielectric constant of vacuum
$\zeta$	limiting energy of Fermi distribution (Fermi level)
$\eta$	number of free electrons per atom
$\vartheta$	valency
$\kappa$	conductivity
$\kappa_i$	ionic conductivity
$\lambda$	wavelength
$\mu_0$	permeability of vacuum
$\nu$	frequency
$\xi$	ionization potential
$\xi^*$	electron affinity
$\rho$	space-charge density
$\sigma$	interference level of a semi-conductor
$\tau$	total potential barrier at the surface
$\phi$	internal work function
$\chi$	lower limit of conduction band
$\psi$	external work function
$\omega$	average energy of emitted electrons after leaving the surface
$\Delta$	denoting differences
$\Gamma$	activation energy for diffusion and ionic conduction
$\Theta$	fraction of the surface of an atomic film cathode covered with adsorbed atoms or ions (coverage)
$\Sigma$	energy of disorder
$\Xi$	potential barrier in front of an interstitial site in a crystal lattice
$\Phi$	energy of adsorption
$\Psi$	total work function
$\Psi^{(ph)}$	photo-electric work function

## SYMBOLS

### Values of Constants

$c$	$= 2 \cdot 977 \times 10^8$ m. sec. $^{-1}$
$e$	$= 1 \cdot 602 \times 10^{-19}$ coulomb
$h$	$= 6 \cdot 622 \times 10^{-34}$ watt sec. $^2$
$k$	$= 1 \cdot 380 \times 10^{-23}$ watt sec. degree $^{-1}$
$m$	$= 9 \cdot 107 \times 10^{-31}$ kg.
$L$	$= 6 \cdot 023 \times 10^{23}$ molecules/M gram
$\epsilon_0$	$= 8 \cdot 855 \times 10^{-12}$ amp. sec. volt $^{-1}$ m. $^{-1}$
$\mu_0$	$= 1 \cdot 257 \times 10^{-6}$ volt. sec. amp. $^{-1}$ m. $^{-1}$
$e/m$	$= 1 \cdot 759 \times 10^{11}$ coulomb kg. $^{-1}$
$e/k$	$= 1 \cdot 161 \times 10^4$ degree volt $^{-1}$
$\omega$	$= kT/e = 8 \cdot 617 \times 10^{-5} T$ eV
$C$	$= 1 \cdot 801 \times 10^{14}$ m. $^{-2}$ degree $^{-1}$
$A_0$	$= 120$ amp. cm. $^{-2}$ degree $^{-2}$

## CHAPTER 1

# THE THERMAL EMISSION OF ELECTRONS FROM METALS

## 1. The Fermi-Dirac Distribution of Energy of the Electrons in a Metal

The problems of electron emission may be approached either by the thermodynamical or by the statistical method. As already discussed in the preface, only one of these methods will be employed in this work for reasons of lucidity. The statistical method was chosen, as it allows the behaviour of electrons to be more clearly visualized in any particular emission problem. This is accomplished by assuming the energy of the electrons to be entirely electrostatic and by combining plots of the appropriate potential with the statistical calculus. When applying this method, the concepts of the quantum theory will be used from the beginning and the classical laws will only be discussed when necessary for completeness of understanding.

The first problem to be considered is that of emission from the surface of a clean metal. The laws valid for this emission must be derived from the distribution of the electrons in the interior of the metal. Such a metal is built up from a geometrical configuration of identical atoms. According to Bohr, the positive nucleus of such an atom, carrying  $Z$  elementary charges, is surrounded by  $Z$  electrons. Each of these electrons possesses a definite energy depending on the state of the atom at that particular time. It is the essence of Bohr's theory that there is only a number of discrete energy values which are possible for every electron. These energy values may be derived from the various spectra of the atom. They can be conveniently represented by energy levels, the separation of which corresponds to the difference between the respective energies. A typical example is given in Fig. 1. The levels are classified into groups which are distinguished by arabic numbers, the number 1 referring to the group of lowest energy. These numbers are called principal quantum numbers. The levels within a particular group are assigned small letters in the sequence  $s, p, d, f, g$ , etc., called azimuthal quantum numbers. The number of levels belonging to

any one group is equal to the principal quantum number of the group. The scheme therefore takes the following form:

$$1s; \quad 2s; \quad 2p; \quad 3s; \quad 3p; \quad 3d; \quad \text{etc.}$$

The energy levels converge with increasing values towards an upper limit corresponding to the series limit of the spectrum. If the electron exceeds this energy limit then it becomes detached and the atom is ionized.

In practice the absolute values of the energy levels are less important than the differences between them. These differences

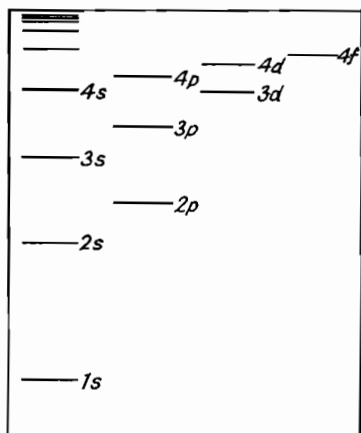


Fig. 1.—Schematic.

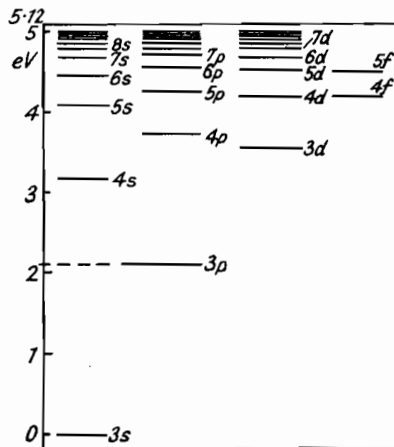


Fig. 2.—For Sodium (outer Electrons).

Figs. 1-2.—Energy Levels of the Electrons of an Atom.

determine the change of energy experienced by the electron when it passes from one level to another. The absolute value of the levels may therefore be fixed in any arbitrary and convenient manner. The magnitude of the energy differences is measured in watt sec. or electron-volts, one electron-volt (abbreviated eV) corresponding to the energy change of an electron passing through a potential difference of 1 volt. In general, energies measured in electron-volts will be denoted by the later Greek letters, e.g.  $\phi$ ,  $\chi$ ,  $\psi$ , etc., whilst corresponding energies measured in watt sec. will take the form  $E_\phi$ ,  $E_\chi$ ,  $E_\psi$ , etc. Then if the charge of the electron is denoted by  $e$ :

$$E_\phi = e\phi$$

$$E_\phi (\text{watt sec.}) = 1.60 \times 10^{-19} \phi (\text{eV}) \dots \dots \quad (1)$$

Fig. 2 shows as an example the values of the differences between the energy levels of sodium from the third group, expressed in eV.

The method of representing the energy of the electrons by means of energy levels has given rise to a pictorial mode of expression, using the electrons instead of the energy levels. It is said, for instance, that an energy level is occupied by an electron, meaning that its energy has a value corresponding to the level concerned. In the same manner one speaks of the passing of an electron from one energy level to another—meaning that its energy has changed from that corresponding to the first level to that corresponding to the second level. This conversion will be frequently employed on account of its clarity, but its figurative meaning must be borne in mind.

The distribution of the  $Z$  electrons on the energy levels is given by the Pauli Principle. According to this a definite energy level of an isolated system, e.g. a metal atom, may be occupied by a definite number of electrons only. This number, called their occupation number or occupancy  $G$ , depends on the azimuthal quantum number according to the following scheme:

Azimuthal quantum number	Occupancy $G$
$s$	2
$p$	6
$d$	10
$f$	14

An  $s$ -state can therefore only be occupied by two electrons, a  $p$ -state by 6 electrons, etc. This occupancy results from the fact that the electron possesses an angular momentum, the electron spin. This angular momentum, together with the momentum belonging to the electron orbit concerned, has only a definite number of positions in a magnetic field. This number of possible positions is equal to the occupancy  $G$  given above.

If the atoms are considered in the “ground” state in which the electrons have their least possible energy values, then a definite distribution of electrons on the energy levels is obtained for every atomic number  $Z$  by means of the Pauli Principle. This distribution has been compiled for the second row of the periodic system in Table I on next page.

When a large number  $N$  of individual metallic atoms coalesce to form a solid, they do so in a regular geometric manner forming up

into the so-called crystal lattice. What happens to the energies of the electrons during the formation of this lattice? According to the Pauli Principle, which is also valid for the system of the lattice, it is not possible for all the electrons on the same energy levels of the single atoms and denoted by a definite quantum number, to occupy the same energy level in the metal lattice. As the occupation number of an energy level is limited by the number  $G$ , the energy levels of the atoms which are of equal magnitude before crystallization, have to be different after crystallization. For a state of definite principal and azimuthal quantum number of the solid metal there will therefore appear a large number  $N$  of energy levels lying close together and forming an energy band in place of the one sharp level of the single atom. The conditions resulting are shown schematically in Fig. 3. Instead of the plot of sharp energy levels for the single atom (cf. Fig. 1) a corresponding plot of energy bands, becoming wider with increasing principal quantum number, is now obtained. Little knowledge exists of the exact position of the bands, but the separation and width of the outermost bands are of the order of some electron-volts.

TABLE I

Element	Number of electrons in the energy level					
	1s	2s	2p	3s	3p	3d
Na	2	2	6	1	—	—
Mg	2	2	6	2	—	—
Al	2	2	6	2	1	—
Si	2	2	6	2	2	—
P	2	2	6	2	3	—
S	2	2	6	2	4	—
Cl	2	2	6	2	5	—
Ar	2	2	6	2	6	—

In Fig. 3, valid for sodium, only one-half of the highest occupied energy band—the 3s-band—is filled by electrons. This is due to the fact that Na has only one 3s electron, whereas the occupancy of the 3s-band is  $G=2$ . This incomplete occupation of the 3s-band gives the reason for the electrical conductivity of Na, i.e. for the mobility of its electrons in an applied electric field. The explanation is most easily approached by first considering an element whose highest energy band is completely filled. According to Pauli, the occupancy of each level is fixed by the number  $G$  and cannot be

exceeded. Since each level is filled, then motion of an electron from one level to another must involve the equal and opposite motion of another electron. Any general motion of electrons in a fixed direction is therefore impossible. A completely filled band cannot therefore support electronic conduction. For a partially filled band such as exists in the case of sodium, the conditions are very different. Electrons which are near the boundary of the occupied part of the  $3s$ -band may have their energies raised by an applied electric field and pass to unoccupied levels above the boundary. The vacated levels may then be occupied by lower energy electrons moving in under the influence of the same applied field. A directed flow thus arises and the phenomenon of

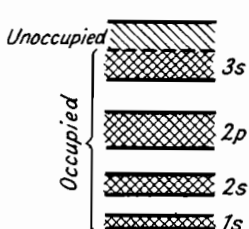


Fig. 3.—Sodium.

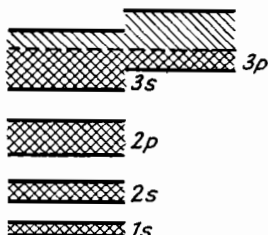


Fig. 4.—Magnesium.

Figs. 3-4.—The Energy Bands of a Metal.

electronic conduction is observed. Such a conduction is therefore only possible in the case of elements whose highest energy band is partially filled. Elements with only completely filled bands must be insulators.

If magnesium, the element following sodium in the periodic table, is considered it will be found that a difficulty arises. The second  $3s$ -electron, absent in sodium, is present in magnesium and it would appear that the highest energy band is likely to be filled—and electronic conduction impossible. This is not in accordance with fact and steps must be taken to explain the contradiction. The difficulty is overcome by assuming that in this and similar cases, the higher energy bands overlap as shown in Fig. 4. The upper limit of the  $3s$ -band is higher than the lower limit of the  $3p$ -band, and there is consequently a series of energy levels in the two bands which have nearly the same height. Because a state with the lowest energy is always the most stable, the electrons in the ground state will occupy the two energy bands up to a level of common height—corresponding to the dashed line in Fig. 3. Parts of the two

overlapping bands therefore remain unoccupied and electronic conduction becomes possible.

So far the atom has been considered in its "ground" state or state of minimum energy. This state is associated with the absolute zero of temperature and results in all the lower levels being completely occupied up to a certain limiting level determined by the total number of electrons. For metals this limiting level lies in the interior of an energy band (cf. Figs. 3 and 4).

What are the conditions when we leave the absolute zero of temperature? A number of electrons gain additional energy and pass to higher levels than those occupied for the state at  $T=0$ . The distribution that the electrons take up on the levels as a result of increasing temperature is governed by one of the three forms of quantum statistics, the so-called Fermi-Dirac system, named after its discoverers. This system, which contains the classical Boltzmann system as a special case, involves two of the later principles of the quantum theory. The first of these is the Exclusion Principle of Pauli which has already been considered in connection with the occupancy of levels. The second is the Principle of Indistinguishability introduced by Bose and Einstein. According to this principle an electron can only be distinguished by its energy and position, and not by characteristic personal to its individual self. Consequently two electron distributions which are obtained from each other by a mere exchange of electrons must be considered as identical in physics and statistics. Let us consider, for example, the Na-atom shown in Fig. 2, in a state in which one electron is on the  $3s$ -level and another one on the  $3p$ -level. Then this state cannot be distinguished by means of experimental physics from the opposite state in which the two electrons have exchanged their places. The two states therefore must be considered as a single one in the Fermi statistics contrary to the statistics previously employed.

The required distribution function is derived in the following manner. All possible distributions are first considered and then the most probable one selected according to the rules of the probability calculus. For this purpose we consider for each electron the three position co-ordinates  $q_i (i=x, y, z)$  and the three associated momentum co-ordinates  $p_i = m \times dq_i/dt$ , which are obtained by differentiating the position co-ordinates. The totality of six co-ordinates of position and momentum together constitute a 6-dimensional space—the so-called phase space. Every value of energy corresponds to

a definite group of values of  $p_i$  and  $q_i$  and therefore to a definite position in phase space. Consequently every possible distribution of electrons on an energy basis may be represented by a corresponding distribution on a position basis in phase space.

According to Heisenberg's Uncertainty Principle not all of the values of position and momentum can be known exactly at any one time. The uncertainties  $\Delta p_i$  and  $\Delta q_i$  for a pair of these values have a lower limit,

$$\Delta p_i \times \Delta q_i \geq \hbar$$

where  $\hbar$  is Planck's Quantum Number. As there are three values for each of the  $p_i$  and  $q_i$  in the case considered, the lower limit for the product of the uncertainties of all six co-ordinates will have the

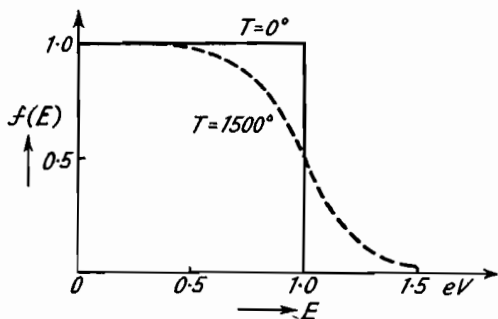


Fig. 5.—Fermi's Distribution Function  $f(E)$ .

value  $\hbar^3$ . If, therefore, phase space is divided into cells of magnitude  $\hbar^3$ , then the position of an electron in phase space can only be located as within the confines of such a cell. Due to the Uncertainty Principle, precision of location has been lost and the positional point replaced by the positional "cell" of magnitude  $\hbar^3$ .

By means of the probability calculus the so-called distribution function  $f(E)$  is derived, giving the probability that a cell in the energy interval  $E$  and  $E+dE$  is occupied by an electron at temperature  $T$ : \*

$$f(E) = \frac{1}{e^{(E-E_b)/kT} + 1} \quad \dots \quad (2)$$

If the behaviour of  $f(E)$  (cf. Fig. 5) is first considered for  $T=0$ , it will be found that  $f(E)=1$  for all values of  $E$  lower than  $E_b$ , and that the associated cell is definitely occupied by an electron for this

\* For the details cf. M. Born, *Atomic Physics*, London, 1944, p. 226.

range of energy values. If, however,  $E > E_\zeta$ , then  $f(E) = 0$  and the respective cell is unoccupied. This behaviour of  $f(E)$  corresponds with the considerations set out above. The energy  $E_\zeta$  is called the "limiting energy" or the "Fermi-level," this name also being employed for temperatures other than zero.

If temperatures  $T > 0$  are considered, the distribution function and the probability that a cell is occupied remain equal to 1 for small values of  $E$ . When approaching the value of  $E_\zeta$ , however, the distribution function falls exponentially and approaches zero for very large values of  $E$ . The fall of the function near  $E_\zeta$  occurs progressively more gradually as the temperature increases. If  $E = E_\zeta$ , the probability  $f(E)$  is always  $\frac{1}{2}$ .

By means of the distribution function  $f(E)$ , which gives the probability for the occupation of the cells, the number  $N(E)dE$  of electrons existing in the energy interval between  $E$  and  $E+dE$  may be calculated. To achieve this,  $f(E)$  must be multiplied by the number of cells  $n(E)$  existing in the energy interval, and by the occupancy  $G$  which gives the number of electrons occupying one cell. Then

$$N(E)dE = G \times n(E) \times f(E)dE = \frac{G \cdot n(E)dE}{e^{(E-E_\zeta)/kT} + 1} \quad . . . \quad (3)$$

The calculation of  $n(E)dE$  is difficult, as it is dependent on the computation of the energy bands. It is possible, however, to compute  $n(E)$  in a relatively simple manner if only the highest and partly occupied energy band of the metal is considered, and if the electrons in this band are assumed to be completely free. This assumption infers that the influence of the potential of the individual ions in the interior of the metal may be neglected. The assumption is justified on account of the relatively great distance existing between the energy band of the free electrons and the next energy band below. The zero point of the energy scale is laid to the lower limit of the highest energy band and all energy values, as for example  $E_\zeta$ , are related to this zero point.

The energy of free electrons is purely kinetic. Hence if  $p = p_x^2 + p_y^2 + p_z^2$  denotes the total momentum of the electrons, then

$$E = \frac{1}{2m} p^2 \quad . . . . . \quad (4)$$

The cells in the energy interval  $E$  and  $E+dE$  make up a spherical shell in the phase space. The volume  $dV$  of this spherical shell is

equal to the product of the volume of the metal concerned and of a spherical shell in the space of the momentum co-ordinates, limited by the radii  $p$  and  $p+dp$ . Therefore, if the unit volume of the metal is considered

$$dV = 4\pi p^2 dp \quad . . . . . \quad (5)$$

and with:

$$p = (2mE)^{1/2} \text{ and } dp = \left(\frac{m}{2E}\right)^{1/2} dE \quad . . . . \quad (6)$$

$$dV = 4\pi \sqrt{2m^{3/2} E^{1/2}} dE \quad . . . . . \quad (7)$$

As the size of the cells is  $\hbar^3$ , the number of cells in the energy interval is obtained by dividing  $dV$  by  $\hbar^3$ :

$$n(E)dE = 4\pi \sqrt{2} \frac{1}{\hbar^3} m^{3/2} E^{1/2} dE \quad . . . . \quad (8)$$

Introducing this into (3) gives the number of free electrons in the energy interval:

$$N(E)dE = 4\pi \sqrt{2} \frac{G}{\hbar^3} \frac{m^{3/2} E^{1/2} dE}{e^{(E-E_\xi)/kT} + 1} \quad . . . . \quad (9)$$

This equation is called Fermi's distribution law. Only the limiting energy  $E_\xi$  in it is unknown and must be determined. The value of  $E_\xi$  may be obtained from the condition that the total number of all the free electrons must have a definite value  $N$ . An integration of (9) over all energy values from zero to infinity therefore gives the equation:

$$\int_0^\infty N(E)dE = 4\pi \sqrt{2} \frac{G}{\hbar^3} m^{3/2} \int_0^\infty \frac{E^{1/2} dE}{e^{(E-E_\xi)/kT} + 1} = N \quad . . \quad (10)$$

After introduction of the abbreviation  $w = E/kT$ , this condition may be written as follows:

$$J(E_\xi) = \int_0^\infty \frac{w^{1/2} dw}{e^{w-E_\xi/kT} + 1} = \frac{N}{4\pi \sqrt{2}} \times \frac{\hbar^3}{G} (mkT)^{-3/2} \quad . . \quad (11)$$

The integral  $J$  can be calculated for two different cases in a relatively simple manner, at first for large positive and secondly for large negative values of  $E_\xi$ . The conditions for the two cases are:

$$\left. \begin{array}{l} (a) \quad \frac{E_\xi}{kT} \gg 1 \\ (b) -\frac{E_\xi}{kT} \gg 1 \end{array} \right\} \quad . . . . . \quad (12)$$

It will easily be seen that the integral  $J$  has very large values in case (a) and very small values in case (b), i.e.:

$$\left. \begin{aligned} (a) \quad J &= \frac{\hbar^3}{4\pi\sqrt{2}G} \times \frac{N}{(mkT)^{3/2}} \gg 1 \\ (b) \quad J &= \frac{\hbar^3}{4\pi\sqrt{2}G} \times \frac{N}{(mkT)^{3/2}} \ll 1 \end{aligned} \right\} \quad \dots \quad (13)$$

Case (a) is realized for a high electron density  $N$  and for low temperatures  $T$ ; and case (b) for small density and high temperatures.

The two cases are separated by a critical temperature  $T_k$  for which  $J=1$ . According to (11):

$$T_k = \frac{\hbar^2}{2mk} \left( \frac{N}{2\pi G} \right)^{3/2} \quad \dots \quad (14)$$

and for electrons

$$T_k = 5 \cdot 1 \times 10^{-11} \left( \frac{N}{G} \right)^{2/3}$$

( $N$  referring to 1 cm.<sup>3</sup>).

The distribution function belonging to (a) is valid for temperatures which are small compared with the temperature  $T_k$ , while the distribution function belonging to (b) is valid for temperatures which are large compared with  $T_k$ .

The approximate calculation of  $J$  in the two cases will not be dealt with here. If the value obtained for  $J$  is introduced into (11), the following two equations for  $E_\zeta$  are obtained: \*

*Case (a):*

$$E_\zeta = \frac{\hbar^2}{2m} \left( \frac{3N}{4\pi G} \right)^{2/3} - \frac{\pi^2}{12} \frac{2m(kT)^2}{\hbar^2} \left( \frac{4\pi G}{3N} \right)^{2/3} + \dots \quad (15)$$

Let  $E_\zeta = E_{\zeta_0}$  for  $T=0$ . Then:

$$E_{\zeta_0} = \frac{\hbar^2}{2m} \left( \frac{3N}{4\pi G} \right)^{2/3} \quad \dots \quad (16)$$

and

$$E_\zeta = E_{\zeta_0} \left[ 1 - \frac{\pi^2}{12} \frac{(kT)^2}{E_{\zeta_0}} + \dots \right] \quad \dots \quad (17)$$

The further terms, which are not given, may be neglected. According to (16) the total number of electrons per unit volume is:

$$N = \frac{4\pi G}{3} \left( \frac{2mE_{\zeta_0}}{\hbar^2} \right)^{3/2}$$

\* For the details cf. R. H. Fowler, E. A. Guggenheim, *Statistical Thermodynamics*, 1939, p. 456.

and introducing this into (9) gives the relative number of electrons in the energy interval  $E$  to  $E+dE$ :

$$\frac{N(E)dE}{N} = \frac{3}{2E_{\zeta_0}^{3/2}} \times \frac{E^{1/2}dE}{e^{(E-E_{\zeta})/\kappa T} + 1} \quad \dots \quad (18)$$

*Case (b):*

In this case

$$J(E_{\zeta}) = \frac{1}{2} \sqrt{\pi} e^{E_{\zeta}/\kappa T} \quad \dots \quad (19)$$

and therefore from (11):

$$e^{E_{\zeta}/\kappa T} = \frac{Nh^3}{G} (2\pi m k T)^{-3/2}$$

This value may be introduced directly into the distribution law (9) and the unity value in the denominator may be neglected, since the exponential function takes very high values in this case. Therefore:

$$\frac{N(E)dE}{N} = \frac{2}{\sqrt{\pi}} (\kappa T)^{-3/2} E^{1/2} e^{-E/\kappa T} dE \quad \dots \quad (20)$$

This equation is the well-known distribution law of Maxwell, which was originally obtained by means of the classical Boltzmann statistics and which occurs here as a special case of the Fermi-Dirac statistics. It is valid for temperatures which are large compared with the critical temperature  $T_k$  given by (14).

If  $T_k$  is to be calculated numerically the number  $N$  of the electrons per unit volume must be known. If  $A_w$  is the atomic weight of the metal,  $\delta$  its density (in g./cm.<sup>3</sup>),  $\eta$  the number of free electrons per atom and  $L$  Loschmidt's number (number of atoms in  $A_w$  gram of the metal), the number of electrons per cm.<sup>3</sup> is:

$$N = \eta \frac{\delta}{A_w} L \text{ cm.}^{-3} \quad \dots \quad (21)$$

The number of free electrons per atom is certainly a small number, being of the order of the occupancy  $G$ . We may put  $\eta=1$  as an estimate. Then with  $G=2$ , with an average atom weight  $A_w=100$  and an average density  $\delta=10$ ,  $N=6 \times 10^{23} \times 10/100=6 \times 10^{22}$  electrons/cm.<sup>3</sup> and from (14)  $T_k \approx 50,000^\circ \text{K}$ . are obtained. Hence case (a) is always valid for the electrons in the interior of a metal, if the temperature is in the normal range between 0 and some 1000 degrees.

Case (b) occurs if the electrons are in a vacuum, e.g. in a discharge tube. The electron density  $N$  then is considerably smaller than in the interior of the metal and Maxwell's distribution law is

therefore valid. This law is also valid for gas molecules. If hydrogen is considered as an example, then because of the smaller density (at 273° K.  $N=6 \times 10^{23}/22.4 \times 10^3 = 2.7 \times 10^{19} \text{ cm.}^{-3}$ ) and the larger mass ( $m=3.3 \times 10^{-27} \text{ kg.}$ ) of the hydrogen molecules  $T_k \approx 0.1^\circ \text{ K.}$  Thus the gases also belong to case (b) at normal temperatures and therefore have an energy distribution according to Maxwell.

The two energy distributions, the Fermi distribution itself according to (18) and the Maxwell distribution according to (20), are plotted in Fig. 6 for  $E_{\zeta_0}=1 \text{ eV}$  and  $dE=0.01 \text{ eV.}$  The considerable difference between the two distribution laws will be seen. Only if the energy values are very high ( $E > E_\zeta$ ), the fall of the Fermi distribution curve corresponds to that according to Maxwell

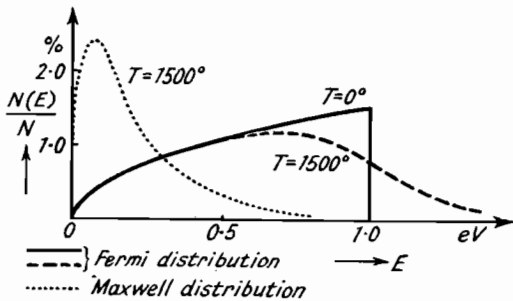


Fig. 6.—Energy Distributions according to Fermi and to Maxwell.

with close approximation. In the case of the Maxwell distribution the maximum of the relative number of electrons  $N(E)/N$ , which is obtained by differentiating (20), is  $E_{max} = 1/2kT.$

As stated above, the energies of the electrons in the interior of a metal are always distributed according to Fermi's law, represented in Fig. 6. Equation (9), for this distribution law is exactly valid for the ideal case of completely free electrons, while in reality there will be differences from the ideal case which may alter the factor of (9). A statement of the magnitude of these differences cannot be made here. The limiting energy  $\zeta_0$  is according to (16), if  $G=2$  (corresponding to an *s*-band):

$$\zeta_0 = 26.1 \left( \frac{\delta\eta}{A_w} \right)^{2/3} \text{ eV} \quad \dots \quad (22)$$

The value of  $A_w/\delta$  in this equation is equal to the volume of a gram-atom and is called the atomic volume. In addition to this atomic volume, the number  $\eta$  of free electrons per atom must be

known, if the limiting energy  $\zeta_0$  is to be calculated. As exact values for  $\eta$  are not available, only the values of  $\zeta_0\eta^{-2/3}$  are given for some metals in Table No. II. As will be seen from this table, the limiting energy  $\zeta_0$  is of the order of 1 to 10 eV, if  $\eta$  is small, as is normally the case.

TABLE II  
*The Limiting Energy  $\zeta_0$  of some Metals*

$\zeta_0\eta^{-2/3}*$	$\zeta_0\eta^{-2/3}$	$\zeta_0\eta^{-2/3}$
Li 4.7 eV	Be 9.0 eV	Th 3.5 eV
Na 3.2 „	Mg 4.5 „	Ta 5.3 „
K 2.1 „	Ca 3.0 „	Mo 5.8 „
Rb 1.8 „	Sr 2.5 „	W 5.8 „
Cs 1.5 „	Ba 2.4 „	Fe 7.1 „
Cu 7.0 „	Al 5.6 „	Ni 7.4 „
Ag 5.5 „		Pd 6.1 „
Au 5.5 „		Pt 6.0 „

\*  $\eta$ =number of free electrons per atom.

The temperature-dependence of  $\zeta$  is produced at first by the correction term in the square brackets of equation (17) and secondly by the temperature-dependence of  $N$  due to the increase of volume with increasing  $T$ . The influence of the correction term may be neglected in practice. Therefore if a linear coefficient of thermal expansion  $h$  is assumed and  $V=V_0(1+hT)^3$  the following equation is obtained from (16) and (17):

$$\zeta_T = \zeta_0(1-2hT) \quad \dots \quad \dots \quad \dots \quad \dots \quad (23)$$

With an average value  $h=1 \times 10^{-5}$ , for example, it is  $\zeta_{1000}=0.98\zeta_0$ .

As shown by Sun Nien Tai and Band<sup>1</sup> and by Wohlfahrt,<sup>1</sup> the temperature dependence of the Fermi level will be different from that given by (23) if the highest energy bands are overlapped (cf. Fig. 4) and if the Fermi level is very close to the top or bottom of the respective bands. The difference then obtained is due to the transfer of electrons from one band to the other with rising temperature. For the case of nickel a positive temperature dependence of  $\zeta$  instead of the negative one given by (23) has been calculated.

## 2. The Potential Barrier at the Surface of a Metal

In Sec. 1 it was assumed that the metal under consideration was a crystal lattice of infinite extent, but when discussing thermal electron emission, that is, the emission of electrons from hot bodies, it will

be necessary to consider the boundaries of the lattice. In so doing the problem will be simplified by neglecting the potential differences produced by the individual metal ions and by assuming an average constant potential for every electron in the interior of the metal. It is then clear that the potential of an electron, moving from the interior of the metal towards a metal-vacuum boundary, must rise as the boundary is crossed. If no such increase in potential occurs, electrons would leave the metal in great numbers even at absolute zero temperature by virtue of their energy at that temperature, and the metal lattice would eventually disintegrate. Considerations of stability make it necessary therefore to conclude that a potential barrier exists at the metal-vacuum boundary opposing the emission of electrons into the vacuum.

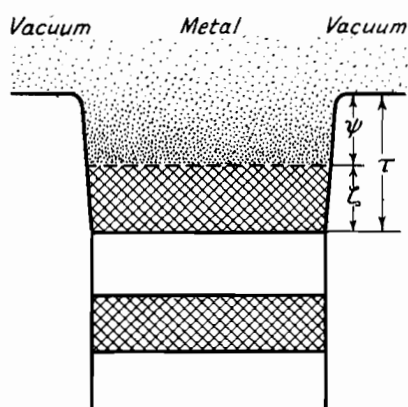


Fig. 7.—Potential Variation at the Surface of a Metal, represented by "the potential box".

The potential distribution in the interior and at the boundary may be represented by the potential box shown in Fig. 7. The bottom of this box corresponds to the lower limit of the energy band of the free electrons, while the sides of the box represent the relatively steep rise of the potential at the boundary between metal and vacuum. The height represented by the broken line is equal to the limiting or maximum energy  $\zeta$  of the electrons at absolute zero.

The total potential barrier  $\tau$  at the boundary can be conveniently divided into two parts, one part which corresponds to the limiting energy  $\zeta$ , and a second part, denoted by  $\psi$ , which is equal

\* Strictly speaking it is necessary to distinguish between the potential energy of an electron in eV and its potential in volts. As both have the same numerical value, however, it is possible for the sake of simplicity to denote them by the same Greek letter without risk of confusion.

to the difference between the potential values  $\tau$  and  $\zeta$ . This potential difference:

$$\psi = \tau - \zeta \quad \dots \dots \dots \quad (24)$$

when multiplied by the electron charge  $e$ , is equal to the work necessary to remove any electron from the metal by means of, for example, increase of temperature. The value of this potential difference, expressed in electron-volts, is called the work function. On the other hand, when an electron enters the metal from the vacuum an equal amount of energy  $e\psi$  is gained.

In the plot in Fig. 7 showing the potential of the electrons at the metal surface, the sign of the potential has been chosen opposite to that generally used. In most cases, as, for example, in the theory of electricity, an increase in the potential energy of the electrons is associated with a decrease in potential, owing to their negative charge. The potential in Fig. 7, however, increases with the potential energy of the negative electrons. This convention is regarded as being more suitable, as it makes clear visualization of the phenomena possible, and it will therefore be used throughout.

It is possible to imagine two physical causes for the origin of the potential barrier at the boundary of a metal. One cause supposes the existence of an electrical double layer at the boundary produced by the polarization of the metal ions near the boundary due to the inward direction of the electric field. Such a double layer, as is well known, would produce a potential barrier of the required form. The second possible cause is the image force which arises in the following manner. If an electron is emitted from a metal and is at a distance  $z$  from the surface, it induces a charge of equal magnitude but opposite sign in the interior of the metal. This induced charge is located, using the optical analogy, at the position of the mirror image of the emitted electron in the metal surface. The induced charge, at a distance  $z$  from the surface, attracts the emitted electron with a force determined in accordance with Coulomb's law and known as the image force. An image potential may be associated with this image force which increases as the electron leaves the boundary of the metal and which contributes to the total barrier  $\tau$ .

The image potential was first calculated by Schottky.<sup>3</sup> According to Coulomb's law the image force is:

$$F_i = \frac{e^2}{4\pi\epsilon_0(2z)^2} \quad \dots \dots \dots \quad (25)$$

and consequently the field strength corresponding to this image force:

$$\mathbf{E}_i = \frac{e}{16\pi\epsilon_0 z^2} \quad \dots \quad \dots \quad \dots \quad (26)$$

The absolute value of the image force potential  $V_i$ , associated with  $\mathbf{E}_i$ , is defined in such a way that it tends to zero as  $z$  approaches infinity. Then:

$$V_i = \int_z^\infty \mathbf{E}_i(z) dz = \frac{-e}{16\pi\epsilon_0 z} \quad \dots \quad \dots \quad \dots \quad (27)$$

The equation for  $V_i$  (cf. Fig. 8), giving an infinite potential for  $z=0$ , can only be valid for values of  $z$  which are different from zero. This can easily be explained. Equation (27) was calculated for a

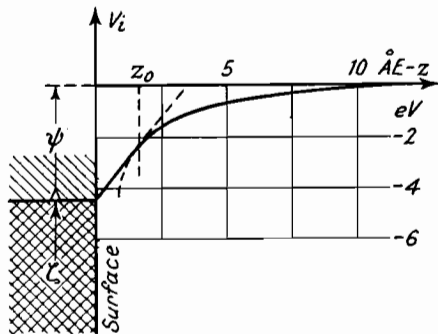


Fig. 8.—The Potential  $V_i$  associated with the Image Force.

uniform distribution of charge, but in the limit  $z=0$ , as the surface is approached, the influence of the discrete ionic charges cannot be neglected. The shape of the image potential curve as  $z$  tends to zero may be approximated, using a suggestion made by Schottky, by constructing the tangent to the potential curve valid for larger values of  $z$  from the point  $V_i=\psi$  on the ordinate axis. In this way the part of the total potential barrier  $\tau$  corresponding to the work function  $\psi$  is obtained by using the conception of the image force. The potential is linear from  $z=0$  to the tangential point  $z=z_0$  of the curve given by equation (27). From this point to higher values of  $z$  the potential is represented by equation (27).

A relation between the work function and the critical distance  $z_0$  can be derived by dividing the work function, i.e. the energy necessary to take the electron to infinity, into two parts. The first of these parts refers to the distance from  $z=0$  to  $z=z_0$  and is equal to the constant field strength  $e/16\pi\epsilon_0 z_0^2$  multiplied by the electronic

charge  $e$  and by the distance  $z$ . The second part, appropriate to the distance from  $z=z_0$  to  $z=\infty$ , is determined by equation (27) and equals  $e \times e / 16\pi\epsilon_0 z_0$ . Therefore the work function expressed as the sum of the two parts is:

$$E_\psi = \frac{e^2}{8\pi\epsilon_0 z_0} \text{ watt sec. . . . .} \quad (28)$$

or expressed in electron-volts:

$$\psi = \frac{e}{8\pi\epsilon_0 z_0} = \frac{7.2 \times 10^{-10}}{z_0} \text{ eV . . . .} \quad (29)$$

The critical distance  $z_0$ , defining the lower limit for the validity of equation (27) for the image force potential, will be of the order of inter-atomic distances, i.e. of some  $10^{-8}$  cm. It is only within such a small distance that the image force potential will be influenced by the discrete ionic charges. Consequently the value of  $\psi$  obtained from the above equation will be of the order of a few electron-volts and will therefore be in good correspondence with the measured values (cf. Table V, p. 97). If  $z_0$  is put equal to the lattice spacing  $d$  of the crystal lattice of the metal concerned, the value of the work function so obtained will be nearly proportional to  $1/d$ . This relation is also in reasonable agreement with experiment. The alkali metals, for instance, have a large lattice spacing and a small work function (for Cs,  $d=6.05 \text{ \AA.}$  and  $\psi=1.9 \text{ eV}$ ), while the heavy metals have a small lattice spacing and a large work function (for W,  $d=3.16 \text{ \AA.}$  and  $\psi=4.5 \text{ eV}$ ). It may be concluded that Schottky's assumptions mentioned above are justified by the relatively good agreement between the experimental results and the equation for the work function derived from the image force potential.

Calculations of the work function using the methods of wave mechanics have been carried out by Tamm and Blochinzew,<sup>1</sup> Mrowka and Recknagel,<sup>2</sup> Bartelink,<sup>1</sup> Wigner and Bardeen,<sup>1</sup> Bardeen<sup>1</sup> and Hellmann and Kossatotschkin.<sup>1</sup> The methods used are always based on calculations of the energy of the metal lattice with all electrons included and of the respective energy which is obtained with one electron excluded. The difference between these two energies then gives the value of the work function. The above calculations confirm the proportionality between  $\psi$  and the reciprocal of the lattice spacing. The later calculations also give a relatively good correspondence between theory and experiment for the alkali metals.

The experimental methods used for the measurement of the work function are discussed in a later chapter (Chapter 2) and exact values for the work function of different metals are given there (cf. Table V).

Of the other two potential barriers occurring at the metal-vacuum boundary, only the total potential barrier  $\tau$  can be measured by application of electron diffraction methods. In accordance with the theory of wave mechanics a wave property or electron wave is associated with every electron. These electron waves, when impinging upon a crystal lattice, are diffracted and the position of the diffraction maxima is influenced by the coefficient of diffraction of the waves:

$$n_e = \sqrt{\left(\frac{E+E_\tau}{E}\right)} \quad \dots \quad (30)$$

( $E$  being the energy of the electrons outside the crystal). From the position of these diffraction maxima it is therefore possible to calculate the coefficient of diffraction and the potential  $\tau$ . According to Davisson and Germer<sup>2</sup> and Bethe<sup>1</sup> the value  $\tau=14.8$  eV is obtained for nickel. With a measured work function  $\psi$  equal to 4.9 eV (cf. Table V), the value  $\zeta=9.9$  eV is obtained. The value obtained for  $\zeta$  from Table II, if the number of free electrons per atom,  $\eta$ , is put equal to unity, is  $\zeta=7.4$  eV. This degree of correspondence may be regarded as good in view of uncertainty in the exact value of  $\eta$ .

The work function of a metal is not constant, but depends, as will be seen in detail later, on the temperature of the metal concerned, on the magnitude of the electrical field existing outside the surface of the metal, and on the orientation of the surface to the crystal lattice of the metal.

The existence of a temperature-dependence of the work function  $\psi$  can be concluded from the fact that the Fermi level  $\zeta$  is temperature dependent. (Herzfeld,<sup>1</sup> Reimann<sup>1</sup>). If the total potential barrier  $\tau$  were independent of temperature the sign of the temperature coefficient of  $\psi$  would be opposite to that of the coefficient of  $\zeta$ . An increase of work function with temperature would then be obtained in most cases. The total potential barrier, however, depends on the distance between the ions of the metal lattice and will therefore also depend on temperature. Calculations of this latter dependence as undertaken by Seeley,<sup>1</sup> Wigner<sup>2</sup> and Herring and Nichols,<sup>1</sup> show that the temperature coefficient of  $\tau$  is negative and of the same order as that of the Fermi level  $\zeta$ . The calculations are

as yet not accurate enough to allow more quantitative conclusions. The temperature-dependence of  $\psi$  will be indicated by a subscript,  $\psi_T$  denoting the work function at temperature  $T$  and  $\psi_0$  the work function at  $T=0$ .

The dependence of the work function on the magnitude of the external electrical field may be seen from the potential curves in Fig. 9. The external field is in such a direction as to attract electrons from the surface of the metal. Under these circumstances the potential due to this external field of strength  $E_e$  is superimposed on the image force potential corresponding to the work function. The superposition of the two potentials results in a potential maximum existing at a finite distance  $z_m$  from the surface. The height of this potential maximum, which replaces the continuously

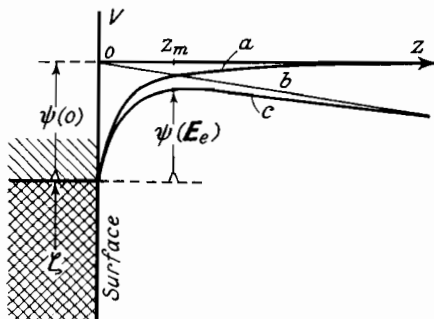


Fig. 9.—Superposition of Image Potential and External Potential.

- (a) Potential due to Image Force.
- (b) Potential due to External Field.
- (c) Resulting Potential.

rising image potential, is less than the potential rise due to the image force alone. In the presence of an external field, the work function, i.e. the work necessary to extract an electron from the metal, will therefore be equal to the height of this potential maximum. Since this height depends on the magnitude of the external field, the work function will also depend on the magnitude of this field. The dependence of the work function on the external field may be indicated by a superscript,  $\psi^{(o)}$  denoting the work function with zero external field.

The fact that the total field strength, the sum of image field and external field, is equal to zero at the potential maximum may be used for the derivation of the numerical relation between work function and external field. Using equation (26) we then have:

$$E_i + E_e = -\frac{e}{16\pi\epsilon_0 z^2} + E_e = 0$$

Solving this equation for  $z$  gives the position of the potential maximum:

$$z_m = \frac{1}{4} \sqrt{\left( \frac{e}{\pi \epsilon_0 E_e} \right)} \dots \dots \dots \quad (31)$$

According to this equation for

$$E_e = 100 \text{ volt/cm.}, \quad z_m = 2 \times 10^{-5} \text{ cm.}$$

$$E_e = 10,000 \text{ volt/cm.}, \quad z_m = 2 \times 10^{-6} \text{ cm.}$$

The distance between the potential maximum and the metal surface is therefore of the order of  $10^{-5}$  or  $10^{-6}$  cm.

The total potential is derived by adding the potential corresponding to the external field,

$$V_e = -E_e z \dots \dots \dots \quad (32)$$

to the image force potential given by equation (27). Then:

$$V(z) = \frac{-e}{16\pi\epsilon_0 z} - E_e z \dots \dots \dots \quad (33)$$

From this equation the value of the potential at the maximum is obtained as:

$$V_m = -\frac{1}{2} \sqrt{\left( \frac{e E_e}{\pi \epsilon_0} \right)} \dots \dots \dots \quad (34)$$

Finally we know that the work function with an external field is equal to the height of the potential maximum and consequently will be obtained by adding the value found for  $V_m$  to the work function  $\psi^{(o)}$  without external field. Therefore:

$$\psi^{(E_e)} = \psi^{(o)} - 3.78 \cdot 10^{-5} \cdot \sqrt{E_e} \dots \dots \dots \quad (35)$$

According to this equation the work function is dependent on the square root of the external field strength.

The work function of a metal surface depends on the orientation of this surface to the crystal lattice of the metal as well as on temperature and external field. This fact was first observed when the electron emission of multicrystalline metal surfaces was examined by means of the electron microscope. It can be seen from the electron images that the single crystals lying in the surface emit electrons with different intensities (cf. Fig. 10). These differences in electron emission can be explained on the assumption that crystal areas with different orientations have different work functions. Other investigations were made by Martin,<sup>1</sup> who examined single hemispherical crystals of tungsten by means of the electron microscope. Parts of these hemispheres with different orientations to

the crystal lattice emitted with different intensities (cf. Fig. 11). The conclusion that the work function has different values for areas of different orientation was confirmed by direct measurements of the work functions of single crystals (for methods of measurement cf. Chapter 2). According to Mendenhall and de Voe<sup>1</sup> the work function of tungsten is 4.35 eV for a (013)-plane and 4.50 eV for a (112)-plane, while according to Nichols<sup>1</sup> the work function of tungsten lies between a lowest value of 4.35 eV for a (111)-plane and a highest value of 4.66 eV for a (112)-plane. There is not complete agreement between these results.

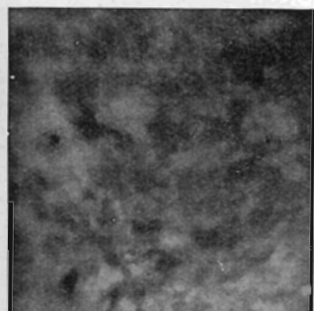


Fig. 10.—A Multicrystalline Tungsten Cathode (Brueche<sup>2</sup>).



Fig. 11.—A Hemispherical Single Crystal of Tungsten (Martin<sup>1</sup>).

Figs. 10–11.—Electron Microscope Images.

A theoretical explanation of the influence of the orientation on the work function was tried by Mrowka,<sup>1</sup> Mueller,<sup>1</sup> Smoluchowski,<sup>1</sup> and Stranski-Suhrmann.<sup>1</sup> In the two latter investigations a good correspondence was found between the results of the calculation and the values measured by Nichols.<sup>1</sup> In further discussion we shall initially neglect the differences between the work functions of parts of the surface having different orientations and assume a uniform value. The influence of these differences in work function on observed phenomena will be discussed in Sec. 6.

### 3. The Passage of the Electrons across the Metal-Vacuum Boundary

After the preparatory work of the first two sections we can now proceed to derive the laws for thermal electron emission from pure metals; that is, for the emission of electrons from such metals due

to increasing temperature. The conditions may be visualized by re-examination of the potential box (Fig. 7). At a temperature different from zero some of the electrons are on energy levels above the limiting energy  $\zeta$ , and the number of these electrons increases with increasing temperature according to the distribution law. Of these electrons only the few whose energy exceeds the total potential barrier can leave the metal, i.e. can be emitted. The process can be made clear, according to Schottky,<sup>6</sup> if the electrons are represented by balls which run along the bottom of the box and up its sloping walls, the latter representing the total potential barrier  $\tau$ . The distribution of the velocities of the balls is assumed to correspond to Fermi's law. Under these conditions most of the balls will run up the walls to a certain height and will then return, because their velocity is not sufficient for reaching and surpassing the rim of the walls. Only very few of the balls, whose velocity is especially large, will reach the rim, leave the box with a residual velocity and thus represent the emitted electrons. An increase in temperature of the metal is represented by an increase in the velocities of all the balls. In this way many more balls are enabled to leave the box and the increase of electron emission with increasing temperature is demonstrated.

Let  $v_z$  denote the velocity component of the electrons in the direction  $z$  perpendicular to the metal surface and let  $E^{(n)}$  denote the energy associated with this component. Then at a definite temperature  $T$  of the metal, those electrons are emitted whose velocities are large enough to overcome the potential barrier existing at the surface. The condition for emission is therefore:

$$E^{(n)} = \frac{mv_z^2}{2} = \frac{p_z^2}{2m} \geq E_\tau \quad \dots \quad (36)$$

In order to calculate the number of emitted electrons the distribution law (9) must be written in terms of the momentum co-ordinates  $p_x$ ,  $p_y$ ,  $p_z$ . The value of the phase volume  $dV$  in (9), which results from (7), has therefore to be replaced by the phase volume  $dp_x$ ,  $dp_y$ ,  $dp_z$ , referring to the momentum co-ordinates. Accordingly equation (9) must be divided by (7) and multiplied by  $dp_x$ ,  $dp_y$ ,  $dp_z$ , and the new form of distribution law is obtained:

$$N(p)dp_x dp_y dp_z = \frac{G}{h^3} \frac{dp_x dp_y dp_z}{e^{(p^2/2m - E_\zeta)/kT} + 1} \quad \dots \quad (37)$$

Equation (37) is integrated over all possible values of  $p_x$  and  $p_z$ ,

thus giving the number of electrons whose momentum co-ordinate  $p_z$  lies between  $p_z$  and  $p_z + dp_z$ :

$$N(p_z)dp_z = \frac{G}{\hbar^3} dp_z \int_{-\infty}^{+\infty} \int_{-\infty}^{+\infty} \frac{dp_x dp_y}{e^{[(p_z^2 + p_y^2 + p_t^2)/2m - E_\zeta]/kT} + 1} . \quad (38)$$

This integral may be calculated by the introduction of polar co-ordinates. If the energy  $E^{(n)}$ , resulting from (36) is introduced instead of  $p_z$ , the integration gives the number of electrons whose energy in the direction  $z$  is between  $E^{(n)}$  and  $E^{(n)} + dE^{(n)}$ :

$$N(E^{(n)})dE^{(n)} = G \frac{\pi m k T}{\hbar^3} \sqrt{\left(\frac{2m}{E^{(n)}}\right)} \ln(1 + e^{-(E^{(n)} - E_\zeta)/kT}) dE^{(n)} \quad (39)$$

Multiplying this equation by  $v_z = \sqrt{(2E^{(n)}/m)}$  gives the number of electrons with energies between  $E^{(n)}$  and  $E^{(n)} + dE^{(n)}$  striking the unit area of the surface in a second:

$$N(E^{(n)})dE^{(n)} = G \frac{2\pi m k T}{\hbar^3} \ln(1 + e^{-(E^{(n)} - E_\zeta)/kT}) dE^{(n)} . \quad (40)$$

For the electrons emerging from the surface  $E^{(n)} \geq E_\tau$  according to (36), and therefore  $(E^{(n)} - E_\zeta)/kT \gg 0$ . Instead of (40) the approximate formula:

$$N(E^{(n)})dE^{(n)} \simeq \frac{GC}{\hbar} T e^{-(E^{(n)} - E_\zeta)/kT} dE^{(n)} . . . . \quad (41)$$

will therefore be used for the emerging electrons with:

$$C = \frac{2\pi m k}{\hbar^2} = 1.801 \times 10^{14} \text{ m.}^{-2} \text{ degree}^{-1} . . . . \quad (41a)$$

This universal constant  $C$  will be found frequently in the calculations referring to phenomena of emission and conductivity.

Equation (41) may be considered as the distribution law for the energy of the emerging electrons. It is similar to Maxwell's distribution law (20), as the term  $E^{1/2}$  in that law may be neglected. From this it follows that the emerging electrons are distributed according to Maxwell's law.

The mean value of the energy of the emerging electrons (in the direction of the normal) may be derived from (41):

$$E_\omega^{(n)} = \frac{\int_{E_\tau}^{\infty} E^{(n)} e^{-(E^{(n)} - E_\zeta)/kT} dE^{(n)}}{\int_{E_\tau}^{\infty} e^{-(E^{(n)} - E_\zeta)/kT} dE^{(n)}} . . . . \quad (42)$$

The kinetic energy of the electrons after emission is obtained by subtracting  $E_\zeta$  from the above value. Hence the mean value of the kinetic energy is:

$$E_\omega^{(n)} = kT$$

or

$$\omega = \frac{kT}{1.6 \times 10^{-19}} = 8.61 \times 10^{-5} T \text{ eV} \dots \quad (43)$$

Accordingly the mean kinetic energy of the emerging electrons at  $T=1000^\circ$  is 0.086 eV.

In order to obtain the total number of emerging electrons, equation (41) has to be integrated for all values of  $E^{(n)} \geq E_\tau$ . The number so obtained is not, however, directly equal to the number of emitted electrons, as another fact, not previously mentioned, must be taken into consideration. The electron waves associated with the electrons may be reflected from regions in which a high potential gradient exists, in the same manner as light waves are reflected from regions in which there is a sudden change in the refractive index. Such reflection of electron waves, and therefore of the electrons themselves, will be possible at the surface since the potential barrier there represents a very high potential gradient. Consequently it will be possible for a certain fraction of those electrons impinging upon the metal surface, and possessing sufficient energy for emission, to be reflected back into the metal. Only the remaining fraction, given by a coefficient of transmissivity  $D_e$ , will pass the metal surface.

Using the coefficient of transmissivity, the total number of emitted electrons is obtained by integration of (41):

$$N_e = \frac{GC}{h} T \int_{E_\tau}^{\infty} D_e(E^{(n)}) e^{(E_\zeta - E^{(n)})/kT} dE^{(n)} \dots \quad (44)$$

This integral may be calculated if a mean coefficient of transmissivity  $\bar{D}_e$  is introduced. Then:

$$N_e = GC \bar{D}_e \frac{k}{h} T^2 e^{-(E_\tau - E_\zeta)/kT} \dots \quad (45)$$

Multiplication by the electronic charge  $e$  gives the emission current per unit area of the metal surface:

$$j_s = GeC \bar{D}_e \frac{k}{h} T^2 e^{-(E_\tau - E_\zeta)/kT} \dots \quad (46)$$

This equation, in which the term  $E_r - E_\zeta$  in the exponent is equal to the work function  $E_\psi$ , is Richardson's well-known emission equation. It was at first obtained in a slightly different form, containing the factor  $T^{1/2}$  instead of  $T^2$ . It has not been found possible to carry out an experimental proof which would distinguish between the older  $T^{1/2}$  law and the  $T^2$  law derived here, the reason being the overriding magnitude of the exponential function and the consequent fact that the precision of the measurements is not sufficient for distinguishing between the two  $T$ -terms. The  $T^2$  law was derived by Dushman, v. Laue, Richardson, Schottky and H. A. Wilson by means of thermodynamical methods; the statistical derivation shown here was given by Sommerfeld<sup>1</sup> and Nordheim.<sup>2</sup> The factor  $G$  in the emission equation and the fixing of the energy levels  $E_\zeta$  and  $E_r$ , as described above, were the new results of the statistical derivation.

The mean coefficient of transmissivity  $\bar{D}_e$  has to be calculated by means of wave mechanics. The calculation carried out by Nordheim<sup>1</sup> and MacColl,<sup>1</sup> assuming a continuous variation of the potential at the metal surface, gives  $\bar{D}_e \approx 1$ . Making this substitution, the emission equation for a surface area  $S$  has the form:

$$I_s = A_0 S T^2 e^{-e\psi/kT} = A_0 S T^2 e^{-11610\psi/T}. \dots \quad (47)$$

In this equation:

$$A_0 = G e C \frac{k}{h} = G \times 60 \text{ amps./cm.}^2 \text{ degree} \dots \quad (48)$$

The factor  $A_0$  in the emission equation is called the emission constant. The occupation number  $G$  in  $A_0$  is usually put equal to 2, as the highest occupied energy band is an *s*-band in the case of almost all the metals used in practice for electron emission. Values of the occupation number  $G$  differing from 2 are, however, also possible on account of the overlapping of the highest energy bands in some metals as discussed above.

With  $G=2$ ,  $A_0=120$  amps./cm.<sup>2</sup> degree. Deviations from this value may be due not only to an occupation number  $G \neq 2$ , but also to a coefficient of transmissivity  $D_e$  different from 1 in exceptional cases. Further deviations may be caused if the electrons, contrary to our previous supposition, cannot be regarded as completely free. In this case the variation of the emission constant would result from a corresponding variation of the factor in the distribution law (9) or (37).

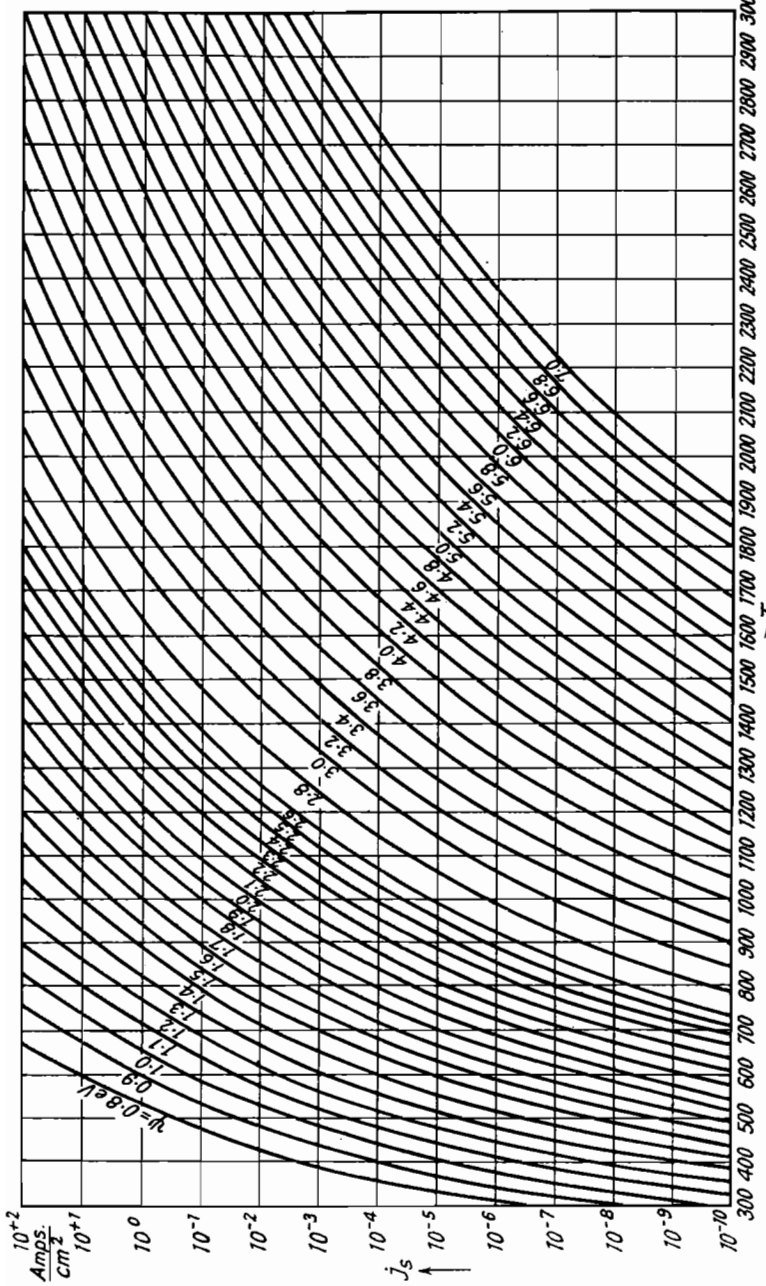


Fig. 12.—Density  $j_s$  of the Saturated Current as a Function of Temperature  $T$  (Work Function  $\phi$  as a Parameter).

The emission current given by equation (47) can only be measured if all the electrons emitted by the cathode are drawn away from it by an adequate positive field. In this case the emission current is termed saturated and will be denoted by  $I_s$ . Because of the exponential function in (47) the magnitude of the saturated current depends on the values of work function and temperature to a high degree. The nature of this dependence in the ranges of work function and temperature which apply in practice may be seen from the diagram in Fig. 12 giving  $j_s = I_s/S$  as a function of  $T$  with the work function as a parameter.

Finally it is possible to determine the velocity distribution of the

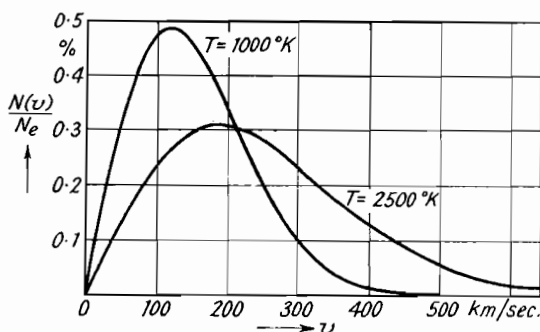


Fig. 13.—Maxwellian Velocity Distribution of the emitted Electrons.

emitted electrons. The energy of these electrons is obtained from equation (41), which gives, on division by equation (45):

$$\frac{N(E^{(n)})dE^{(n)}}{N_e} = \frac{1}{kT} e^{-(E^{(n)} - E_\zeta)/kT} dE^{(n)}$$

The velocity in the direction of the normal after emission is obtained from:

$$\frac{mv^2}{2} = E^{(n)} - E_\zeta$$

Converting to  $v$  as variable gives:

$$\frac{N(v) dv}{N_e} = \frac{mv}{kT} e^{-mv^2/kT} dv \quad . . . . . \quad (49)$$

The distribution of the velocities of the emitted electrons resulting from the above equation is of Maxwellian form and is plotted in Fig. 13 for two different temperatures  $T=1000^\circ$  and  $T=2500^\circ$  and for  $dv=1$  km./sec.

The mean velocity of the emitted electrons is obtained from (43). The mean square of the velocity is:

$$\overline{v^2} = \frac{2E_{\omega}^{(n)}}{m} = \frac{2kT}{m} = 30.5T \text{ (km./sec.)}^2$$

and therefore:

$$\sqrt{\overline{v^2}} = 5.53\sqrt{T} \text{ km./sec. . . . .} \quad (50)$$

Hence for  $T=1000^\circ$ :

$$\sqrt{\overline{v^2}} = 175 \text{ km./sec.}$$

#### 4. The Characteristics of a Diode

Only the source of emitted electrons, the cathode, has been considered in the previous sections. If the emission current is to be

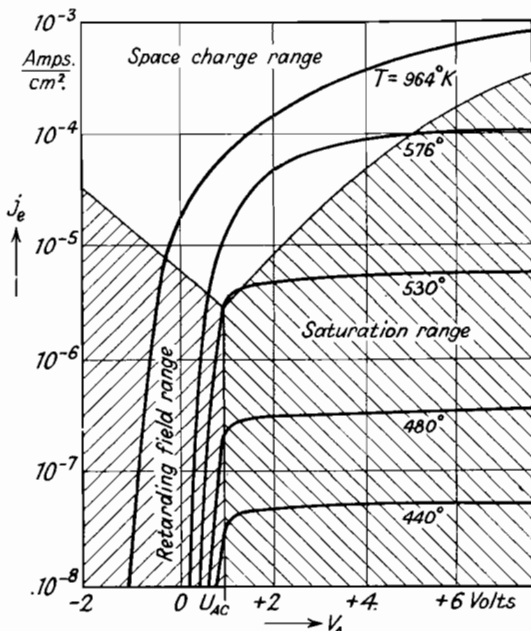


Fig. 14.—The three Ranges of the Characteristics. Emission Densities  $j_e$  as a Function of Anode Voltage for different Temperatures of the Cathode (Work Function of the Cathode about 1.4 eV).

measured or used, at least one other electrode, the collecting electrode or anode, will be needed in addition to the cathode. The saturated current  $I_s$  given by (47), in such a diode system only flows if an adequate positive voltage  $V_A$  is applied to the anode. If the

anode voltage is not sufficient for saturation, the emission current depends on the magnitude of the anode voltage to a higher degree than can be explained by the dependence of the work function on the external field according to (35). Plotting the emission current  $I_e$  as a function of the anode voltage  $V_A$  in the region of small anode voltages gives what are known as the diode characteristics of the system. These characteristics, which are an important feature of electron emission, are shown in Fig. 14 for different temperatures of a cathode with a work function of about 1.4 eV. Three different ranges of these characteristics can be distinguished according to the magnitude of the anode voltage, the saturation range, the retarding field range and the space-charge range. A special equation is valid and must be derived for each of these three ranges. While the emission current increases slowly with increasing anode voltage under saturated conditions (on the right-hand side of Fig. 14), under retarding field conditions the logarithm of the current is represented by a steeply rising straight line (left-hand side of Fig. 14). The space-charge range, lying between the two former ones, becomes narrower with decreasing temperature and disappears entirely for sufficiently low temperatures where the emission current passes directly from the retarding field to the saturation range.

Before discussing the laws valid for the three different ranges we have to consider the potential distribution existing in the diode system if the electrodes are connected together, i.e. if no voltage is applied between them.

#### 4.1. Galvani and contact potential

Fig. 15 shows the variation of potential in the diode system for the simplest case in which the two electrode metals I and II have two plane parallel surfaces of infinite extent with the vacuum in between. When equilibrium has been reached, as many electrons must cross the junction between the two metals from metal I to metal II as cross in the opposite direction from metal II to metal I. This equilibrium is realized if the two Fermi levels,  $\zeta_1$  and  $\zeta_2$  have the same height, which implies a potential difference  $\bar{U}_{12} = \zeta_2 - \zeta_1$ , existing at the junction between the two metals. This potential difference is called the galvani potential.

The galvani potential is of little practical importance. The potential difference, however, which exists in the vacuum between the two points  $X$  and  $Y$ , delimiting the region of the image force in front of the metal surfaces, is important. This potential difference

is called the contact potential  $U_{12}$ . Its magnitude is, as can be seen directly from Fig. 15:

$$U_{12} = -(\psi_2 - \psi_1) = \psi_1 - \psi_2 \quad . . . . \quad (51)$$

The contact potential, so defined, always arises if the work functions of the two metals are different, and it is equal to the difference of the two work functions.

Equation (51) for the contact potential is exactly valid only in the case when the two electrodes have the same temperature. If the temperatures of the electrodes are different, additional thermo-voltages occur which add to the contact potential and which can be accounted for by a corresponding correction term in (51). The thermo-voltages of metals are, however, only of the order of some millivolts, while the contact potential normally has a value of some

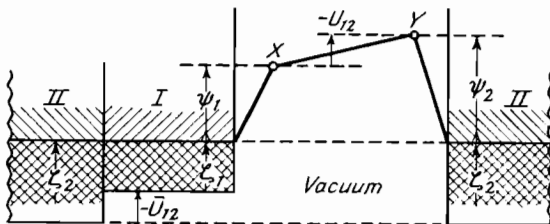


Fig. 15.—Potential Variation between two Directly Connected Metal Electrodes.

tenths of a volt or even of some volts. Consequently the thermo-voltage correction term may be neglected in most cases.

The contact potential, sometimes termed the volta potential, must not be confused with the potential resulting from the contact between metals and ionic conductors, which is also and more frequently called the volta potential or, alternatively, the standard electrode potential. There is no direct connection between this electrochemical phenomenon and the contact potential described above (Gysae and Wagener<sup>1</sup>). The experimental proofs for the validity of equation (51) relating contact potential and work function are discussed later on, when the methods for measuring the contact potential are dealt with (cf. Sec. 10).

The potential variations associated with the contact potential may be clearly visualized if each metal is again represented by a potential box. At  $T=0$  the two boxes representing the electrodes are filled with electrons up to a height  $\zeta_1$  and  $\zeta_2$  respectively. An equilibrium can only exist if the surfaces of the two boxes filled by electrons are at the same height. Hence the bottom of one box

must be higher than the bottom of the other by an amount equal to the galvani potential (cf. Fig. 15). The walls of the two boxes which bound the vacuum are then connected by a sloping plane, corresponding to the potential in the vacuum. The difference between the heights of the ends of this sloping plane corresponds to the value of the contact potential.

After this preparatory work the three ranges of the characteristics may be discussed in detail. According to the classification given above the emission current in these ranges will be called retarding field current, space-charge current, and saturated current respectively, and the equations for these different currents will be derived now.

#### 4.2. Equation for the retarding field current

As the electrons leave the cathode with definite velocities, distributed according to equation (41), they can travel some distance

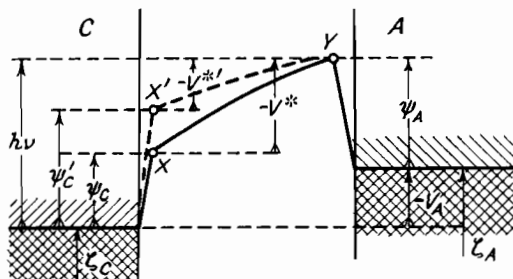


Fig. 16.—Variation of Potential in the Retarding Field Range.

against the opposition of a negative (retarding) potential applied between cathode and anode. Those electrons whose velocities are large enough will overcome the retarding field and reach the anode with a corresponding loss in velocity. The current, consisting of these electrons, is called retarding field current, and the potential distribution, existing between cathode and anode in this case, is shown in Fig. 16 (for two different work functions of the cathode  $\psi_C$  and  $\psi'_C$ ). If the potential distribution is described by means of potential boxes, the bottom of the box, representing the anode, must be lifted by an amount which is equal to the negative voltage  $V_A$  applied to the anode. Then the level of the limiting energy  $\zeta_A$  is also higher than the corresponding level  $\zeta_C$  of the cathode by an amount  $V_A$ .

The anode voltage  $V_A$  and all other voltages must take a negative sign in our potential diagram. This will be understood from the fact that a positive voltage increases the energy of the electrons and thus acts in the opposite manner to a potential barrier, having a positive sign in the diagram. On the other hand a negative voltage has the same effect as a potential barrier.

The electrons emerging from the cathode may again be visualized as rolling balls. In order to reach the anode, they must have sufficient energy to pass the point  $X$  at the rim of the cathode box and to run up the sloping plane towards the point  $Y$  in front of the anode. Only if this point  $Y$  is reached can the electrons fall over the rim of the anode box on to the surface of the anode, and so once more gain energy. The total potential difference which has to be overcome by the electrons when passing to the anode is equal to the difference between the potential of the point  $Y$  and the potential corresponding to the energy level  $\zeta_C$ . The value of this difference, which may be seen directly from Fig. 16, is equal to  $-|V_A| + \psi_A$ . If this total potential is put into the emission equation (47) instead of the work function  $\psi_C$ , the electron current passing to the anode, i.e. the retarding field current, is obtained:

$$I_r = A_0 S T^2 e^{(V_A - \psi_A)/kT} \quad \dots \quad (52)$$

Another way of representing the retarding field current can be found by introducing the effective voltage  $V^*$  which is applied between the two points  $X$  and  $Y$  (cf. Fig. 16):

$$V^* = V_A + U_{CA} \quad \dots \quad (53)$$

The contact potential in this equation may be replaced by the value  $U_{CA} = \psi_C - \psi_A$  from (51) and the work function of the cathode may be taken from the emission equation (47). Then

$$I_r = I_s e^{V^*/kT} = I_s e^{V^*/\omega} = I_s e^{11610 V^*/T} \quad \dots \quad (54)$$

The value of the retarding field current, as given by (54) for different temperatures and effective voltages, can be obtained from the nomographic chart in Fig. 17.

Plotting the logarithm of the retarding field current as a function of the voltage must give a straight line, according to both (52) and (54). On the other hand, the confirmation of such a linear dependence will be a proof that the electrons in vacuum have a Maxwellian distribution. This proof was given for example by Schottky<sup>4</sup> and Germer.<sup>1</sup>

It will be seen from equation (52) that the retarding field current

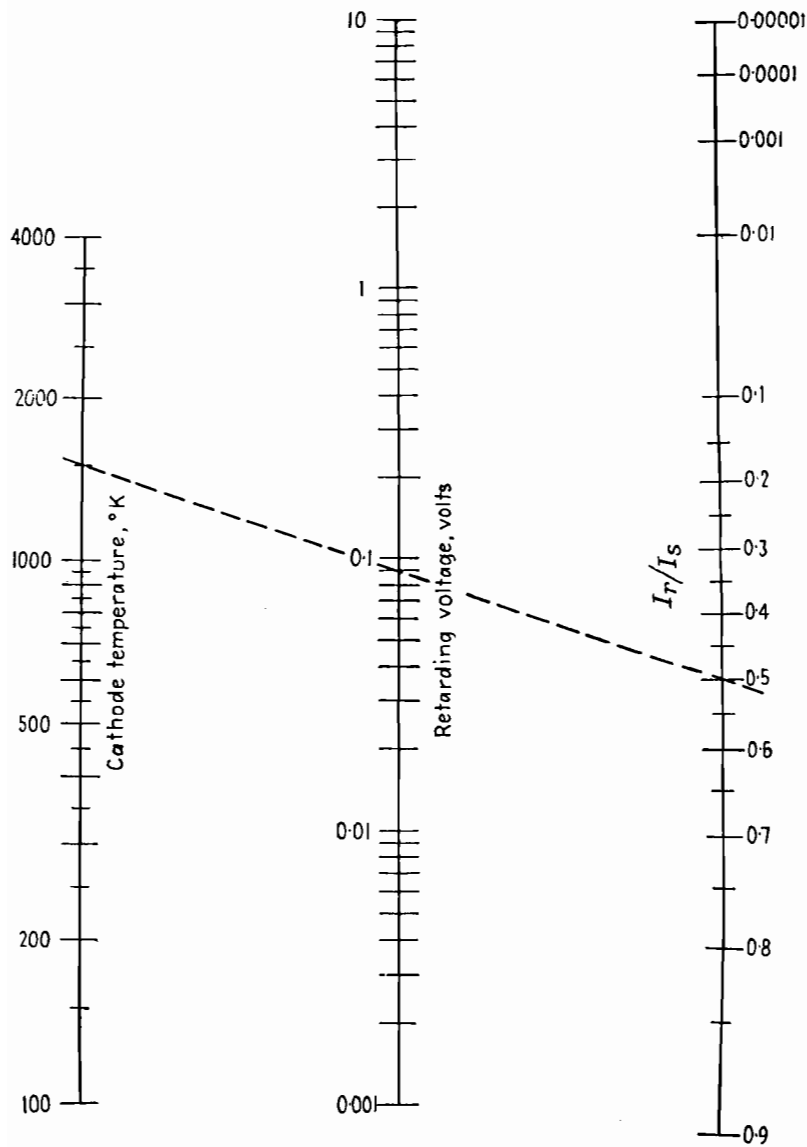


Fig. 17.—Nomographic Chart for Evaluation of the Retarding Field Current  $I_r$ .

only depends on the temperature of the cathode and on the voltage and work function of the anode, and that this current is independent of the work function of the cathode. This fact, which is clearly indicated in Fig. 16, was recognized by Davisson.<sup>1</sup>

The equations given above are only valid for plane, parallel electrodes. The calculation of the retarding field current in a system of coaxial cylindrical electrodes is more difficult, as in such a system the tangential component of the electron velocity has to be considered in addition to the normal component.

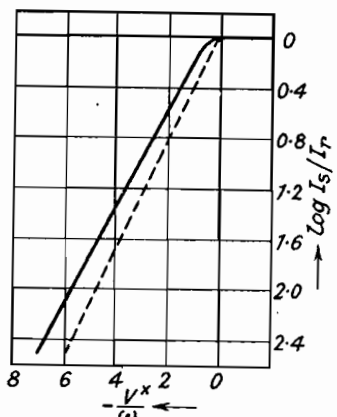


Fig. 18.—Calculated Retarding Field Current in a Cylindrical (full line) and a Plane Field (dashed line). (Rothe-Kleen, Vol. I, Fig. 5.)

The solution was given by Schottky,<sup>4</sup> who showed that the logarithmic plot of the retarding field current in a cylindrical system gives a straight line if the applied negative voltages are sufficiently high. This line is slightly shifted towards negative voltages compared with the line for the plane system. Fig. 18 shows a curve from which the retarding field current  $I_r$ , flowing in a cylindrical field may be determined as a function of the ratio  $V^*/\omega$ .

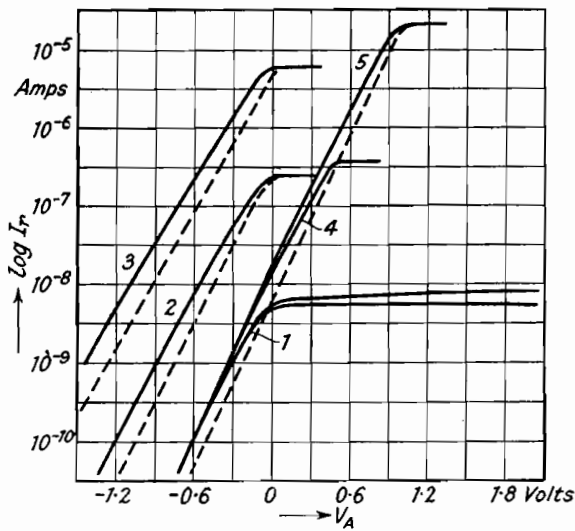


Fig. 19.—Theoretical Retarding Field Curves (Becker<sup>5</sup>).  
 (1, 2, 3) Pure Tungsten at Different Temperatures.  
 (4) Tungsten Thorium,  $\Delta\psi = 0.5$  eV } Same Temperatures as  
 (5) Tungsten Thorium,  $\Delta\psi = 1.0$  eV } with 1.

— Plane Field  
 - - - Cylindrical Field.

The retarding field current also is independent of the work function of the cathode in the cylindrical field as shown in Fig. 19, the full curves representing the cylindrical system and the dashed curves representing the plane system. The curves 1, 2 and 3 refer to pure tungsten at three different temperatures, while curves 4 and 5 refer to tungsten contaminated by thorium, the contaminated tungsten having a smaller work function than pure tungsten (cf. Sec. 5). The lower parts of the curves 1, 4 and 5 which have been obtained for the same temperature are identical in spite of the considerable differences in work function. Differences between these curves are only obtained if the retarding field current approaches the saturated current.

#### 4.3. Equation for the space-charge current

As the anode voltage becomes less negative, the number of electrons entering the interspace between cathode and anode

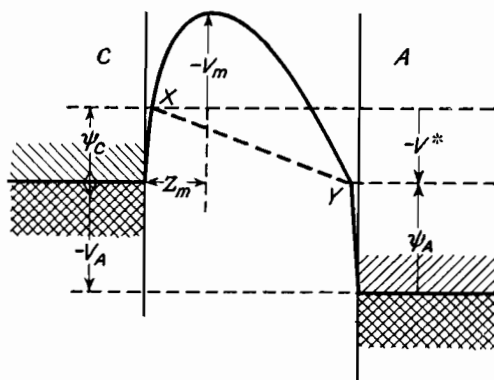


Fig. 20.—Variation of Potential in the Space-charge Range.

increases and finally a negative space-charge of detectable density is formed in front of the cathode. This space-charge causes an increase in potential in front of the cathode, adding to the potential barrier corresponding to the work function. The potential distribution thus resulting is plotted in Fig. 20 in the usual way, assuming that the anode voltage is now positive. The additional potential barrier produced by the space-charge (full line) is superimposed on the fall in potential which exists without space-charge (dashed line). If  $V_m$  denotes the height of the potential barrier due to space-charge, then the electrons emerging from the cathode have to overcome the total potential barrier  $\psi_c - V_m$  in order to reach

the anode. Only the faster electrons can do this, while the slower ones will overcome the work function, but will have to return to the cathode after having penetrated some distance into the vacuum.

The effect of the space-charge is, in fact, noticed at small negative anode voltages (from an effective voltage  $V^*$  of about  $-1$  volt). The electron current passing to the anode—now called space-charge current—will be smaller than that corresponding to equation (54) for the retarding field current. Therefore, the curve obtained in the logarithmic plot of the emission current deviates from the straight line representing the retarding field current, as shown by Fig. 14. The exact voltage at which the equation for the retarding field current becomes invalid can only be calculated approximately. Such approximate formulæ have been given by Schottky<sup>5</sup> and Moeller and Detels.<sup>1</sup> In a plane field the maximum current for which equation (52) or (54) is valid is:

$$j_{max} = 6 \times 10^{-10} T^{3/2} \frac{1}{d^2} \text{ amp./cm.}^2. \quad . . . \quad (55)$$

( $d$ =distance between cathode and anode in mm.). According to this equation the influence of the space-charge begins at  $10^{-5}$  amp./cm.<sup>2</sup> for the usual distances  $d$  of the order of 1 mm. If the cathode temperature is so low that the saturated current does not exceed  $10^{-5}$  amp./cm.<sup>2</sup>, the emission current passes directly from the region of the retarding field to that of the saturated current.

The existence of a space-charge and of the additional potential barrier due to space-charge has been proved experimentally by Wehnelt and Bley.<sup>1</sup> In these experiments an electron beam passing between cathode and anode was diverted by the space-charge.

The height  $V_m$  of the additional potential barrier is obtained if the space-charge current  $I_{sp}$  is considered as a retarding field current flowing against the voltage  $V_m$ . Accordingly  $V_m$  is derived from equation (54) for the retarding field current  $I_r = I_{sp}$  and for  $V^* = V_m$ :

$$V_m = \frac{kT}{e} \ln \frac{I_{sp}}{I_s} = -1.98 \times 10^{-4} T \log \frac{I_s}{I_{sp}} \quad . . . \quad (56)$$

The potential  $V_m$  is of the order of some tenths of a volt for the temperatures between  $1000^\circ$  and  $2000^\circ$  normally used.

The dependence of the space-charge current on anode voltage  $V_A$  can be calculated by means of Poisson's equation which, for a

co-ordinate  $z$  perpendicular to the surfaces of cathode and anode, may be written:

$$\frac{d^2V}{dz^2} = \frac{\rho}{\epsilon_0} \quad \dots \dots \dots \quad (57)$$

( $\rho$ =density of space-charge). The relation between the density  $\rho$  of the space-charge occurring in this equation and the space-charge current is given by the well-known equation:

$$I_{sp} = S \rho v \quad \dots \dots \dots \quad (58)$$

$v$  denoting the velocity of the electrons. The solution of the problem is relatively simple if the initial velocities of the electrons are neglected. Then:

$$\frac{1}{2}mv^2 = eV$$

and by means of (57) and (58):

$$\frac{d^2V}{dz^2} = \frac{\rho}{\epsilon_0} = \frac{I_{sp}}{S\epsilon_0 v} = \frac{I_{sp}}{S\epsilon_0 \sqrt{(2e/m)V}} \quad \dots \dots \quad (59)$$

This is a differential equation of the second order for the function  $V(z)$ . The boundary conditions are  $V(0)=0$  and  $\left(\frac{dV}{dz}\right)_{z=0}=0$ .

The second condition is obtained because the potential barrier due to space-charge is located directly at the cathode surface, if the initial velocities are neglected.

The differential equation above can be integrated twice without difficulty. The result is:

$$V^{3/4} = \left( \frac{9}{4\sqrt{2}\epsilon_0} \sqrt{\frac{m}{e}} \times \frac{I_{sp}}{S} \right)^{1/2} \times z$$

from which, for  $z$  equal to the distance  $d$  between cathode and anode the equation:

$$I_{sp} = \frac{4\sqrt{2}\epsilon_0}{9} \sqrt{\frac{e}{m}} S \frac{V_A^{3/2}}{d^2} = 0.233 S \frac{V_A^{3/2}}{d^2} \text{ mA} \quad \dots \quad (60)$$

is derived ( $S$  in  $\text{cm}^2$ ,  $d$  in  $\text{mm}$ ). This equation, according to which the space-charge current depends on the  $3/2$ th power of the anode voltage, is called Child's law. This law, only with other constants, is valid for every configuration of electrodes, e.g. cylindrical and spherical configurations (cf. Langmuir and Compton <sup>7</sup>).

As the initial velocities of the electrons are neglected in (60), this equation only gives a rough approximation. The exact calculation, making use of Maxwell's velocity distribution of the emerging

electrons, is more difficult and was carried out by Schottky,<sup>1, 2</sup> Epstein,<sup>1</sup> Fry,<sup>1</sup> and Langmuir.<sup>1</sup> Only the result of this calculation, which is obtained from the first two terms of a series development of an integral, can be given here. Let  $z_m$  denote the position of the maximum of the potential barrier due to space-charge (cf. Fig. 20). Then, if the effective voltage  $V^*$  defined by (53) is used, the space-charge current for plane electrodes is, with an error of  $2\frac{1}{2}\%$  for  $V^* - V_m > 1$  volt:

$$j_{sp} = \frac{I_{sp}}{S} = \frac{4\sqrt{2\epsilon_0}}{9} \sqrt{\frac{e}{m}} \times \frac{(V^* - V_m)^{3/2}}{(d - z_m)^2} + \left[ 1 + \frac{2.66}{\sqrt{[(e/kT)(V^* - V_m)]}} \right] \quad (61)$$

The term  $V^*$  in this equation is different from the anode voltage  $V_A$ , while  $V_m$  depends again on the space-charge current  $I_{sp}$  according to (56). If the values (53) and (51) for  $V^*$  and (56) for  $V_m$

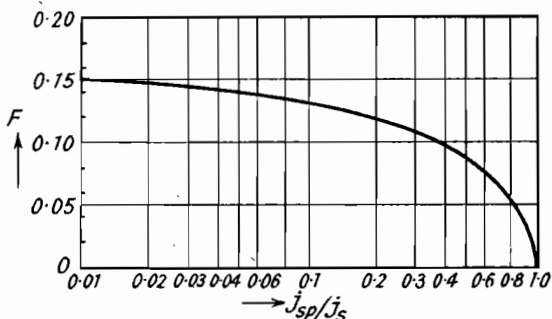


Fig. 21.—Factor  $F$ , necessary for Evaluation of the Distance between Cathode and Potential Barrier due to Space Charge.

are used and the work function  $\psi_C$  is calculated by means of equation (47):

$$V^* - V_m = V_A - \psi_A + \psi^*(T, j_{sp}) \dots \dots \quad (62)$$

with

$$\psi^*(T, j_{sp}) = \frac{kT}{e} \ln \frac{A_0 T^2}{(j_{sp}/1000)} = 0.198 \times \log \frac{1.2 \times 10^{11} (T/1000)^2}{j_{sp}} \quad (63)$$

( $j_{sp}$  in mA/cm.<sup>2</sup>). Furthermore, the distance  $z_m$  occurring in (61) is given by:

$$z_m = F(j_{sp}/j_s) \times \frac{(T/1000)^{3/4}}{\sqrt{j_{sp}}} \text{ mm.} \dots \dots \quad (64)$$

( $j_{ps}$  in mA/cm.<sup>2</sup>). In this equation the factor  $F$ , depending on the ratio of space-charge current to saturated current, can be taken from Fig. 21.

If the value of  $V^* - V_m$  in (62) is used, an equation better suited for a calculation of the space-charge current can be obtained from (61):

$$j_{sp} = 0.233 \left\{ \frac{(V_A - \psi_A + \psi^*)^{3/2}}{(d - z_m)^2} \left( 1 + \frac{\Delta}{100} \right) \right\} \text{mA/cm.}^2. \quad (65)$$

The value of the percentage increase:

$$\Delta = 78 \sqrt{\left( \frac{T/1000}{V_A - \psi_A + \psi^*} \right)} \% \quad . . . . \quad (66)$$

represents the increase of the space-charge current when the initial velocities are taken into account. In addition to this percentage

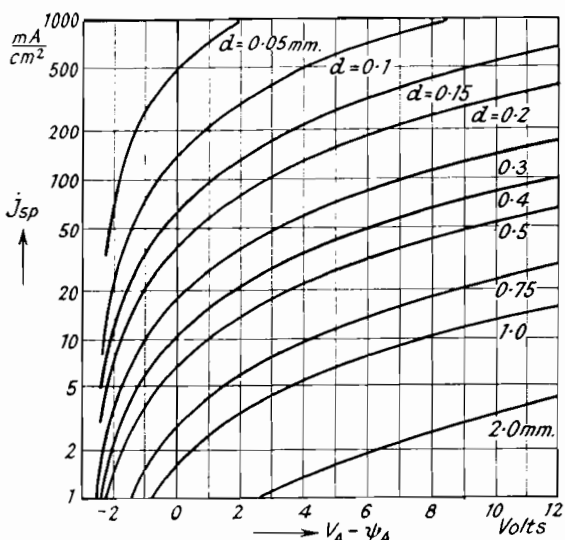


Fig. 22.—Density  $j_{sp}$  of Space-charge Current as a Function of the Difference  $V_A - \psi_A$  between Anode Voltage and Work Function of the Anode (Distance  $d$  between Cathode and Anode as Parameter) (Liebmann <sup>1</sup>).

increase there are two more differences between the approximate equation (60) and the more exact equation (65). The distance between cathode and anode is replaced by the distance between potential barrier and anode, and the anode voltage is replaced by the term (62) representing the effective potential difference between potential barrier and anode. We see by a comparison of equations (63) and (47) that the function  $\psi^*(T, j_{sp})$  represents the value of the work function of the cathode which would exist at the cathode, if the space-charge current were a saturated current. Hence the value of  $\psi^*$  may be determined easily by means of the curves in Fig. 12.

A chart allowing a general evaluation of equations (64)–(66) for the space charge current has been given by Ferris.<sup>1</sup>

For the special values  $T=1050^\circ\text{ K}$ . and  $j_s=1 \text{ amp./cm.}^2$  the space-charge current can be obtained from Fig. 22, as a function of the difference  $V_A - \psi_A$  between anode voltage and work function of the anode.

Comparisons between theoretical values of the space-charge current, based on (60) or (65), and experimental values were carried

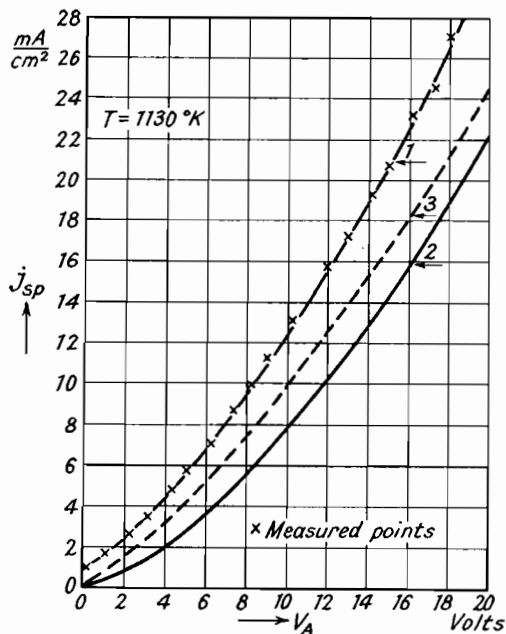


Fig. 23.—Comparison of Measured and Calculated Values of the Space-charge Current. 1. Calculated according to (65). 2. Calculated according to (60). 3. Calculated according to (65), the correction term  $A$  being neglected (Kleen<sup>1</sup>).

out by Kleen<sup>1</sup> and Ferris.<sup>1</sup> A good correspondence between the space-charge characteristic calculated by means of the exact formula (65) and the measured values was found. The values obtained from the approximate equation (60) gave considerable deviations (cf. Fig. 23).

The equation for the space-charge current in a cylindrical system is:

$$I_{sp} = 0.233 \frac{S}{Br_1 r_2} \{V_A - \psi_A + \psi^*(T, j_{sp})\}^{3/2} \text{ mA} \quad . \quad (67)$$

$r_1$  denoting the radius of the cathode,  $r_2$  that of the anode. In this equation a small correcting term has been neglected. The term  $B$  depending on  $r_2/r_1$ , has been calculated by Langmuir and Blodgett<sup>2</sup>; its value can be taken from Fig. 24. For  $1 \leq r_2/r_1 \leq 2$  it is approximately (with 10% maximum error):

$$B = \left(1 - \frac{r_1}{r_2}\right)^2$$

Then:

$$\frac{S}{Br_1 r_2} = \frac{S}{(r_2 - r_1)^2} \times \frac{r_2}{r_1} = \frac{S \cdot (r_2/r_1)}{d^2} \quad \dots \quad (67a)$$

$d$  again denoting the cathode-anode distance. In this special case, which holds for most indirectly heated cathodes, equation (67) changes into equation (60) valid for the plane system, the difference being that the surface area  $S$  of the cathode has to be replaced by the surface area  $S \times r_2/r_1$  of the anode.

In two publications by Page and Adams<sup>1,2</sup> another solution for the space-charge current in a cylindrical system has been given which is especially suitable for large values of  $r_2/r_1$ .

The dependence of the space-charge current on temperature according to equations (65) or (67) is chiefly determined by the function  $\psi^*(T, j_{sp})$ , while the influence of the factor  $\sqrt{T}$  in (66) and the temperature-dependence of  $z_m$  according to (64) may be neglected in practice. Hence, applying (63):

$$\begin{aligned} \left(\frac{\partial V_A}{\partial T}\right)_{j_{sp}=\text{const}} &= -\frac{\partial \psi^*}{\partial T} \\ &= 1.98 \times 10^{-4} \log \frac{1.2 \times 10^{11}(T/1000)^2}{j_{sp}} + 1.72 \times 10^{-4} \quad . \quad (68) \end{aligned}$$

For temperatures between  $800^\circ$  and  $1200^\circ$  K. and currents between 1 and 100 mA values for  $\partial \psi^*/\partial T$  between  $1.9 \times 10^{-3}$  and  $2.4 \times 10^{-3}$



Fig. 24.—The Constant  $B$  in Equation (67) for the Space-charge Current as Function of  $r_2/r_1$ .

are obtained. The space-charge characteristic therefore is shifted to negative voltages by about 0.2 volt for an increase in temperature of 100°. For the variation of the space-charge current with constant anode voltage the value:

$$\left(\frac{\partial j_{sp}}{\partial T}\right)_{V_A=const.} = - \left(\frac{\partial j_{sp}}{\partial V_A}\right)_{T=const.} \times \left(\frac{\partial V_A}{\partial T}\right)_{j_{sp}=const.} \simeq \frac{G_A}{S} \times \frac{\partial \psi^*}{\partial T}. \quad (69)$$

is derived,  $G_A$  denoting the anode conductance of the anode-cathode system.

Finally it will be interesting to consider if and by how much the space-charge current is influenced by the magnitude of the work function  $\psi_C$  of the cathode. As can be seen from equations (65) and (67), the work function does not directly occur in these equations. Apart from a special case to be discussed later on, the space-charge current will therefore not depend on the work function of the cathode. This fact, which was confirmed by an experiment of Gysae and Wagener,<sup>2</sup> may be visualized by considering the potential distribution between cathode and anode shown in Fig. 25. The total potential barrier in front of the cathode which must be overcome by the electrons has the value:

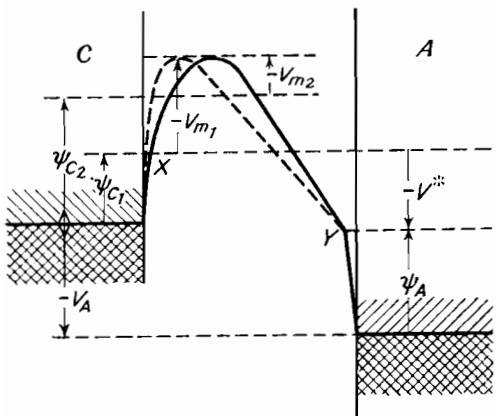


Fig. 25.—Variation of Potential in the Space-charge Range, assuming two Different Values for the Work Function of the Cathode.

according to equations (47), (56), and (63), and is therefore independent of the work function of the cathode. This independence can be explained in the following manner. If the work function of the cathode is decreased, more electrons will emerge from the surface of the cathode, but these electrons increase the space-charge, and hence the height of the potential barrier due to space-charge, by an amount which exactly compensates for the decrease of the

$$\psi_C - V_m = \frac{kT}{e} \ln \frac{A_0 ST^2}{I_{sp}} = \psi^*(T, j_{sp}) \dots \quad (70)$$

work function. Consequently the current passing the potential barrier remains the same in spite of the increased number of electrons emerging from the cathode.

The influence of the distance  $z_m$ , between potential barrier and cathode surface, on the magnitude of the space-charge current has not been considered yet.  $z_m$  may have relatively large values for small space-charge currents; for example, for  $j_{sp}=1$  mA/cm.<sup>2</sup>,  $T=1000^\circ$  K. and  $I_s \geq 100 I_{sp}$ ,  $z_m=0.15$  mm. Because of the factor  $F$  in equation (64)  $z_m$  depends on the saturated current  $I_s$  and therefore on the work function of the cathode. Consequently  $z_m$  increases with decreasing work function. Considerable variations of  $z_m$  (more than 10%) only occur, however, if the saturated current is smaller than ten times the space-charge current. In this case alone, provided the distance  $d$  between cathode and anode is small (<1 mm.), can the magnitude of the denominator of equation (65), and consequently the magnitude of the space-charge current, be influenced by variations of the work function of the cathode.

Apart from this special case the position of the (retarding field and space-charge current) characteristic in a diode system with unvarying emitting surface is determined solely by the configuration of the system, by the temperature of the cathode, and by the work function of the anode.

If the valve system contains one or several grids in addition to the anode, the equivalent voltage resulting from the anode and grid voltages has to be introduced into the equations for the characteristics given above, in place of the anode voltage.\* In this case the statements relating to the influence of the anode work function refer to a mean value of the work functions of the anode and the grids which has to be determined in the same way as the equivalent voltage. The details may be obtained from the appropriate sources.†

Finally it may be pointed out that the formulæ given for both the retarding field and the space-charge current are only valid on the supposition that the cathode has a uniform temperature and that there is no potential drop along the cathode due to heater current, i.e. that the cathode is indirectly heated. If these two suppositions

\* Cf. K. R. Spangenberg, *Vacuum tubes*, MacGraw-Hill Comp., 1948; or H. Rothe, W. Kleen, *Grundlagen und Kennlinien der Elektronenröhren* (*Fundamentals and Characteristics of Electronic Valves*), Leipzig, 1948.

† An exception to the rule stating that the characteristic is independent of the cathode work function is obtained in the case of valves with grids if the retarding field current flowing to anode or positive outer grids is considered (Adam<sup>1</sup>).

are not fulfilled, the real characteristic is obtained by a superposition of a series of characteristics, valid for the different temperatures and voltages of the discrete parts of the cathode. If this is done the real characteristics no longer have the simple shape resulting from the equations given above.

#### 4.4. Equation for the saturated current

Proceeding to higher anode voltages, we come to the saturation range, in which the potential barrier due to space-charge disappears and all electrons emerging from the cathode surface reach the anode. As can be seen from Fig. 14, the characteristic passes into the saturated current region gradually without any marked discontinuity. The increase of the current with increasing anode voltage becomes less, but a slight increase remains, even when the space-charge has disappeared, owing to the dependence of the work function on the external field according to equation (35).

If the conditions in the saturation range are also described by means of potential boxes, the dependence of the saturated current on the external field may be visualized in the following manner (cf. Fig. 26). With increasing external field (or anode voltage) the rim of the potential box representing the cathode will be bent down more and more. Consequently the rolling balls, representing the electrons, will need a lower minimum velocity to reach the rim and will thus arrive at the rim in larger numbers. This increased number of balls will all roll towards the anode over the sloping plane representing the external field. The potential distribution in the saturation range may be compared with the corresponding distributions in the other ranges by comparing Fig. 26 with the Figs. 15, 16, 20, and 25.

The numerical relation between saturated current and anode voltage is obtained by introducing the value (35) for the work function into the emission equation (47). The saturated current flowing with external field strength zero may be denoted by  $I_s^{(o)}$  although it cannot be measured directly. Then for plane electrodes and with  $E_e = V_A/d$  the saturated current  $I_s$  flowing with anode voltage  $V_A$  is:

$$I_s = I_s^{(o)} e^{(e/kT) \times 3.78 \times 10^{-5} \sqrt{V_A/d}} \\ \log I_s = \log I_s^{(o)} + \frac{6.0}{T\sqrt{d}} \sqrt{V_A} \quad . . . . \quad (71)$$

( $d$  in mm.).

According to this equation, formulated by Schottky<sup>3</sup> and therefore called the Schottky law, the logarithm of the saturated current plotted as a function of the square root of the anode voltage gives a straight line, the Schottky line. An exact experimental check of this equation is difficult, as the ideal conditions of perfectly plane surfaces assumed for the derivation of the equation do not exist in reality. As the surface of the cathode is always rough to a certain

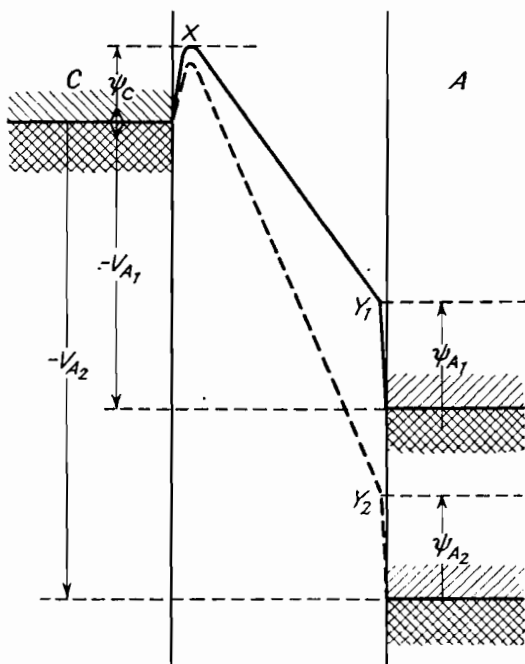


Fig. 26.—Variation of Potential in the Saturation Range for two different Work Functions of the Cathode.

degree, there are regions in which the field strength is larger than the value  $dV/dz$  calculated from the applied anode voltage and the geometric configuration. Because of this influence of the roughness, which cannot be calculated exactly, the saturated current obtained in experiments will always be larger than the current calculated from (71). In addition to this, the fact that the work function is not the same over all regions of the surface area must be taken into consideration, for differences in work function also produce deviations from Schottky's law (cf. Sec. 6).

For tungsten Schottky obtained a correspondence to within 20%

between measured and calculated saturated currents, if the anode voltages were more than 100 volt (corresponding to a field strength of about 10,000 volt/cm.). The result obtained by Nottingham<sup>1</sup> shown in Fig. 27 is similar. In this case also deviations from the law are obtained for smaller field strengths which are chiefly due to the differences in work function over the surface as discussed above. With higher field strengths the measured values in a logarithmic plot show the linear dependence demanded by equation (71).

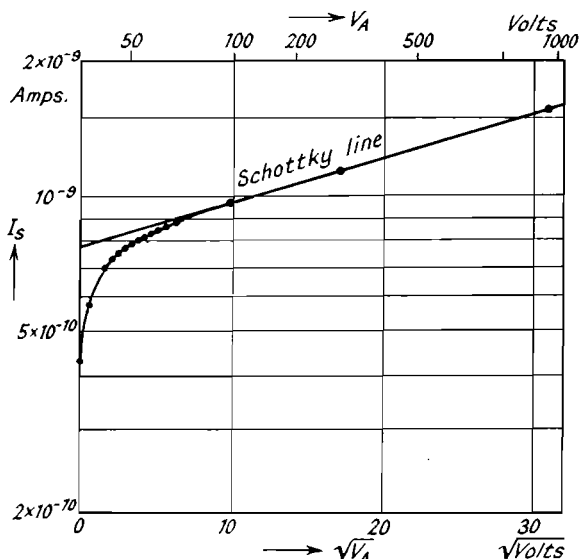


Fig. 27.—Measured and Calculated Values of the Saturated Current as a Function of Anode Voltage ( $T=1434^\circ\text{ K.}$ ) (Nottingham<sup>1</sup>).

An additional effect is observed with field strengths of more than  $5 \times 10^4$  volt/cm. According to Seifert and Phipps,<sup>1</sup> Turnbull and Phipps,<sup>1</sup> Mott-Smith<sup>1</sup> and Guth and Mullin,<sup>1, 2</sup> deviations from the Schottky line are then obtained which are periodic in  $\sqrt{E_e}$  or  $\sqrt{V_A}$  and which are explained by reflection of the electron waves associated with the emitted electrons at the potential barrier in front of the cathode.

Finally it may be mentioned that an entirely new effect, the so-called tunnel effect of wave mechanics, occurs with very high field strengths. In this case the potential barrier in front of the cathode becomes so narrow that the electrons can pass through unimpeded. Consequently with these very high field strengths there is electron

emission even at room temperatures, termed either cold emission or field emission.

The potential distribution in the three ranges of the characteristics discussed above may be characterized in the following manner:

In the retarding field range (cf. Fig. 16) the height of the total potential barrier to be overcome by the electrons is equal to the difference between the work function of the anode  $\psi_A$  and the anode voltage  $V_A$  (having due regard to sign).

In the space-charge range (cf. Fig. 20) the height is equal to a value which is obtained from equation (70) and which only depends on the temperature  $T$  of the cathode and on the magnitude of the space-charge current  $I_{sp}$ .

In the saturation range (cf. Fig. 26) the height is equal to that given by equation (35), its magnitude being determined only by the work function of the cathode for zero external field and by the external field strength.

The maximum of the potential barrier lies closely in front of the surface of the anode under retarding field conditions, at about  $10^{-5}$  to  $10^{-6}$  cm. distance from the surface of the cathode under saturation conditions, while it may occupy any point of the anode-cathode region under space-charge conditions.

## 5. The Influence of Adsorbed Foreign Materials on Electron Emission from Metals

### 5.1. Influence of foreign materials on the work function

The emission properties of a pure metal are considerably changed if atoms or ions of any other material are adsorbed at the emitting surface of the metal. The phenomena occurring are of technical importance, as the emission current can be greatly increased and the heater power which is necessary for obtaining a certain emission can be as much decreased by a suitable selection of the foreign material. Adsorption is also important in the case of the oxide-coated cathode, and it will therefore be necessary to discuss some of the details, especially the physics of the adsorption process, which is essential for clearly understanding the effect of adsorption on emission.

Adsorption at metal surfaces may take place in different ways, and these will be discussed first:

(a) *Adsorption of ions.*—If an ion—assumed to be charged positively—is near a metal surface it will be attracted by an image

force in the same way as an electron (cf. Sec. 2). Image force attraction may again be visualized by a potential curve. For convenience the sign of the potential in this curve will be chosen opposite to that used in the case of the electron. A reduction in the energy of the ion as it approaches the metal surface will then

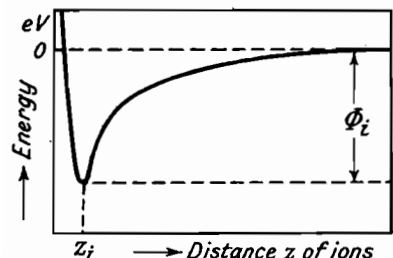


Fig. 28.—Potential Curve for the Adsorption of an Ion at a Metal Surface (J. H. de Boer, *Electron Emission and Adsorption Phenomena*, 1935).

minimum distance  $z_i$  between ion and metal surface. The adsorption energy set free during the process is then obtained from equation (27) for the image force potential and, for a single charged ion, is:

$$\Phi_i = \frac{e^2}{4\pi\epsilon_0 \times 4z_i} = \frac{3.6 \times 10^{-10}}{z_i} \text{ eV. . . . . (72)}$$

(b) *Adsorption of dipoles.* In this case distinction has to be made between permanent and induced dipoles. Permanent dipoles can only consist of molecules, for in an undisturbed atom the centres of gravity of positive and negative charges are the same, lying together in the nucleus, and the formation of a dipole is therefore not possible. Induced dipoles are more important. They are produced by an inducing electrical field which removes the electrons of the clouds, together with their centre of gravity, from their normal places. In the latter case the induced dipole moment  $M$  is determined by the field strength  $E$  by using a proportionality factor called polarization constant:

$$M = \alpha E \quad . . . . . (73)$$

(c) *Adsorption by van der Waal's forces.* If an atom is not ionized and if there is no electrical field to induce a dipole, the atom can nevertheless be adsorbed by means of van der Waals' forces, acting between normal atoms. These van der Waals' forces result from the continually varying field of the electrons of the one atom

producing a continually varying dipole in the other atom. The interaction between the two dipoles thus produced gives, as a mean value, an attractive force between the two atoms in spite of the average complete electrical symmetry.

Considering the last two cases of adsorption by dipoles and adsorption by van der Waals' forces, potential curves may be plotted in the same way as for the adsorption of ions, provided the potential energy of the adsorbed atom, expressed in electron-volts, is plotted as a function of the distance from the metal surface.

The adsorption of ions and dipoles always produces an electrical double layer at the surface of the metal. In the first case this double layer consists of adsorbed ions on the one side and of charges induced in the metal on the other side, while in the second case the double layer is formed by the adsorbed dipoles themselves. The effect of such a double layer on the work function of the metal concerned can be determined. Let  $M$  denote the dipole moment and  $s$  the surface density of the dipoles, i.e. their number per  $\text{cm}^2$ . Then the electric double layer gives a jump in potential the magnitude of which is:

$$\Delta V = \frac{1}{\epsilon_0} s |M| \quad \dots \dots \dots \quad (74)$$

(cf. Fig. 29).

If adsorption of dipoles is considered, the dipole moment results from (73). In case of adsorption of ions, however, the fact that the charges induced by these ions lie in the interior of the metal must be taken into account. As a potential difference cannot exist in the interior of the metal, only those parts of the dipoles, of length  $z_i$ , lying outside the metal will be effective.

It is quite clear that the work function of the metal concerned is changed by the amount  $\Delta V$ . The work function is decreased if the positive pole of the double layer is directed to the outside, while it is increased if the negative pole is outside. If the work function of the pure metal is denoted by  $\psi_M$  and the work function of the metal plus double layer by  $\psi_{M-Dip}$  then according to (74):

$$\psi_{M-Dip} = \psi_M - \frac{1}{\epsilon_0} s |M| \quad \dots \dots \dots \quad (75)$$

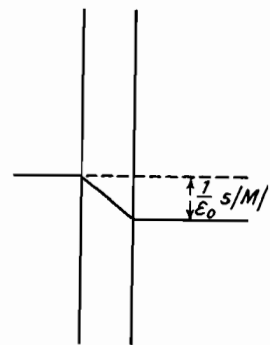


Fig. 29.—The Potential Jump produced by an Electric Double Layer.

We shall now consider in detail some different types of cathodes having such an adsorbed film consisting of foreign material. Tungsten is mainly used as a basic material for all these atomic film cathodes, as it can be heated to the highest temperatures and can consequently be most efficiently cleaned from other undesirable contaminations. The atomic film cathodes will be denoted by a symbol M-A, the chemical symbol of the basic material being given first and the symbol of the material of the adsorbed film second.

## 5.2. Adsorption of cæsium (W-Cs)

The first experiments with this film cathode, the one on which most investigations have been made, were carried out by Langmuir and Kingdon.<sup>4, 5</sup> They measured the emission of a tungsten wire in a valve containing a certain quantity of cæsium. As the vapour pressure of cæsium at room temperature is about  $5 \times 10^{-6}$  mm. mercury, a detectable quantity of cæsium vapour will be present in such a valve. Langmuir and Kingdon<sup>5</sup> measured a maximum emission current of the tungsten wire of  $8.8 \times 10^{-5}$  amp./cm.<sup>2</sup> for a temperature of the wire of 690° K. and a temperature of the valve of 30° C. In contradiction to this the corresponding saturated current of pure tungsten in a high vacuum is calculated from the emission equation as  $3.6 \times 10^{-26}$  amp./cm.<sup>2</sup>. Hence the emission of the tungsten wire has been increased by the very considerable factor  $10^{21}$  by the cæsium vapour present in the valve.

If the emission of this W-Cs cathode is measured as a function of the temperature of the cathode at sufficiently low temperatures, an increase of emission according to Richardson's equation (47) is found, giving a nearly straight line in the logarithmic plot of emission as a function of  $1/T$  owing to the exponential function in (47) (cf. Fig. 30).

If, however, the temperature of the cathode is increased to a certain value depending on the vapour pressure and therefore on the temperature of the valve, the curve bends, reaches a maximum, and subsequently drops suddenly until the emission of pure tungsten is reached. The work function of the W-Cs cathode was determined by Langmuir and Kingdon from the straight rise on the right-hand side in Fig. 30 (cf. Sec. 8). The value obtained was 1.38 eV, which means that the work function of pure tungsten (4.54 eV) has been decreased by about 3.2 eV, and that a very large increase in emission has been produced in this way. Langmuir

and Kingdon explained the observed decrease of the work function by assuming an electrical double layer on the tungsten surface consisting of adsorbed caesium ions as discussed above. The adsorbed ions evaporate from the cathode at higher temperatures,

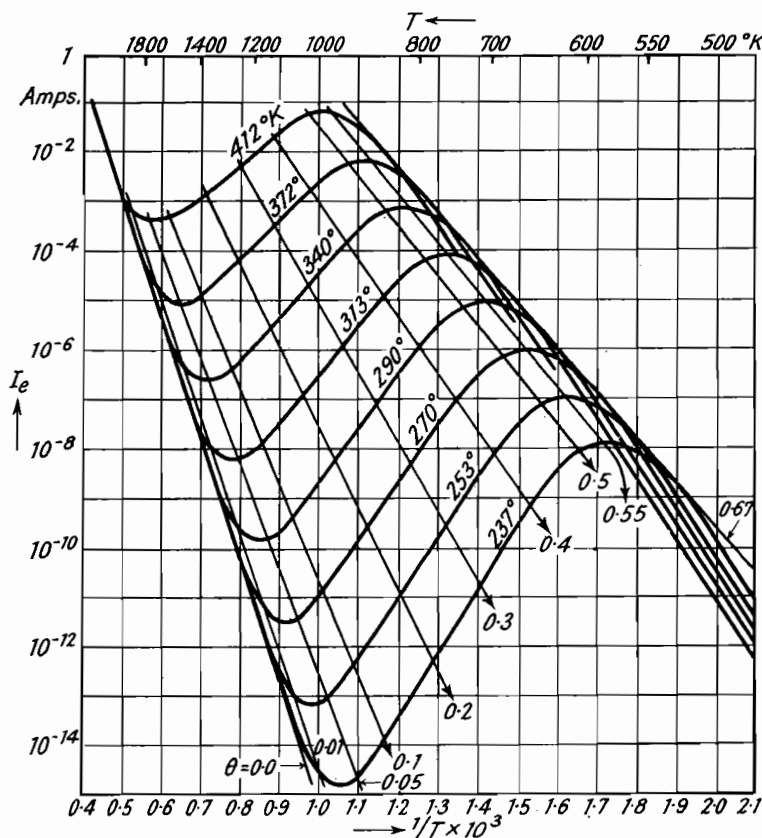


Fig. 30.—Electron Emission of the W-Cs Cathode as a Function of Temperature (Temperature of the Valve as Parameter) (Langmuir and Taylor<sup>8</sup>).

thus producing the deviation from the straight line and the final decrease of the emission with increasing temperature.

The origin of the ions may be explained by realizing that the caesium has an ionization voltage of  $\xi_{Cs} = 3.88$  eV, which is 0.66 eV lower than the work function of pure tungsten (4.54 eV, cf. Table V). If, therefore, a caesium atom is near a tungsten surface an energy of 3.88 eV is necessary for its ionization, while, on the other hand, an energy of 4.54 eV, corresponding to the work function of tungsten,

is set free, when the electron resulting from the ionization enters the tungsten. Thus an energy of  $\psi_w - \xi_{Cs} = 0.66$  eV is gained during the total process, which is therefore possible without any supply of energy from outside. The proof that ions are in fact adsorbed at the tungsten surface was given, by applying a negative voltage to the anode of the valve and by detecting a current of positive ions evaporating from the tungsten cathode.

These investigations were completed by experiments of Becker,<sup>1</sup> who examined the relation between the emission current and the

fraction  $\theta$  of the tungsten surface covered by caesium. The tungsten cathode was at first cleaned by heating it to a high temperature, and then an activation curve was taken by measuring the emission current as a function of time at a definite temperature of the cathode. The result of such measurements is shown in Fig. 31 with the cathode temperature as parameter. At low temperatures (up to 625° K.) when the caesium atoms impinging upon the tungsten do not re-evaporate, a maximum emission is reached in a certain time  $t_m$  which is independent of the magnitude of the temperature.

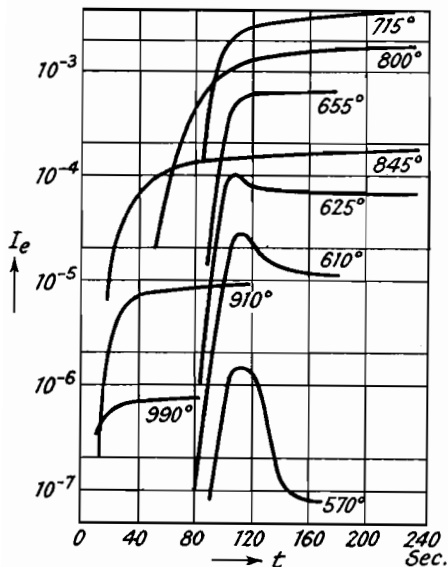


Fig. 31.—Activation of a W-Cs Cathode (Cathode Temperature as Parameter) (Becker<sup>1</sup>).

temperature. The time  $t_m$  only depends on the value of the vapour pressure  $p$  of the caesium, the product  $p \times t_m$  being constant according to Becker's measurements. As the number of the impinging caesium atoms is proportional to  $p$ , this result means that the maximum of the emission is reached at a definite density of caesium atoms on the surface, this density being independent of the temperature. Let  $\theta_m$  denote the fraction of the surface covered with caesium for maximum emission, then for smaller fractions

$$\frac{\theta}{\theta_m} = \frac{t}{t_m}$$

By means of this relation the emission and the decrease in work

function can be plotted as a function of  $\theta/\theta_m$  (cf. Fig. 32). A maximum variation of the work function is obtained for  $\theta=\theta_m$ , and a decrease of the variation for  $\theta>\theta_m$ , the value of  $\theta_m$  being so far unknown.

More detailed ideas of the mechanism of the W-Cs cathode were given by Langmuir and Taylor<sup>8</sup> and de Boer and Veenemans.<sup>1, 2, 3, 4</sup> The latter authors specially examined the variation of potential in front of the cathode surface during the adsorption of the caesium ions (cf. Fig. 27). As these investigations are beyond the scope of this work, they cannot be dealt with here. It may be pointed out that according to these investigations only that part of the caesium which is first deposited is adsorbed as ions, while the rest is adsorbed as uncharged atoms. If the methods developed by Langmuir and Taylor and de Boer and Veenemans are applied, the value of the covering fraction  $\theta_m$  corresponding to maximum emission can be calculated. For the W-Cs cathode a value of  $\theta_m=0.67$  is obtained, from which it is seen that two-thirds of the total tungsten surface is covered with caesium at maximum emission.

In an investigation of Stran-sky and Suhrmann<sup>2</sup> it is assumed that the Cs is adsorbed as atoms only, but an experimental decision between this new idea and the idea of adsorption mainly by ions generally accepted before, is still outstanding.

### 5.3. Adsorption of barium (W-Ba)

This type of atomic film cathode is obtained by evaporating barium from some source in the experimental valve (e.g. a barium getter) on to a previously cleaned tungsten wire. Such a cathode was experimentally examined by Becker,<sup>3, 4</sup> and the phenomena observed are mainly the same as for W-Cs. Fig. 33 shows the emission current of the W-Ba cathode as a function of the fraction  $\theta$ , covered with barium, for  $T=1100^\circ\text{K}$ . (The ratio of the emission current of W-Ba and of pure W has been plotted.)

As barium can be either singly or doubly ionized it has to be decided whether the single or the double-charged ion is adsorbed

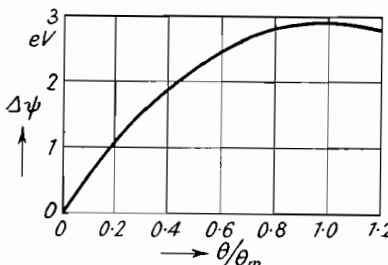


Fig. 32.—Variation  $\Delta\psi$  of the Work Function of a W-Cs Cathode as a Function of the Fraction  $\theta$  covered with Cæsium (Langmuir and Taylor<sup>8</sup>).

at the tungsten surface. This question can be answered by means of calculations based on potential curves similar to those of Fig. 28. The result of such calculations, the details of which cannot be given here, shows that barium is adsorbed as a double-charged ion, in the initial stage of adsorption. Furthermore, the relative density of the barium on tungsten corresponding to maximum emission is obtained as  $\theta_m = 0.29$  in a similar manner as in the case of the W-Cs cathode.\*

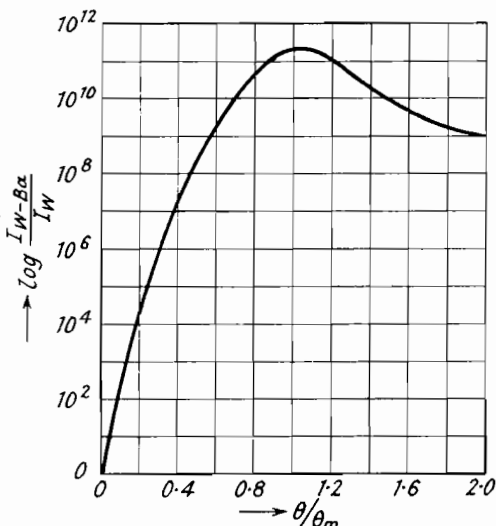


Fig. 33.—Emission Current of a W-Ba Cathode as a Function of the Fraction  $\theta$  covered with Barium (Becker<sup>4</sup>).

#### 5.4. Adsorption of thorium (W-Th)

This type of cathode was first investigated by Langmuir,<sup>3</sup> when examining tungsten wires containing about 1% ThO<sub>2</sub> which are used for the manufacture of incandescent lamps owing to their superior recrystallization properties. The ThO<sub>2</sub> is reduced to thorium by the tungsten at temperatures above 2600° K. The thorium, thus produced, diffuses to the surface and forms there a dipole layer which decreases the work function. The cathodes obtained in this way are of considerable technical importance. Contrary to the case of the W-Ba cathode, the thorium when evaporated can be replaced by diffusion and the cathode can thus

\* Cf. J. H. de Boer, *Electron Emission and Adsorption Phenomena*, 1935, pp. 100–104.

be regenerated. In addition to this the emission of the W-Th cathode is not influenced by variations of the vapour pressure and of the temperature of the valve, as is, for example, the W-Cs cathode.

The mechanism of the emission of the W-Th cathode is exactly the same as that of the W-Cs and the W-Ba cathodes. This can be seen from experiments of Brattain and Becker,<sup>1</sup> who evaporated the thorium from a wire containing thorium on to a second wire which was at first completely pure. In this way a thorium film was produced on the second wire, and its emission was measured as a function of the relative density  $\theta$  of the thorium. Fig. 34 shows the result of the experiments. Apart from the absolute values, the relation between emission current and density is the same as for the W-Ba cathode (cf. Fig. 33). It may be concluded from this that the mechanism of the emission is the same for both cathodes. The final value of the emission current of W-Th obtained for large values of  $\theta/\theta_m$  is the same as the emission current measured for pure thorium metal.

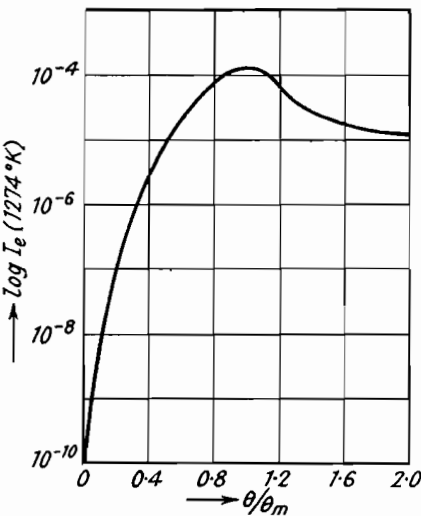


Fig. 34.—Electron Emission of the W-Th Cathode as a Function of the Fraction  $\theta$ , covered with Th (Brattain and Becker<sup>1</sup>).

## 5.5. Adsorption of oxygen (W-O)

Adsorption of oxygen is obtained by exposing the cathode to an atmosphere of oxygen. As oxygen preferably forms negative ions, such negative ions will be adsorbed at the metal surface establishing a dipole layer with a dipole moment the negative pole of which is directed outwards, contrary to the cases considered before. Hence the work function of the metal is increased in this case and the emission decreased correspondingly; the cathode is poisoned by the oxygen. The processes occurring during the adsorption of the oxygen atoms have been discussed in detail by Vervey and de Boer.<sup>1</sup> For chemical reasons they assume that a surface oxide is formed

during this adsorption. The surface oxide consists of a monomolecular layer of metal oxide molecules, forming permanent dipoles, the negative poles of which are directed outwards as mentioned above (cf. Fig. 35).

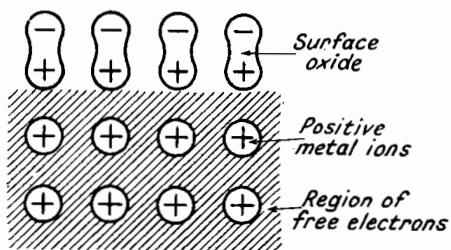


Fig. 35.—Formation of a Surface Oxide on a Metal Surface (J. H. de Boer, *Elektronen emission und Adsorptions erscheinungen* (1937)).

## 5.6. Adsorption of several materials (W-O-Cs, W-O-Ba, W-Ba-O)

When examining the emission of a tungsten wire in caesium vapour, the emission may be increased by using a tungsten wire previously poisoned with oxygen instead of the pure tungsten. This phenomenon was observed first by Langmuir and Kingdon.<sup>5, 6</sup> The tungsten wire in their experiments was first exposed to oxygen, and then caesium was adsorbed in the same manner as discussed under subsection 2. If the wire was then heated at a temperature of 1600° K. for a short time a considerable increase of the emission was observed, giving up to  $10^6$  times the emission current of a normal W-Cs cathode. Thus by the adsorption of both oxygen and caesium on tungsten a new type of cathode is obtained which has a work function still lower than that of the pure W-Cs cathode, and which will be denoted by the symbol W-O-Cs. Apart from the absolute magnitudes the emission of this W-O-Cs cathode depends on the temperature of the cathode and on the vapour pressure of the caesium in quite the same way as does the emission of the pure W-Cs cathode. Emission values of W-O-Cs are shown in Fig. 36 as a function of temperature and are compared there with the emission of the other types of cathodes discussed before.

In order to explain the mechanism of the W-O-Cs cathode, de Boer\* assumed that the heating of the cathode carried out at 1600° produces the distribution of the adsorbed Cs-ions which is

\* J. H. de Boer, *Electron Emission and Adsorption Phenomena*, 1935, pp. 156–158.

shown in Fig. 37. According to this the Cs-ions are deposited beside the metal oxide dipoles and are thus more tightly bound than

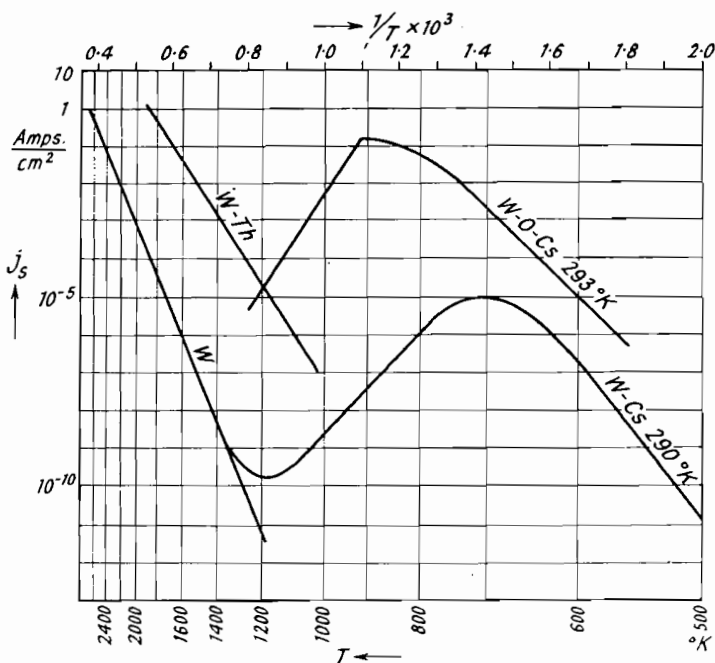


Fig. 36.—Electron Emission of different Atomic Film Cathodes as a Function of Temperature.

by simple adsorption at the pure metal surface in the case of the W-Cs cathode. The energy of adsorption therefore is larger than in the case of the W-Cs cathode, and more Cs-ions can be adsorbed than on pure tungsten, a lower work function being thereby produced.

Because of the stronger binding between the Cs-ions and the oxide dipoles, the evaporation of these ions is less than from pure W-Cs, and consequently higher temperatures can be reached without decreasing the optimum density of the ions (cf. Fig. 36). As measured by Langmuir and Kingdon,<sup>5</sup> the maximum emission

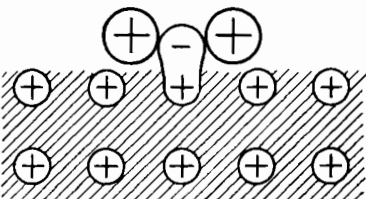


Fig. 37.—Arrangement of the Cs-ions on the Surface of a W-O-Cs Cathode (J. H. de Boer, *Elektronen emission und Adsorptionserscheinungen*, 1937).

current of W-O-Cs occurs at a temperature of  $1000^{\circ}$  K., the value of the current being  $0.35$  amp./cm.<sup>2</sup> (valve temperature  $30^{\circ}$  C.). The maximum emission of W-Cs (cf. p. 50) is thus increased by a factor  $4 \times 10^3$  by the additional adsorption of oxygen.

Barium can also be adsorbed together with oxygen, and an increase of the emission of the pure W-Ba cathode can thus be obtained, according to Ryde and Harris.\* The phenomena observed in this case change considerably if the cathode is exposed to oxygen not before but after depositing the barium, a decrease of the emission instead of an increase being then obtained. Obviously the oxygen ions are then deposited on top of the barium ions previously adsorbed, and the work function of the W-Ba cathode is increased by the negative dipole moment of the oxygen layer on top. Such a cathode is denoted by the symbol W-Ba-O. Similar phenomena may also be observed with W-Cs (for the work function of these cathodes cf. Table VII).

Concluding this section, we may state that the work function of atomic film cathodes such as W-Ba, W-Cs, etc., can be both decreased and increased by the adsorption of oxygen, and that the position of the oxygen relative to the other adsorbed material is decisive in determining the effect.

## 6. The Surface Fields and their Influence on the Work Function

It has been tacitly assumed in the previous section that the foreign atoms which are absorbed on an atomic film cathode exist in the same density over all parts of the surface. This assumption, however, is refuted by some well-known investigations which have been carried out by means of the electron microscope. The electron images obtained in the electron microscope give an exact magnified picture of the distribution of the electron emission over the surface of the cathode. The brightness of each area in the image is a measure of the intensity of the emission in the corresponding area of the cathode surface. Fig. 38 shows some of these images which were taken by Brueche and Mahl<sup>1</sup> during the activation of a W-Th cathode. One sees from these images that the emission is limited to small emission patches in the early stages of activation, and that these patches spread over the surface as the activation proceeds. Obviously the thorium moves from these patches over

\* Cf. A. L. Reimann, *Thermionic Emission*, 1934, p. 159.

the surface until the whole surface is covered by thorium and emits nearly uniformly when the activation is finished. A similar movement of the activating material on the surface of the basic metal can be observed with barium on tungsten according to Becker and Moore.<sup>7</sup>

The differences in emission observed in the electron images can be explained by assuming that the density of the adsorbed atoms or ions (either the absolute density  $s$  or the relative density  $\theta$ ) varies

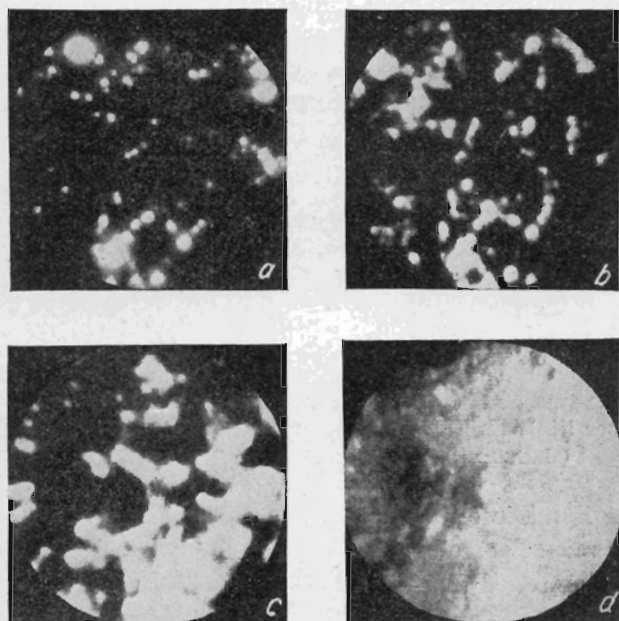


Fig. 38.—Electron Images of a W-Th Cathode, taken at different Stages of Activation (Brueche and Mahl).

over the surface of the cathode and is a function  $s(x, y)$  or  $\theta(x, y)$  of the co-ordinates on this surface. This assumption must be made for all atomic film cathodes, as can be seen from the electron images in Figs. 39 and 40 showing the distribution of the emission of a Ni-Cs and a Ni-Ba cathode.

The considerations of the previous section, assuming a constant density  $\theta$  over the entire surface, are therefore only valid for small areas of the cathode. The work function in these small areas can no longer be calculated directly from equation (75), because this equation is only valid for surfaces of infinite extent with uniform

density of the adsorbed material. Because of the differences in density the potential jump  $\Delta V$  resulting from (74) will have different values in different surface areas. Consequently there will be potential differences between these surface areas, and the potential differences are connected with additional electrical fields in front of the surface of the cathode, which are called surface fields. These surface fields are superposed on the image force field and on the external field and they will influence the work function in the same manner as the external field influences the work function in the Schottky-effect.

The surface fields to a certain extent also exist with pure metals where the emission patches are formed by crystal planes of different



Fig. 39.—Electron Images of a Ni-Cs Cathode (mag.  $\times 5$ ) (Brueche<sup>2</sup>).

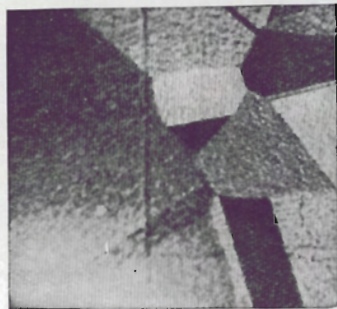


Fig. 40.—Electron Images of a Ni-Ba Cathode (mag.  $\times 60$ ) (Brueche<sup>2</sup>).

orientations (cf. Fig. 10/11). On account of this general importance the phenomena produced by surface fields will be discussed in more detail. The effect of the surface fields may be calculated in the same way as the effect of the external field on the work function was calculated before (cf. Sec. 2). The resulting potential which exists in front of a definite area of the surface will again be plotted as a function of the distance  $z$  from the surface. If the surface field and the image force field are taken together as one field, the internal field, the conditions are mainly the same as in Fig. 9. It is only necessary to replace the curve for the image force potential by the curve representing the appropriate potential of the internal field, while the external field is again represented by a straight line falling with increasing  $z$ . The superposition of the two curves again gives a potential maximum, the position of which being once more denoted by  $z_m$ .

The potential  $V$  resulting from the superposition is calculated as the sum of the potential belonging to the internal field:

$$V_i = \int_z^\infty \mathbf{E}_i(z) dz \quad . . . . . \quad (76)$$

and of the external potential given by equation (32). Hence:

$$V = \int_z^\infty \mathbf{E}_i(z) dz - \mathbf{E}_e z \quad . . . . . \quad (77)$$

By means of this value the work function existing in the case considered can be related to the work function  $\psi^{(0)}$  existing without external field and without any surface fields, i.e. for a completely uniform density. This is done by adding to  $\psi^{(0)}$  the value of the potential  $V$  at the position of the potential maximum where  $z=z_m$ , thus giving:

$$\psi = \psi^{(0)} + \int_{z_m}^\infty \mathbf{E}_i(z) dz - \mathbf{E}_e z_m \quad . . . . . \quad (78)$$

Differentiation of this equation gives:

$$\frac{d\psi}{d\mathbf{E}_e} = -\mathbf{E}_i(z_m) \frac{dz_m}{d\mathbf{E}_e} - z_m - \mathbf{E}_e \frac{dz_m}{d\mathbf{E}_e}$$

On the other hand, the internal field is equal to the negative of the external field for  $z=z_m$ . Hence, if the external field  $\mathbf{E}_e$  is calculated from the anode voltage  $V_A$  on the assumption of a plane system, then:

$$\mathbf{E}_i(z_m) = -\mathbf{E}_e = -\frac{V_A}{d}$$

From the last two equations the following equation for the work function is obtained (Becker and Mueller<sup>2</sup>):

$$\frac{d\psi}{dV_A} = -\frac{z_m}{d} \quad . . . . . \quad (79)$$

If the work function is known as a function of the anode voltage applied, the distance  $z_m$  from the surface at which internal and external field are equal can be ascertained by means of (79). Then the external field at the position  $z=z_m$ , being equal to the internal field at the same position, is known too. If the anode voltage is suitably varied, it will therefore be possible to determine the internal field  $\mathbf{E}_i$  as a function of the distance  $z$ . The only supposition is that the external field  $\mathbf{E}_e$  can be calculated from the geometric configuration of the electrode system with sufficient accuracy, i.e.

assuming that the influence of the roughness of the surface is not too large. Apart from this the field strength must not be so large that cold emission occurs.

In Fig. 41 the internal field is given as a function of the distance  $z$  from the surface in a logarithmic plot according to measurements by Linford<sup>1</sup> carried out with W-Th cathodes. The straight line in this figure represents the field strength appropriate to the image force according to equation (26). In the medium range between  $10^{-5}$  and  $10^{-4}$  cm. the measured values of the internal field strength are considerably larger than the image force field on account of the

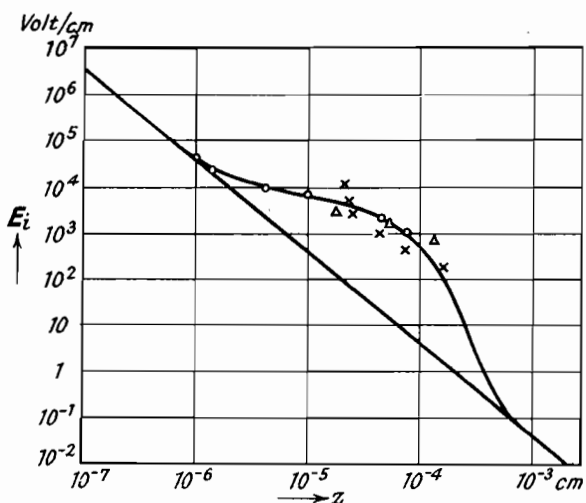


Fig. 41.—The Internal Field  $E_i$  as a Function of the distance  $z$  from the Surface (Linford<sup>1</sup>).

surface fields. For example, at  $z=10^{-4}$  cm. the internal field amounts to about 1000 volts/cm., while the field strength appropriate to the image force at the same position is only 3.5 volts/cm. according to (26).

As the surface fields extend considerably further outwards from the surface than the image force field, they are influenced substantially more by the magnitude of the external field. This may be visualized by means of Fig. 42 showing potential curves in front of the surface of a metal for the two cases with or without surface fields. The full curves always represent the potential of the internal field only, while the dashed curves represent the potential resulting from the superposition of this internal field and an external field.

The large influence of the external field on the potential in front of a cathode with surface fields (curves *c* and *d*) will be seen from Fig. 42. Consequently the work function and the saturated current of atomic film cathodes depend more on the magnitude of the external field than do those of pure metal cathodes which have surface fields of a smaller intensity.

The saturated current of an atomic film cathode may be plotted on a logarithmic scale as a function of the square root of the anode voltage in the same way as for pure metals (cf. Sec. 4.4). In such a plot considerable deviations from the Schottky line, which is

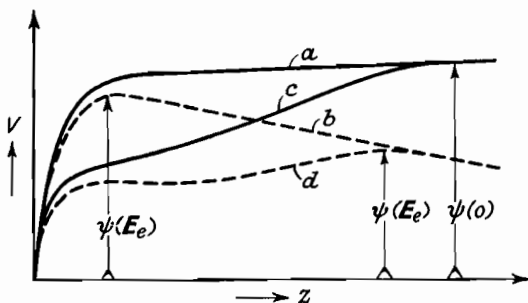


Fig. 42.—Schematic Plot of the Potential of an Electron in front of a Metal Surface

- (a) Without Surface Field and Without External Field.
- (b) Without Surface Field and With External Field.
- (c) With Surface Field and Without External Field.
- (d) With Surface Field and With External Field.

valid for cathodes without differences in work function, are obtained with small anode voltages (cf. Fig. 43, in which *C* is an appropriate factor chosen in such manner that the different curves ultimately coincide at a definite voltage). Only at very high field strengths ( $> 10,000$  volts/cm.), strong enough to remove most of the surface fields, do the observed curves approach the Schottky line. The deviations from the Schottky line are largest for medium densities of the absorbed material (values of  $\theta/\theta_m$ ), due to the fact that the differences in density are also large in this case (cf. the electron images, Fig. 38).

If the relation between saturated current and anode voltage observed in Fig. 43 is to be computed, it is necessary to make a suitable assumption for the distribution of the density *s* of the foreign material over the surface. The accuracy of this assumption, which will be more or less schematic, can only be decided by the

correspondence between the result of the calculation and the experimental result. A relatively good correspondence is obtained by Becker's<sup>5</sup> assumption of a chequerboard distribution of density, introducing the density  $s$  within each chequerboard square as the product of two cosine functions of the two edges of the squares. The details of Becker's calculations cannot be discussed here and only the result can be given. According to this the calculated relation between saturated current and external field corresponds best to the experimental curves (cf. Fig. 43), if the length  $l$  of the chequerboard squares is assumed to be between  $10^{-4}$  and  $10^{-3}$  cm. and if the maximum variation  $\Delta\psi$  of the work function is between

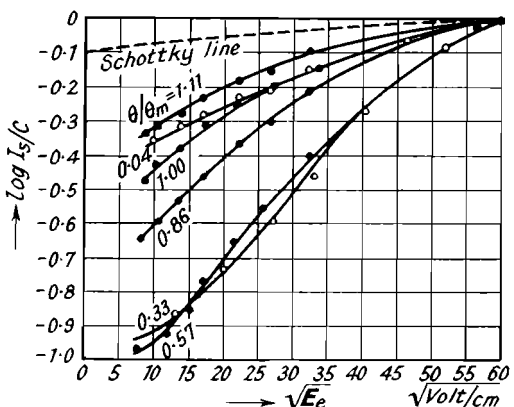


Fig. 43.—Saturated Current of a W-Th Cathode as a Function of Square Root of the Applied Field Strength for Different Densities of Adsorbed Material (Becker<sup>5</sup>).

0.5 and 1 eV. The values thus obtained for the dimensions of the squares correspond with the size of the emission centres observed in the electron images. Also the variation of the work function is of the right order, as Becker and Ahearn<sup>6</sup> measured differences in work function up to 0.6 eV with a W-Th cathode, while according to Morgulis and Djatlowizka<sup>1</sup> differences can even be as much as 1.9 eV. If the internal field strength  $E_i(z)$  is computed using the values calculated for  $l$  and  $\Delta\psi$ , a curve is obtained which corresponds well with Linford's measured values in Fig. 41.

The existence of emission patches also influences the velocity distribution of the emitted electrons, because the slow electrons will preferentially be prevented from overcoming the surface fields. In agreement with this Nottingham<sup>1</sup> when examining the emission of W-Th cathodes, observed a deficiency in slow electrons. A

quantitative explanation of this effect has, however, not been given yet.

On the basis of the above considerations the work function of the atomic film cathode will be a function  $\psi(x, y)$  of the co-ordinates  $x$  and  $y$  of the surface, and this function will depend on the external field and on the temperature. A suitable formula for this function is given by:

$$\psi(x, y) = \bar{\psi} + \frac{\Delta\psi}{2} \cos \frac{\pi x}{l} \cos \frac{\pi y}{l} . . . . . \quad (80)$$

according to Becker,<sup>6</sup> King<sup>1</sup> and Gysae and Wagener.<sup>3</sup> In this formula  $\bar{\psi}$  is the arithmetic mean value of the work function, given by the equation:

$$\bar{\psi} = \frac{1}{S} \iint \psi(x, y) dx dy . . . . . \quad (81)$$

This arithmetic mean value is not important so far as the emission current of the cathode is concerned. Because of the exponential function in the emission equation, the emission current is obtained using quite another form of mean value. This mean value of the work function, which is really decisive in determining the emission current may be denoted by  $\bar{\psi}$ , and is obtained as a solution of the emission equation, written with this mean value inserted:

$$I_s = SA_0 T^2 e^{-e\bar{\psi}/kT} . . . . . \quad (82)$$

This equation, in which  $I_s$  denotes the total saturated current and  $S$  the total surface of the cathode, defines the emissive mean value.

In order to find a relation between this emissive mean value and the individual values of the work function, the emission equation may be written for a single surface element  $dxdy$ :

$$dI_s(x, y) = A_0 T^2 e^{-e\psi(x, y)/kT} dx dy . . . . . \quad (83)$$

From this equation the total saturated current is obtained by an integration over the whole cathode surface:

$$I_s = A_0 T^2 \iint e^{-e\psi(x, y)/kT} dx dy . . . . . \quad (84)$$

By equating (82) to (84) the following equation for the mean value  $\bar{\psi}$  of the work function is derived:

$$\bar{\psi} = \frac{kT}{e} \ln \frac{S}{\iint e^{-e\psi(x, y)/kT} dx dy} . . . . . \quad (85)$$

When taking the arithmetic mean value, all the individual values of the work function over the surface have equal weight, but in determining the emissive mean the low values of the work function predominate due to the exponential function in the denominator of (85). It may be assumed for the purpose of calculation that only two values  $\psi_{max}$  and  $\psi_{min}$  of the work function exist at the cathode surface. Let  $S_{max}$  and  $S_{min}$  denote the fractions of the surface

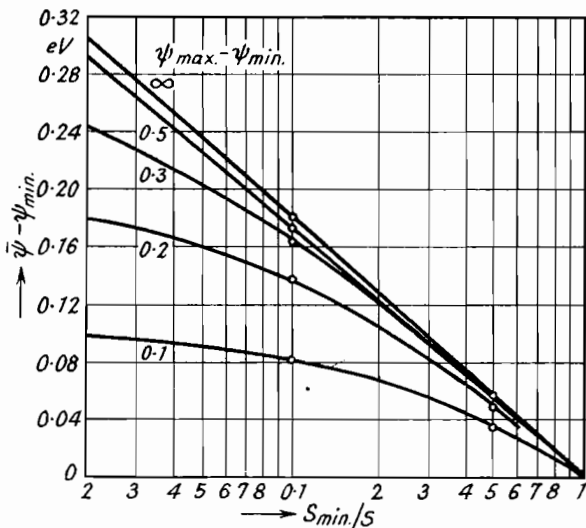


Fig. 44.—Difference between the Mean Value  $\bar{\psi}$  of the Work Function and the smallest Work Function  $\psi_{min}$  as a Function of the Fraction  $S_{min}/S$  of Highly Emitting Surface (Heinze and Wagener<sup>1</sup>).

appropriate to these work functions. Then the following formula is derived from (85) for the difference between the mean value  $\bar{\psi}$  and the smallest value  $\psi_{min}$  of the work function:

$$\bar{\psi} - \psi_{min} = -\frac{kT}{e} \ln \frac{1}{S} [S_{min} + S_{max} e^{-e(\psi_{max} - \psi_{min})/kT}] \quad . \quad (86)$$

The differences  $\bar{\psi} - \psi_{min}$  calculated from this equation are plotted in Fig. 44 as a function of the ratio  $S_{min}/S$  and for different values of  $\psi_{max} - \psi_{min}$ . The difference between the mean value and the lowest value of the work function is small, even for infinite differences  $\psi_{max} - \psi_{min}$  in work function and for small values  $S_{min}/S$  of the highly emitting part of the surface. We see from this that the areas with smallest work function contribute most to the emission of a cathode of non-uniform work function.

As can be seen from equation (85), the mean value  $\bar{\psi}$  varies with temperature, even if the individual work functions  $\psi(x, y)$  are independent of temperature for all areas of the surface. This temperature-dependence results from the fact that the surface areas with large work function contribute to the emission relatively more at high temperatures than at low temperatures, as can be observed from the emission equation.

The magnitude of this temperature-dependence was estimated by Gysae and Wagener,<sup>3</sup> the formula (80) for the work function being used. The result obtained for  $T=1000^\circ$  is set out in Fig. 45, from which it is seen that the temperature coefficient  $d\bar{\psi}/dT$  is of the order  $10^{-4}$  eV/degree. This temperature coefficient is only due to the differences in work function and it exists even if the work function  $\psi(x, y)$  of the surface elements of the cathode is entirely independent of temperature. A temperature coefficient of  $\psi(x, y)$  and of the arithmetic mean value  $\bar{\psi}$  would add to the temperature coefficient of the emissive mean value discussed above.

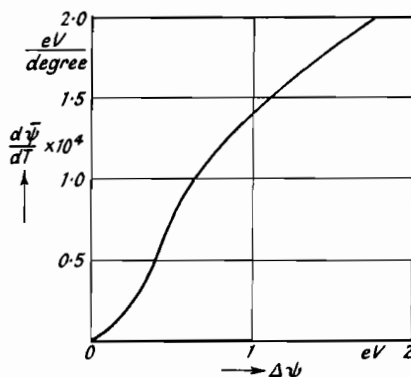


Fig. 45.—Temperature Coefficient  $d\bar{\psi}/dT$  of the Emissive Mean Value of Work Function as a Function of the Maximum Variation  $\Delta\psi$  of Work Function.

## REFERENCES

- ADAM, H. (1) *Z. techn. Physik* 22 (1940), 251.
- BARDEEN, D. (1) *Physic. Rev.* 49 (1936), 653.
- BARTELINK, E. H. B. (1) *Physica* 3 (1936), 193.
- BECKER, J. A. (1) *Physic. Rev.* 28 (1926), 341.  
 (2) and MUELLER, W., *ibid.*, 31 (1928), 431.  
 (3) *Trans. electrochem. Soc.* 55 (1929), 153.  
 (4) *Trans Faraday Soc.* 28 (1932), 151.  
 (5) *Rev. mod. Phys.* 7 (1935), 107.  
 (6) and AHEARN, I., *Physic. Rev.* 54 (1938), 448.  
 (7) and MOORE, G. E., *Phil. Mag.* 29 (1940), 129.
- BETHE, H. (1) *Ann. Phys.* 87 (1928), 60.
- BRATTAIN, W. H. (1) and BECKER, J. A., *Physic. Rev.* 43 (1933), 428.
- BRÜCHE, E. (1) and MAHL, H., *Z. techn. Physik* 16 (1935), 623.  
 (2) *Jahrb. Forsch. Inst. AEG* 4 (1933–35), 25.

THE OXIDE-COATED CATHODE

- DAVISSON, C. (1) *Physic. Rev.* 23 (1924), 299.  
 (2) and GERMER, L. H., *Physic. Rev.* 30 (1927), 705.
- EPSTEIN, P. S. (1) *Verh. dtsch. phys. Ges.* 21 (1919), 89.
- FERRIS, W. R. (1) *R.C.A. Review* 10 (1949), 134.
- FRY, TH., C. (1) *Physic. Rev.* 17 (1921), 441.
- GERMER, L. H. (1) *Physic. Rev.* 25 (1925), 795.
- GUTH, E. (1) and MULLIN, C. I., *Physic. Rev.* 59 (1941), 575.  
 (2) *ibid.* 61 (1942), 339.
- GYSAE, B. (1) and WAGENER, S., *Z. Physik* 110 (1938), 145.  
 (2) and WAGENER, S., *Z. techn. Physik* 19 (1938), 264.  
 (3) and WAGENER, S., *Z. Physik* 115 (1940), 296.
- HEINZE, W. (1) and WAGENER, S., *Z. Physik* 110 (1938), 164.
- HELLMANN, H. (1) and KASSATOTSCHKIN, W., *Acta Physica Chimica* 5 (1936), 23.
- HERRING, C. (1) and NICHOLS, M. H., *Rev. Mod. Phys.* 21 (1949), 185.
- HERZFELD, K. F. (1) *Physic. Rev.* 35 (1930), 248.
- KING, A. (1) *Physic. Rev.* 53 (1938), 570.
- KLEEN, W. (1) *Telefunkenröhre* 66 (1937).
- LANGMUIR, I. (1) *Physic. Rev.* 21 (1923), 419.  
 (2) and BLODGETT, K. B., *ibid.* 22 (1923), 347.  
 (3) *Physic. Rev.* 22 (1923), 357.  
 (4) and KINGDON, K. H., *Science* 57 (1923), 58.  
 (5) and KINGDON, K. H., *Physic. Rev.* 23 (1924), 112.  
 (6) and KINGDON, K. H., *Proc. Roy. Soc. (A)* 107 (1925), 61.  
 (7) and COMPTON, K. T., *Rev. mod. Phys.* 3 (1931), 237.  
 (8) and TAYLOR, J. B., *Physic. Rev.* 44 (1933), 423.
- LIEBMAN, G. (1) *Journ. of the I.E.E.* 93 (III) (1946), 138.
- LINFORD, L. B. (1) *Rev. mod. Phys.* 5 (1933), 47.
- MACCOLL, L. A. (1) *Physic. Rev.* 56 (1939), 699.
- MARTIN, S. T. (1) *Physic. Rev.* 56 (1939), 947.
- MENDENHALL, C. E. (1) and DE VOE, Ch. F., *Physic. Rev.* 51 (1937), 346.
- MÖLLER, G. H. (1) and DETELS, F., *Jb. d. drahtl. Telegr. u. Teleph.* 27 (1926), 74.
- MORGULIS, N. O. (1) and DJATLOWIZKAJA, B. I., *J. exp. theoret. Physics* 9 (1939), 293.
- MOTT-SMITH, H. M. (1) *Physic. Rev.* 56 (1939), 668.
- MROWKA, B. (1) *Z. techn. Physik* 18 (1937), 572.  
 (2) and RECKNAGEL, A., *Physik Z.* 38 (1937), 758.
- MÜLLER, E. W. (1) *Naturw.* 27 (1939), 820.
- NICHOLS, M. H. (1) *Physic. Rev.* 57 (1940), 297.
- NORDHEIM, L. W. (1) *Proc. Roy. Soc.* 121 (1928), 626.  
 (2) *Physik Z.* 30 (1929), 177.
- NOTTINGHAM, W. B. (1) *Physic. Rev.* 49 (1936), 78.
- PAGE, L. (1) and ADAMS, N. I., *Physic. Rev.* 68 (1945), 126.  
 (2) and ADAMS, N. I., *Physic. Rev.* 76 (1949), 381.

## THERMAL EMISSION OF ELECTRONS FROM METALS

- REIMANN, A. L. (1) *Nature* 133 (1934), 833.  
SCHOTTKY, W. (1) *Physik Z.* 15 (1914), 526.  
(2) *ibid.* 624.  
(3) *ibid.* 872.  
(4) *Ann. Phys.* 44 (1914), 1011.  
(5) *Verh. dtsch. physik Ges.* 16 (1914), 490.  
(6) *Z. Physik* 14 (1923), 63.
- SEELEY, S. (1) *Physic. Rev.* 59 (1941), 75.
- SEIFERT, R. L. E. (1) and PHIPPS, T. E., *Physic. Rev.* 56 (1939), 652.
- SMOLUCHOWSKI, R. (1) *Physic. Rev.* 60 (1941), 661.
- SOMMERFELD, A. (1) *Z. Physik* 47 (1928), 27.
- STRANSKI, I. N. (1) and SUHRMANN, R., *Ann. Phys.* 1 (1947), 153.  
(2) *ibid.* 1 (1947), 169.
- SUN NIEN TAI (1) and BAND, W., *Proc. Camb. Phil. Soc.* 42 (1946), 72.
- TAMM, I. (1) and BLOCHINZEW, D., *Z. Physik* 77 (1932), 774.
- TURNBULL, O. (1) and PHIPPS, T. E., *Physic. Rev.* 56 (1939), 663.
- VERVEY, E. J. W. (1) and DE BOER, J. H., *Recueil Trav. Chim. Pays-Bas* 55 (1936), 675.
- WEHNELT, A. (1) and BLEY, H., *Z. Physik* 35 (1926), 338.
- WIGNER, E. (1) and BARDEEN, D., *Physic. Rev.* 48 (1936), 84.  
(2) *Physic. Rev.* 49 (1936), 696.
- WOHLFAHRT, E. P. (1) *Proc. Phys. Soc.* 60 (1948), 360.

## CHAPTER 2

### METHODS OF MEASURING THE WORK FUNCTION OF METALS

#### 7. Importance and Fundamentals of the Measurement of the Work Function

When utilizing electron emission, one of the objects is to find suitable materials for the cathode which give the largest possible emission at the lowest possible temperature and heater power. For comparison of different materials measurements may be made of the saturated currents of these materials at the same temperatures. Such a procedure, however, is not satisfactory to the physicist, and he will therefore try to measure the physical constant which determines the emission, namely the work function of the material concerned. Apart from this a measurement of the work function under different conditions will give information of the mechanism upon which the electron emission of the examined material is based. As pointed out in the previous chapter, the work function  $\psi$  depends on temperature and external field. Ideally one would expect the method to give the value of  $\psi$  at the operating temperature. However this is not always so and it is therefore important to know the suitability of the various methods and their limitations. For this reason the existing methods will be discussed critically and in full detail.

Thin filaments or ribbons of metal are normally used for measuring the work function, the same as are employed for the cathodes of commercial valves. The anode of the electrode system is best made of three parts (guard ring structure), as shown in Fig. 46. The two outer anodes of this assembly which are connected together, cover the ends of the cathode, which are at a lower temperature because of the heat conduction towards the ends, while the centre anode with a separate lead is located over the centre part of the cathode with uniform temperature. The three anodes are connected to the same voltage supply, but only the emission current flowing to the centre anode is measured. Effects of non-uniformity of the potential field and of differences in the cathode temperature which would produce faulty results are thus avoided.

It may, moreover, be pointed out that all the known means of

vacuum technique must be applied when carrying out the measurement of the work function, in order to obtain a metal surface which is really pure and free from undesired foreign materials. According to the discussion in Sec. 5 it is quite clear that slight traces of foreign materials on the surface which only form fractions of a monatomic layer may considerably influence the value obtained for the work function. Consequently all foreign materials which may exist on the surface of the cathode to be examined must be removed before the measurement. A good pumping equipment with diffusion pumps of large exhaustion speed and with wide connecting tubes which do not reduce the exhaustion speed is necessary for this. The glass vessel used for the measurement has to be baked at temperatures between 400° and 600° C., depending on the type of glass, in order to remove water vapour. The metal parts of the measuring system must consist of metals which can be heated to a temperature of at least 1000° C., either by eddy current or by electron bombardment, without melting and evaporating. For improving the vacuum the well-known barium- and other getters should be employed, a selection of these getters with respect to their vapour pressure, and their position relative to the cathode, being of considerable importance. Many of the earlier investigators did not pay sufficient attention to these points and the results they obtained must therefore be open to doubt.

If directly heated cathodes are employed, the potential in the electrode system is non-uniform due to the potential drop along the cathode produced by the heater current (cf. the remark at the end of Sec. 4.3). This non-uniformity, whose influence on the result is difficult to account for, can be avoided if the switching circuit of Germer<sup>1</sup> and Demski,<sup>1</sup> shown in Fig. 47, is used. The cathode in this circuit is heated by interrupted D.C. which is generated from an A.C. source by means of a half-wave rectifier. This heater current produces across a blocking resistor in the heater circuit a large potential drop which drives the anode negative during the heating period and which thus cuts off the flow of the emission current during this period. Consequently the emission current can only flow during the times when the heater

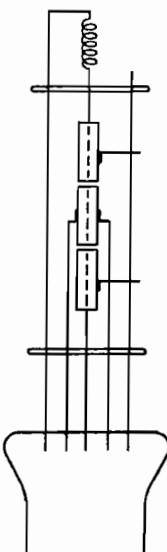


Fig. 46.—Assembly for Measurement of the Work Function.

current is interrupted, and when there is no disturbing potential drop along the cathode.

Precise values of the work function can be obtained without special methods of preparation only for such refractory metals as W, Mo, Nb, Ta. Only these metals can be degassed sufficiently without evaporating and melting. Metals with low melting point can be produced in vacuum by evaporating them from a special source on to a suitable base. By this procedure, which was first carried out with barium by Anderson,<sup>1</sup> a cathode is obtained which is extremely free from foreign material. Surfaces with a similar good purity are obtained by splitting a single crystal in vacuum and by using the cleavage planes thus produced as the emitting surface,

according to Kluge<sup>1</sup> and Kluge and Steyskal.<sup>2</sup> Finally it may be noted that platinum which is difficult to degas was successfully degassed by Oatley<sup>2</sup> by a bombardment with argon ions.

The measurement of the work function of atomic film cathodes is certain to be less accurate than the measure-

ments with pure metals. The atomic films are only stable in a definite range of temperatures, while above this range the foreign material evaporates and the emission qualities are changed. The temperature range over which measurements can be taken therefore is small, being limited at the upper end by the evaporation of the material and at the lower end by the fact that the emission current becomes too small to be measured. Hence the accuracy of the measurements will also be small. As the work function of such a cathode varies considerably along the surface any method used for measuring  $\psi$  must give one of the mean values derived in Sec. 6, either the emissive mean value or the arithmetic mean value. When the special methods are dealt with, it will be discussed which of these mean values is obtained in each special case.

### 8. Richardson Line Method

The simplest way of determining the work function is by measuring the saturated current  $I_s$  at a definite temperature  $T$  and by calculating the work function from the emission equation (47)

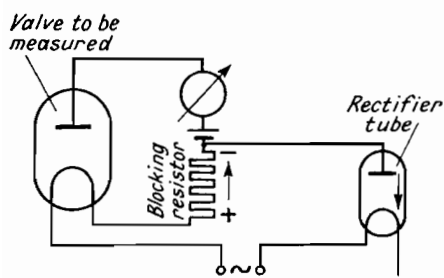


Fig. 47.—Switching Circuit for the Examination of Directly Heated Cathodes.

using these two values of  $I_s$  and  $T$  and  $A_0 = 120$ . But as there were many doubts if the emission constant  $A_0$  is really equal to the theoretical value 120, this simple method has only rarely been employed. The doubts originally resulted from the simultaneous existence of two emission equations, the  $T^{1/2}$  and the  $T^2$  equations. They were increased by the uncertainty of the exact values of the coefficient of transmissivity  $D_e$  and of the occupation number  $G$ , occurring in equation (48) for the emission constant  $A_0$ . On account of these doubts a method for determining the work function has mostly been used which gives the value of the emission constant in addition to that of the work function. This is the so-called Richardson line method.

According to equation (47) for the saturated current:

$$\log \frac{I_s}{T^2} = 5040\psi \frac{1}{T} + \log A_0 S \quad \dots \quad (87)$$

If, therefore,  $\log I_s/T^2$  is plotted against  $1/T$ , a straight line with the slope  $-5040\psi/T$  and the intersection  $\log A_0 S$  on the ordinate axis is obtained. Such a Richardson line, measured for tungsten, is shown in Fig. 48. The work function required can be ascertained from the slope of this line.

The accuracy of the work function measured by this method is determined by the following aspects:

(a) If the saturated current  $I_s$  measured for a definite anode voltage is introduced in equation (87), the value of the work function obtained corresponds to the same voltage. The value  $\psi^{(0)}$  of the work function belonging to zero external field can be determined by introducing into (87) the saturated current  $I_s^{(0)}$  belonging to zero field. This current, however, cannot directly be measured but must be derived from saturated currents measured for higher field strengths. Such a derivation is possible for pure metals by an extrapolation by means of the Schottky line. This Schottky line, however, does not precisely correspond to the conditions existing on account of the influence of surface roughness and differences in work function discussed in Sec. 4.4. Hence the extrapolation will not be very accurate, and the work function for zero external field will be obtained with some error. If atomic film cathodes are examined, a simple procedure for determining the work function belonging to zero field cannot be given (cf. Sec. 6).

(b) When determining the work function, account must be taken of the fact that it may depend on the temperature (cf. Schottky,<sup>1</sup>

Becker and Brattain,<sup>2</sup> Wigner<sup>1)</sup>. If assuming a linear dependence as a first approximation, then

$$\psi_T = \psi_0 + \frac{d\psi}{dT} T \quad \dots \dots \dots \quad (88)$$

and by introducing this value into the emission equation:

$$I_s = A_0 S T^2 e^{-e[\psi_0 + (d\psi/dT)T]/kT} = A_0 S e^{-e(d\psi/dT)/k} T^2 e^{-e\psi_0/kT}$$

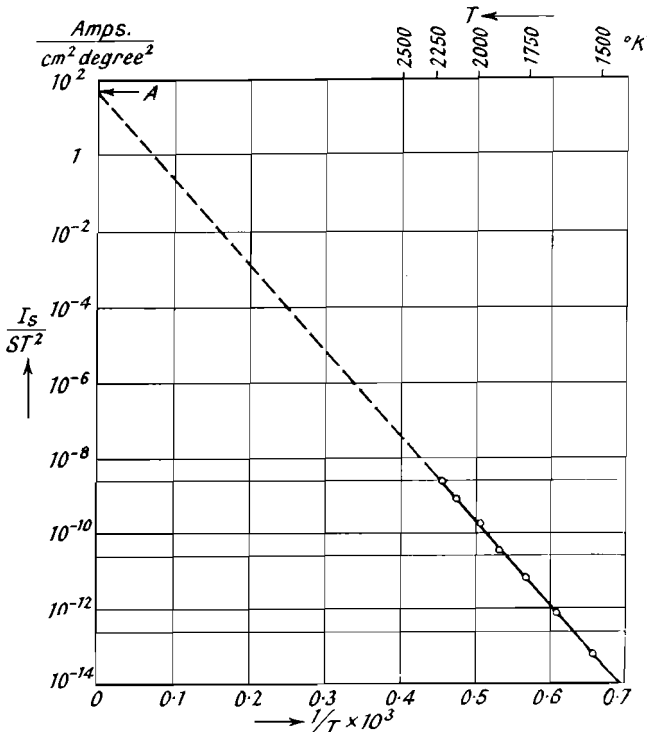


Fig. 48.—Richardson Line for Tungsten.

If this equation is plotted as a Richardson line, the slope of this line gives the work function at zero temperature and the intersection on the ordinate the value:

$$A = A_0 e^{-e(d\psi/dT)/k} \quad \dots \dots \dots \quad (89)$$

This value may be considerably different from the theoretical value  $A_0 = 120$ , if the temperature-dependence of the work function is large, the details being shown by Fig. 49. As the measured value of  $A$  is influenced by many experimental errors, it is, however, not possible to derive the temperature coefficient  $d\psi/dT$  by means of (89). Consequently, when using the Richardson line, only the

value of the work function existing at  $T=0$  and not the value for the operating temperature can be obtained. Furthermore, it will be practically impossible to recognize a temperature dependence of the work function, if this dependence is only linear.

(c) The differences in work function, which have been discussed in detail in the previous section, also exist on the surface of pure metals due to the dependence of the work function on the orientation of the emitting crystal plane. Strictly speaking, the integral equation (84) is therefore valid instead of the emission equation (47). This integral equation, when plotted on a logarithmic scale, gives instead of a straight line a curve whose curvature of course is too small to be determinable within the spread of the measured values. Hence the straight line, drawn through the measured points for the evaluation, is really the tangent to the curve concerned.

Application of the Richardson method then gives the emissive mean  $\bar{\psi}$  of the work function which is related to the individual work functions of the patches by equation (85).\* The relation between this emissive mean  $\bar{\psi}$  and the experimental curve is obtained by differentiating (82):

$$\bar{\psi} = -\frac{k}{e} \frac{d}{d(1/T)} \ln(I/T^2) = \frac{kT^2}{e} \frac{d}{dT} \ln(I/T^2) . . . \quad (90)$$

For  $\bar{\psi}$  the term "apparent work function" has also been used.

In Table III some values measured for the metals tungsten and molybdenum by means of the Richardson method are given. Only the values measured since 1930, which are more reliable than the earlier ones, are quoted. These values are calculated for zero external field and they are valid for  $T=0$  according to the above.

\* Footnote added during proof reading: It may be noted that the Richardson method gives  $\bar{\psi}_0$ , the emissive mean value at zero temperature, whilst equation (85) defines  $\bar{\psi}_T$ , the value at temperature  $T$ .

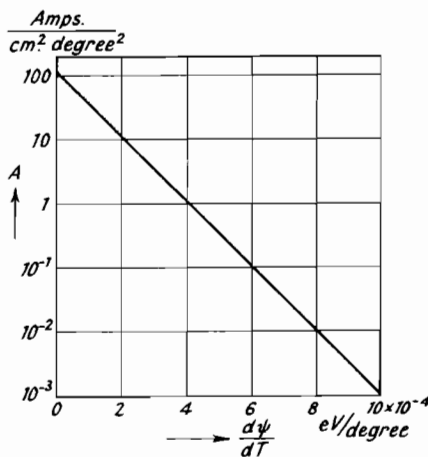


Fig. 49.—Measured Value  $A$  of the Emission Constant as a Function of the Temperature Coefficient  $d\psi/dT$  of the Work Function.

TABLE III

*Values of the Work Function of Tungsten and Molybdenum, measured by Means of the Richardson Method (since 1930)*

Material	Year of measurement	Measured by	Work function (eV)	A
W	1933	Ahearn <sup>1</sup>	4.58	—
W	1934	Freitage and Krueger <sup>1</sup>	4.53	22
W	1936	Wahlin and Whitney <sup>3</sup>	4.63	212
W	1937	Johnson and Vick <sup>1</sup>	4.55	90
W	1937	Reimann <sup>2</sup>	4.52	84
W	1939	Seifert and Phipps <sup>1</sup>	4.54	—
Mo	1932	Du Bridge and Roehr <sup>4</sup>	4.15	55
Mo	1933	Ahearn <sup>1</sup>	4.32	—
Mo	1934	Freitage and Krueger <sup>1</sup>	4.33	24.6
Mo	1935	Wahlin and Reynolds <sup>2</sup>	4.17 4.30 4.38	51 96 175
Mo	1937	Grover <sup>1</sup>	4.19	—
Mo	1941	Wright <sup>1</sup>	4.20	55

The table shows that the values of the work function measured for the same metal by different authors correspond fairly well. A much better correspondence cannot be expected because only a mean value of work function is obtained due to the dependence of the work function on crystal orientation. The magnitude of this mean value will therefore depend on the crystal planes and on the individual values of the work function which preferably exist at the surface of the multi-crystalline cathode.

On the other hand, as seen from Table III, considerable differences exist between the values  $A$ , measured for the emission constant and its theoretical value  $A_0=120$ . There are several possible explanations for these differences which, having a bearing on the accuracy of the work function, will be discussed now:

(a) Firstly the method of measuring  $A$  is in itself not accurate. Only the error in  $A$  due to the error in determining the temperature will be considered. The temperature can be measured to 1%; then, for  $\partial T/T = 0.01$ ;  $\psi = 5$  eV; and  $T = 1000^\circ$ , equation (50) gives:

$$\partial A/A = e\psi/kT \times \partial T/T = 0.58 \dots \quad (90)$$

Accordingly the emission constant can only be ascertained with an error of about  $\pm 50\%$ .

(b) For determining  $A$  from the intercept in the Richardson plot the total emitting surface  $S$  must be known. This surface area is

larger than the geometric surface due to the roughness of the surface and is only known for a few special cases (cf. Tonks<sup>1</sup> and R. P. Johnson<sup>1</sup>). In general the uncertainty in  $S$  does not allow  $A$  to be measured very accurately.

(c) According to the above considerations the temperature-dependence of the work function enters into the value of  $A$  and hence a value of  $A$  different from 120 is to be expected.

(d) The curvature of the Richardson line produced by the differences in work function also influences the value of  $A$  which is reduced by this influence (cf. Recknagel<sup>1</sup>).\*

(e) The value  $A_0 = 120$  is obtained from the simplifying assumptions made on page 25 (coefficient of transmissivity  $D_e = 1$ , occupancy  $G = 2$ , existence of completely free electrons). If these assumptions are not correct then  $A_0$  will differ from the calculated value.

For all these reasons an accurate determination of the emission constant seems hardly possible. For the same reasons it is not possible to derive from measurements of the emission constant  $A$  accurate values of the temperature dependence of the work function. Also since  $A$  cannot be measured accurately, knowledge of the transmission coefficient  $D_e$  or of the occupancy  $G$  cannot be derived.

It was previously assumed that for atomic film cathodes the coefficient of transmissivity  $D_e$  would be very different from 1 and that consequently the value of  $A_0$  would be much smaller for these cathodes than for pure metals (cf. Nordheim<sup>1</sup>). This assumption is disproved by an experiment of Gysae and Wagener,<sup>2</sup> based on equation (65) for the space-charge characteristic. As the right-hand side of this equation according to (63) contains the term  $kT/e \times \log A_0$ , every variation of  $A_0$  will shift the characteristic along the voltage axis. In the experiment of Gysae and Wagener, therefore, the space-charge characteristic was measured twice in the same assembly, the cathode consisting of pure tungsten during the first and of the same tungsten covered with a film of barium during the second measurement. No shift of the characteristic could be found within the accuracy of the measurements. Hence it must be concluded that tungsten, covered with a barium film (W-Ba), has the same value  $A_0$  as pure tungsten. For an estimate, therefore, a calculation of the work function from the emission equation may be sufficient in many cases (cf. King<sup>1</sup>). Exact examinations, however, have to rely on the Richardson method or on the other methods to be discussed later on.

\* Footnote added during proof reading : For further details see Arizumi.<sup>1</sup>

Concluding this section, the values measured for the work function and the emission constant of platinum are given as an example for the considerable spread which is produced by bad vacuum conditions. Platinum is especially difficult to degas, and the values given in Table IV show that particularly the results of the earlier investigations spread considerably and that only by gradually improving vacuum technique could accurate and reproducible values be obtained.

TABLE IV  
*Work Function of Pt in Chronological Order*

Year	Author	eV	A
1908	H. A. Wilson <sup>1</sup>	2.18	$10.7 \times 10^4$
1908	H. A. Wilson <sup>1</sup>	5.45	366
1908	H. A. Wilson <sup>1</sup>	6.00	620
1913	Langmuir <sup>1</sup>	6.62	$10.7 \times 10^6$
1921	Richardson <sup>1</sup>	4.10	39.8
1921	Richardson <sup>1</sup>	5.65	265
1928	Du Bridge <sup>1</sup>	4.69	11.5
1928	Du Bridge <sup>1</sup>	5.60	235
1928	Du Bridge <sup>1</sup>	6.20	6450
1928	Du Bridge <sup>1</sup>	6.30	8130
1928	Du Bridge <sup>1</sup>	6.40	14000
1928	Du Bridge <sup>2</sup>	6.27	17000
1933	Van Velzer <sup>1</sup>	5.40	170
1936	Whitney <sup>1</sup>	5.32	132

## 9. Calorimetric Measurement of the Work Function

The discussions in the previous section show the importance of a method by which the work function can be measured at the operating temperature of the cathode. Such a method is given by the cooling effect, which is based on the following phenomenon.

When an electron is emitted, a certain energy is required which enables the electron to overcome the work function and to leave the surface with the initial velocity. This energy has to be taken from the heater power. When the anode voltage is applied the cathode cools, the decrease in the amount of heat radiated being equal to the energy necessary for electron emission.

On the supposition that the emission current is saturated, the magnitude of this cooling effect is only determined by the work function and by the energy given to the emitted electrons as initial velocity. The emitted electrons have a Maxwellian energy distribution, the normal component having an energy  $E_w = kT$ , while

the energy of the two tangential components is  $kT/2$  each. The total energy associated with the initial velocity of emission is  $kT + 2 \times kT/2 = 2kT$  and hence the total energy required for the emission of one electron is:

$$E = E_\psi + 2kT \dots \dots \dots \quad (91)$$

A more detailed thermodynamical investigation shows that on the right-hand side of this equation an additional term must be added which accounts for the amount of heat convected from the interior to the surface by the current (cf. Wagner,<sup>1</sup> Herring<sup>1</sup>). This additional term which contains the Thomson coefficient of the metal concerned is estimated to amount to a few hundredths of a volt and is therefore negligible in most cases.

The cooling power which is equal to the decrease of the energy irradiated from the cathode per unit time is obtained from equation (91) by multiplying with the electron current  $I_s$ :

$$P_{cool} = I_s \psi + 2I_s \frac{kT}{e} \text{ watt} \dots \dots \dots \quad (92)$$

Accordingly the work function  $\psi$  can be ascertained from the cooling power  $P_{cool}$ , the value for  $\psi$  being:

$$\psi = \frac{P_{cool}}{I_s} - 1.72 \times 10^{-4} T \text{ eV} \dots \dots \dots \quad (93)$$

In this manner a method has been found which allows the measurement of the work function at only one definite temperature, which, for instance, may be the operating temperature.

The influence of the emission patches on equation (93), relating work function and cooling power, has been investigated by Herring.<sup>1</sup> It was shown that  $\psi$  in (93) can be replaced by the mean value  $\bar{\psi}$ , provided a correction term is introduced the magnitude of which is about  $1/10$  eV.

Many experimental difficulties arise if the cooling power,  $P_{cool}$  is to be measured directly from the decrease of the cathode temperature. The radiation law for the cathode is normally not well known and has to be used in the calculation. Also the result has to be corrected for the heat conduction through the support wires and this varies with temperature. Such a direct measurement was at first carried out by Davisson and Germer,<sup>1,2</sup> who compared this calorimetric measurement with the Richardson line method. The values of Davisson and Germer were obtained by means of the old  $T^{1/2}$  emission law and neglected the correction term  $2kT/e$  in

equation (92). If they are converted to the  $T^2$  law and the correction term taken into account the appropriate values are:

Richardson line

$$\psi_0^{(0)} = 4.55 \text{ eV}$$

Calorimetric method

$$\psi_{2270}^{(0)} = 4.52 \text{ eV}$$

This agreement is very good, and the temperature-dependence of the work function of tungsten can only be very small.

Another method for measuring the cooling effect was given by Wehnelt and Jentzsch.<sup>1</sup> They equalized the decrease in temperature, obtained after switching on the emission current, by a corresponding increase in heater power. Then the cooling power is directly equal to the amount by which the heater power must be increased, in order to establish the same cathode temperature as existing before switching on the emission. The criterion for the equality of the temperature before and after switching is given by the electrical resistance of the cathode, which can be adjusted in a Wheatstone bridge.

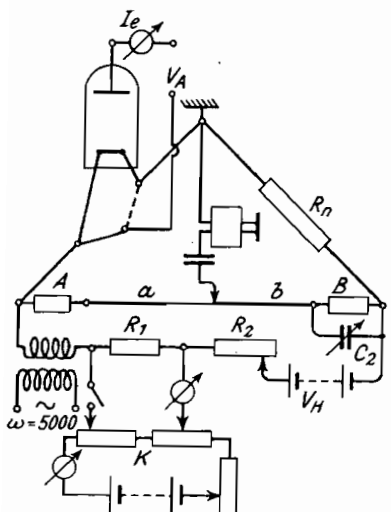


Fig. 50.—Principal Circuit for Measuring the Cooling Power.

bridge for the minimum in a receiver in the usual way. A suitable blocking of the detector arm will then prevent the emission current superposing on the measuring current (cf. the circuit in Fig. 50). If the measurement is carried out with all these refinements, according to Heinze,<sup>1</sup> the resistance and the temperature of the cathode can be kept constant to  $5 \times 10^{-3}\%$ .

The following possible errors must be accounted for during the measurement of the cooling effect by the bridge method:

(a) After applying the anode voltage, the cathode, due to its Ohmic resistance, is heated by the emission current, and this heating effect opposes the cooling effect. The heating effect can be eliminated by minor modifications to the circuit, for instance by

centre tapping the cathode and so producing a symmetric distribution of the emission current on the two halves of the cathode. The residual heating effect can then be accounted for by modifying the formulæ (cf. the special papers).

(b) The anode is heated by the bombarding emission current, and this heating influences the temperature of the cathode by radiation. Consequently the anode has to be cooled.

(c) The plate resistance of the diode system cathode-anode is parallel to a part of the cathode and is therefore measured in the bridge after switching on the emission current. As the saturated current increases with increasing anode voltage, this plate resistance is not infinite. If the resistance is measured with A.C. the shunting effect of the plate resistance can be avoided by inserting an adequate choke in the anode circuit.

Some authors tried to utilize the cooling effect in the space-charge range for a measurement of the work function. The following discussion shows that this is not possible.

The electrons in the space-charge range have to overcome the potential barrier due to space-charge, in addition to the work function  $\psi$  (cf. Sec. 4.3). Hence the value of the total barrier  $\psi - V_m$ , must be put into equation (93) instead of the work function  $\psi$ . In this manner the equation:

$$\psi = \frac{P_{cool}}{I_{sp}} - 1.72 \times 10^{-4}T + V_m \quad . . . \quad (94)$$

is obtained for the space-charge region. In the investigations quoted above equation (94) has been used for the calculation of  $\psi$ , but it has not been taken into consideration that  $V_m$  also depends on  $\psi$  according to (70). If the value for  $V_m$  from (70) is introduced into the equation above, we have:

$$\psi = \frac{P_{cool}}{I_{sp}} - 0.86 \times 10^{-4}T \left( \ln \frac{SA_0 T^2}{I_{sp}} + 2 \right) + \psi \quad . . \quad (95)$$

The work function can be cancelled from the equation thus obtained and can therefore not be calculated by means of that equation.

The reason for this fact may be seen by reference to Fig. 25, showing the potential distribution in the space-charge range. The total potential barrier  $\psi - V_m$  to be seen in front of the cathode in this figure only depends on the temperature and on the magnitude of the space-charge current according to (70) and is independent of the magnitude of the work function. Consequently, when

measuring the cooling power in the space-charge range, that is the energy necessary for overcoming the total potential barrier, a value is obtained which is completely independent of the work function and which can therefore not be used for calculating the work function. If, however, determination of the work function is attempted employing equation (94), the term  $V_m$  in this equation has to be ascertained by measuring the saturated current and using equation (56). Then the work function, obtained from (94) with that value of  $V_m$ , is only apparently determined by the cooling power, but really derived from the emission equation by means of the saturated current which was measured for ascertaining  $V_m$ .

## 10. Measurement of the Work Function by Means of the Contact Potential

A further method for measuring the work function is obtained if equation (51) is used, according to which the contact potential between cathode and anode is equal to the difference of the work functions of these two electrodes. Accordingly, if the work function of the one electrode is known, the work function of the other electrode can be ascertained by measuring the contact potential, or if the work function of the one electrode is constant, variations of the work function of the other one can be detected and measured. The methods resulting in this manner, which can also be carried out at one definite temperature, correspond with the methods existing for measuring the contact potential. Hence the latter methods are to be discussed now, but only the most important of them will be dealt with.\*

Before discussing the methods in detail, it may be pointed out that the reference electrode whose work function is supposed to be known or constant must consist of a refractory metal (the best being tungsten). Only such a metal can be sufficiently degassed and freed from contaminating layers influencing the work function, but nevertheless it will never be absolutely certain that a completely pure metal surface is produced by such a treatment and that the value of the work function, measured for this surface by other authors, has been obtained. Consequently the methods using the contact potential are more suitable for measuring variations of the work function, produced either by variations of temperature or by a contamination of the cathode to be examined. In this case the

\* For a compilation of all these methods cf. Gericke.<sup>1</sup>

absolute values need not be known. If absolute measurements are to be carried out by means of the contact potential, it will be necessary to determine the work function of the reference electrode by one of the other methods. In this case, of course, using the contact potential method will only be worth while for such (non-metallic) cathodes which are difficult to be measured by other methods.

### 10.1. Kelvin's method

The principal idea of this, the earliest method for measuring the contact potential, is as follows. The contact potential, as every other potential, will be produced by an electrical charge whose magnitude results from the capacity of the condenser formed by the two electrodes (cf. Fig. 16). Consequently a decrease of capacity,

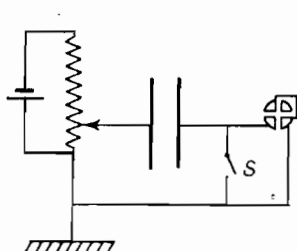


Fig. 51.—Circuit for Measuring the Contact Potential according to Lord Kelvin (Gericke<sup>1</sup>).

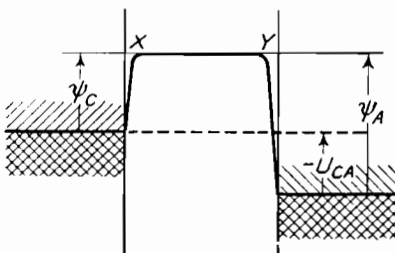


Fig. 52.—Potential Distribution During the Measurement according to Lord Kelvin.

produced by removing the two electrodes from one another, will increase the contact potential, if the charge remains unchanged. When using the circuit shown in Fig. 51, the one electrode is connected to earth by a potentiometer, while the second one is connected to an electrometer whose second pair of quadrants is earthed too. If after opening the earth switch  $S$ , one of the two electrodes is removed, the increase of the potential produced by the decrease in capacity is detected by the electrometer. The magnitude of the detected potential depends on the magnitude of the voltage adjusted at the potentiometer tap. If in a special case this voltage is equal to the contact potential, the potential distribution in the condenser formed by the two electrodes is as shown in Fig. 52. There is no potential drop across the condenser. In this case and this case only there will be no deflection of the electrometer on removing one of the electrodes. The value of the potentiometer voltage is then equal to the contact potential.

The agreement between the differences in work function obtained by this and by other methods has been proved experimentally by Glasoe<sup>1</sup> and by Farnsworth and Winch.<sup>1</sup> They measured the difference in work function between Fe and Ni, or between the (100)- and the (111)-plane of a single crystal consisting of silver. The second method, used for checking the contact potential method, was the method of the frequency limit of photo-electrons (cf. Sec. 11.1).

A refinement of the Kelvin method was given by Meyerhof and Miller.<sup>1</sup> By making the electrodes approach each other quickly, a voltage pulse was produced which was made visible by means of an electrometer valve, an amplifier, and a cathode-ray tube. In this manner an accuracy of 0.01 volt could be obtained for a surface area of 2 mm.<sup>2</sup> of the electrodes.

### 10.2. Zisman's method

Zisman<sup>1</sup> mounted the two electrodes, consisting of two parallel metal sheets, inside a valve envelope and vibrated the one with respect to the other. Instead of a D.C. potential being produced as before, an alternating voltage whose frequency is that of the vibration is so developed between the electrodes. This frequency can be amplified and detected in a receiver. As before, an adjustable voltage is applied to one electrode and when this is equal to the contact potential no oscillation is heard in the receiver. According to Zisman the contact potential can be measured to an accuracy of 1/1000 of a volt in a few seconds. This method has, for instance, been used to measure the temperature-dependence of the work function of tungsten (cf. Sec. 12).

### 10.3. Intersection method

This method, which was given by Rothe<sup>1</sup> and Germer,<sup>2</sup> uses equation (52) for the retarding field current in a plane field which by taking the logarithm is given by:

$$\log I_r = \frac{5040}{T} (V_A - \psi_A) + \log SA_0 T^2 \dots \quad (96)$$

If the logarithm is also taken of equation (47) for the saturated current, we get:

$$\log I_s = \frac{5040}{T} \psi_c + \log SA_0 T^2 \dots \quad (97)$$

where the work function  $\psi_c$  of the cathode may depend on the anode voltage.

If a logarithmic plot is made of the retarding field current and the saturated current against the anode voltage as abscissa, the former is represented by a straight and the latter by a slightly curved line. The value of the anode voltage at the intersection of the two curves, i.e. when  $I_r = I_s$ , is:

$$V_A^* = \psi_A - \psi_C = U_{AC} \quad . . . . . \quad (98)$$

Thus the contact potential may be determined from the abscissa of the intersection point and, if the work function of the anode is known, the work function of the cathode can be ascertained (cf. Fig. 54).

If the electrode system is not plane but cylindrical, the logarithmic plot also gives a straight line for the retarding field current provided the anode voltage is sufficiently low. This line has to be extended to intersect the curve representing the saturated current. The intersection point obtained in this manner has, however, to be corrected using the equation for the retarding field current in a cylindrical field (cf. Fig. 18).

The method discussed is in practice limited to plane or cylindrical electrode configurations, as explicit equations for the retarding field current are only known for these configurations. The determination or the elimination of the work function of the anode may be carried out in two different ways.

(a) According to Heinze and Wagener<sup>3</sup> (cf. Fig. 53), a cathode, consisting of a tungsten wire  $W$ , is attached to the cathode  $C$  to be examined. The anode of the experimental design, consisting of three cylindrical parts, can be moved along the axis of the two cathodes. This special arrangement allows the measurement of the two contact potentials between the anode and both the cathode  $C$  to be examined and the tungsten cathode  $W$ . If the two measurements of the contact potential are carried out, the following values for the abscissæ of the intersection points are obtained according to (98):

$$\left. \begin{aligned} V_A^{*(1)} &= \psi_A - \psi_C \\ V_A^{*(2)} &= \psi_A - \psi_W \end{aligned} \right\}$$

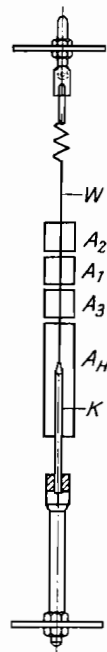


Fig. 53.—Experimental Design for the Intersection Method (Heinze and Wagener<sup>3</sup>).

## 2. 10.3

## THE OXIDE-COATED CATHODE

The work function of the cathode to be examined is derived from this as:

$$\psi_c = \psi_w + (V_A^{*(2)} - V_A^{*(1)}) \quad . . . \quad (99)$$

As the work function  $\psi_w$  of tungsten can be determined by the Richardson method the work function  $\psi_c$  of the cathode to be examined may be ascertained, without knowing the work function of the anode. This method therefore is especially suitable for measurements of the absolute value of the work function, as opposed to the methods for measuring the contact potential discussed before.

The Richardson method gives the value of  $\psi_w$  for  $T=0$  while its

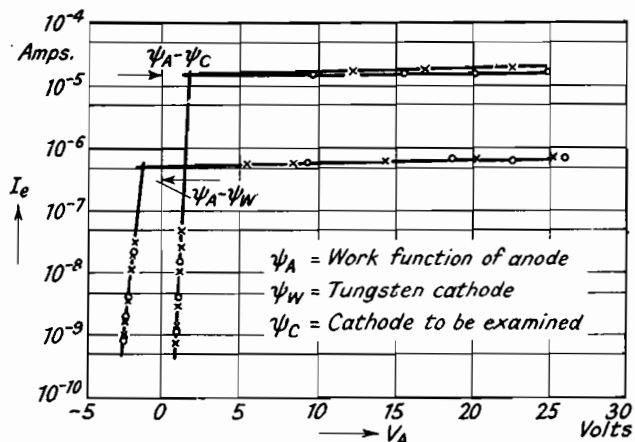


Fig. 54.—Determination of the Contact Potential by the Intersection Method (Heinze and Wagener<sup>3</sup>).

value at the measuring temperature has to be used in equation (99). The difference between these two values, resulting from the temperature-dependence of the work function of tungsten, must be accounted for by an appropriate correction, if accurate values are desired. A practical example for carrying out this method is given by Fig. 54.

(b) A way for determining the work function of the anode was given by Sano,<sup>1</sup> who measured the retarding field current at different temperatures of the cathode. If, then, equation (96) is written in the following manner:

$$\log \frac{I_r}{T^2} = 5040 (V_A - \psi_A) \frac{1}{T} + \log SA_0 \quad . . . \quad (100)$$

the left-hand side of this equation will give a straight line, when

plotted as a function of  $1/T$  for fixed values of the voltage  $V_A$ . The desired value of  $\psi_A$  can be derived from the slope of that line.

The agreement of the work function obtained by the intersection method with values obtained by the Richardson method was checked by Heinze.<sup>2</sup> The examined cathode was a tantalum wire whose work function could also be measured by the Richardson method. The maximum deviation between the two methods was only 1/100 eV.

When applying the intersection method to cathodes with emission patches (in particular atomic film cathodes), the shape of the curve representing the retarding field current is not altered by the differences in work function, as the retarding field current is independent of the work function of the cathode (cf. Sec. 4.2). Hence equation (96) for the logarithm of the retarding field current is valid for atomic film cathodes too. If the logarithm of the emission equation (82) is taken and if the right-hand side of the equation thus obtained is put equal to the right-hand side of (96), the abscissa of the intersection point is:

$$V_A^* = \psi_A - \bar{\psi}_C \dots \dots \dots \quad (101)$$

This value exactly corresponds to the value obtained for pure metals, with the only difference that the work function  $\psi_C$  which is assumed to be constant over all the surface is replaced by the mean value  $\bar{\psi}_C$  of work function. The latter can therefore be ascertained by means of the intersection method in the same manner as the work function of pure metals.\* The only difference results from the fact that extrapolating the saturated current to the intersection with the line representing the retarding field current will be more difficult for atomic film cathodes. However, by introducing the saturated current, valid for anode voltages greater than zero, the mean value of the work function corresponding to that anode voltage can be obtained.

#### 10.4. Displacement of the characteristic

This method, which was much used, utilizes equations (52) or (65) for the retarding field or space-charge characteristic respectively. Both equations contain the work function of the anode in addition to the anode voltage, and a variation of this work function will therefore shift the characteristic along the voltage

\* Footnote added during proof reading: It may be pointed out that the intersection method gives the value  $\bar{\psi}_1$  at the measuring temperature as opposed to the Richardson method which gives  $\bar{\psi}_0$  (cf. Arizumi<sup>2</sup>).

axis. Hence such a variation of the work function of the anode can be ascertained from the shift, the variation being directly equal to the magnitude of the shift.

This method in itself does not belong to the contact potential methods, as it provides no direct way for determining the contact potential. It only gives the variation of the work function of the anode, but for historical reasons it will be discussed here. Before it was known that the characteristics are independent of the work function of the cathode it was assumed that the position of the characteristics would be determined directly by the contact potential. In early investigations, therefore, special arrangements were made for keeping the work function of the cathode constant in order to avoid the influence of variations of this work function. Such arrangements are really not necessary, for the reasons discussed above. Only the temperature and the emitting surface of the cathode have to be kept constant during the measurement, as only these influence the position of the characteristic in addition to the work function of the anode.

The method has been checked experimentally by Gysae and Wagener,<sup>2</sup> who measured the characteristic between a revolving cathode, consisting of a tungsten wire, and two different anodes, a tungsten and a tantalum wire. The two characteristics obtained in this manner will be displaced against another by an amount which is equal to the difference between the work function of tungsten and tantalum. A good correspondence between the shift of the characteristics and the difference in the work functions was found in the experiment mentioned.

In addition to this Moench<sup>1</sup> showed by suitable experiments that the results of this method correspond with those obtained according to Kelvin. The deviation between the result of the two methods was only 1/100 volt, which was within the experimental error.

When applying this method to atomic film cathodes it must be remembered that then the cathode to be examined forms the anode of the experimental arrangement. Consequently the value measured for the work function is determined by quite another manner of taking the mean as with the methods discussed before. This manner of taking the mean was examined experimentally by Gysae and Wagener.<sup>3</sup> The anodes of their valves were split into a number of parts insulated from each other, and a variable voltage could be applied between the different parts of the anode. In this manner an anode with patches of different work functions and

different contact potentials between them could be roughly imitated. The result was that the arithmetic mean value  $\bar{\psi}$  of the work function, defined by equation (81), is measured by the displacement of the characteristic. In the same manner the arithmetic mean value of the work function will be measured by the specific contact potential methods given by Kelvin and Zisman which have been discussed above.

### 10.5. Magnetic method

Another method for measuring the contact potential which has not been used much is connected with the well-known principle of the magnetron. An electrode system consisting of a cylindrical cathode (e.g. a tungsten wire) and a concentric cylindrical anode is brought into an axial magnetic field. The emitted electrons are deviated from their paths to the anode and travel spirally round the cathode. If the magnetic field is increased gradually, the electrons eventually are diverted from their normal path so much that they are no longer able to reach the anode, and in the same moment, when a critical value  $H_0$  of the field strength is reached, the emission current is suddenly cut off. This critical field strength  $H_0$  depends on the magnitude of the anode voltage  $V_A$  and on the contact potential  $U_{CA}$ . There is a relation between these three values, and the contact potential can be calculated from the critical field strength by means of this relation which accounts for the initial velocities of the electrons by a correction term.

The method was given by Oatley,<sup>1</sup> and the details may be found in his paper. Oatley employed the method for determining the work function of molybdenum, a value  $\psi_{Mo}=4.1$  eV being found (using  $\psi_{tungsten}=4.54$  eV, cf. Table V). The main disadvantage of this method is that a very exact concentric assembly is needed in order to fulfil the equation between critical field strength, anode voltage, and contact potential.

## 11. Application of Photo- or Field-Emission

Other methods for determining the work function are obtained, if the electrons are emitted not by an increased temperature but by irradiation of light on the surface of the cathode. In this case the energy necessary for overcoming the work function is supplied by impinging photons instead of by the increased temperature. The energy of these photons is partly absorbed by the electrons, thus enabling them to leave the metal over the potential barrier at the

surface (cf. the potential box, Fig. 8). The irradiation by light thus produces an electron current, the photo-electric or photo-current which may already flow at the lowest temperatures.

If  $\nu$  denotes the frequency of the light, the energy of the photons, as is well known, is  $h\nu$ . The energy which can be given to the electrons by the photons therefore decreases with decreasing frequency. Finally a frequency limit  $\nu_0$  is reached at which the energy of a photon is just sufficient to lift an electron over the potential barrier representing the work function. Hence in this case:

$$h\nu_0 = E_\psi = e\psi \quad \dots \quad \dots \quad \dots \quad \dots \quad \dots \quad (102)$$

or

$$\psi = \frac{h}{e}\nu_0 = \frac{hc}{e} \frac{1}{\lambda_0} = \frac{1.239}{\lambda_0(\mu)} \text{ eV} \quad \dots \quad \dots \quad \dots \quad \dots \quad \dots \quad (103)$$

$c$  denoting the velocity of light and  $\lambda_0$  the limiting wavelength belonging to the frequency  $\nu_0$  and measured in  $\mu$ . For a work function of 1 eV the limiting wavelength  $\lambda_0$  is about  $1.2 \mu$ , i.e. lying in the infra-red, while for a work function of 5 eV  $\lambda_0$  is about  $0.25 \mu$ , which is in the far ultraviolet.

If the frequency of the impinging light is greater than  $\nu_0$ , the photons have an excess energy which gives a certain initial velocity to the electrons. This initial velocity is not the same for all the emitted electrons, as for frequencies  $\nu > \nu_0$  not only those electrons can be detached whose energy is exactly equal to the limiting energy, but also some of those which have a lower energy and which have to be considered as in lower regions of the potential box. The latter electrons, when leaving the metal, have to overcome a larger opposing potential and consequently their initial velocities, resulting from the energy excess, will be smaller. The equation for the maximum initial velocity is, similar to (102):

$$h\nu = E_\psi + \frac{1}{2}mv_{max}^2 \quad \dots \quad \dots \quad \dots \quad \dots \quad \dots \quad (104)$$

Hence it is:

$$\frac{1}{2}mv_{max}^2 = h(\nu - \nu_0) \quad \dots \quad \dots \quad \dots \quad \dots \quad \dots \quad (105)$$

The distribution of the initial velocities may be determined experimentally by measuring the photo-electric current as a function of a negative voltage applied to the anode. If this negative (retarding) voltage is gradually increased, at first only the slowest of the emitted electrons and later on also the faster ones are prevented from reaching the anode. In this manner a curve for the photo-electric current as a function of the negative voltage is obtained

which is schematically given in Fig. 55. The current gradually falls until at a definite negative voltage, the stopping voltage  $V_{st}$ , the fastest electrons can no longer reach the anode. The distribution of the energies of the emitted electrons may be obtained by differentiating the retarding field curve shown in Fig. 55.

As already mentioned, electrons with an energy which is smaller than the limiting energy can be emitted if the employed frequency is higher than the frequency limit. Consequently the number of electrons which may be emitted and the probability for an electron to be emitted increases with increasing frequency. Hence the photo-electric current also increases with increasing frequency or decreasing wavelength. This increase is shown by Fig. 56 for three different metals.

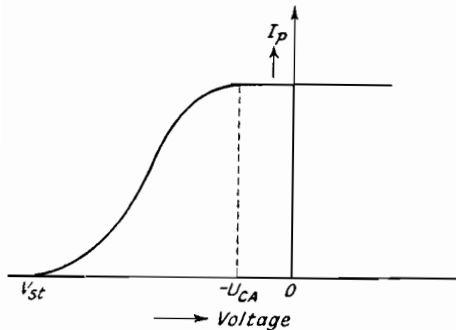


Fig. 55.—Photo-electric Current as a Function of a Retarding Voltage (Schematic).

The laws which are valid for the photo-electric emission give a number of different methods for determining the work function. Only the three most important of these methods will be discussed here.

### 11.1. Measurement of the frequency limit of photo-electrons

If the photo-electric emission is measured as a function of frequency and the frequency limit  $\nu_0$  is determined by extrapolating the emission measured for higher frequencies, the work function  $\psi$

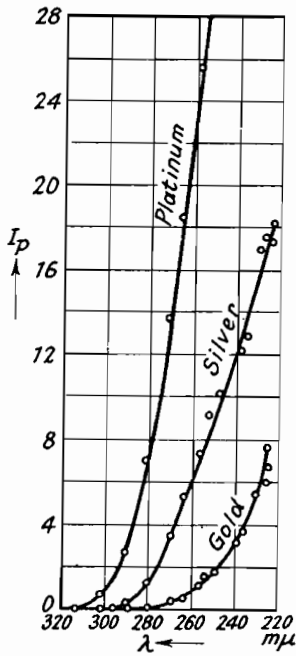


Fig. 56.—Photo-electric Current  $I_p$  as a Function of the Wavelength  $\lambda$ . (Müller Pouillet, *Lehrbuch der Physik*, Vol. IV/4, 1934).

can be ascertained from this frequency limit by means of equation (103). The determination of  $\nu_0$  in this simple way is rather difficult, as the temperature of the cathode is usually different from zero and some of the electrons are then in energy levels above the limiting energy. These electrons can be emitted by photons whose frequency is less than the limiting frequency  $\nu_0$ . Consequently the limiting frequency is not very sharp at these temperatures and an exact determination of the work function is made difficult.

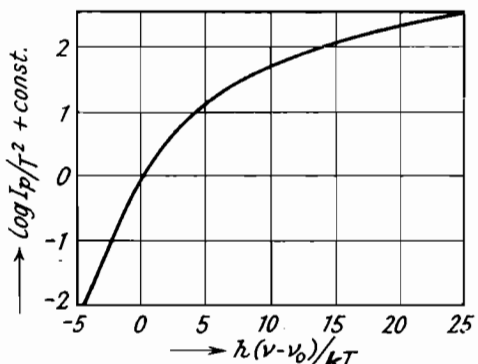


Fig. 57.—Plot of the Photo-electric Current according to Fowler (Du Bridge and Roehr<sup>3</sup>).

For temperatures greater than zero an exact equation for the photo-electric emission has been derived by Fowler<sup>1</sup> of the form:

$$\log I_p/T^2 = K + f\left(\frac{h\nu - h\nu_0}{kT}\right) \dots \quad (106)$$

where  $I_p$  is the photo-electric current,  $K$  is a constant, and the last term is a complicated function of  $(h\nu - h\nu_0)/kT$  (cf. Fig. 57). If  $I_p$  is measured experimentally as a function of  $\nu$  and then plotted as a function of  $h\nu/kT$  a curve is obtained which has the same shape as that of Fig. 57. It is, however, displaced and the amount of the displacement between the two curves in the  $h\nu$  direction is equal to  $h\nu_0/kT$ . The value of  $\nu_0$  can be found in this way and hence  $\psi$ , the work function.

When applying this method to atomic film cathodes, the mean value obtained for the work function is quite different from the emissive mean value on account of the difference between the Fowler law (106) and the emission equation (47). It must therefore be assumed that a mean value which is interesting for the thermionic

emission cannot be ascertained by this photo-electric method. This assumption was confirmed by both experiment and calculation by King<sup>1</sup> and Farnsworth and Winch.<sup>1</sup>

## 11.2. Measurement of the stopping potential

An equation for the stopping potential  $V_{st}$  which stops photo-electrons from reaching the anode (cf. Fig. 55) can easily be derived by using Fig. 16. If the electrons are to reach the anode with zero velocity the quantity of photoelectric energy to be supplied must be equal to the height of the arrow indicated by  $\hbar\nu$  in Fig. 16. As is seen from this figure, the relation

$$-V_{st} + \psi_A = \hbar\nu$$

or

$$V_{st} = -(\hbar\nu - \psi_A) \dots \dots \dots \quad (107)$$

then holds. By measuring the stopping voltage  $V_{st}$  and using the above equation, the work function  $\psi_A$  of the anode can be determined.

## 11.3. The photo-electric line

When applying this method, the cathode is irradiated by a black body of the variable temperature  $T_s$ . Then the energy of the photons impinging upon the cathode surface is distributed according to Planck's law for black body radiation, and the energy of the electrons in the irradiated cathode, after having absorbed the photons, will be distributed in the same manner. Planck's radiation law, for the energy distribution of the photons, is:

$$N(E)dE = \frac{2\pi c m^{3/2}}{\hbar^3} \times \frac{E^{1/2}}{e^{E/kT} - 1} \dots \dots \quad (108)$$

Neglecting an unessential factor, this law differs from Fermi's distribution law (9) only in two details. The  $+1$  in the denominator of (9) is replaced by  $-1$  and the limiting energy  $E_\zeta$  in the exponent of (9) is missing. These differences are unimportant if only the higher energies which are needed to overcome the potential barrier are considered. For these energies the two distribution laws degenerate into Maxwell's distribution law. Hence the electrons in the metal, irradiated by the black body of the temperature  $T_s$ , will have the same energies as they would have if the cathode were heated to the temperature  $T_s$ . Consequently the number of emitted electrons will be the same in both cases and is given by

Richardson's emission equation, in which the temperature of the cathode must be replaced by the temperature  $T_s$  of the black body. The emission current thus obtained, which is called the total photo-electric emission, is:

$$I_p' = A'T_s^2 e^{-e\psi/kT_s} \dots \dots \quad (109)$$

This equation differs from Richardson's law for the thermionic emission only in the constant  $A'$ . This constant is different from the emission constant  $A_0$ , as the probability for the absorption of a photon by an electron (quantum yield) occurs in it. A value for  $A'$  which is generally valid therefore cannot be given.

Equation (109) was confirmed experimentally by Suhrmann,<sup>1</sup> who found that the index of  $T_s$  was slightly different from 2. As pointed out by Herring and Nichols<sup>2</sup> such deviations from the index in (109) are to be expected because the quantum yield occurring in  $A'$  will be dependent on temperature to a considerable extent.

The work function can be determined from equation (109) in the same manner as from Richardson's equation, by measuring the current  $I_p$  as a function of the temperature  $T_s$  and by plotting the Richardson line. This method has the advantage that the temperature of the cathode need not be varied during a series of measurements. Any temperature-dependence of the work function can therefore be detected and measured which is not possible with Richardson's method.

The method can also be adapted to other sources of radiation instead of the black body, provided the difference between the spectral distributions of the two radiations is duly taken into account (cf. Suhrmann<sup>1</sup>).

If the method is applied to atomic film cathodes, the emissive mean value of the work function is measured in the same manner as with Richardson's and the intersection method. This can be understood from the fact that the only difference between the Richardson method and the method discussed now is the manner of supplying the energy, while the electrons leave all areas of the cathode in exactly the same way with both methods. The photo-electric line was used by Suhrmann and v. Eichborn<sup>4</sup> for measuring the work function of a Pt-Ba cathode as a function of the external field.

#### 11.4. Application of field emission

The field emission, mentioned at the end of Sec. 4, can also be used for determining the work function. The electron current

which is emitted, if a field strength of more than  $10^7$  volt/cm. is applied, is given by:

$$I_F = 6 \cdot 2 \times 10^{-6} S \frac{\zeta^{1/2}}{(\zeta + \psi)\psi^{1/2}} E^2 e^{-6 \cdot 85 \times 10^7 \psi^{3/2}/E} \quad . . \quad (110)$$

In this equation a small correction term, taking account of the image force field, has been neglected. If, corresponding to Richardson's method,  $\log I_F/E^2$  is plotted against  $1/E$ , the work function can be ascertained from the slope of the straight line obtained in this way. This method was checked experimentally by Haefer.<sup>1</sup> It

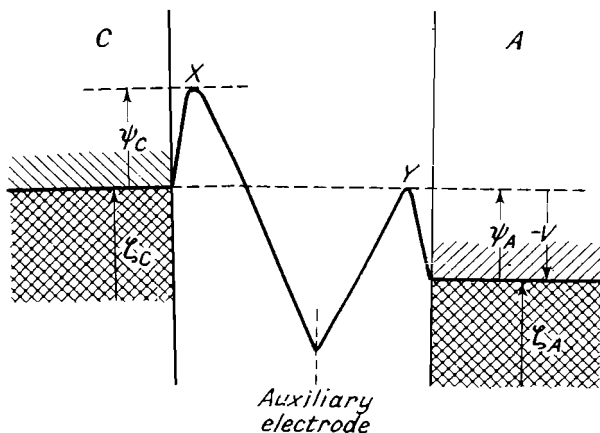


Fig. 58.—Potential Distribution in the Experimental Set of Goss and Henderson.<sup>1</sup>

gives the value of the work function at the measuring temperature, but this temperature must not be very high, as the thermionic emission must be small compared with the field emission.

Another method, using the field emission, was given by Goss and Henderson.<sup>1</sup> They used the material to be examined as a collector for field electrons which were accelerated by an auxiliary electrode. Fig. 58 shows the potential distribution in their experimental set. As the field electrons pass through the potential barrier, representing the work function, they leave the cathode with an energy equal to the limiting energy  $E_\zeta$  and without any initial velocity. If the voltage between cathode and collector is varied from zero to positive values, the electrons will only be able to meet the collector if they reach the point  $Y$  immediately in front of the anode surface with at least zero velocity. It is therefore necessary that the

collector voltage is at least equal to the work function of the collector (cf. Fig. 58). When the collector voltage has reached this value, the field emission current rises suddenly. This behaviour is quite contrary to thermionic and photo-electric emission, which rise gradually with increasing voltage, because the electron velocities in these cases are distributed according to Maxwell (cf. Fig. 55). This may be understood as a proof that the field emission is really produced by electrons passing through the potential barrier (cf. Henderson and Dahlstrom<sup>1)</sup>). It is quite clear that the work function of the collector material can be determined by measuring the voltage of the sudden rise of the field emission current.

When applying the methods using field emission to atomic film cathodes, the two different methods discussed must be distinguished. If equation (110) for the field emission is used, a different mean value which is unimportant for the thermionic emission is obtained, in a similar manner as when ascertaining the work function by the frequency limit. There are two reasons for this, the difference between the equations for field emission and thermionic emission and the fact that the surface fields are considerably altered by the strong field which is applied for field emission. The second method, however, in which the work function of the anode is measured, gives the arithmetic mean value of the work function in the same manner as the displacement of the characteristic.

## 12. Experimental Values of the Work Function and Dependence on Temperature

The most reliable values of the work function measured by the methods discussed above have been compiled in the following tables. Table V gives the values for pure metals and Table VII for metals covered with atomic films. Only values which have been obtained with multicrystalline surfaces have been taken, and all the measurements before 1930, which mostly are less reliable, have been omitted. The values given are valid for zero external field and those by the Richardson and the calorimetric method refer to zero temperature (the values by the calorimetric method were extrapolated to  $T=0$ ). The values obtained by contact potential, photo- and field-emission methods refer to room temperature.

The work functions of the heavy metals, to be seen from Table V, are between  $3\frac{1}{2}$  and  $5\frac{1}{2}$  eV, the highest known value is that of platinum. The alkaline earth metals have values between  $2\frac{1}{2}$  and

4 eV, while the alkali metals with about 2 eV have the lowest values of all metals. In Table VI the mean values of the work function of pure metals are given in the order of their magnitude together with the corresponding values for the ionization potential and the atomic volume ( $A/8$ ). It is seen from this table that roughly, apart from some deviations, the ionization potential increases and the atomic volume decreases in the same direction.

The figures given for atomic film cathodes in Table VII are not complete, because the scrutiny of the numerous measured values is beyond the scope of this book. The table only gives an idea of the magnitude of the work functions concerned. The values given in Table VII for the work functions of W-Cs and W-O-Cs are considerably higher than those measured in earlier experiments where values under 1 eV were obtained. But if the values in Table VII are introduced into the emission equation, the saturated currents obtained correspond well with the emission currents measured directly by Langmuir and Kingdon<sup>2</sup> and Langmuir and Taylor.<sup>3</sup> The values of the work function given here, therefore, are likely to be more accurate than the lower values obtained in the earlier experiments.

TABLE V  
*Work Functions  $\psi$  of Pure Metals  
(arranged in columns of the periodic system)*

Material	Year of measurement	Method	Measured by	$\psi^0$ (eV)
Li	1949	contact potential (displacement of characteristic).	Anderson <sup>6</sup>	2.48†
Na	1937 1940	photo-electric photo-electric	Mann and du Bridge <sup>1</sup> Maurer <sup>1</sup> mean value	2.29 2.28 2.28
K	1937 1940	photo-electric field emission	Mayer <sup>1</sup> Haefer <sup>1</sup> mean value	2.26 2.18 2.22
Cs	1938	photo-electric field emission	Mayer <sup>2</sup> Haefer <sup>1</sup> mean value	1.94 1.92 1.93
Cu	1949	contact potential (displacement of characteristic).	Anderson <sup>7</sup>	4.45†

† For  $\psi_{Ba} = 2.51$  eV.

TABLE V—*continued*

Material	Year of measurement	Method	Measured by	$\psi^{(0)}$ (eV)
Ag	1931	photo-electric contact potential (displacement of characteristic). " "	Fowler <sup>1</sup>	4.75
	1936		Anderson <sup>2</sup>	4.45†
	1941		Anderson <sup>5</sup>	4.46†
Au	1931	photo-electric	Fowler <sup>1</sup>	4.89
Be	1934	photo-electric	Suhrmann and Schallmanach <sup>3</sup>	3.32
	1937	photo-electric	Mann and Du Bridge <sup>1</sup>	3.92
Mg	1937	photo-electric	Mann and Du Bridge <sup>1</sup>	3.68
	1938	photo-electric contact potential (displacement of characteristic).	Cashman <sup>1</sup>	3.67
	1938		Anderson <sup>3</sup>	3.66†
Ca	1932	photo-electric	Rentschler <sup>1</sup>	3.20
	1936	photo-electric	Jamison and Cashman <sup>1</sup>	2.71
Ba	1933	photo-electric (total emission).	Suhrmann and Deponte <sup>2</sup>	2.70
	1935	contact potential (displacement of characteristic).	Anderson <sup>1</sup>	2.43*
	1936	photo-electric	Jamison and Casman <sup>1</sup>	2.51
	1939	photo-electric	Cashman and Bassoe <sup>2</sup>	2.51
	1940	field emission	Haefer <sup>1</sup>	2.49
	1940	photo-electric	Maurer <sup>1</sup>	2.45
Zn	1940	contact potential (displacement of characteristic). photo-electric	Anderson <sup>4</sup>	2.48
	1944			2.51
Cd	1944	photo-electric	Suhrmann and Pietrzik <sup>5</sup>	4.10
			mean value	4.29
Al	1944	photo-electric	Suhrmann and Pietrzik <sup>5</sup>	4.20
Ce	1932	photo-electric	Rentschler <sup>1</sup>	2.84

\* For  $\psi_w = 4.54$  eV.† For  $\psi_{Ba} = 2.51$  eV.

TABLE V—*continued*

Material	Year of measurement	Method	Measured by	$\psi^{(0)}$ (eV)
Zr	1932	photo-electric	Rentschler <sup>1</sup>	3.73
Th	1932	photo-electric	Rentschler <sup>1</sup>	3.38
C‡	1938	Richardson method	Reimann <sup>3</sup>	4.34
	1947	Richardson method	Braun and Busch <sup>1</sup>	4.39
	1949	Richardson method	Glockler and Sausville. <sup>1</sup>	4.35
	1949	Richardson method	Ivey <sup>1</sup>	4.60
Si‡	1947	Richardson method	Braun and Busch <sup>1</sup>	3.59
Nb	1934	Richardson method	Wahlin and Sordahl <sup>1</sup>	3.96
Ta	1931	photo-electric	Cardwell <sup>1</sup>	4.15
	1931	photo-electric	Fowler <sup>1</sup>	4.13
	1932	photo-electric	Rentschler <sup>1</sup>	4.12
	1935	Richardson method	Cardwell <sup>2</sup>	4.10
	1935	photo-electric	Cardwell <sup>2</sup>	4.13
	1935	cooling effect	Krueger and Stabenow <sup>1</sup>	4.08
	1942	Richardson method	Fiske <sup>1</sup> mean value	4.19 4.13
Bi	1934	photo-electric	Suhrmann and Schallmanach. <sup>3</sup>	4.48
	1941	photo-electric	Jupnik <sup>1</sup>	4.24
Cr	1948	Richardson method	Wahlin <sup>6</sup>	4.60
Mo	1932	Richardson method	Du Bridge and Roehr. <sup>4</sup>	4.15
	1932	photo-electric	Du Bridge and Roehr. <sup>4</sup>	4.14
	1933	Richardson method	Ahearn <sup>1</sup>	4.32
	1934	Richardson method	Freitag and Krueger <sup>1</sup>	4.33
	1935	Richardson method	Wahlin and Reynolds. <sup>2</sup>	4.17
				4.30
	1935	cooling effect	Krueger and Stabenow <sup>1</sup>	4.38
	1936	contact potential (magnetic).	Oatley <sup>1</sup>	4.40
	1937	Richardson method	Grover <sup>1</sup>	4.19
	1941	Richardson method	Wright <sup>1</sup> mean value	4.20 4.24

\* For  $\psi_w = 4.54$  eV.

† C and Si are probably semi-conductors, but as their properties are closely connected to those of metals they are quoted here.

TABLE V—*continued*

Material	Year of measurement	Method	Measured by	$\psi^{(0)}$ (eV)
W	1931	photo-electric	Warner <sup>1</sup>	4.54
	1932	photo-electric	Rentschler <sup>1</sup>	4.60
	1933	Richardson method	Ahearn <sup>1</sup>	4.58
	1934	Richardson method	Freitag and Krueger <sup>1</sup>	4.53
	1935	cooling effect	Krueger and Stabenow <sup>1</sup>	4.44
	1935	Richardson method	Nottingham <sup>1</sup>	4.52
	1936	Richardson method	Wahlin and Whitney <sup>3</sup>	4.63
	1937	Richardson method	Johnson and Vick <sup>1</sup>	4.55
	1937	Richardson method	Reimann <sup>2</sup>	4.52
	1939	Richardson method	Seifert and Phipps <sup>1</sup>	4.54
	1940	cooling effect	Fleming and Henderson <sup>1</sup>	4.63 §
	1948	photo-electric	Apker, Taft and Dickey <sup>1</sup> mean value	4.49 <b>4.54</b>
U	1932	photo-electric	Rentschler <sup>1</sup>	3.63
	1939	photo-electric	Hole and Wright <sup>1</sup>	3.27
Fe ( $\alpha$ ) ( $\beta$ )	1931	photo-electric	Glasoe <sup>1</sup>	4.77
	1942	Richardson method	Wahlin <sup>5</sup>	4.23
	1942	Richardson method	Wahlin <sup>5</sup>	4.48
			mean value	<b>4.49</b>
Co	1942	Richardson method	Wahlin <sup>5</sup>	4.41
Ni	1931	photo-electric	Glasoe <sup>1</sup>	5.01
	1933	Richardson method	Fox and Bowie <sup>1</sup>	5.03
	1939	contact potential (displacement of characteristic).	Bosworth <sup>1</sup>	4.94*
	1942	Richardson method	Wahlin <sup>5</sup>	4.61
	1949	Richardson method	Cardwell <sup>3</sup>	5.24
	1949	photo-electric	Cardwell <sup>3</sup>	5.05
			mean value	<b>4.96</b>
Rh	1931	Richardson method	Dixon <sup>1</sup>	4.58
	1938	Richardson method	Wahlin and Whitney <sup>4</sup>	4.80
Pd	1932	photo-electric	Du Bridge and Roehr <sup>3</sup>	4.99
	1932	photo-electric	Du Bridge and Roehr <sup>3</sup>	4.96
			mean value	<b>4.98</b>
Pt	1933	Richardson method	Van Velzer <sup>1</sup>	5.40
	1936	Richardson method	Whitney <sup>1</sup>	5.32
	1939	contact potential (magnetic).	Oatley <sup>2</sup>	5.36
			mean value	<b>5.36</b>

\* For  $\psi_w = 4.54$  eV.§ Measured at  $T = 1800^\circ$ .

TABLE VI

*Work Function, Ionization Potential and Atomic Volume of Metals*

	Cs	K	Na	Li	Ba	Ce	Th	Mg
Work function	1.93	2.22	2.28	2.48	2.51	2.84	3.38	3.67
Ionization potential	3.86	4.32	5.09	5.37	5.21	6.54	—	7.63
Atomic volume at $T=0^\circ\text{ K}$ .	66	43.4	23	12.5	37.3	20.4	19.7	13.8
	Zr	Nb	Cd	Ta	Al	Mo	Zn	Co
Work function	3.73	3.96	4.10	4.13	4.20	4.24	4.29	4.41
Ionization potential	6.92	—	8.94	—	5.94	7.20	9.37	7.8
Atomic volume at $T=0^\circ\text{ K}$ .	13.9	10.9	12.7	10.7	9.9	9.4	8.97	6.58
	Cu	W	Fe	Cr	Au	Ni	Pd	Pt
Work function	4.45	4.54	4.49	4.60	4.89	4.96	4.98	5.36
Ionization potential	7.67	—	7.83	6.7	9.20	7.60	8.30	8.80
Atomic volume at $T=0^\circ\text{ K}$ .	7.05	9.49	7.05	7.2	10.12	6.55	8.78	8.99

All the methods discussed, except the Richardson method, can be used for determining the temperature-dependence of the work function. Until now measurements with pure metals have been carried out by the cooling effect, the Zisman method, the displacement of the characteristic, the photo-electric frequency limit (Fowler method) and the photo-electric line. The Zisman method, being used by Waterman and Potter<sup>1</sup> and Potter,<sup>2</sup> is especially suitable. If the two electrodes of a diode system are made of the material to be examined and the temperature of only one of these electrodes is varied, the temperature coefficient of the work function results directly from the contact potential measured between the two electrodes. The values measured for the temperature-dependence of the work function by different authors are compiled in Table VIII; they correspond very well. In addition to this Fig. 59 shows two series of measurements for tungsten and tantalum which were obtained by Krueger and Stabenow<sup>1</sup> by means of the cooling effect.

The experimental values obtained for the temperature coefficient of the work function have been compared with theoretical ones by Seeley.<sup>1</sup> Such a comparison, however, appears to be premature in view of the uncertainty about the temperature coefficient of the total potential barrier  $\tau$  (cf. p. 18). Furthermore, as discussed

in Sec. 6, the differences in work function between crystal areas of different orientation will give rise to an additional temperature coefficient, the coefficient of the emissive mean  $\bar{\psi}$  which must be taken into account (Nottingham<sup>2</sup>).

While the emissive mean  $\bar{\psi}$  always depends on temperature due to the manner of taking the mean, the arithmetic mean value  $\tilde{\psi}$ , defined by (81) only depends on temperature if the work function  $\psi(x, y)$  at the individual surface elements of the cathode is temperature-dependent. Such a temperature-dependence may be produced either by the work function of the basic metal or, if atomic film cathodes are concerned, by the dipole moment  $M$  of the atomic film,

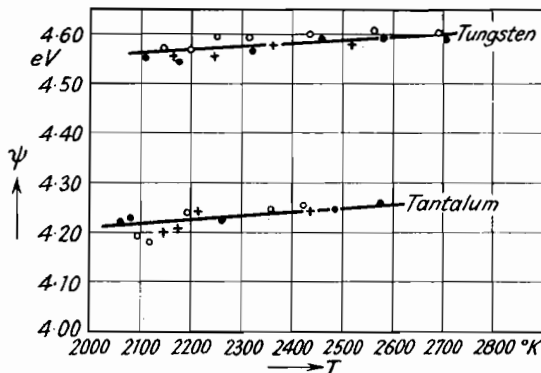


Fig. 59.—Temperature Dependence of the Work Functions  $\psi$  of Tungsten and Tantalum (Krueger and Stabenow<sup>2</sup>).

occurring in equation (75) for the work function of these cathodes. Zwicker<sup>1</sup> assumed such a temperature-dependence and gave some theoretical reasons for it.

The measurements of the temperature coefficient which have been carried out for atomic film cathodes have been discussed in detail by Gysae and Wagener.<sup>3</sup> The temperature coefficient of  $\bar{\psi}$  was determined by direct calculation from the emission equation (King<sup>1</sup> for W-Th) and by means of the photo-electric line (Suhrmann and Deponte<sup>2</sup> for Ni-Ba). A temperature coefficient  $d\bar{\psi}/dT$  of some  $10^{-4}$  eV/degree was obtained, which is of the order of the temperature coefficient, due to taking the mean, which was calculated by Gysae and Wagener<sup>3</sup> (cf. Sec. 6). The temperature coefficient of the arithmetic mean value  $\tilde{\psi}$  was measured several times by the displacement of the characteristic, always for W-Th (D. B. Langmuir,<sup>1</sup> Reimann,<sup>2</sup> and Gysae<sup>1</sup>). The results of these

TABLE VII

*Work Functions  $\psi$  of Atomic Film Cathodes*

Cathode	Year of Measurement	Method	Measured by	$\psi$ (eV)	A
W-Cs	1929	contact potential (displacement of characteristic).	Langmuir and Kingdon <sup>2</sup>	1.74	—
	1933	calculated from the ratio W-Cs-emission by W-emission.	Langmuir and Taylor <sup>3</sup>	1.64	—
	1938	photo-electric	Mayer <sup>2</sup>	1.70	—
	1940	field emission	Haefer <sup>1</sup>	1.50	—
W-Ba	1932	Richardson method	Becker <sup>1</sup>	2.07	—
	1934	Richardson method	Ryde and Harris *	1.56	1.5
	1940	field emission	Haefer <sup>1</sup>	1.63	—
W-Th	1927	Richardson method	Dushman and Ewald <sup>1</sup>	2.62	3.0
	1929	contact potential (displacement of characteristic).	Langmuir and Kingdon <sup>2</sup>	3.08	—
	1933	Richardson method	Brattain and Becker <sup>1</sup>	2.86	15.5
	1937	Richardson method	Reimann <sup>2</sup>	2.77	6.5
	1937	contact potential (displacement of characteristic).	Reimann <sup>2</sup>	2.86	—
Ta-Th	1944	Richardson method	Gallagher <sup>1</sup>	2.52	—
W-O	1929	contact potential (displacement of characteristic).	Langmuir and Kingdon <sup>2</sup>	(5.34)	—
	1935	contact potential (displacement of characteristic).	Reimann <sup>1</sup>	6.24	—
Pt-O	1939	contact potential (magnetic method).	Oatley <sup>2</sup>	6.55	—
Ni-O	1939	contact potential (displacement of characteristic).	Bosworth <sup>1</sup>	6.34	—
W-O-Cs	1929	contact potential (displacement of characteristic).	Langmuir and Kingdon <sup>2</sup>	1.44	—
W-O-Ba W-Ba-O	1934	Richardson method	Ryde and Harris *	1.34	0.18
	1934	Richardson method	Ryde and Harris *	1.9-2.5	—

\* Cf. A. L. Reimann, *Thermionic Emission*, 1934, p. 159.

experiments do not correspond at all; they not only differ in the absolute value, but also in the sign. Further measurements must therefore be carried out in order to find out if the arithmetic mean value  $\bar{\psi}$  and the individual values of the work function are more dependent on temperature than the work functions of pure metals.

TABLE VIII

*Temperature Coefficient  $d\psi/dT$  of the Work Function of Pure Metals*

Material	Year of measurement	Method	Measured by	Temperature range ( $^{\circ}$ K.)	$d\psi/dT$ (eV/degree)
Be	1934	photo-electric line	Suhrmann and Schallmanach. <sup>3</sup>	80–300 $^{\circ}$	$1 \times 10^{-4}$
Bi	1934	photo-electric line	Suhrmann and Schallmanach. <sup>3</sup>	80–300 $^{\circ}$	$1 \times 10^{-4}$
Mo	1932	photo-electric frequency limit.	Du Bridge and Roehr <sup>3</sup>	300 $^{\circ}$ –900 $^{\circ}$	$6 \times 10^{-5}$
Pd	1932	photo-electric frequency limit.	Du Bridge and Roehr <sup>3</sup>	300 $^{\circ}$ –1100 $^{\circ}$	$1.3 \times 10^{-5}$
Ta	1931	photo-electric frequency limit.	Fowler <sup>1</sup>	300 $^{\circ}$ –1000 $^{\circ}$	$7 \times 10^{-5}$
	1935	photo-electric frequency limit.	Cardwell <sup>2</sup>	300 $^{\circ}$ –1000 $^{\circ}$	$7 \times 10^{-5}$
	1935	cooling effect	Krueger and Stabenow <sup>1</sup>	2000 $^{\circ}$ –2600 $^{\circ}$	$6 \times 10^{-5}$
W	1935	cooling effect	Krueger and Stabenow <sup>1</sup>	2100 $^{\circ}$ –2700 $^{\circ}$	$6 \times 10^{-5}$
	1937	Zisman method	Waterman and Potter <sup>1</sup>	300 $^{\circ}$ –950 $^{\circ}$	$6 \times 10^{-5}$
	1937	displacement of characteristic.	Reimann <sup>2</sup>	300 $^{\circ}$ –1100 $^{\circ}$	$6 \times 10^{-5}$
	1940	Zisman method	Potter <sup>1</sup>	300 $^{\circ}$ –950 $^{\circ}$	$6.3 \times 10^{-5}$

## REFERENCES

- AHEARN, A. I. (1) *Physic. Rev.* 44 (1933), 277.  
 ANDERSON, P. A. . (1) *Physic. Rev.* 47 (1935), 958.  
                      (2) *ibid.* 49 (1936), 320.  
                      (3) *ibid.* 54 (1938), 753.  
                      (4) *ibid.* 57 (1940), 122.  
                      (5) *ibid.* 59 (1941), 1034.  
                      (6) *ibid.* 75 (1949), 1205.  
                      (7) *ibid.* 76 (1949), 388.
- APKER, L. (1) TAFT, E., and DICKEY, J., *Physic. Rev.* 73 (1948), 46.
- ARIZUMI, T. (1) *J. Phys. Soc. Japan* 3 (1948), 1.  
                      (2) *Ibid.* 3 (1948), 186
- BECKER, J. A. (1) *Trans. Faraday Soc.* 28 (1932), 151  
                      (2) and BRATTAIN, W. H., *Physic. Rev.* 45 (1934), 694.
- BOSWORTH, R. C. L. (1) *Trans. Faraday Soc.* 35 (1939), 397.
- BRATTAIN, W. H. (1) and BECKER, J. A., *Physic. Rev.* 43 (1933), 428.
- DU BRIDGE, L. A. (1) *Physic. Rev.* 31 (1928), 236.  
                      (2) *ibid.* 32 (1928), 961.  
                      (3) and ROEHR, W. W., *ibid.* 39 (1932), 99.  
                      (4) *ibid.* 42 (1932), 52.
- BRAUN, A. (1) and BUSCH, G., *Helv. Physica Acta* 20 (1947), 33.
- CARDWELL, A. B. (1) *Physic. Rev.* 38 (1931), 2041.  
                      (2) *ibid.* 47 (1935), 628.  
                      (3) *ibid.* 76 (1949), 125.
- CASHMAN, R. J. (1) *Physic. Rev.* 54 (1938), 971.  
                      (2) and BASSOE, E., *ibid.* 55 (1939), 63.
- DAVISSON, C. (1) and GERMER, L. H., *Physic. Rev.* 20 (1922), 300.  
                      (2) *ibid.* 30 (1927), 634.
- DEMSKI, A. (1) *Physik. Z.* 30 (1929), 291.
- DIXON, E. H. (1) *Physic. Rev.* 37 (1931), 60.
- DUSHMAN, S. (1) and EWALD, I. W., *Physic. Rev.* 29 (1927), 857.
- FARNSWORTH, H. E. (1) and WINCH, R. P., *Physic. Rev.* 58 (1940), 812.
- FISKE, M. D. (1) *Physic. Rev.* 61 (1942), 513.
- FLEMING, G. M. (1) and HENDERSON, J. E., *Physic. Rev.* 58 (1940), 887.
- FOWLER, R. H. (1) *Physic. Rev.* 38 (1931), 45.
- FOX, W. (1) and BOWIE, M., *Physic. Rev.* 44 (1933), 345.
- FREITAG, H. (1) and KRUEGER, F., *Ann. Phys.* 21 (1934), 697.
- GALLAGHER, Ch. J. (1) *Physic. Rev.* 65 (1944), 46.
- GERICKE, H. (1) *Physik Z.* 37 (1936), 327.
- GERMER, L. H. (1) *Physic. Rev.* 25 (1925), 795.
- GLASOE, N. (1) *Physic. Rev.* 38 (1931), 1490.
- GLOCKLER, G. (1) and SAUSVILLE, J. W., *J. Electrochem. Soc.* 95 (1949), 292.
- GOSS, W. (1) and HENDERSON, J. E., *Physic. Rev.* 56 (1939), 857.
- GROVER, H. (1) *Physic. Rev.* 52 (1937), 982.

# THE OXIDE-COATED CATHODE

- GYSAE, B. (1) Thesis, Technical University, Berlin, 1938.  
 (2) and WAGENER, S., *Z. techn. Physik* 19 (1938), 264.  
 (3) and WAGENER, S., *Z. Physik* 115 (1940), 296.
- HAEFER, R. (1) *Z. Physik* 116 (1940), 604.
- HEINZE, W. (1) *Ann. Phys.* 16 (1933), 41.  
 (2) *Z. Physik* 109 (1938), 459.  
 (3) and WAGENER, S., *ibid.* 110 (1938), 164.
- HENDERSON, J. E. (1) and DAHLSTROM, R. K., *Physic. Rev.* 55 (1939), 473.
- HERRING, C. (1) *Physic. Rev.* 59 (1941), 889.  
 (2) and NICHOLS, M. H., *Rev. mod. Phys.* 21 (1949), 185.
- HOLE, W. L. (1) and WRIGHT, R. W., *Physic. Rev.* 56 (1939), 785.
- IVEY, H. F. (1) *Physic. Rev.* 76 (1949), 567.
- JAMISON, N. C. (1) and CASHMANN, R. J., *Physic. Rev.* 50 (1936), 624.
- JOHNSON, H. C. (1) and VICK, F. A., *Proc. Roy. Soc. (A)* 158 (1937), 35.
- JOHNSON, R. P. (1) *Physic. Rev.* 54 (1938), 459.
- JUPNIK, H. (1) *Physic. Rev.* 60 (1941), 884.
- KING, A. (1) *Physic. Rev.* 53 (1938), 570.
- KLUGE, W. (1) *Physik Z.* 39 (1938), 582.  
 (2) and STEYSKAL, H., *Z. Physik* 116 (1940), 415.
- KRUEGER, F. (1) and STABENOW, G., *Ann. Phys.* 22 (1935), 713.
- LANGMUIR, I. (1) *Physic. Rev.* 2 (1913), 450.  
 (2) and KINGDON, K. H., *ibid.* 34 (1929), 129.  
 (3) and TAYLOR, J. B., *ibid.* 44 (1933), 423.
- LANGMUIR, D. B. (1) *Physic. Rev.* 49 (1936), 428.
- MANN, M. M. (1) and DU BRIDGE, L. A., *Physic. Rev.* 51 (1937), 120.
- MAURER, R. J. (1) *Physic. Rev.* 57 (1940), 653.
- MAYER, H. (1) *Ann. Phys.* 29 (1937), 129.  
 (2) *ibid.* 33 (1938), 419.
- MEYERHOF, W. E. (1) and MILLER, P. H., *Rev. Sci. Instr.* 17 (1946), 15.
- MÖNCH, G. (1) *Z. Physik* 65 (1930), 233.
- NORDHEIM, L. W. (1) *Z. Physik* 46 (1928), 852.
- NOTTINGHAM, W. B. (1) *Physic. Rev.* 47 (1935), 806.  
 (2) *ibid.* 58 (1940), 927.
- OATLEY, C. W. (1) *Proc. Roy. Soc.* 155 (1936), 218.  
 (2) *Proc. Phys. Soc.* 51 (1939), 318.
- POTTER, I. G. (1) *Physic. Rev.* 58 (1940), 623.
- RECKNAGEL, A. (1) *Z. Physik* 98 (1936), 355.
- REIMANN, A. L. (1) *Philos. Mag. J. Sci.* 20 (1935), 594.  
 (2) *Proc. Roy. Soc. (A)* 163 (1937), 499.  
 (3) *Proc. Phys. Soc.* 50 (1938), 496.
- RENTSCHLER, H. C. (1) HENRY, D. E., and SMITH, K. D., *Rev. Sci. Instr.* 3 (1932), 794.
- RICHARDSON, O. W. (1) *Emission of Electricity from Hot Bodies* (1921), 81.  
 (1) *Z. techn. Physik* 6 (1925), 633.  
 (2) *Z. Physik* 36 (1926), 750.  
 (3) *ibid.* 41 (1927), 530.
- SANO, S. (1) *Electrotech. Journal* 5 (1941), 78.

MEASURING THE WORK FUNCTIONS OF METALS

- SCHOTTKY, W. (1) *Handb. d. Experimentalphysik* XIII/2 (1928), 45.
- SEELEY, S. (1) *Physic. Rev.* 59 (1941), 75.
- SEIFERT, R. L. E. (1) and PHIPPS, T. E., *Physic. Rev.* 56 (1939), 652.
- SUHRMANN, R. (1) *Z. Physik* 54 (1929), 99.  
 (2) and DEPONTE, R., *ibid.* 86 (1933), 615.  
 (3) and SCHALLMANACH, A., *Zeitschr. f. Physik* 91 (1934), 775.  
 (4) and v. EICHBORN, J. L., *Z. Physik* 107 (1937), 523.  
 (5) and PIETRZIK, J., *Zeitschr.f. Physik* 122 (1944), 600.
- TONKS, L. (1) *Physic. Rev.* 28 (1931), 1030.
- VAN VELZER, H. L. (1) *Physic. Rev.* 44 (1933), 831.
- WAHLIN, H. B. (1) and SORDAHL, L. O., *Physic. Rev.* 45 (1934), 886.  
 (2) and REYNOLDS, I. A., *ibid.* 48 (1935), 751.  
 (3) and WHITNEY, L. V., *ibid.* 50 (1936), 735.  
 (4) and WHITNEY, L. V., *J. Chem. Phys.* 6 (1938), 594.  
 (5) *Physic. Rev.* 61 (1942), 509.  
 (6) *ibid.* 73 (1948), 1458.
- WAGNER, C. (1) *Ann. d. Physik* 6 (1930), 370.
- WARNER, A. H. (1) *Physic. Rev.* 38 (1931), 1871.
- WATERMAN, A. T. (1) and POTTER, J. G., *Physic. Rev.* 51 (1937), 63.
- WEHNELT, A. (1) and JENTZSCH, F., *Ann. Physik* 28 (1909), 537.
- WHITNEY, L. V. (1) *Physic. Rev.* 50 (1936), 1154.
- WIGNER, E. (1) *ibid.* 49 (1936), 696.
- WILSON, H. A. (1) *Philos. Trans. Roy. Soc. London (A)* 208 (1908), 251.
- WRIGHT, R. W. (1) *Physic. Rev.* 60 (1941), 465.
- ZISMAN, W. A. (1) *Rev. Sci. Instr.* 3 (1932), 367.
- ZWIKKER, C. (1) *Physik Z.* 30 (1929), 578.

## CHAPTER 3

### PHENOMENA IN IONIC SOLIDS

In the previous two chapters thermionic emission from metals, which is of fundamental importance for the physics of the oxide-coated cathode, has been discussed in detail. As the oxide cathode, however, is not a metal but an ionic solid, many phenomena, only observed with such solids, are also of importance. These phenomena will now be dealt with.\*

#### 13. Formation of Ionic Solids and Lattice Defects in such Solids

The best example to use in our discussion is sodium chloride, which has been the subject of most investigations. The two components of this compound, considered as independent atoms, have the following electron configuration (cf. Table I):

	1s	2s	2p	3s	3p	3d
Na	2	2	6	1	—	—
Cl	2	2	6	2	5	—

In order to calculate the formation of the NaCl crystal lattice from the atoms concerned, it will be convenient to consider one sodium and one chlorine atom at an infinite distance from each other. It may be assumed that these two atoms are at first ionized. During this ionization the 3s-electron of the Na passes into the 3p-level of the Cl, and the highest energy levels of the resulting two ions will therefore be fully occupied as are the corresponding levels in a rare gas atom. The two oppositely charged ions attract each other according to Coulomb's law, and they will approach up to a distance of half the lattice constant  $d$ . During this process the energy  $e^2/(d/2)$  is gained for every pair of ions. The sum of this energy for all the pairs of ions forming the NaCl crystal gives the so-called lattice energy which is gained during the formation

\* Only the fundamentals of some of these phenomena can be given here. Details are obtained from *Electronic Processes in Ionic Crystals*, N. F. Mott, R. W. Gurney, Oxford, 1940.

of the whole NaCl crystal lattice. If the sum is calculated for the sodium chloride lattice and the result related to one pair of ions, the value  $1.75e^2/(d/2)$  is obtained.\*

This value is only a first approximation, as the ions should not be considered as inelastic balls with the radius  $d/4$ . The approach of the ions to a distance of less than  $d/2$  is prevented by repulsive forces between the electrons of the two ions, which are the exchange forces of wave mechanics. When the equilibrium distance  $d/2$  is reached, these repulsive forces are as large as the attracting Coulomb force and prevent a further approach. The energy  $E_{rep}$  which must be supplied for overcoming these repulsive forces must be deducted from the energy which is gained due to the Coulomb force. A more accurate value of the lattice energy therefore is:

$$E_L = 1.75 \frac{e^2}{d/2} - E_{rep} \quad . . . . . \quad (111)$$

As the repulsive forces are only effective for very small distances between the two ions and as they decrease rapidly with increasing distance, the work  $E_{rep}$  which must be done against these forces is relatively small. Exact calculations show that this work amounts to only 10% of the total lattice energy. For sodium chloride, for instance ( $d=5.628 \text{ \AA.}$ ), the first term in (111) gives 8.9 eV, while the work  $E_{rep}$  only amounts to 1.0 eV, giving a total lattice energy  $E_L=7.9 \text{ eV}$ .

It has been assumed so far that the crystal lattice considered is ideal, which means that all ions are bound to sites determined by the geometry of the lattice. But really such an ideal lattice will only exist at zero temperature. As was first pointed out by Wagner and Schottky,<sup>1</sup> a crystal lattice at higher temperatures will show deviations from the ideal array which are due to the thermal vibrations of the ions. These vibrations are statistically distributed and in some cases are so large that the ions concerned can gain the energy which is necessary for escape from their normal sites.

By such a removal a so-called lattice defect is produced and the two main possibilities for such a defect are illustrated for a compound AB in Figs. 60 and 61. As shown in Fig. 60, the ions may move into the interstices of the crystal lattice, leaving a vacancy in the lattice behind them. Such a defect, consisting of a vacancy and an interstitial ion, is called a Frenkel defect. The second possibility,

\* The details of this calculation may be obtained from F. Seitz, *The Modern Theory of Solids*, 1940.

shown in Fig. 61, is that some ions leave the crystal lattice completely, and that only a corresponding number of vacancies remain. The stoichiometric equilibrium in this case can only be maintained

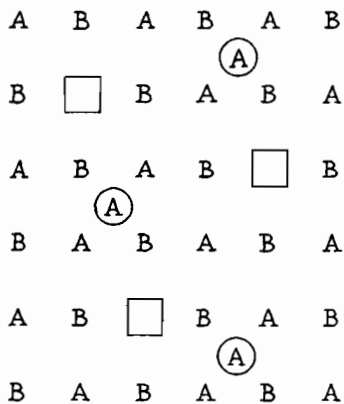


Fig. 60.—Frenkel Defects.

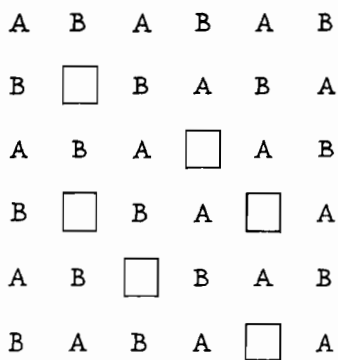


Fig. 61.—Schottky Defects.

Figs. 60–61.—The Different Possibilities for Lattice Defects.

if equal numbers of vacancies in the lattice of A-ions and in the lattice of B-ions are formed. An appropriate pair of vacancies is then called a Schottky defect.

As Wagner and Schottky<sup>1</sup> showed, there is a thermodynamical

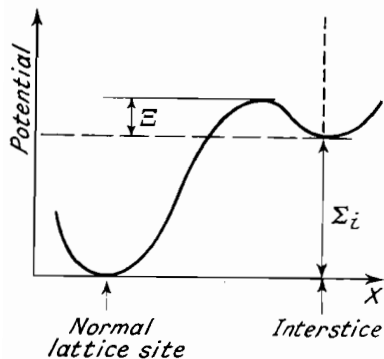


Fig. 62.—Potential Variation for the Passage of an Ion from a Normal Lattice Site to an Interstice.

equilibrium between the ions in normal positions and the ions which have moved from their normal positions and have so given rise to the formation of defects. For estimating the number of defects the Frenkel type (Fig. 60) may be considered first. The passage of an ion from its normal place to an interstice can be connected with a potential variation, which is shown in Fig. 62. According to this figure,  $E_{\Sigma_i}$  denotes the total change in the potential energy of the ion

as it passes from a normal place to an interstice, while the potential barrier, which must be assumed to exist in front of the interstice, is denoted by  $E_z$ . Then the number  $n_1$  of ions passing

from normal places to interstices per unit time will be proportional to the total number  $n$  of the ions and to the number of those ions whose kinetic energy is larger than  $E_{\Sigma_i} + E_S$ . As this latter number is proportional to  $\exp[(E_{\Sigma_i} + E_S)/kT]$  according to Maxwell's distribution law,  $n_1$  is given by:

$$n_1 = n e^{-(E_{\Sigma_i} + E_S)/kT} \dots \dots \dots \quad (112)$$

The number  $n_2$  of ions passing from an interstice to a normal lattice site will be proportional to the number  $n_i$  of interstices occupied, to the probability  $n_i/n$  of finding a normal lattice site unoccupied, and to the number of those ions in the interstices whose kinetic energy is larger than  $E_S$ . Hence:

$$n_2 = \frac{n_i^2}{n} e^{-E_S/kT} \dots \dots \dots \quad (113)$$

If an equilibrium is established the number of ions passing in the two directions must be the same, or  $n_1 = n_2$ . From this and the two above equations it follows:

$$\gamma = \frac{n_i}{n} = e^{-E_{\Sigma_i}/2kT} \dots \dots \dots \quad (114)$$

where  $\gamma$  is called the degree of disorder. According to this equation the degree of disorder depends exponentially on the energy  $E_\Sigma$ , named energy of disorder.

If considering the Schottky defects, let  $E_{\Sigma_v}$  denote the energy which must be supplied for producing a pair of vacancies (one at an A-lattice site and one at a B-lattice site, cf. Fig. 61). Then according to Schottky<sup>1</sup> the degree of disorder  $\gamma = n_v/n$ , where  $n_v$  denotes the number of pairs of vacancies, is also given by an equation similar to (114):

$$\gamma = \frac{n_v}{n} = e^{-E_{\Sigma_v}/2kT} \dots \dots \dots \quad (115)$$

The calculation of  $E_{\Sigma_v}$  in this case was carried out by Schottky<sup>1</sup> and Mott and Littleton.<sup>1</sup> Only a brief outline of the method of calculation will be given here. The removal of a positive ion from its normal place in the crystal lattice to infinity is considered first. The energy necessary for this removal would be equal to the lattice energy  $E_L$  if the variation of the electrical field inside the crystal, produced by the removal, could be neglected. This variation, however, cannot be neglected. The electrical field produced by

the absence of the ion polarizes the medium surrounding the vacant ion site. As the energy of the polarization field is of the same order as the lattice energy, the former must be taken into account when calculating  $E_{\Sigma v}$ . Let  $E_{pol}^+$  denote the polarization energy at the vacant positive ion site. Then the energy necessary for bringing the positive ion to infinity will be  $E_L - E_{pol}^+$ . The value of the polarization energy  $E_{pol}$  is:

$$E_{pol} = \frac{e^2}{2r} \left(1 - \frac{1}{\epsilon}\right) \quad . . . . . \quad (116)$$

where  $\epsilon$  denotes the dielectric constant and  $r$ , referring to the extension of the polarization field in the crystal, is of the order of the interatomic distance.

An amount of energy corresponding to that given above must be supplied for removing a negative ion from its normal place. Ultimately the two ions must be brought from infinity to the surface of the crystal and placed there. The energy gained during this latter process is equal to the lattice energy, and the total energy necessary for producing a pair of vacancies will be:

$$\begin{aligned} E_{\Sigma v} &= 2E_L - E_{pol}^+ - E_{pol}^- - E_L \\ \text{or } E_{\Sigma v} &= E_L - E_{pol}^+ - E_{pol}^- \quad . . . . . \end{aligned} \quad (117)$$

If now a special compound is considered, the type of defect which requires the smallest energy  $E_{\Sigma}$  will have the highest degree of disorder and will be preferred. The calculation of the respective energies, therefore, gives a means for discriminating between the different types of lattice defects. In this manner Schottky<sup>1</sup> found that the type shown in Fig. 61 (Schottky type) is realized for sodium chloride.

TABLE IX

*The Energy of Disorder  $E_{\Sigma}$  and its Constituents for Different Alkali Halides  
(Mott and Littleton<sup>1</sup>)*

Material	NaCl	KCl	KBr
$E_{pol}^+$	3.32	2.71	2.68
$E_{pol}^-$	2.76	2.39	2.31
$E_L$	7.94	7.18	6.91
$E_{\Sigma}$	1.86	2.08	1.92

The value of the energy  $\Sigma_v$  calculated for NaCl is  $\Sigma_v = 1.86$  eV. The values of the individual terms in equation (117) as calculated

by Mott and Littleton<sup>1</sup> for different alkali halides are given in Table IX. The number of pairs of vacancies calculated from equation (115) for sodium chloride is shown by Fig. 63.

The question as to which type of defect predominates may also be roughly decided from geometrical considerations. If, for instance, one of the ions in the lattices is small compared with the other, these small ions will readily fit into the interstices, and Frenkel defects

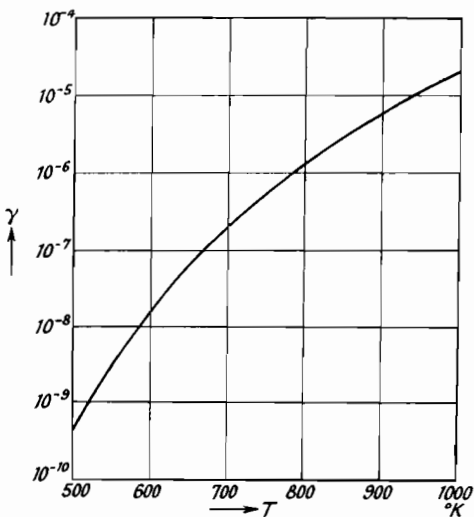


Fig. 63.—Number of Pairs of Vacancies in Sodium Chloride as a Function of Temperature.

will be preferred. If, on the other hand, the two types of ions are of about the same size, the Schottky defects will have a higher probability.

#### 14. Diffusion \*

The interstitial ions and the vacancies have not fixed positions in the crystal lattice but can move through the lattice with a certain mobility. This mobility of interstitial ions and vacancies is important if the thermodynamical equilibrium between ions in normal places and interstitial ions or vacancies is to be rearranged due to variations of temperature. Let us consider a crystal lattice with vacancies and assume that the temperature is increased. Then the

\* For the details of diffusion phenomena see R. M. Barrer, *Diffusion in and through Solids*, Cambridge, 1941.

equilibrium in the crystal must be adjusted to the new temperature by additional vacancies which can primarily only be formed at the boundaries of the crystal. Such a new vacancy, formed at the surface, will subsequently be occupied by an ion which is located in the layer below and a new vacancy will be produced at the position of such an ion. If this process is repeated many times, the vacancy gradually moves inwards, and the equilibrium can thus be adjusted to the value corresponding to the new temperature. A certain time will be necessary for this adjustment, and this time will depend on the mobility of the vacancies.

Furthermore, the mobility of the vacancies is important for equalizing differences in the concentration of different parts of the

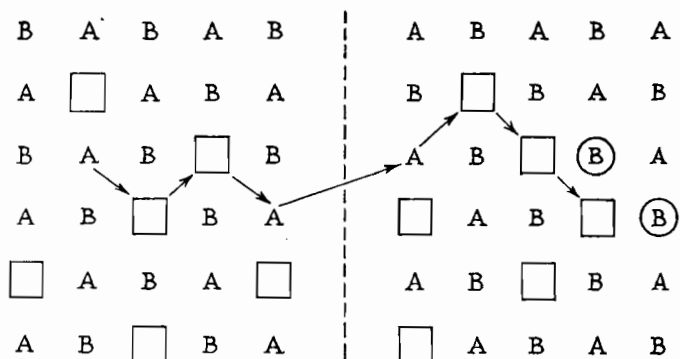


Fig. 64.—A Crystal Lattice AB with a Difference in Composition between the Two Sides.

crystal. Let us consider a compound AB whose composition is stoichiometric on the one side (left-hand side of Fig. 64) while on the other side there is a stoichiometric excess of B-ions due to an increased number of vacancies in the lattice of the A-ions (right-hand side of Fig. 64). Consequently there is a difference in the concentration of both the A- and B-ions between the right- and the left-hand side of the compound AB, and this difference in concentration will be equalized with a speed depending on temperature. This equalizing may be done by the A-ions moving over the vacancies from left to right or—expressed in another manner—by the vacancies in the lattice of the A-ions travelling from right to left. A possible path for the A-ions has been marked by arrows in Fig. 64.

The process thus resulting is called diffusion. In the case considered the A-atoms diffuse from left to right, so removing the difference in concentration and establishing the stoichiometric

equilibrium again. An example of such a diffusion is given by the tarnishing reactions which are observed during the formation of thin oxide layers at the surface of metals, e.g. iron. In this case the A-ion in Fig. 64 corresponds to iron and the B-ion to oxygen. The pure iron must be imagined on the left- and the oxidizing atmosphere on the right-hand side of the figure.

Similar diffusion phenomena are observed with metals. For example, when two metals make contact at sufficiently high temperatures one metal may diffuse into the other and a mixed crystal may be produced. Another example of these phenomena is given by the diffusion of nitrogen and carbon in iron. In this case the diffusion is not produced by the formation of vacancies but by N- or C-atoms built into the interstices of the Fe-lattice.

A short mathematical analysis of the diffusion phenomena may be given here. Let us denote the concentration of the excess material (B in Fig. 64) by  $c$ , the cross section of the material in which the diffusion occurs by  $q$ , and the amount of diffusing material moving through this cross section in the  $x$ -direction per second by  $S_x$ . Then the fundamental equation for the diffusion is:

$$S_x = -Dq \frac{dc}{dx} \quad \dots \dots \dots \quad (118)$$

The proportionality factor  $D$  in this equation is called the diffusion coefficient and is normally measured in  $\text{cm.}^2 \text{ sec.}^{-1}$ .

The relation between diffusion flow, diffusion constant, and concentration gradient given by equation (118) is of the same form as the relation between heat flow, heat conductivity, and temperature gradient. Apart from the symbols the same differential equation is therefore valid:

$$\frac{\partial c}{\partial t} = D \frac{\partial^2 c}{\partial x^2} \quad \dots \dots \dots \quad (119)$$

A main supposition for this equation is that the diffusion coefficient must be independent of concentration; this supposition is not always fulfilled. If the concentration varies not only with  $x$  but with all three co-ordinates, the second differential coefficient on the right-hand side of equation (119) is replaced by Laplace's operator. The solution of equation (119), taking account of any special boundary conditions, gives the distribution  $c(x)$  of the concentration as a function of time  $t$  with the diffusion coefficient  $D$  as a parameter.

If the diffusion coefficient  $D$  is to be ascertained, the distribution of the concentration must be computed for the experimental configuration and the values obtained must be compared with the measured distribution. In order to simplify calculations and measurements, the experimental configuration will be made as simple as possible. The concentration may be measured at different places of the material by the usual methods of chemical analysis. If the measurement needs to be more sensitive, either spectographic analysis or radioactive methods, using radioactive tracers as

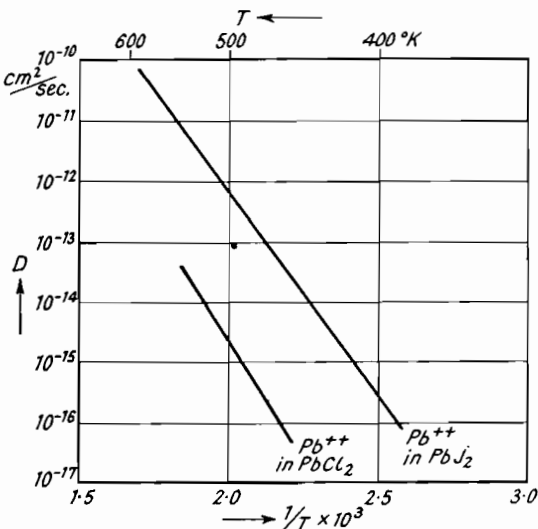


Fig. 65.—Diffusion Coefficient  $D$  of  $\text{PbCl}_2$  and  $\text{PbI}_2$  as a Function of Temperature (Hevesey and Seith,<sup>1</sup> Seith<sup>2</sup>).

diffusing material, can be employed. If the diffusion of thin surface layers into a basic material is examined, these layers can be detected by measuring their lattice spacing by electron diffraction.

The diffusion coefficient depends on temperature to a high degree. The law for this temperature-dependence is obtained by using equation (114) for the degree of disorder as a function of temperature. If the Frenkel type of lattice defect is considered, the number of diffusing ions is proportional firstly to the total number  $n_i$  of the ions in the interstices resulting from (114) and secondly to the number of ions of this total which can pass from the interstices to the vacancies. As this latter number is proportional to  $e^{-E_d/kT}$

the number of diffusing ions and the diffusion coefficient  $D$ , according to (118), is given by:

$$D = D_0 e^{-(\frac{1}{2}E_{\Sigma i} + E_S)/kT} \dots \dots \dots \quad (120)$$

Accordingly the diffusion coefficient depends on temperature by an exponential function which may be written in a shorter form:

$$D = D_0 e^{-E_r/kT} \dots \dots \dots \quad (121)$$

The energy  $E_r$  is called activation energy.

If the logarithm of the diffusion coefficient is plotted against  $1/T$  in the usual manner, a straight line will be obtained and the activation energy can be calculated from the slope of this line. Experiments confirm this result, as shown by Fig. 65 for the diffusion of  $Pb^{++}$  ions in  $PbCl_2$  and  $PbI_2$  measured by Hevesey and Seith<sup>1</sup> and Seith<sup>2</sup> by means of radioactive lead. The activation energies calculated for the two above cases are 1.55 eV for  $Pb^{++}$  in  $PbCl_2$  and 1.3 eV for  $Pb^{++}$  in  $PbI_2$ ; the corresponding values for  $D_0$  are 7.8 and 4.0 respectively.

## 15. Ionic Conduction

The motion of ions in a crystal lattice cannot only be brought about by differences in concentration but also by applying an electrical field to the crystal. Ionic conduction is then produced which is measured by the ionic conductivity  $\kappa_i$ . The principal laws for ionic conduction in solids are similar to those for conduction in liquids (electrolytes) and are the following:

(a) Faraday's law is valid, according to which an electrical charge of the amount  $Le=96,500$  coulomb is needed for depositing at the electrodes a gram-equivalent of the ions concerned, i.e. the quantity  $A/\vartheta$  ( $\vartheta$ =valency).

(b) The velocity of the ions per unit electrical field is called the ionic mobility  $u_i$ . The density  $j_i$  of the ionic current is then obtained in the usual way as the product of electrical charge and velocity:

$$j_i = n\vartheta eu_i E \dots \dots \dots \quad (122)$$

$n$  denoting the number of ions per unit volume. Using Ohms' law:

$$j_i = \kappa_i E \dots \dots \dots \quad (123)$$

the relationship:

$$u_i = \frac{\kappa_i}{n\vartheta e} \text{ cm.}^2 \text{ sec.}^{-1} \text{ volt}^{-1} \dots \dots \dots \quad (124)$$

is derived ( $n$  referring to a  $\text{cm.}^3$ ,  $\kappa_i$  in  $\Omega^{-1}\text{cm.}^{-1}$ ).

This equation is valid if the ionic conduction is produced by only one type of ions, otherwise the transport number, characterizing the share of the particular type of ion in the total ionic conductivity, must be introduced on the right-hand side of the equation.

(c) There will be a relation between the mobility  $u_i$  and the diffusion coefficient  $D$ , as both are produced by ions travelling by means of lattice defects. This relation was thermodynamically derived for solids by Wagner.<sup>2</sup> Only the result of this derivation will be given here, which is:

$$D = \frac{kT}{\vartheta e} u_i = \frac{8.62}{\vartheta} \times 10^{-5} T u_i \text{ cm.}^2 \text{ sec.}^{-1} \dots \quad (125)$$

The validity of this equation was proved experimentally by Tubandt, Reinhold, and Jost<sup>1</sup> and by Seith,<sup>1</sup> who found correspondence to within 25% between the experimental and theoretical values.

If equations (124) and (125) are combined, the following relation between the diffusion coefficient and the ionic conductivity is obtained:

$$D = \frac{5.38 \times 10^{14}}{\vartheta^2 n} T \kappa_i \dots \dots \dots \quad (126)$$

By means of this equation derivation of the diffusion coefficient may be reduced to a measurement of the ionic conductivity and *vice versa*.

The main difference between ionic and electronic conduction results from the fact that the composition of the conducting material is altered by the deposition of ions. The products of deposition accumulate at the electrodes and produce an electromotive force which is directed against the primary voltage and is called the polarization voltage. When measuring with D.C. this polarization voltage must be overcome, and ionic current only flows when this voltage has been exceeded. When the current is switched off, the polarization electromotive voltage remains and drops gradually.

The best method of measuring the ionic conductivity is by means of an A.C. bridge, as the polarization voltages are then avoided. If the measurement is carried out with D.C., attention must be paid to the polarization phenomena and to variations of chemical composition produced by electrolytic dissociation. In many cases polarization phenomena can be used for distinguishing between ionic and electronic conduction. On the other hand, the absence of polarization voltages is no proof of the non-existence of ionic conduction, because the processes at the electrodes may mask the

polarization phenomena. The most exact proof for the existence of ionic conduction is obtained by establishing Faraday's law.

On account of equation (126) the ionic conductivity depends on temperature in a similar way to the diffusion coefficient, i.e.:

$$\kappa_i = \frac{D_0}{T} e^{-E_\Gamma/kT} = A^* e^{-E_\Gamma/kT} \dots \quad (127)$$

This equation is to be replaced by a sum of two exponential functions if both ions participate in the ionic conduction, but the experimental evidence shows that in most cases only one exponential function is obtained and that usually one type of ion predominates in the phenomenon. Table XI gives conductivity values which were measured by Lehfeldt<sup>1</sup> for different alkali halides and for silver halides. These values have been extrapolated to the melting point of the materials concerned and the values so obtained together with the appropriate melting points are also included for comparison. The last row of the table gives the values for lead iodide measured by Seith.<sup>1</sup> It will be seen that the activation energy measured for ionic conduction in this case corresponds very well with the activation energy measured for diffusion in PbI<sub>2</sub> as given above.

TABLE X  
*Ionic Conductivities and Activation Energies of Ionic Solids*

Material	Activation energy (eV)	A* ( $\Omega^{-1} \text{cm.}^{-1}$ )	Melting point (°K.)	$\kappa_i$ at melting point ( $\Omega^{-1} \text{cm.}^{-1}$ )
NaF	2.25	$1.5 \times 10^6$	1265	$1.7 \times 10^{-3}$
NaCl	1.90	$1 \times 10^6$	1075	$1.3 \times 10^{-3}$
NaBr	1.78	$1 \times 10^6$	1010	$1.3 \times 10^{-3}$
NaI	1.42	$1.5 \times 10^5$	935	$4.0 \times 10^{-3}$
KF	2.35	$3 \times 10^7$	1130	$9 \times 10^{-4}$
KCl	2.06	$2 \times 10^6$	1040	$2 \times 10^{-4}$
KBr	1.97	$1.5 \times 10^6$	1015	$2 \times 10^{-4}$
KI	1.77	$3 \times 10^5$	955	$1.5 \times 10^{-4}$
AgCl	0.90	$1 \times 10^5$	730	$0.6 \times 10^{-1}$
AgBr	0.66	$6.3 \times 10^3$	700	$1 \times 10^{-1}$
PbI <sub>2</sub>	1.30	$1.2 \times 10^5$	685	$3 \times 10^{-5}$

When ionic conductivity or diffusion is measured over a wide range of temperatures, the logarithmic plot of the measured values against  $1/T$  often gives not one but two straight lines (cf. Fig. 66). Only the one of these straight lines which lies at higher temperatures is reproducible. The other one, lying at lower temperatures, has

always the same slope, but its height depends on the preceding treatment of the material in question (cf. Lehfeldt<sup>1</sup>).

For explaining this phenomenon it is assumed that the thermodynamical equilibrium of the lattice defects freezes in below a definite temperature  $T_f$ , because the time necessary for reaching the equilibrium increases more and more with decreasing temperature. Hence the degree of disorder will become constant below  $T_f$ . Then the factor  $\exp(\frac{1}{2}E_{\Sigma i}/kT)$  in equations (120) and (127) also becomes constant and the ionic conductivity (or diffusion coefficient) is given by:

$$\kappa_i = \overline{A^*} e^{-E_S/kT} \dots \dots \quad (128)$$

A plot of the ionic conductivity below  $T_f$  will therefore give a straight line with a smaller slope which only results from the energy  $E_S$ , corresponding to the potential barrier in Fig. 62.

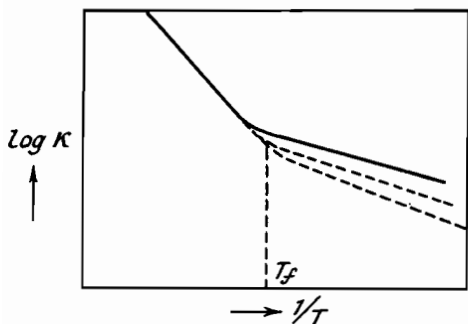


Fig. 66.—Ionic Conductivity as a Function of Temperature (Schematically)

The fact that the ionic conductivity below  $T_f$  depends on the preceding treatment may be explained by assuming this treatment to influence the number of lattice defects freezing in. Hence the

constant  $A$  varies with the preceding treatment, while the potential barrier  $E$ , determining the slope of the straight line in the conductivity plot, remains the same. Furthermore, ionic conductivity and diffusion in this temperature range are influenced by excess atoms or by atoms of foreign materials which may be built into the crystal lattice. Ionic conductivity and diffusion are therefore called "structure-sensitive" in the range below the temperature  $T_f$  which marks the beginning of freezing in, while these phenomena are called "structure-insensitive" in the range above  $T_f$  which is determined by the thermodynamical equilibrium. The "temperature of freezing in  $T_f$ " which separates the two ranges may have completely different values for different samples of the same material.

The above considerations refer to ionic solids consisting of single crystals. The phenomena observed are, of course, more involved

if agglomerations of many small crystals are investigated, as diffusion and ionic conduction may also occur along the grain boundaries in this case. It is, however, not possible at the present time to give reliable data on these additional phenomena.

### 16. Electronic Conduction

The solids considered so far were mainly halides in which ionic conduction is predominant. Conduction by electrons, however, is chiefly observed in compounds showing a small ionic conductivity, for instance in metal oxides. These compounds will be dealt with in this chapter, but for the sake of simplicity alkali halides such as

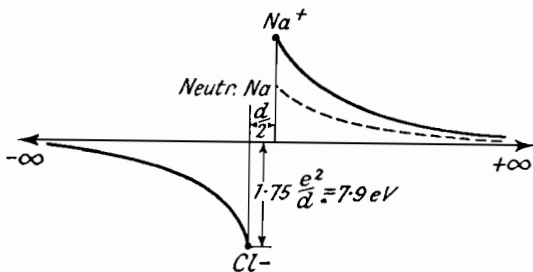


Fig. 67.—Variation of the Potential of the Electrons during the Formation of Sodium Chloride (Schematic).

sodium chloride will also be discussed, as their composition is better known than that of the metal oxides which behave in an analogous manner.

In Sec. 13 the formation of the crystal lattice of sodium chloride has been discussed in detail by considering the gradual approach of sodium and chlorine ions. During this approach the potential of the electrons of the positive sodium ion will increase by an amount equal to the lattice energy, while the potential of the electrons of the negative chlorine ion decreases by the same amount. The variation of potential which is thus obtained for the electrons of the two approaching ions is shown in Fig. 67.

The permissible energy levels of the electrons of the sodium and chlorine atoms, as given by the quantum rules (Figs. 1 and 2), will all be displaced by a similar amount. When the solid is formed these discrete energy levels widen into bands in the same manner as discussed for metals in Sec. 1. Two groups of energy bands are obtained, one associated with the sodium ion and the other with the chlorine ion. The sodium ion bands are on the average 7.9 eV

higher than the electron levels of a sodium atom, and the chlorine ion bands are depressed by a similar amount from the levels of a chlorine atom.

The configuration of the energy bands of the NaCl lattice resulting in this manner was calculated by Slater,<sup>1</sup> Shockley<sup>1</sup> and Fisher<sup>1</sup> and is shown in Fig. 68 for a cross section in the 100-direction of the NaCl crystal. As can be seen from this diagram, the 3s and 3p energy bands of Cl are still higher than the highest occupied band of Na in spite of the energy bands of Na being lifted by 7.9 eV during the formation of the lattice. As distinct from pure Na and pure Cl, all the energy bands are either fully occupied or empty, because as mentioned in Sec. 13, the 3s electron of Na has entered and filled the 3p-band of Cl. Conduction of electrons in the NaCl lattice is therefore not possible according to the considerations of Sec. 1, and hence sodium chloride is an insulator.

The same conditions as shown for NaCl exist for all saturated ionic solids in which the valencies of the constituent ions are mutually bound. All these saturated solids are therefore insulators. On the other hand, if unsaturated valencies which are not claimed chemically, exist, electronic conduction occurs (Friederich<sup>1</sup>). The electrons appropriate to these unclaimed valencies then only partly fill the highest energy band and can move in this band if an electrical field is applied. Some examples of this are quoted in Table XI, which shows that the electrical conductivity of TiO, TiN, and VC is of the same order as that of metals due to the existence of unclaimed valencies. The saturated compounds TiO<sub>2</sub>, AlN, and Al<sub>4</sub>C<sub>3</sub>, however, having no unclaimed valencies, are insulators.\*

TABLE XI  
*Conductivity and Valency of Chemical Compounds (Weise<sup>1</sup>)*

Compound	Valency electrons of the metal			Conductivity at 293° K. ( $\Omega^{-1}$ cm. <sup>-1</sup> )
	Existing	Claimed	Free	
TiO <sub>2</sub>	4	4	0	$<10^{-12}$
TiO	4	2	2	$\approx 2500$
AlN	3	3	0	$<10^{-12}$
TiN	4	3	1	$\approx 8000$
Al <sub>4</sub> C <sub>3</sub>	12	12	0	$<10^{-12}$
VC	5	4	1	$\approx 11000$

\* For exceptions from this rule and for their explanation, cf. Meyer.<sup>5</sup>

Returning to the saturated ionic compounds, electronic conduction would be possible if electrons in the full  $3p$ -Cl-band could be lifted into the empty  $3s$ -Na-band (Fig. 68). These electrons would be free to move under an applied field, thus producing electronic conductivity. Such a transference of electrons is theoretically possible at sufficiently high temperatures. The number of electrons lifted into the empty band and consequently the conductivity would then considerably increase with increasing temperature, contrary to metals which show a slight decrease in conductivity with increasing temperature. Such a conductor, which is practically an insulator at low temperatures but the conductivity of which becomes high at sufficiently high temperatures, is called a semi-conductor.

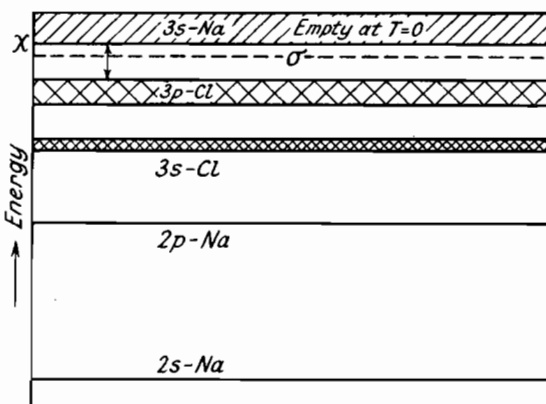


Fig. 68.—Energy Bands of Sodium Chloride.

In the case of sodium chloride, of course, the energy difference of about 7 eV between the upper limit of the  $3p$ -Cl-band and the lower limit of the  $3s$ -Na-band is so large that temperatures of about  $100,000^\circ$  would be necessary in order to lift an adequate number of electrons into the empty band. This type of electronic conduction therefore cannot be observed with NaCl, and the experimental evidence shows that there are only a few solids in which the difference between the two energy bands concerned is small enough to enable the electrons to reach the empty band at temperatures below the melting point. The phenomenon of semi-conduction when observed in compounds is usually produced by a slight deviation from the stoichiometric composition of the compound concerned. For understanding this we must consider in detail the

structure of chemical compounds whose composition is not exactly equal to the molecular proportions (non-stoichiometric).

When discussing the defects in crystal lattices in Sec. 13, it was assumed that the lattice was composed stoichiometrically. This supposition will now be dropped and in this manner two possibilities for producing a deviation from stoichiometric composition will be obtained from the two different types of defect considered in Sec. 13. The two possibilities are as follows:

(a) The interspersion of one type of the constituent ions, for instance B, into the interstices (cf. Fig. 69). An excess of B-ions or atoms is produced in this way.

(b) The formation of vacancies at the sites of only one type of the constituent ions, for instance A in Fig. 70. A defect of A-ions or, what is the same, an excess of B-ions or atoms is so obtained.

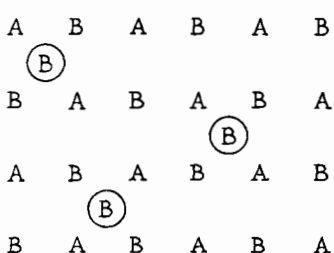


Fig. 69.—Interspersion into the Interstices.

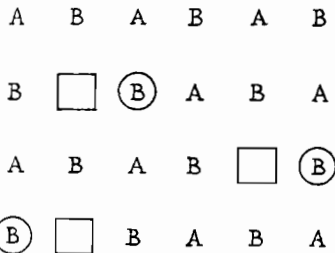


Fig. 70.—Formation of Vacancies.

Figs. 69-70.—Possibilities for Building Excess Atoms into a Crystal Lattice (Excess Atoms marked by a Circle).

The existence of this latter case was proved experimentally for iron oxide by Jette and Foote<sup>1</sup> who investigated FeO containing an excess of oxygen. The lattice constant  $d$  of this FeO which crystallizes in the cubic system was determined by taking an X-ray pattern, and the density  $\delta$  was measured too. Then the volume  $M/\delta L$  ( $M$ =molecular weight) appropriate to one molecule FeO could be calculated from the density. It was found that this volume was larger than the elementary cell  $d^3$  of the crystal lattice of FeO, which can only be explained by the existence of vacancies in the crystal lattice.

The two examples illustrated by Figs. 69 and 70 have been highly generalized, by assuming that the lattice defects are restricted to one of the constituent ions only. Actually there will always be defects for both constituents given by a thermodynamical equili-

brium, and the stoichiometric excess will be produced by the predominance of the defects for one constituent. Considering the formation of defects by vacancies, the conditions are shown by the right-hand side of Fig. 64, where there is a certain number (4) of vacancies at A-lattice sites and a smaller number (2) at B-sites, resulting in an excess in the component B.

The formation of excess atoms due to the existence of additional vacancies in the crystal lattice is especially important for the oxide-coated cathode. Another example is sodium chloride, in which, as pointed out in Sec. 13, vacancies are the preferred type of lattice defect. If a crystal of sodium chloride is heated in sodium vapour, an excess of sodium is produced in the crystal, this excess being recognized by a variation in the optical properties of the crystal.

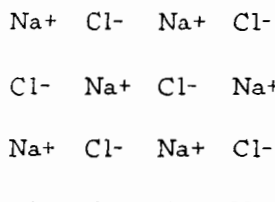


Fig. 71.—Stoichiometrically Composed.

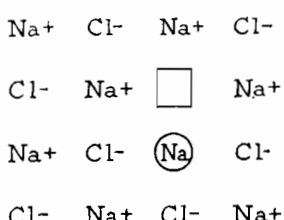


Fig. 72—With Excess Sodium.

Figs. 71-72.—The Crystal Lattice of Sodium Chloride

An additional absorption band arises which is in the visible range of frequencies and which gives a yellow colour to the crystal. These phenomena, which are also observed with other alkali halides, have been especially studied by the school of Pohl.

The excess of sodium in sodium chloride is produced by additional vacancies at the Cl-ion sites, as illustrated by Figs. 71 and 72 showing the crystal lattice without and with excess sodium. As the whole crystal must remain electrically neutral, the excess sodium cannot exist as ions. When a vacancy at a Cl-ion site is formed, an additional electron will be taken up by the crystal, and this electron will be associated with the vacant lattice site, so neutralizing the positive charge created by the vacancy. Such a combination consisting of a negative-ion site plus an electron is called an F-centre. It is, of course, also possible to think of the additional electron as being directly associated with one of the Na-ions surrounding the vacant ion site. The Na-ion concerned which is so transformed into a neutral atom is indicated by a circle in Fig. 72.

The electron which is bound to the vacancy or to the excess atom adjacent to this vacancy has special energy levels. These special energy levels are usually named impurity levels, because in the early theory of semi-conductors they were assumed to be produced by impurities.\* As the levels concerned are in fact due to the interference of the additional defects which are responsible for the deviation from the stoichiometric equilibrium, these levels will be called interference levels here. One of these levels, denoted by  $\sigma$ , has been marked in Fig. 68, showing the energy bands of sodium chloride.

The position of the interference levels has been calculated by Tibbs<sup>1</sup> and Simpson<sup>1</sup> for alkali and silver halides. An approximate idea of their position can be obtained according to Mott and Gurney † by using the analogy of a hydrogen atom. The vacant negative ion site, having a positive charge, can be compared with the positive hydrogen nucleus. Both are associated with only one electron which is bound to the positive charge. Bohr's formula for the energy levels of the hydrogen electron can therefore be applied to the interference levels of the vacant site, provided the different dielectric behaviour of the interior of the ionic lattice is accounted for. The formula so obtained for the gap between the empty band and the lowest interference level is

$$\chi - \sigma = \frac{2\pi^2 m^* e^4}{h^2 \epsilon_{eff}^2} = \frac{1}{\epsilon_{eff}^2} \frac{m^*}{m} \times 13.5 \text{ eV} . . . \quad (129)$$

$m^*$  denotes the so-called effective mass of the electron in the crystal lattice which is slightly different from the electronic mass in vacuum, while  $\epsilon_{eff}$  is an effective dielectric constant which is somewhere in between the dielectric constant for a statical field and that for optical wavelengths. The above formula shows that the position of the interference levels depends on the value of the dielectric constant and that their distance from the empty band above will decrease with increasing dielectric constant.

An important factor to note is that the energy difference between such an interference level and the empty 3s-Na-band is much smaller

\* The term "impurity levels" is justified in semi-conductors consisting of one element only such as: As, B, Ge, Si, Te. These element-semi-conductors whose conductivity is produced by impurities foreign to the element in question will not be considered here. The discussion will be confined to compound-semi-conductors such as oxides, sulphides, etc.

† N. F. Mott, R. W. Gurney, *Electronic Processes in Ionic Crystals*, Oxford, 1940, p. 113.

(a few tenths of 1 eV) than that existing between the  $3s$ -Na-band and the fully occupied  $3p$ -Cl-band. A relatively small energy is therefore necessary for lifting an electron from the interference level into the empty  $3s$ -band and for obtaining an electronic conduction in this band. This energy can be supplied either photo-electrically or thermally. The photo-electrical excitation of the electrons in the interference levels of alkali halides was studied by Pohl and his co-workers and will not be discussed in detail here. If the thermal excitation is considered, the number of electrons in the energy band empty at  $T=0$  and hence the electronic conductance will again increase very much with increasing temperature. Another type of semi-conduction is obtained which is due only to the existence of excess atoms. As will be shown below, this type of semi-conductance is divided into two sub-types, and three types of semi-conductors are therefore distinguished altogether. They are:

(a) *Intrinsic Semi-Conductors.* This type is obtained if the electrons, as discussed above, are excited from the highest energy band which is fully occupied at  $T=0$  ( $3p$ -Cl in NaCl) to the lowest empty energy band ( $3s$ -Na). The latter band is called the conduction band, as conduction takes place in it. As pointed out above, this type of semi-conduction does not occur frequently.

(b) *Reduction Semi-Conductors* (electron-excess or N-type semi-conductors). In these semi-conductors a part of the non-metal ions is removed by a reducing treatment (e.g. by hydrogen) and an excess of metal atoms is thus produced. The number of removed non-metal ions or of excess metal atoms then depends on time and temperature of the reduction. The energy conditions in these semi-conductors are exactly the same as described above for NaCl, with Na in excess. A semi-conduction is produced which increases with increasing number of excess atoms. Examples of this excess semi-conduction are given in Table XII.

TABLE XII  
*Excess Semi-Conduction (Weise<sup>1</sup>)*

Compound	$\kappa$ at 293° K. ( $\Omega^{-1}$ cm. $^{-1}$ )	Compound	$\kappa$ at 293° K. ( $\Omega^{-1}$ cm. $^{-1}$ )
ZnO	$\leq 10^{-12}$	ZnO-xO	$\leq 4$
WO <sub>3</sub>	$\leq 10^{-5}$	WO <sub>3</sub> -xO	$\leq 5.5$
TiO <sub>2</sub>	$\leq 10^{-12}$	TiO <sub>2</sub> -xO	$\leq 5.0$
Fe <sub>2</sub> O <sub>3</sub>	$\leq 10^{-12}$	Fe <sub>2</sub> O <sub>3</sub> -xO	$\leq 3.4$
UO <sub>2</sub>	$\leq 10^{-6}$	UO <sub>2</sub> -xO	$\leq 10$

(c) *Oxidation Semi-Conductors* (electron-defect or P-type semi-conductors). This type of semi-conductor is the exact opposite of the type discussed previously. The compound concerned is treated in an oxidizing atmosphere, and some of the metal ions are removed from the compound by oxidation. Additional vacancies in the lattice of the metal ions are formed in this way and a defect of metal ions is produced.

As the crystal must remain electrically neutral the removal of positive metal ions must be compensated by a simultaneous removal of electrons, which may be taken from the negative ions surrounding the additional vacancies. Interference levels  $\sigma'$  are then obtained which are due to the missing electrons and which differ from

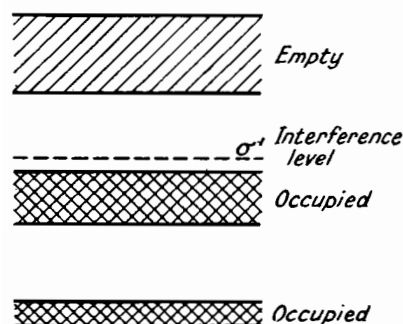


Fig. 73.—Energy Bands and Levels of an Oxidation Semi-conductor.

the interference levels in reduction semi-conductors in two ways. Firstly the interference levels now considered are normally not occupied but empty, and secondly they do not lie slightly below the conduction band but are situated a little higher than the fully occupied energy band (cf. Fig. 73). The electrons of the fully occupied band can therefore easily be lifted into the empty interference

levels by temperature excitation. In this manner a defect of electrons is produced in the highest energy band which was fully occupied before, and a conduction of electrons in this energy band is made possible. With this type of conduction the free places in the energy band, which are called electron holes, move instead of the electrons in the normal type of conduction. The type of conduction discussed now is therefore also called conduction by electron holes. Examples for this type are given in Table XIII.

TABLE XIII  
Defect Semi-Conduction (Weise<sup>1)</sup>)

Compound	$\kappa$ at 293° K. ( $\Omega^{-1}$ cm. <sup>-1</sup> )	Compound	$\kappa$ at 293° K. ( $\Omega^{-1}$ cm. <sup>-1</sup> )
CuI	$\leq 10^{-5}$	CuI + xI	$\leq 1$
Cu <sub>2</sub> O	$\leq 10^{-10}$	Cu <sub>2</sub> O + xO	$\leq 10^{-2}$
CoO	$10^{-7}$ (573° K.)	CoO + xO	$10^{-2}$ (573° K.)
UO <sub>2</sub>	$\leq 10^{-6}$	UO <sub>2</sub> + xO	$\leq 10^{-1}$

The steep rise of conductivity with increasing temperature, produced by the increasing number of electrons which are excited into the conduction band, makes the semi-conductors interesting and important for technical applications. The calculation of conductivity as a function of temperature, which was first given by A. H. Wilson,<sup>1, 2</sup> will be dealt with in the next section.

### 17. The Energy Distribution of Electrons in an Excess Semi-Conductor and the Relation between Conductivity and Temperature

Before calculating the relation between conductivity and temperature of a semi-conductor, we must discuss conduction in metals once more. Metallic conduction exists, according to the considerations in Sec. 1, if the highest energy band occupied by electrons is not fully occupied. It can then be assumed as a first approximation that the electrons in this highest energy band are able to move freely. In order to find a formula for the metallic conductivity the free electrons are assumed to move with a mean velocity  $\bar{v}$ , the three components of which have equal weight. If an electrical field is applied to the metal, the electrons acquire an additional mean velocity  $\Delta\bar{v}$  in the direction of the field. In this manner a drift of the electrons in the direction of the field is obtained, producing an electric current of density  $j$  which is equal to the product of the density of charge  $Ne$  ( $N$ , the number of the free electrons per unit volume) and of the increase in velocity  $\Delta\bar{v}$ :

$$j = Ne\Delta\bar{v} \quad \dots \quad (130)$$

On the other hand, according to Ohm's law:

$$j = \kappa E \quad \dots \quad (131)$$

$\kappa$  representing the conductivity. By comparing these two equations it is seen that the increase  $\Delta\bar{v}$  in the mean velocity, which is the only variable on the right-hand side of (130), will be proportional to the field strength. If the velocity of the electrons in the unit field, the electron mobility, is denoted by  $u$ , then  $\Delta\bar{v} = uE$  and hence:

$$j = NeuE$$

By comparing this equation with Ohm's law (131), the formula for the conductivity is derived:

$$\kappa = Neu \quad \dots \quad (132)$$

The mobility  $u$  can be obtained by considering the collisions between the electrons moving in the metal and the metal ions. The average distance which the electrons travel between two such collisions is called the mean free path. The mean free path may be

denoted by  $l$ , the time necessary for travelling this distance by  $t$ , and the acceleration, produced by the field  $E$  during the time  $t$ , by  $b$ . Then the total increase in velocity during the time  $t$  will be:

$$v = bt = \frac{eE}{m} \bar{v} \quad . . . . . \quad (133)$$

The mean increase in velocity may be equated to a half of this value, and the mobility (for  $E=1$ ) will therefore be:

$$u = \frac{el}{2mv} = 8.80 \times 10^{14} \frac{l}{\bar{v}} \text{ cm.}^2 \text{ sec.}^{-1} \text{ volt}^{-1} \quad . . . \quad (134)$$

If this value is introduced into (132) the conductivity is:

$$\kappa = \frac{Ne^2 l}{2mv} = 1.41 \times 10^{-4} N \frac{l}{\bar{v}} \Omega^{-1} \text{ cm.}^{-1} \quad . . . \quad (135)$$

( $N$  referring to 1 cm.<sup>3</sup>).

If the quantum theory is used instead of the classical laws applied above,\* the electronic mass in vacuum used in the above formulæ must be replaced by the "effective mass" of the electrons in the crystal lattice (see p. 126). The mean velocity  $\bar{v}$  is then replaced by the velocity appropriate to the limiting energy  $E_\zeta$ , as given by equation (16). The mean free path in quantum theory depends on the probability of propagation of the electron waves associated with the electrons (cf. Bloch<sup>1</sup> and Peierls<sup>2</sup>). If the crystal lattice is ideal, the propagation of the electron waves at  $T=0$  is completely unhindered, as is the propagation of light in a transparent crystal. Both the mean free path and the conductivity therefore become infinitely large for  $T=0$ . The propagation of the electron waves will be hindered only by irregularities of the lattice due to heat oscillations and to interspersed foreign atoms which produce a finite value of mean free path and conductivity. In this manner the observed decrease of the conductivity of metals with increasing temperature is explained by the fact that the heat oscillations also increase with temperature. If copper is considered, the velocity  $\bar{v}$  is  $1.58 \times 10^8$  cm./sec., the mean free path  $l=842 \times 10^{-8}$  cm. and the mobility  $u=46.8$  cm.<sup>2</sup> sec.<sup>-1</sup> volt<sup>-1</sup>; the corresponding values for nickel are  $\bar{v}=1.36 \times 10^8$  cm./sec.,  $l=266 \times 10^{-8}$  cm., and  $u=17.1$  cm.<sup>2</sup> sec.<sup>-1</sup> volt<sup>-1</sup>.

While the number  $N$  of free electrons is practically independent of temperature for metals, the conditions are quite different for semi-conductors. If an excess semi-conductor is considered the

\* Cf. N. F. Mott, H. Jones, *The Theory of the Properties of Metals and Alloys*, Oxford, 1936, p. 240.

conductivity depends on the number of electrons in the conduction band (cf. Fig. 68). This number depends very much on temperature, as has been indicated in the previous section. If therefore the electronic conductivity of semi-conductors is to be ascertained, equation (138), which was obtained for metallic conduction, can be used again, but the number  $N$  of the free electrons occurring in (135) must be calculated first. For this purpose the energy distribution of the electrons in a semi-conductor will be investigated in a similar way as was adopted for metals in Sec. 1.

It will be assumed throughout this investigation that the number of excess metal atoms per unit volume, which will be denoted by

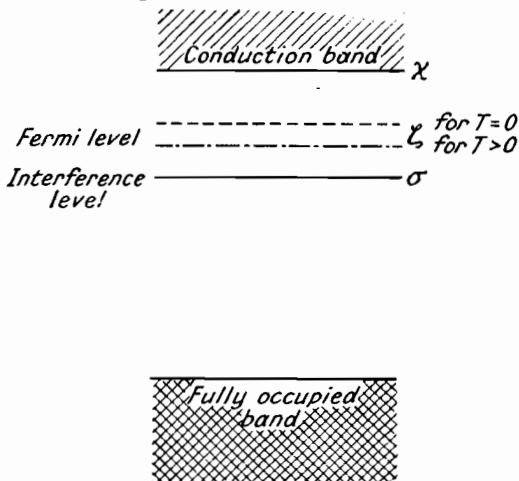


Fig. 74.—The Highest Energy Bands and Levels in an excess Semi-conductor.

$n_o$ , is independent of temperature. In agreement with Meyer and Möglich,<sup>4</sup> we confine ourselves to temperatures below the temperature  $T_f$  of "freezing in," discussed in Sec. 15, where processes such as diffusion, ionic conduction, and chemical reaction which tend to change  $n_o$  are negligibly small. The excess atoms may then be assumed to be frozen in and their number will therefore be independent of temperature.

Two more assumptions will be made for the calculation of conductivity. Firstly it will be assumed that there is only one interference level  $\sigma$  below the conduction band (cf. Fig. 74), and secondly that the number  $n_o$  of excess atoms supplying electrons to the conduction band is identical with the number of places in the crystal lattice at which the electrons may be attached at  $T=0$ . Both

assumptions will not always be fulfilled, and it will be discussed later how the result of the calculation is influenced, if one of them is not complied with.

The Fermi-statistics are again used for the investigation. The symbols for the energy values will be seen from Fig. 74, which shows the highest energy bands and levels of an excess semi-conductor. The number of excess electrons belonging to an individual excess atom at  $T=0$  will be denoted by  $G^*$ . The total number of electrons of the excess atoms is therefore equal to  $G^*n_o$ . If  $T>0$ , these  $G^*n_o$  electrons are distributed in the interference level  $E_o$  and in the conduction band, the lower limit of which is denoted by  $E_x$ .

Let  $N_o$  and  $N_x$  denote the densities of electrons in the interference level and in the conduction band respectively (numbers per unit volume), then:

$$N_o + N_x = G^*n_o \dots \dots \dots \quad (136)$$

The density  $N_o$  is obtained from the Fermi-distribution (3) for  $E=E_o$  and  $n(E)dE=n_o$ :

$$N_o = \frac{G^*n_o}{e^{(E_o - E_\zeta)/kT} + 1} \dots \dots \dots \quad (137)$$

The relation for the limiting energy  $E_\zeta$  occurring in this equation will be quite different from the relation for  $E_\zeta$  which was derived for the electrons in a metal. The new relation for semi-conductors will be calculated below.

The density  $N_x$  of electrons in the conduction band is obtained by an integration of the Fermi-distribution (3). The upper limit of this integral is independent of the width of the conduction band and can be assumed as infinite, because the number of electrons in the conduction band decreases rapidly when moving from the lower limit  $E_x$ . Hence it is:

$$N_x = \int_{E_x}^{\infty} \frac{Gn_x(E)dE}{e^{(E-E_\zeta)/kT} + 1} \dots \dots \dots \quad (138)$$

The value  $n_x(E)$  representing the number of cells in the phase volume per energy interval is given by equation (8), if the variable  $E$  in this equation is replaced by  $E^*=E-E_x$ . Then:

$$\begin{aligned} N_x &= 4\pi\sqrt{2}\frac{Gm^{3/2}}{\hbar^3} \int_0^{\infty} \frac{E^{*1/2}dE^*}{e^{[E^*-(E_\zeta-E_x)]/kT} + 1} \dots \dots \quad (139) \\ &= \frac{2G}{\sqrt{\pi}}(CT)^{3/2}J(E_\zeta - E_x) \end{aligned}$$

where  $J$  denotes the integral given by (11) and  $C$  the universal constant defined by (41a).

When evaluating  $J$  in Sec. 1, two cases were distinguished. In the applications of interest here, the condition  $(E_x - E_\zeta)/kT = -(E_\zeta - E_x)/kT \gg 1$  is normally complied with (for exceptions see p. 135). This, according to (12), means that case (b) is valid and that the approximate value of  $J$  from (19) can be used. The electron density  $N_x$  in the conduction band therefore is:

$$N_x = G(CT)^{3/2} e^{-(E_x - E_\zeta)/kT} \dots \quad (140)$$

The unknown limiting energy  $E_\zeta$  is obtained by means of equations (136) and (137), from which:

$$N_x = G^* n_\sigma - N_\sigma = G^* n_\sigma - \frac{G^* n_\sigma}{e^{(E_\sigma - E_\zeta)/kT} + 1} = \frac{G^* n_\sigma}{1 + e^{(E_\zeta - E_\sigma)/kT}} \quad (141)$$

or with  $N_x$  from (139)

$$\frac{G^* \sqrt{\pi}}{2G(CT)^{3/2}} \frac{n_\sigma}{1 + e^{(E_\zeta - E_\sigma)/kT}} = J(E_\zeta - E_x) \dots \quad (141a)$$

Using again the approximate value (19) for  $J$  and solving for  $(\chi - \zeta)$  we have:

$$\chi - \zeta = \chi - \sigma - \frac{kT}{e} \ln \frac{1}{2} \left[ \sqrt{1 + \frac{4G^* n_\sigma}{G(CT)^{3/2}} e^{(x-\sigma)/kT}} - 1 \right] \quad (142)$$

The energy  $\chi - \zeta$  (cf. Fig. 74) which must be supplied in order to lift an electron from the interference level  $\sigma$  to the lower limit of the conduction band  $\chi$  is called the internal work function.\* An approximate value for this work function can be obtained if (for  $G = G^*$ ):

$$e^{(x-\sigma)/kT} \gg \frac{(CT)^{3/2}}{4n_\sigma}$$

or according to (41a):

$$\chi - \sigma \gg \frac{kT}{e} \ln \left( 0.61 \times 10^{15} \frac{T^{3/2}}{n_\sigma} \right) \dots \quad (143a)$$

( $n_\sigma$  referring to 1 cm.<sup>3</sup>).

Using this condition, the approximate value for  $\chi - \zeta$  is given by:

$$\begin{aligned} (\chi - \zeta)^{\text{approx}} &= \frac{1}{2}(\chi - \sigma) + \frac{kT}{2e} \ln \frac{(CT)^{3/2}}{n_\sigma} \dots \dots \dots \quad (143) \\ &= \frac{1}{2}(\chi - \sigma) + 0.99 \times 10^{-4} T \times \ln \left( 2.43 \times 10^{15} \frac{T^{3/2}}{n_\sigma} \right) \end{aligned}$$

It can easily be shown that:

$$\chi - \zeta \geq (\chi - \zeta)^{\text{approx}}$$

\* The term "activation energy" which is sometimes used for  $\chi - \zeta$  will not be employed here, since this term is likewise used for  $\frac{1}{2}(\chi - \sigma)$ .

Equation (143) therefore gives a lower limit for the internal work function.

The exact value of the internal work function and the magnitude of the deviation between the exact and the approximate values can

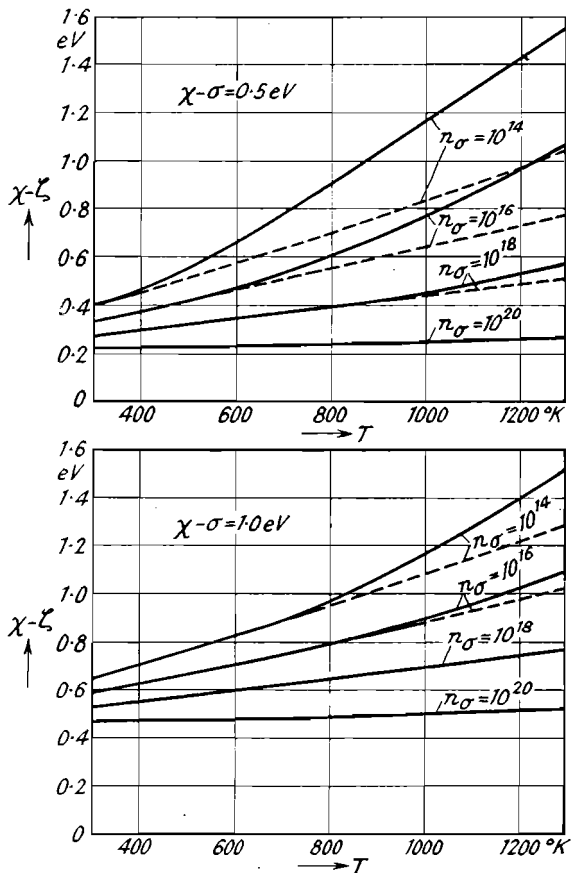


Fig. 75.—Internal Work Function  $\chi - \zeta$  of a Semi-conductor as a Function of Temperature. Exact Values full lines, Approximate Values, broken lines.

be seen from Fig. 75 for two different values of  $\chi - \sigma$ . According to this figure, the internal work function is equal to nearly half the energy difference  $\chi - \sigma$  for large values of  $n_\sigma$ , while considerably larger work functions are obtained for smaller values of  $n_\sigma$ , especially if the temperature is high at the same time. The curves given for the internal work function in Fig. 75 have not been confirmed experimentally yet, but it may be noted that the same

relations as shown in Fig. 75 are obtained by the thermodynamical calculations of Schottky.<sup>2</sup>

Apker, Taft, and Dickey<sup>1</sup> gave a method for determining the position of the Fermi-level  $\zeta$  in semi-conductors. Their method is based on the measurement of the photo-electric stopping potential described in Sec. 11.2. The semi-conductor to be examined is used as the cathode from which the photo-electrons are emitted, while the anode consists of a metal. If an excess semi-conductor is considered, the photo-electrons are emitted from the interference level  $\sigma$  while with a metal they are emitted from the Fermi level  $\zeta$ . Comparing the two cases of semi-conductor and metal emitter, the energy necessary for the emission will therefore be larger by an amount  $\zeta - \sigma$  in the case of a semi-conductor (cf. Figs. 16 and 74). This amount of energy must be added on the right-hand side of equation (107) for the stopping potential, giving

$$V_{st} = -(\hbar v - \psi_A) + \zeta - \sigma \quad \dots \quad (144)$$

from which the position of  $\zeta$  with reference to  $\sigma$  can be calculated, provided the work function of the anode is known. This method has so far only been applied to element-semi-conductors such as B, Ge, Te, As (cf. Taft and Apker<sup>1</sup>) which were measured at room temperature. Measurements for different temperatures are not known yet.

By using equation (143) the condition  $-(E_\zeta - E_\chi)/kT \gg 1$ , assumed when evaluating equation (139), can be reduced to:

$$\chi - \sigma \gg \frac{2kT}{e} = 1.72 \times 10^{-4} T \quad \dots \quad (145)$$

For  $T = 1000^\circ$  K., for example,  $\chi - \sigma \gg 0.17$  eV. If the above condition is not complied with, an exact evaluation of the integral  $J$  in (139) and (141a) is necessary. Such an evaluation has been undertaken by Shifrin,<sup>1</sup> Bush and Labhart,<sup>3</sup> and Putley.<sup>1</sup>

Equation (140) gives the density  $N_x$  of electrons in the conduction band as a function of the internal work function  $\chi - \zeta$  in the exponent. As this internal work function depends on  $T$  and  $n_o$  according to (142) and (144), it will be desirable to find another formula with an exponent which is independent of  $T$  and  $n_o$  as far as possible. Such a formula is obtained if the internal work function is replaced by the energy difference  $\chi - \sigma$  by using the respective equations. Then by means of (142):

$$N_x = \frac{1}{2} G C^{3/2} T^{3/2} e^{-e(\chi-\sigma)/kT} \left[ \sqrt{1 + \frac{4n_o}{(CT)^{3/2}} e^{e(\chi-\sigma)/kT}} - 1 \right] \quad (146)$$

while by using (143) the approximate equation:

$$N_x = GC^{3/4} n_o^{1/2} T^{3/4} e^{-e(x-\sigma)/2kT} \dots \dots \dots \quad (147)$$

or

$$N_x = 4.93 \times 10^7 G n_o^{1/2} T^{3/4} e^{-e(x-\sigma)/2kT} \text{ cm.}^{-3}$$

is obtained which is subject to the validity of condition (143a).

Finally the equation for the conductivity is derived by introducing the above values into (135). The mean velocity  $\bar{v}$  occurring in (135) may be obtained by equating the kinetic energy  $\frac{1}{2}m\bar{v}^2$  to  $\frac{3}{2}kT$ , as the number of electrons in the conduction band is small enough for the Maxwell distribution law to be valid.

Therefore:

$$\begin{aligned} \frac{1}{2}m\bar{v}^2 &= \frac{3}{2}kT \\ \bar{v} &= 0.674 \times 10^6 T^{1/2} \text{ cm./sec.} \dots \dots \end{aligned} \quad (148)$$

Using this value, we obtain from (135) and (147):

$$\begin{aligned} \kappa &= a_0 T^{1/4} e^{-5800(x-\sigma)/T} \Omega^{-1} \text{ cm.}^{-1} \\ a_0 &= 1.4 \times 10^4 \frac{l \sqrt{(n_o) T^{1/2}}}{\bar{v}} = 2.06 \times 10^{-2} l \sqrt{n_o} \dots \end{aligned} \quad (149)$$

( $l$  in cm.,  $n_o$  in  $\text{cm.}^{-3}$ ).

According to the above equation a plot of the logarithm of conductivity against  $1/T$  will give a straight line, because the effect of the factor  $T^{1/4}$  is as negligible as was the factor  $T^2$  in the Richardson equation (see Fig. 76 at lower temperatures).

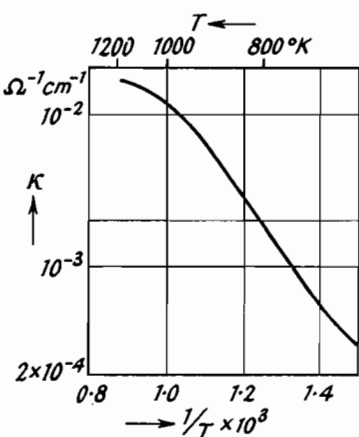


Fig. 76.—Conductivity of ZnO as a Function of Temperature (Miller<sup>1</sup>).

occurs in the constant  $a_0$ , but the determination of  $n_o$  from this constant is only possible if the mean free path or the mobility  $u$  in the conduction band is known. In addition to this a possible

temperature-dependence of the interference energy  $\chi - \sigma$  would influence the measured value of  $a_0$  to a certain degree in the same manner as the emission constant in the Richardson equation is influenced by a temperature-dependence of the work function. If such a temperature-dependence of  $\chi - \sigma$  exists, only the value of  $\chi - \sigma$  extrapolated to  $T=0$  is obtained from (149).

If condition (143a) is not fulfilled, equations (142) and (146) must be used for the internal work function and the number  $N_x$  of electrons in the conduction band, instead of the approximate equations (143) and (147). The straight line, representing the number  $N_x$  or the conductivity  $\kappa$  in the logarithmic plot, will then also be obtained at lower temperatures, but this line will bend towards the temperature axis at higher temperatures (cf. Fig. 76), thus showing that almost all the electrons from the interference levels have moved into the conduction band. A saturation condition will thus be obtained and eventually a further increase in conductivity will no longer be possible. In this event a decrease of conductivity with increasing temperature may even be observed at sufficiently high temperatures due to the decrease of the mean free path  $l$  in (135) with increasing temperature (cf. Fig. 81).

The above formulæ were derived for excess semi-conductors. They can also be applied to the other two classes, the defect and the intrinsic semi-conductors. The formulæ remain exactly the same for defect semi-conductors,  $n_o$  then denoting the number of electron holes.

After having undertaken these calculations, using the two simplifying assumptions made on page 131, we shall now consider more general cases in which one or the other of these assumptions is not fulfilled. At first we assume that the  $n_o$  electrons coming from the level  $\sigma$  in the excess atoms may not only be attached to those  $n_o$  excess atoms but that there are more places in the crystal lattice to which these electrons may go, even when they are not located in the conduction band. An example for such a case may be given by considering the right-hand side of Fig. 64 showing a crystal lattice AB with a certain number (4) of vacancies at A-lattice sites and a smaller number (2) at B-lattice sites. There is an excess of B-atoms (encircled) in this lattice due to the difference in the respective numbers of vacancies. One can easily see, however, that in this case the electrons in the conduction band need not necessarily return to their original (encircled) B-ions, but may be trapped by other B-ions near the two additional vacancies at A-lattice sites.

The number of such additional vacancies or electron traps will be

denoted by  $n_a$ , and it will be assumed that the electrons in these traps have the same energy as in the  $n_\sigma$  interference levels. Then instead of (136):

$$N_\sigma + N_a + N_x = G^* n_\sigma \quad \dots \quad (150)$$

and instead of (137):

$$N_\sigma + N_a = \frac{G(n_\sigma + n_a)}{e^{(E_\sigma - E_\zeta)/kT} + 1} \quad \dots \quad (151)$$

Equations (138) to (140) remain unchanged, while (141) becomes:

$$N_x = \frac{G^* n_\sigma - G^* n_a e^{(E_\zeta - E_\sigma)/kT}}{1 + e^{(E_\zeta - E_\sigma)/kT}} \quad \dots \quad (152)$$

The limiting energy  $\zeta$  must be calculated from this equation. Only the result of this calculation obtained with the simplifying condition  $n_a \gg N_x$  will be given here. It is:

$$\zeta \approx \sigma - \frac{kT}{e} \ln \frac{n_a}{n_\sigma} \quad \dots \quad (153)$$

One sees from this that the Fermi-level may be either higher or lower than the interference energy level  $\sigma$ , depending on the ratio  $n_a/n_\sigma$ .

From (153) the internal work function  $\chi - \zeta$  is obtained as:

$$\chi - \zeta \approx \chi - \sigma + \frac{kT}{e} \ln \frac{n_a}{n_\sigma} \quad \dots \quad (154)$$

If this equation is introduced into (140), the formula for the number  $N_x$  of electrons in the conduction band, valid for this case, is:

$$N_x = G C^{1/32} \frac{n_a}{n_a} T^{3/2} e^{-e(\chi - \sigma)/kT} \quad \dots \quad (155)$$

This equation replaces (147) if  $n_a$ , the number of trapping sites, is not negligible. If, however,  $n_a \ll N_x$ , (147) remains valid. Equation (155) was first derived by Nijboer.<sup>1</sup>

After having discussed the influence of the trapping sites we shall now assume that there is not only one interference level  $\sigma$  but a small band of such levels (cf. Fig. 77). As outlined by Mott and Gurney,\* the excess atoms will interact with each other if their concentration exceeds a certain value and the energy levels of the electrons of these excess atoms are therefore no longer all the same. They spread over a certain range and form an interference energy band in the semi-conductor, which is separated from the conduction

\* N. F. Mott, R. W. Gurney, *Electronic Processes in Ionic Crystals*, Oxford, 1940, p. 166.

band by a small gap ( $\chi - (\sigma + \Delta\sigma)$  in Fig. 77). The width  $\Delta\sigma$  of this interference band increases with the number of excess atoms.

The Fermi-level and the number of electrons in the conduction band for this case were calculated by Busch.<sup>2</sup> Let  $n_o(E)$  denote the

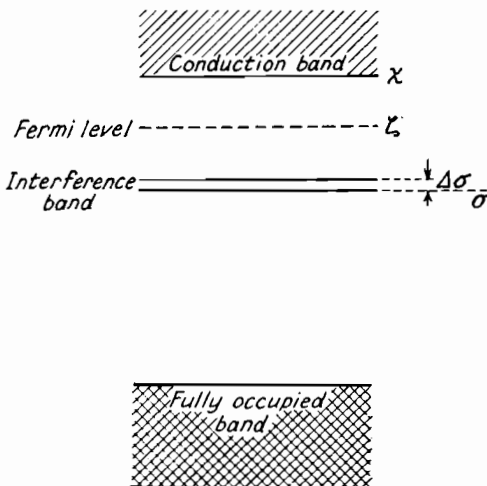


Fig. 77.—Energy Bands in an Excess Semi-conductor having a Large Number of Excess Atoms.

number of energy levels in the interference band between  $E$  and  $E+dE$ , and  $N_o(E)$  the number of electrons in these levels. Equation (136) (for  $n_a=0$ ) must then be replaced by:

$$N_x + \int_{\sigma}^{\sigma+\Delta\sigma} N_o(E)dE = G^* \int_{\sigma}^{\sigma+\Delta\sigma} n_o(E)dE \quad \dots \quad (156)$$

The equations (136) to (140) used in the first case are valid, but (141) must be replaced by:

$$N_x = \int_{\sigma}^{\sigma+\Delta\sigma} \frac{G^* n_o(E)dE}{1 + e^{(E_x - E)/kT}} \quad \dots \quad (157)$$

This integral can easily be evaluated if it is assumed that  $n_o(E) = n_a/e\Delta\sigma$  and  $(E_x - E)/kT \gg 1$ . The further calculation is then quite similar to that for only one energy level  $\sigma$  as carried out on page 133 and the value obtained for the internal work function is:

$$\chi - \zeta = \frac{\chi - \sigma}{2} + \frac{kT}{2e} \ln \left[ \frac{(CT)^{3/2} \times e\Delta\sigma}{n_a} \right] - \frac{kT}{2e} \ln [e^{e\Delta\sigma/kT} - 1] \quad (158)$$

The number  $n_o$  of interference levels occurring in equation (143)

for  $\Delta\sigma=0$  is now replaced by the ratio between  $n_\sigma$  and the width  $e\Delta\sigma$  of the interference band measured in units  $kT$ . This ratio, which gives the number of interference levels in a strip of the interference band of width  $kT$ , may be called the interference density and is denoted by:

$$n_{(kT)} = \frac{n_\sigma}{e\Delta\sigma/kT} . . . . . \quad (159)$$

With this value and for  $e^{e\Delta\sigma/kT} \gg 1$  the internal work function from (158) may be related to the internal work function valid for  $\Delta\sigma=0$  as given by (143). If  $(\chi-\sigma)_{\Delta\sigma=0}$  denotes the value obtained from (143) or from Fig. 75 with  $n_{(kT)}$  instead of  $n_\sigma$ , then :

$$\chi - \zeta = (\chi - \sigma)_{\Delta\sigma=0} - \Delta\sigma/2 . . . . . \quad (160)$$

According to this equation the Fermi-level will be half-way between the lower limit of the conduction band and the upper limit of the

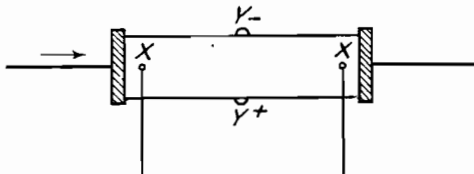


fig. 78.—Experimental Design for Measuring Conductivity and Hall Effect.

interference band, if the value of  $n_{(kT)}$  is large or the temperature low (cf. Fig. 77).

The formula now obtained for the number  $N_x$  of electrons in the conduction band is:

$$N_x = GC^{3/4}n_{(kT)}^{1/2}T^{3/4}e^{-e[(x-(\sigma+\Delta\sigma))/2kT]} . . . . . \quad (161)$$

This is the equation that has to be used when the width of the interference band cannot be neglected. Equation (161) is also valid on the condition  $E_\zeta - E_x/kT \gg 1$ , which for a sharp interference level gave (145) and which now, taking into account (160), becomes:

$$\chi - (\sigma + \Delta\sigma) \gg \frac{2kT}{e} . . . . . \quad (161a)$$

The equations derived above for the conductivity of semiconductors can only be checked experimentally by measurements in the low-temperature range, where the chemical composition and the number of excess atoms do not vary with temperature but remain appreciably constant during the measuring time. Fig. 78 shows

an experimental set for measuring the conductivity in which the semi-conducting material is in the form of a slab or rod. In order to avoid faulty results produced by the contact resistances of the electrodes, the voltage necessary for calculating the conductivity is taken from the two points  $X$ . The auxiliary electrodes applied at these points  $X$  and also the electrodes  $Y$  which are used for measuring the Hall-effect (cf. p. 145) are best made by evaporating thin metal layers on to the required areas.

Further examples of measurements of the conductivity as a function of temperature are given by Fig. 79 for  $\text{TiO}_2$  (according to Meyer<sup>2</sup>) and Fig. 80 for  $\text{ZnO}$  (according to Fritsch<sup>1</sup>). These

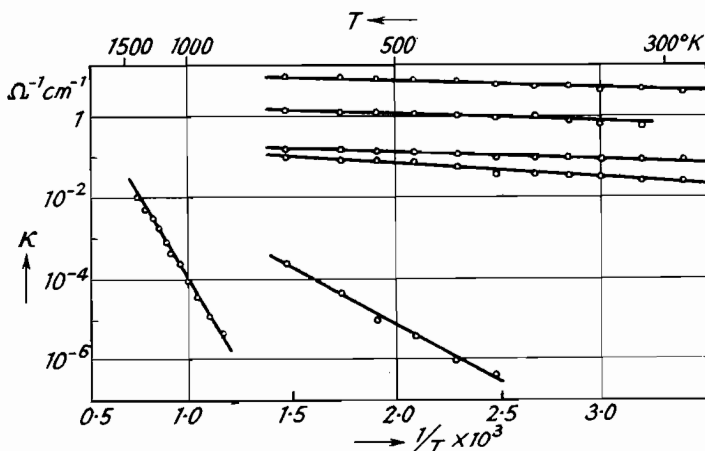


Fig. 79.—The Conductivity  $\kappa$  of a Semi-conductor as a Function of Temperature for Different Densities of Excess Atoms :  $\text{TiO}_2$  (Meyer<sup>2</sup>).

measurements were carried out for different numbers of excess atoms  $n_a$  obtained by varying the reducing treatment of the oxide. All the curves shown are straight lines in a plot  $\log \kappa$  against  $1/T$ , and represent exponential functions:

$$\kappa = a \cdot e^{-E_B/kT} \dots \dots \dots \quad (162)$$

as required by the formulæ derived above. Sometimes, as shown by Fig. 81, the slope of the lines changes from one value to another when passing a certain temperature. This is not surprising, since in the formulæ derived above for the number of electrons in the conduction band, quite different values of the exponent appear, depending on the value of  $n_a$ . For  $n_a \ll N_x$  equation (147) is valid

and the factor  $(\chi - \sigma)/2$  appears in the exponent, whilst for  $N_a \gg N_x$  equation (155) is correct, and here the exponent is  $\chi - \sigma$ . The one formula may be valid in one range of temperatures and the other

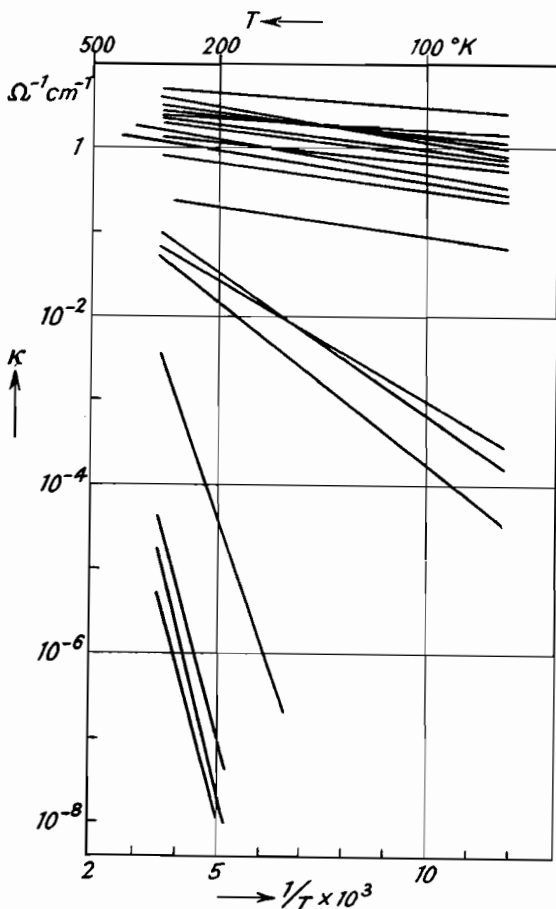


Fig. 80.—The conductivity  $\kappa$  of a Semi-conductor as a Function of Temperature for Different Densities of Excess Atoms: ZnO (Fritsch<sup>1</sup>).

formula in another range. It may also be possible that a semiconductor is an excess (defect) semi-conductor at lower temperature and an intrinsic semi-conductor at higher temperatures, and lines of different slope may be observed for this reason. One can see from this short outline that it will generally be difficult to obtain accurate values of the interference energy and the internal work function

from the slopes observed unless the details of the mechanism producing the semi-conduction are known.

An important result shown by Figs. 79 and 80 is that an increase in the amount of excess material in the semi-conductor decreases not only the conductivity itself but also the slope of the line representing the conductivity. This phenomenon, which was quite unexpected, was first observed by Meyer<sup>1</sup> for  $\text{WO}_3$ . It has been confirmed by Hartmann<sup>1</sup> for  $\text{Al}_2\text{O}_3$  and  $\text{Ta}_2\text{O}_5$ , by Meyer and Neldel<sup>3</sup> who measured  $\text{Fe}_2\text{O}_3$  in addition to the compounds quoted, and by Busch<sup>1</sup> for SiC. Table XIV gives some numerical values for the variation of the energy  $\beta$  in (162) with increasing number of excess atoms as measured by Meyer and Neldel.

Furthermore, Meyer and Neldel found a relation between  $\beta$  and the constant  $a$  in (162) if these two values were ascertained for different states of a semi-conductor (different numbers of excess atoms). This relation, which was confirmed by Busch,<sup>1</sup> is:

$$\beta = K_1 \log a + K_2 \quad \dots \quad (163)$$

where  $K_1$  and  $K_2$  are two constants ( $K_1 > 0$ , Meyer's rule). The relation is valid for  $\beta \geq 0.06$  eV.

TABLE XIV

*Variation of the Energy  $\beta$  in the Exponent of the Semi-Conductor Formula with Increasing Number of Excess Atoms (Meyer and Neldel<sup>3</sup>)*

Semi-conductor	$\beta$	
	From	To
$\text{TiO}_2$	1.73 eV	0.004 eV
$\text{ZnO}$	1.04 "	0.05 "
$\text{Fe}_2\text{O}_3$	1.18 "	0.005 "

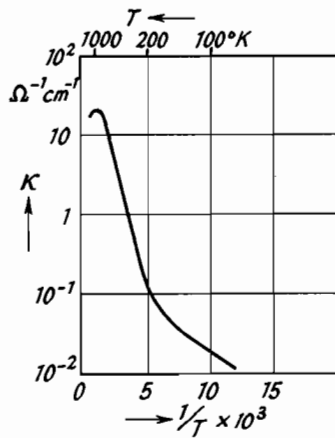


Fig. 81.—Conductivity  $\kappa$  of Silicon Carbide as a Function of Temperature (Busch<sup>1</sup>).

Various attempts have been made to explain the decrease of  $\beta$  with increasing number of excess atoms. Möglich<sup>1</sup> and Nijboer<sup>1</sup> assumed that the dielectric constant of a semi-conductor varies with increasing number of excess atoms and that this variation influences the distance between the two energy levels  $\chi$  and  $\sigma$ . But such a variation of the dielectric constant with the number of excess atoms has not been proved experimentally yet. Gisolf,<sup>1</sup> contrary to the assumptions normally made, assumed that the energy levels of the excess electrons lie within the conduction band and that the electrons go from there to special trapping sites which form a band below the conduction band. Gisolf explains the relation (163) in this way, but does not justify the special assumptions that have to be made. An equation for the constant  $K_1$  in (163) has been given by Busch<sup>2</sup> who related it to the temperature of "freezing in" which was defined in Sec. 15.

A plausible explanation for the relationship represented by equation (163) was given by Mott and Gurney.\* Their reasoning may be discussed by using equation (161), which gives the number of electrons in the conduction band if the interference levels make up an interference band (cf. Fig. 77). As discussed on p. 139 the width  $\Delta\sigma$  of the interference band will then increase with increasing number of excess atoms. Consequently the exponent of (161) will decrease and the decrease of  $\beta$  in (162) is thus explained. The relation (163) is more difficult to explain. If  $a$  is calculated by combining (161) and (135) and  $\beta$  is expressed by the values occurring in the exponent of (161), the following equation is obtained from (163):

$$\sigma = k_1 \log \frac{1}{l^2 n_{(kT)}} + k_2(T) \quad \dots \quad (164)$$

( $k_1 > 0$ ). A decrease either in the mean free path  $l$  or in the interference density  $n_{(kT)}$  with increasing  $\Delta\sigma$  and  $n_\sigma$  must be assumed in order to fulfil (163). A decrease in  $l$  was considered by Meyer and Neldel.<sup>3</sup> On the other hand, a relation similar to (163) is also observed for the thermionic emission of semi-conductors in which the mean free path has no importance, and an explanation of relation (163) by assuming only a variation of  $l$  seems therefore to be unsatisfactory.

The value of the number  $n_\sigma$  of excess atoms can only be obtained

\* N. F. Mott, R. W. Gurney, *Electronic Processes in Ionic Crystals*, Oxford, 1940, p. 166.

by chemical analysis for semi-conductors with relatively large  $n_o$  and correspondingly high conductivity. The interference energy will be small in this case and condition (145) is then no longer fulfilled. The following values were measured by Meyer<sup>2</sup> for  $TiO_2$ :

TABLE XV

*Experimental Values for the Density  $n_o$  of Excess Atoms in  $TiO_2$  (Meyer<sup>2</sup>)*

$\kappa (T=293^\circ K.)$	$n_o$
0.22 $\Omega^{-1} \text{cm.}^{-1}$	$0.3 \times 10^{20} \text{ atoms/cm.}^3$
0.78	$4 \times 10^{20}$
4.46	$21 \times 10^{20}$

The determination of smaller values of  $n_o$  is made possible by the Hall-effect, which at the same time allows a discrimination between excess and defect semi-conductors. This Hall-effect is observed in an experimental set similar to Fig. 78, if a magnetic field  $H$ , perpendicular to the plane of the paper (directed from above), is applied. The electrons producing the current through this semiconductor are diverted towards the upper side in the figure by the magnetic field. Consequently there will be a potential difference  $V_H$  between the contacts  $Y$  which is proportional to the current density  $j$ , to  $H$ , and to the width  $b$  of the slab perpendicular to the direction of the current. If the thickness of the slab in the direction of the magnetic field is denoted by  $d_0$  then with  $j=I/bd_0$ :

$$V_H = 10^{-6} \mu_0 H \frac{IH}{d_0} \quad \dots \quad (165)$$

The factor  $H$  in this formula is assumed to be given in units  $\text{cm.}^3/\text{Coul.}$  (instead of  $\text{m.}^3/\text{Coul.}$ ). This factor is called the Hall-constant and is normally of the order of  $10^{-4}$  for metals. For  $I=10$  amp.,  $H=10^6$  amp.  $\text{m}^{-1}$ , and  $d_0=0.1$  mm., the value of the potential difference  $V_H$  then is about  $10^{-5}$  volt.

The Hall-constant  $H$  can be calculated by means of electronic theory, which gives the value:

$$H = \frac{3\pi}{8Ne} = \frac{7.35 \times 10^{18}}{N} \text{ cm.}^3/\text{Coul.} \quad \dots \quad (166)$$

( $N$  the number of conduction electrons per  $\text{cm.}^3$ ). If an excess

semi-conductor is considered, the value of  $N$  must be replaced by  $N_x$  from either (140) or (147). Using (140) and with  $G=2$

$$H = \frac{3\pi}{8eGC^{3/2}} T^{-3/2} e^{e(x-\zeta)/kT} = \frac{4.8 \times 10^{-2}}{(T/1000)^{3/2}} e^{e(x-\zeta)/kT} . \quad (167)$$

Or

$$\log H = 5040 \frac{\chi - \zeta}{T} - \log \frac{(T/1000)^{3/2}}{0.048}$$

For  $T=1000^\circ$  and  $\chi - \zeta = 0.5$ ,  $\log H \approx 1$ . One sees from this that the Hall coefficient may take much higher values for semi-conductors than it does for metals.

Equations (167) may be used for determining the position of the Fermi level as this is the only characteristic of the semi-conductor occurring in these equations. If formula (147) for  $N_x$  is used instead of (140)

$$H = \frac{7.5 \times 10^{10}}{\sqrt{n_\sigma} T^{3/4}} e^{e(x-\sigma)/2kT} . . . . . \quad (168)$$

This equation can be used for evaluating the number  $n_\sigma$  of excess atoms by plotting a straight line against  $1/T$  in the usual way and determining the intercept. Miller<sup>1</sup> for instance who measured the Hall effect of ZnO found a value  $n_\sigma = 10^{18}$  for  $\chi - \sigma = 1.4$ . If equation (161) were used instead of (147) for deriving (168),  $n_\sigma$  would be replaced by the interference density  $n_{(kT)}$ .

Equations (166)–(168) are also valid for defect semi-conductors, with the only difference that the opposite sign must be applied (Peierls<sup>1</sup>). It is therefore possible to decide by measuring the Hall-effect, if a given material is an excess or a defect semi-conductor. In addition to this the Hall-effect may be used for discriminating between electronic and ionic conductors, as no Hall-effect can exist for ionic conduction.

The mobility  $u$  of the electrons can be obtained by combining the two equations (132) for the conductivity and (166) for the Hall-constant. It follows:

$$\kappa \times H = \frac{3\pi}{8} u . . . . . \quad (169)$$

The product of conductivity and Hall-constant is nearly equal to the mobility. The values obtained for the mobility of different semi-conductors lie between 0.5 and 100 cm.<sup>2</sup>/volt sec. at temperatures between 200° and 400° K. The mean free path  $l$  calculated from

these mobilities by combining formulæ (134) and (148) is between 1 and 100 Å.

Finally the thermo-electric voltage of semi-conductors is of interest, and a formula for this voltage will therefore be given without derivation. The thermo-electric voltage between two metal contacts (1) and (2), applied to an excess semi-conductor and having different temperatures  $T_1$  and  $T_2$  ( $T_1 < T_2$ ), is given by

$$V_{th(1,2)} = \int_{T_1}^{T_2} \left( \frac{\chi - \zeta}{T} - \frac{2k}{e} \right) dT \quad \dots \quad (170)$$

Therefore

$$\frac{dV_{th}}{dT} = \frac{\chi - \zeta}{T} - \frac{2k}{e} \quad \dots \quad (170a)$$

When deriving this formula the contribution of the metal electrons to the thermo-electric effect has been neglected. This is justified because, for example, with  $\chi - \zeta = 0.5$  and  $T = 800^\circ$ , it follows from (170a) that  $dV_{th}/dT = 0.45$  mV/degree. This value is about 10 times higher than those obtained for metals.

Equation (170a) can be used for determining the position of the Fermi level in a similar way as (167). If the value (143) for  $(\chi - \zeta)$  is introduced in (170a), an equation containing the number of excess atoms  $n_o$  is obtained, and this equation can again be employed for determining  $n_o$ . Furthermore the sign of the thermo-electric voltage  $V_{th}$  in (170) changes if a defect semi-conductor instead of an excess semi-conductor is considered. Hence the measurement of  $V_{th}$  also gives a means for discriminating between the two main types of semi-conductors. Up to the present only very few measurements of the thermo-electric voltage of semi-conductors are known.

Concluding this section, it may be emphasized that many of the equations given above only apply to a particular one of the semiconductor models which have been discussed (e.g. equations (142), (143), (147), (149), (154), (155), (160), (161), 168)). The main formulæ which are valid independently of any particular model are (134), (135), (140), (166), (167), (170). In principle the validity of these formulæ is not even limited to the range below the temperature of "freezing in" (cf. p. 131) to which our discussion has been confined. The equations concerned also refer to the range

\* Cf. F. Seitz, *The Modern Theory of Solids*, New York and London, 1940, p. 191.

above this critical temperature, where the number of excess atoms is no longer constant, but variable and dependent on temperature. In this range, however, the temperature dependence represented by these equations is so much influenced by the temperature dependence of  $n_o$  that the laws which are finally obtained are entirely different.

### REFERENCES

- |                   |  |
|-------------------|--|
| APKER, L.         | (1) TAFT, E., and DICKEY, J., <i>Physic. Rev.</i> 74 (1948), 1462.   |
| BLOCH, F.         | (1) <i>Z. Physik</i> 52 (1929), 555.                                 |
| BUSCH, G.         | (1) <i>Helv. Physica Acta</i> 19 (1946), 167.                        |
|                   | (2) <i>ibid.</i> 19 (1946), 189.                                     |
| FISHER, E.        | (3) and LABHART, H., <i>ibid.</i> 19 (1946), 463.                    |
|                   | (1) <i>Physic. Rev.</i> 73 (1948), 36.                               |
| FRIEDERICH, E.    | (1) <i>Z. Physik</i> 31 (1925), 813.                                 |
| FRITSCH, O.       | (1) <i>Ann. Phys.</i> 22 (1935), 375.                                |
| GISOLF, J. H.     | (1) <i>Ann. Phys.</i> 1 (1947), 3.                                   |
| HARTMANN, W.      | (1) <i>Z. Physik</i> 102 (1936), 709.                                |
| HEVESEY, G. v.    | (1) and SEITH, W., <i>Z. Physik</i> 56 (1929), 790.                  |
| JETTE, E. R.      | (1) and FOOTE, F., <i>J. Chem. Phys.</i> 1 (1933), 29.               |
| LEHFELD, W.       | (1) <i>Z. Physik</i> 85 (1933), 717.                                 |
| MEYER, W.         | (1) <i>Z. Physik</i> 85 (1933), 278.                                 |
|                   | (2) <i>Z. techn. Physik</i> 16 (1935), 355.                          |
|                   | (3) and NELDEL, H., <i>ibid.</i> 18 (1937), 588.                     |
|                   | (4) and MÖGLICH, F., <i>Z. Elektrochem.</i> 45 (1939), 68.           |
| MILLER, P. H.     | (5) <i>Z. f. Elektrochemie</i> 50 (1944), 274.                       |
|                   | (1) <i>Physic. Rev.</i> 60 (1941), 890.                              |
| MÖGLICH, F.       | (1) <i>Z. Physik</i> 109 (1938), 503.                                |
| MOTT, N. F.       | (1) and LITTLETON, M. J., <i>Trans. Faraday Soc.</i> 34 (1938), 485. |
| NIJBOER, B. R. A. | (1) <i>Proc. Phys. Soc.</i> 51 (1939), 575.                          |
| PEIERLS, R.       | (1) <i>Z. Physik</i> 53 (1929), 255.                                 |
|                   | (2) <i>Ann. Phys.</i> 4 (1930), 121.                                 |
| PUTLEY, E. H.     | (1) <i>Proc. Phys. Soc.</i> 62 (1949), 284.                          |
| SCHOTTKY, W.      | (1) <i>Z. physik. Chem.</i> 29 (1935), 335.                          |
| SEITH, W.         | (2) <i>Z. Elektrochemie</i> 45 (1939), 52.                           |
|                   | (1) <i>Zeits. f. Phys.</i> 56 (1929), 804.                           |
| SHIFRIN, K.       | (2) <i>ibid.</i> 57 (1929), 869.                                     |
|                   | (1) <i>Journal of Physics, U.S.S.R.</i> 8 (1944), 242.               |
| SHOCKLEY, W.      | (1) <i>Physic. Rev.</i> 50 (1936), 754.                              |
| SIMPSON, J. H.    | (1) <i>Proc. Roy. Soc. (A)</i> 197 (1949), 269.                      |
| SLATER, J. C.     | (1) and SHOCKLEY, W., <i>Physic. Rev.</i> 50 (1936), 705.            |
| TAFT, E.          | (1) and APKER, L., <i>Physic. Rev.</i> 75 (1949), 118.               |
| TIBBS, S. R.      | (1) <i>Trans. Faraday Soc.</i> 35 (1939), 1471.                      |

PHENOMENA IN IONIC SOLIDS

- TUBANDT, C. (1) REINHOLD, H., and JOST, W., *Z. anorg. Chem.* 177 (1928), 253.
- WAGNER, C. (1) and SCHOTTKY, W., *Z. physik. Chem. (B)* 10 (1930), 163.  
(2) *Z. physik. Chem. (B)* 11 (1931), 139.
- WEISE, E. (1) *E.T.Z.* 59 (1938), 1085.
- WILSON, A. H. (1) *Proc. Roy. Soc. (A)* 133 (1931), 458.  
(2) *ibid.* 134 (1932), 277.

## CHAPTER 4

# THE MECHANISM OF THE EMISSION FROM AN ACTIVATED OXIDE COATING IN EQUILIBRIUM

## 18. Experimental Details and Physical Constants of the Oxide Coating

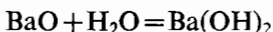
After having discussed the fundamentals in the three previous chapters, we can now proceed to the physics of the oxide-coated cathode. It has previously been pointed out that the oxide cathode, consisting of a chemical compound or a mixture of such compounds, differs essentially from cathodes made of pure or contaminated metals. The physical properties of those compounds, which are quite different from the properties of metals, must therefore be used for explaining the mechanism of the oxide cathode. By not taking this fact into account, false conclusions have been produced in some of the earlier experiments.

The main part of the oxide cathode, the oxide coating, normally consists of one of the three alkaline earth oxides BaO, SrO, and CaO, or of mixtures of these. As the characteristic properties of the oxide cathode occur especially with barium oxide, this oxide is the most important one. For this reason we shall preferably deal with barium oxide in this chapter and shall only refer to the other alkaline earth oxides if they are used in one of the experiments to be discussed. It may be pointed out in this context that the ability to emit electrons is not exclusive to alkaline earth oxides but is a general property of many metal oxides. Details of this general behaviour of metal oxides will be given later, and the emission properties of different metal oxides will then be compared.

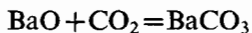
It is assumed that the reader is familiar with the manufacturing process of the oxide cathode as discussed in Vol. I. As the details of the preparation of the cathode do not influence the principles governing its behaviour, the discussion here may be limited to one of the different types of cathodes mentioned in Vol. I, Sec. 2. The most common type, the uncombined cathode, manufactured by decomposition of carbonates, will be chosen. Other types are only considered if they have been used for experiments to be discussed.

On the other hand, it must be taken into consideration that cathodes made by different methods may have different compositions. This will not influence the mechanism of the emission but may affect the individual measured values. Consequently only those experimental values may directly be compared which are obtained for cathodes made in the same way.

When investigating the oxide cathode experimentally, it must be borne in mind that the chemical system of the oxide coating is very sensitive to chemical influences produced by impurities or residual gases. This results from the fact that barium oxide and especially barium metal are very active chemically. BaO combines with water vapour at room temperature according to the formula



and forms barium hydroxide. If water vapour is present, BaO combines with carbon dioxide according to the formula



and forms barium carbonate. Moreover, barium metal has a high affinity for oxygen, hydrogen, and nitrogen. It reacts with oxygen already at room temperature, while it combines with hydrogen above 120° C. forming barium hydride ( $\text{BaH}_2$ ), and with nitrogen above 260° C., forming barium nitride ( $\text{Ba}_3\text{N}_2$ ).\*

Both the susceptibility of the coating to chemical attack and the different methods of manufacture affect the composition of the coating in a very complex manner. When working with oxide cathodes, it is therefore necessary to take into account a number of factors which may influence the measured values. The importance of these factors will be fully understood only in the course of the further discussion in this book. The factors concerned are the following:

(1) The composition of the materials used for manufacturing the alkaline earth oxides (e.g. the alkaline earth carbonates) and the methods by which those materials are made (precipitation method). Both influence the grain size and the crystallographic structure of the oxide coating (cf. Vol. I, Sec. 4).

(2) The ability of the core metal and of the binders in the emission paste to react chemically (cf. Vol. I, Sec. 3 and Sec. 32).

(3) The method of depositing the oxide coating on the core metal, which influences the density, the porosity, and the surface roughness of the coating (cf. Vol. I, Sec. 5 and Sec. 28).

\* For the details cf. Gmelin's *Handbuch der Anorganischen Chemie*, No. 30, Barium (1932).

(4) The composition of the materials used for the other electrodes in the experimental valve (cf. Vol. I, Sec. 12.5 and Sec. 31.3).

(5) The vacuum in the valve, which depends on the pumping procedure and on the type of getter; the best vacuum which is available by modern technical means (at least  $10^{-5}$  mm. mercury) must be provided for exact investigations.

(6) The method of decomposing the cathode for obtaining the alkaline earth oxides (cf. Vol. I, Sec. 7).

(7) The manner of activating the cathode, which is determined by the temperature, the activation current, and the time of activation (cf. Vol. I, Sec. 8 and Sec. 29).

In addition to this the utmost cleanliness must be applied to all the processes needed for making the cathode and the other components of the experimental valve. This necessity has been greatly emphasized in Vol. I. If attention is not sufficiently paid to this, the impurities which then may exist in the cathode will easily produce faulty results.

As the many influences given above cannot be kept completely constant, even in very exact investigations, certain variations of the experimental results must always be expected. Hence all investigations should be carried out with a large number of cathodes. The accuracy of the measured values will be increased in this manner, and judging the reliability of the results will be made easier. Measurements with only one valve which have been carried out sometimes, have a very limited value.

The many conditions which influence the results obtained with oxide-coated cathodes have not been recognized sufficiently in some of the earlier investigations. Some of these conditions could not be taken into account, as the necessary experimental means, for example in vacuum technique, were not available at that time. Consequently the results of those investigations cannot be considered as accurate from our point of view. It is therefore not surprising that the numerous observations which have been made since the discovery of the oxide cathode by Wehnelt,<sup>1</sup> could not at first be explained by a universal concept. As described in Vol. I in detail, many such concepts have been worked out during the development of the oxide cathode. Only some ten years ago a concept was developed which explained the fundamental phenomena without contradiction. This concept will be the basis of the considerations in this book. Before proceeding with it, however,

the fundamental constants of the oxide-coated cathode will be compiled.\*

TABLE XVI  
*Properties of Alkaline Earth Atoms*

	Mg	Ca	Sr	Ba	Unit of measurement										
Atomic number $K$	12	20	38	56											
Atomic weight $A$	24.32	40.08	87.63	137.36	eV										
Ionization voltage $\xi_1$ , f. 1. electron.	7.63	6.25	5.68	5.21											
Ionization voltage $\xi_2$ , f. 2. electron.	15.10	11.87	10.86	9.96	eV										
Polarization constant $a$ of the double-charged ion.	0.10	0.5	0.87	1.6	$10^{-24}$ cm. <sup>3</sup>										
Electron Configuration															
	1s	2s	2p	3s	3p	3d	4s	4p	4d	4f	5s	5p	5d	...	6s
Mg	2	2	6	2	—	—	—	—	—	—	—	—	—	—	—
Ca	2	2	6	2	6	—	2	—	—	—	—	—	—	—	—
Sr	2	2	6	2	6	10	2	6	—	—	2	—	—	—	—
Ba	2	2	6	2	6	10	2	6	10	—	2	6	—	—	2

TABLE XVII  
*Crystal Properties of Alkaline Earth Metals*

	Mg	Ca	Sr	Ba	Unit of measurement
Crystal system	hexagonal	face-centred cubic f. $T \leq 720^\circ$ K. hexagonal f. $T \geq 720^\circ$ K.	face-centred cubic	body-centred cubic	
Lattice constant $d$	3.20 5.21	5.56	6.08	5.02	Å.
Atomic volume $A/\delta$ (calculated from $d$ for $L = 6.02 \times 10^{23}$ ).	14.0	25.9	33.7	38.2	cm. <sup>3</sup> /g.-atom.
Density $\delta$ (calculated from $A$ and $A/\delta$ ).	1.74	1.55	2.60	3.60	g./cm. <sup>3</sup>
Heat of formation $Q_B$ .	36.3	47.8	47	49	k. cal./mol.
Melting point	930	1125	1030	980	° K.
Vapour pressure $p$			cf. Fig. 82		

\* Most of these constants were taken from J. D'Ans and E. Lax, *Taschenbuch für Physiker und Chemiker*, Berlin, 1943.

TABLE XVIII

*Properties of Alkaline Earth Oxides*

	MgO	CaO	SrO	BaO	Unit of measurement
Molecular weight $M$	40.32	56.08	103.63	153.36	
Crystal system	face-centred	cubic	(NaCl-type)		
Lattice constant $d$	4.20	4.80	5.14	5.52	Å.
Density $\delta$ (calculated from $M$ and $d$ ).	3.62	3.38	5.05	6.05	g./cm. <sup>3</sup>
Lattice energy $E_L$	40.9	36.6	34.4	32.5	eV
Heat of formation $Q_B$ .	146.1	151.7	140.8	133	k. cal./mol.
Specific heat at 298° K.	8.96	10.3	10.77	11.34	cal./mol. degree.
Melting point	2920	2840	2700	2200	°K.
Dielectric constant $\epsilon$ for statical field.	9.8	11.8	13.3	14.3*	
Dielectric constant $\epsilon$ for infra-red frequencies.	2.95	3.28	3.31	—	
Vapour pressure $p$			cf. Fig. 83.		
Rate of evaporation			cf. Vol. I, Fig. 54.		

\* Obtained by extrapolation.

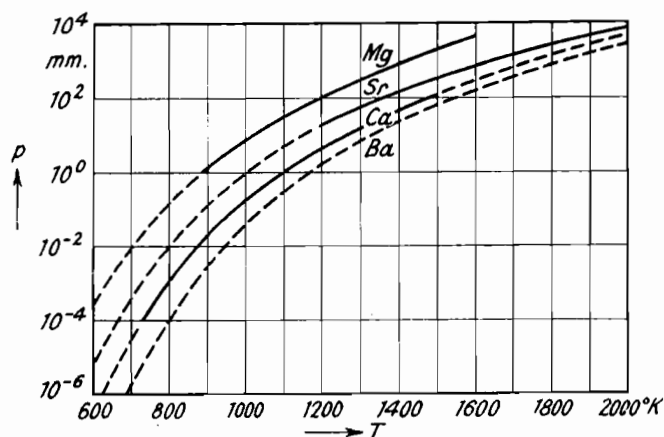


Fig. 82.—Vapour Pressure  $p$  of Alkaline Earth Metals as a Function of Temperature.

### Crystallographic Properties of Alkaline Earth Carbonates

We consider only the three most important carbonates, of which  $\text{BaCO}_3$  and  $\text{SrCO}_3$  occur in the orthorhombic aragonite type at

room temperature. If the temperature is raised to  $1080^{\circ}$  or  $1200^{\circ}$  K., respectively, they pass into a hexagonal crystal structure by an enantiotropic transition (Zimens<sup>1</sup>); the details of this structure are not known.  $\text{CaCO}_3$ , however, occurs in two different structures at room temperature, as aragonite and as calcite, belonging to the rhombohedral division of the hexagonal system. Of these two structures calcite is stable; aragonite, however, is unstable. The

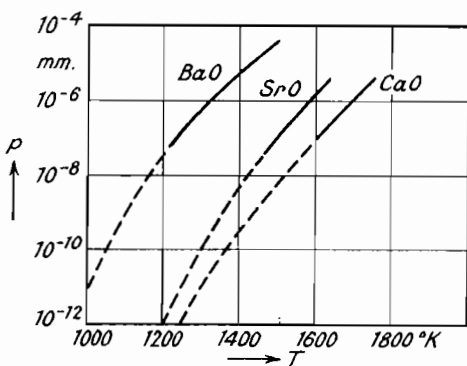


Fig. 83.—Vapour Pressure  $p$  of Alkaline Earth Oxides as a Function of Temperature

latter is only obtained by a slow dropwise precipitation from hot solutions and changes into calcite by a monotropic transition at temperatures above  $800^{\circ}$  K.

If mixtures of alkaline earth carbonates are considered, those formed of  $\text{BaCO}_3$  and  $\text{SrCO}_3$  show the simplest behaviour due to the similarity of their crystallographic properties. These two carbonates form a continuous series of solid solutions according to Cork and Gerhard<sup>1</sup> and Huber and Wagener.<sup>2</sup> The behaviour of the mixtures with  $\text{CaCO}_3$  is less simple. According to Huber and Wagener a simultaneous precipitation of  $\text{BaCO}_3$  and  $\text{CaCO}_3$  gives solid solutions of the aragonite type, if the percentage of  $\text{BaCO}_3$  is higher than 80 mol. %, while solid solutions of the calcite type are obtained below 60%  $\text{BaCO}_3$ . In an intermediate range which is near 70 mol. %  $\text{BaCO}_3$  the two crystal structures occur simultaneously. Similar results were obtained by Kallweit<sup>1</sup> for mixtures between  $\text{SrCO}_3$  and  $\text{CaCO}_3$ ; in this case the concentration limits for the aragonite or calcite type are 50 or 30 mol. % respectively. Table XIX shows the lattice constant for the system  $\text{BaCO}_3 - \text{CaCO}_3$ ,

considering both the pure carbonates and the mixtures. The values for pure  $\text{SrCO}_3$  are  $a=5\cdot1_2$ ,  $b=8\cdot4_0$ , and  $c=6\cdot0 \text{ \AA}$ .\*

TABLE XIX  
*Lattice Constants of Mixtures of  $\text{BaCO}_3$  and  $\text{CaCO}_3$*

Molecular percentages		Aragonite type, orthorhombic structure			Calcite type, rhombohedral structure	
$\text{BaCO}_3$	$\text{CaCO}_3$	$a$	$b$	$c$	$a$	$\alpha$
100%	0%	5·2 <sub>6</sub> Å.	8·8 <sub>1</sub> Å.	6·4 <sub>3</sub> Å.	—	—
80%	20%	5·2 <sub>0</sub> Å.	8·7 <sub>2</sub> Å.	6·3 <sub>9</sub> Å.	—	—
72%	28%	5·0 <sub>6</sub> Å.	8·7 <sub>0</sub> Å.	6·4 <sub>3</sub> Å.	6·5 <sub>9</sub> Å.	45·6°
60%	40%	—	—	—	6·6 <sub>9</sub> Å.	45·0°
50%	50%	—	—	—	6·6 <sub>1</sub> Å.	45·9°
0%	100%	4·9 <sub>4</sub> Å.	7·9 <sub>4</sub> Å.	5·7 <sub>2</sub> Å.	6·3 <sub>6</sub> Å.	46·2°

## 19. The Oxide Coating as an Excess Semi-Conductor

The fundamental consideration in the physics of the oxide-coated cathode is the fact that the composition of the coating does not correspond to the formula  $\text{BaO}$ , due to an excess of barium in the coating. This means according to Sec. 16 that the oxide coating is an excess semi-conductor. All further discussions dealing with the electrons in the coating must therefore start from the energy distribution of electrons in such a semi-conductor which was discussed in Sec. 17.

As the presence of excess barium in the oxide coating is so important, all the experimental evidence for its existence will be compiled first of all. The initial discussion will deal with the investigations in which the existence of excess barium was proved directly. In addition to this the investigations will be quoted which showed that oxygen is developed during the activation of the oxide cathode. The existence of excess barium in the activated cathode can be concluded from these investigations too.

### 19.1. Proof of the existence of excess barium

#### (a) Qualitative Proofs:

Such a proof was first given by Becker,<sup>1</sup> who used a combined  $[\text{BaSr}]O$  cathode on a platinum-iridium core which was

\* For further investigations of the mixtures of alkaline earth carbonates see Faivre and collaborators.<sup>1, 2, 3</sup>

arranged opposite to a carefully cleaned tungsten ribbon. After having brought the temperature of the cathode up to 1260° K., the emission of the tungsten ribbon was measured continuously, and an increase in emission was observed. This increase, which is shown in Fig. 84, completely corresponds to the increase in emission which is obtained during the activation of a W-Ba cathode when evaporating barium on a tungsten wire (cf. Fig. 33). Becker concluded from this that excess barium exists in or on the oxide coating and that this barium, due to the high temperature of the oxide cathode, evaporates on to the tungsten ribbon, changing this into a W-Ba cathode.

Another proof of the excess barium was given by Gehrts,<sup>1</sup> who, when bombarding grid and anode of his experimental valve, observed a green glow in the interspace between cathode and anode. The existence of barium was proved by finding the spectral lines of Ba in the glow.

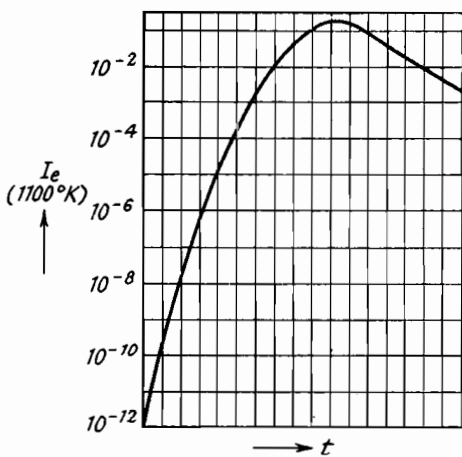


Fig. 84.—Variation of the Emission Current of a Tungsten Ribbon during the Heating of an Oxide Cathode, arranged opposite to the Ribbon (Becker<sup>1</sup>).

#### (b) Quantitative Analyses:

The first chemical analysis of excess barium in the coating was carried out by Berdennikowa,<sup>1</sup> who used combined cathodes made of a mixture of the three usual alkaline earth oxides on platinum-iridium. The excess barium was tested by reduction of water vapour based on the chemical equation  $\text{Ba} + \text{H}_2\text{O} = \text{BaO} + \text{H}_2$ . The water vapour was introduced into the experimental valve, and the pressure of the hydrogen developed during the reaction was measured with a MacLeod gauge. The increase in pressure thus gave a measure for the quantity of excess barium in the cathode. The result was that 5 µg. existed in the fully activated coating of the cathode used by Berdennikowa.

The same method was used by Clausing,\* who in addition to this tested the excess barium by directly measuring the quantity of oxygen needed for the oxidation of the barium. Both methods gave an amount of 0.25 mol. % barium.

However, a more recent application of the former method, undertaken by Jenkins and Newton,<sup>1,2</sup> gave a much lower value of about 0.01 mol. % for the excess barium in [BaSr]O. In this investigation considerable care was taken to ensure that all the barium which might exist on the glass wall and on other components of the experimental valve was excluded from detection by the analysis.

Another method was given by Fritz,<sup>1</sup> who introduced nitrogen into his valves and used the reaction  $3\text{Ba} + \text{N}_2 = \text{Ba}_3\text{N}_2$  occurring at a temperature of 770° K. After finishing this reaction, the oxide-coating was treated in water vapour, giving ammonia by the reaction  $\text{Ba}_3\text{N}_2 + 6\text{H}_2\text{O} = 3\text{Ba}(\text{OH})_2 + 2\text{NH}_3$ . The ammonia could be tested by a colorimetric analysis. Fritz gave a yield of 2 µg., but it is not quite clear if this refers to  $\text{NH}_3$  or to Ba.

Still another method, based on the reduction of  $\text{CO}_2$  by Ba, was employed by Prescott and Morrison.<sup>1</sup> They used cathodes made of a mixture of barium, strontium, and nickelous carbonates on a platinum-iridium core. These cathodes were activated by reduction with methane (cf. Sec. 29.1) and then exposed to carbon dioxide at a temperature of about 1100° K. The carbon dioxide then oxidizes the excess barium according to the reaction  $\text{CO}_2 + \text{Ba} = \text{BaO} + \text{CO}$ , and the quantity of excess barium can be determined by a quantitative analysis of the carbon monoxide developed. Prescott and Morrison obtained in this manner up to 60 µg. excess barium, referring to about 1 mg. BaO. This very high value of about 6 mol. % may be due to the special activation process used by Prescott and Morrison.

When employing these methods for the analysis of the excess barium it must be taken into account that during the activation of a cathode a quantity of barium evaporates which may be considerably larger than the quantity to be detected in the coating (cf. Table XXX). It is therefore important that the evaporated barium which is located on the other parts of the experimental valve is excluded from the analysis. The restriction to the barium in the coating can be achieved either by separating the cathode from the

\* Cf. J. H. de Boer, *Electron Emission and Adsorption Phenomena*, Cambridge, 1935, p. 348.

other parts of the valve before beginning the analysis (Jenkins and Newton), or by using one of the methods which require a higher temperature for the reaction between the barium and the reactive agent (methods by Fritz and by Prescott and Morrison). Furthermore the amount of barium metal on the components of the valve can be reduced by using platinum as core metal of the cathode (cf. Table XXX). The method of Fritz seems to be most reliable, as this method needs a higher temperature and uses gases ( $N_2$ ,  $NH_3$ ) which normally do not occur as residual gases in a valve.

## 19.2. Proof of the development of oxygen during the activation

### (a) Qualitative Proofs:

The first proof of the development of oxygen during the activation was given by Barton,<sup>1</sup> who found by means of a mass spectrograph that negative ions are emitted from a  $[BaSr]O$  cathode at high temperatures. He concluded from the molecular weight  $M=33$ , determined for these ions, that they were  $O_2^-$ -ions. This result was confirmed by Blewett and Jones<sup>1</sup> and Schaefer and Walcher,<sup>1</sup> while Bachman and Carnahan,<sup>1</sup> Broadway and Pearce,<sup>1</sup> and Sloane and Watt<sup>1</sup> found  $O^-$ -ions instead.

A spectroscopical proof for the evolution of oxygen was given by Detels.<sup>1</sup> The gas arising during the activation was pumped into a discharge tube previously evaporated, and the existence of oxygen was confirmed by a spectroscopical examination of the discharge.

Becker, when continuing his experiments described in 19.1 lowered the temperature of the cathode from  $1260^\circ$  to  $800^\circ$  K. and drew an emission current of 1 mA. When doing so, the emission current of the tungsten ribbon which was measured simultaneously fell to  $1/200$  of its original value. This result was explained by assuming that oxygen evaporates from the oxide cathode to the tungsten ribbon and poisons this.

### (b) Quantitative Analysis:

A direct chemical analysis of the oxygen was carried out by Isensee,<sup>1</sup> who also pumped the gas developed during the activation into a container which was previously evacuated. Some hydrogen could also be brought into the container by a palladium tube and could react with the oxygen from the cathode by the catalytic action of a platinum wire. The water vapour so produced was frozen in with liquid air, and the quantity of oxygen developed during the

activation was ascertained from the decrease of pressure in the container. Isensee activated his cathodes, consisting of a mixture of the three usual alkaline earth oxides on a platinum core, at a temperature of about  $1225^\circ\text{ K.}$ , so increasing the saturated current from  $0.2$  to  $70\text{ mA/cm}^2$ . The quantity of oxygen developed during this activation was between  $2$  and  $7\text{ }\mu\text{g.}$  The corresponding amount of excess barium in the oxide coating is about  $0.2\text{ mol. \%}$ .

### 19.3. Location of the excess barium

Considering the result of the experiments described, there cannot be any doubt that excess barium exists in or on an activated oxide coating. The values obtained for the amount of excess barium do not agree very well. They vary between  $10^{-2}\text{ mol. \%}$  (Jenkins and Newton) and  $6\text{ \%}$  (Prescott and Morrison). These differences may partly be due to differences in the state of activation of the cathodes examined. Emission values characterizing the state of activation have been reported by Jenkins and Newton who give  $j_s=9\text{ mA/cm}^2$  at  $T=825^\circ\text{ K.}$  This value, however, is not the optimum one attainable (cf. I, Fig. 50).

If the rather high value of Prescott and Morrison is not taken into account, an average value of the analyses by Clausing, Isensee, and Jenkins is  $p=5\times 10^{-2}\text{ mol. \%}$ ,  $p$  giving the percentage of excess barium in the coating. It was originally assumed that this excess barium would only exist on the surface of the oxide coating or would only be effective there. But this seems to be doubtful in view of the large quantities of excess barium which were measured. Let  $d$  denote the lattice constant of  $\text{BaO}$  and  $d_c$  the thickness of the oxide coating. If only the outer surface of the coating is considered, the quantity of excess barium as given above would make up  $(p/100)\times d_c/(d/2)=100$  atom layers at the surface ( $d\simeq 5\text{ \AA.}$ ,  $d_c\simeq 50\text{ }\mu$ ). A smaller value than this will be obtained for the number of layers at the surface, if it is taken into account that the excess barium may also accumulate at the boundaries of the individual oxide particles in the coating. Nevertheless quite a number of layers of excess barium would remain at the surface as long as this barium is assumed to be located at inner and outer surfaces only. The behaviour of such an accumulation of several atom layers would be similar to that of barium in bulk, and in view of the fact that barium metal has a vapour pressure of  $3\times 10^{-2}\text{ mm.}$  at  $1000^\circ\text{ K.}$ , the existence of so many surface layers of barium seems to be unlikely.

There is therefore good reason to assume that a considerable part of the excess barium is built into the crystal lattice of the oxide coating. This conclusion is confirmed by some experiments showing the effectiveness of the excess barium in the interior of the coating. Becker<sup>1</sup> and Becker and Sears<sup>2</sup> used the experimental arrangement shown in Fig. 85, which consists of two directly heated, combined  $[BaSr]O$  cathodes  $F_1$  and  $F_3$ , and a parallel tungsten ribbon  $F_W$ . By heating the one cathode to a sufficiently high temperature, barium was evaporated from this cathode to the other one which remained cold. The saturated current of the latter cathode was measured during the evaporation at short intervals, during which the temperature was increased to 475–600° K. It was observed that during the evaporation the saturated current rises up to a maximum and subsequently falls again (cf. left-hand side of Fig. 86).

In a second series of experiments one of the oxide cathodes was used as an anode for the tungsten ribbon, and an electron current of  $10 \mu A$  was sent from the ribbon to the cold cathode. The saturated current of this cathode was again measured at short intervals, and a similar curve as before was obtained. The rise and fall of the current in this case only depended on the product of electron current and time, that means on the electrical charge traversing the oxide coating. Becker concluded from this that in this second case barium metal was deposited at the surface by electrolysis.

The shape of the curve in Fig. 86, as obtained in both cases, was explained by the assumption that the barium, accumulating at the surface of the cathode, produces a maximum decrease in work function and a maximum emission, when an optimum concentration of barium at the surface is reached. Until this is achieved the emission current increases with decreasing work function, while after

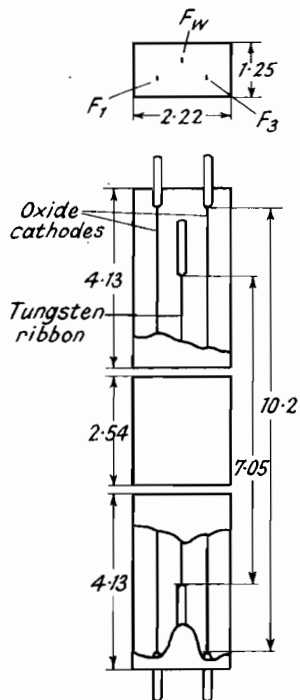


Fig. 85.—Experimental Arrangement of Becker<sup>1</sup> (dimensions in cm.).

exceeding the optimum concentration the current falls with increasing work function.

After the above treatment the oxide cathode was heated to a temperature between 800° and 1040° K. and the saturated current was measured in the same manner as before. It was observed that the current rises again to a maximum and falls afterwards, as seen from the right-hand side of Fig. 86. This phenomenon may be explained by assuming that the barium on the surface diffuses to the interior when the temperature is increased. The amount of barium concentration at the surface therefore decreases, and the emission increases, until the optimum concentration is reached again. When

subsequently this optimum concentration is exceeded, the emission current falls again, until an equilibrium between the excess barium in the interior and at the surface is established.

Becker and Sears repeated this treatment of the cathode—production of barium at the surface by electrolysis and subsequent diffusion of this barium into the interior—several times with the same cathode. Some values measured in this manner (at 500° K.) are plotted in Fig. 87 as a function of the electrical

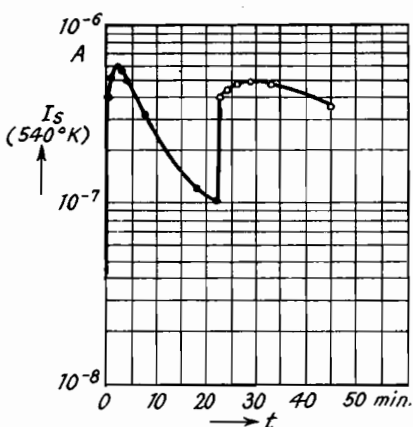


Fig. 86.—Variation of the Saturated Current of an Oxide Cathode during Bombardment by Electrons and Subsequent Heating at 800° K. (Becker<sup>1</sup>).

charge sent into the cathode. The crosses in this figure refer to the maximum currents which were measured when the electrons from the tungsten ribbon were sent into the coating, while the dots denote the emission values which were obtained after establishing the equilibrium of diffusion during the heating of the cathode at 1040° K. One sees from the figure that the emission current in each case increases with the number of repetitions, that means with the total electrical charge sent into the cathode. On the other hand, the different repetitions of the measurement only increase the number of excess barium atoms in the interior of the coating by diffusion, while the state of the surface remains the same within each series of measurements. Hence it follows from the experimental result in

Fig. 86 that the emission current of an oxide cathode not only depends on the qualities of the surface of the coating but also on the qualities of the interior, especially on the number of excess barium atoms in the interior.

If the small number of barium atoms which may be on the surface are neglected, there will be approximately  $p=5 \times 10^{-2}$  mol. % excess barium in the interior of the coating. This result corresponds with that of Schriehl,<sup>1</sup> who found that a maximum amount of about

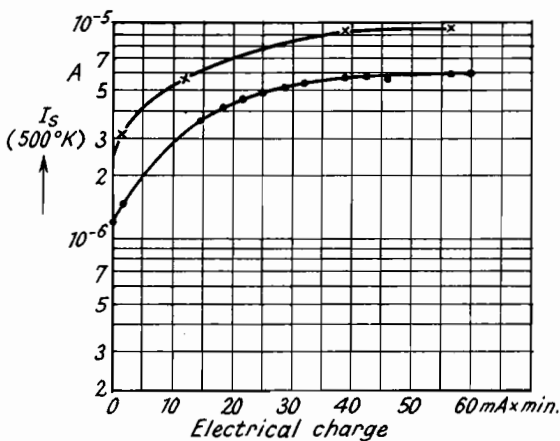


Fig. 87.—Variation of the Saturated Current of an Oxide Cathode during Repeated Electron Bombardments (Becker and Sears<sup>2</sup>).

1% barium is soluble in barium oxide. The total number of excess barium atoms built into a unit volume of barium oxide coating then is:

$$n_o = \frac{\delta L}{M} \times \frac{p}{100} = 2.4 \times 10^{22} \frac{p}{100} \simeq 1 \times 10^{19} \text{ cm.}^{-3} . \quad (171)$$

( $\delta$ =density,  $L$ =Avogadro's number,  $M$ =molecular weight).\*

Finally the question will be discussed, in which way the excess barium atoms are built into the crystal lattice of barium oxide. In order to decide between the two possibilities discussed in Sec. 16, the interspersion into the interstices (Fig. 69) and the formation of vacancies (Fig. 70), calculations or measurements as sketched out in

\* Recently the figure  $n_o=3 \times 10^{17}/\text{cm.}^3$  has been quoted as obtained by Jenkins and Newton<sup>1, 2</sup> for the number of excess atoms. Apparently this is based on an arithmetic error as from Jenkins and Newton's value of  $p=0.01$  mol. %,  $n_o=2.4 \times 10^{18}$  is derived.

Sec. 13 must be undertaken. Schottky<sup>2</sup> and Jost and Nehlep<sup>1</sup> made a theoretical examination of the crystal lattice of sodium chloride and found that vacancies are predominant in both the sodium chloride itself and the alkaline earth oxides which form a lattice of the sodium chloride type, consisting of bivalent ions. The formation of excess barium atoms in the crystal lattice of activated BaO will therefore be due to an increased formation of vacancies in the lattice of the oxygen ions. Fig. 88 shows the configuration of an activated BaO crystal lattice as resulting from such a concept. The residual vacancies in the lattice of the barium ions have been neglected in this figure.

The relationship between BaO and NaCl, as seen by comparing Fig. 88 and Fig. 72, is confirmed by an experimental result of

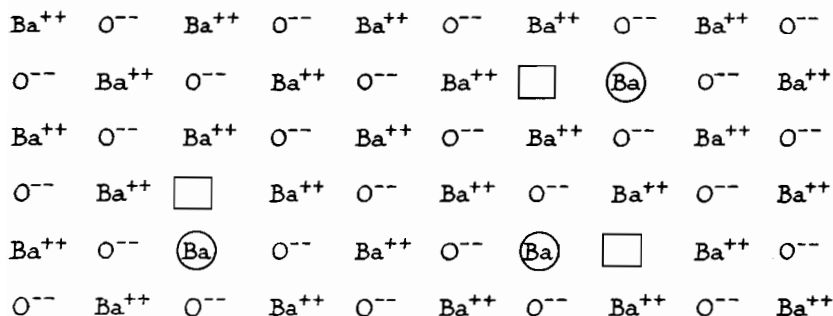


Fig. 88.—Configuration of Excess Barium in the Crystal Lattice of a Barium Oxide Cathode.

Schriehl,<sup>1</sup> according to which BaO is coloured red by taking up excess barium. This colouring effect seems to correspond to the appropriate phenomenon observed with NaCl as described in Sec. 16. The vacancies in the oxygen lattice of BaO producing the excess in barium may therefore be compared with the *F*-centres in NaCl. In drawing Fig. 88 the two electrons necessary for obtaining neutrality of an *F*-centre are associated with one of the surrounding Ba-ions which is indicated by a circle. Such an association, of course, is merely arbitrary; an association of the two electrons with two different ones of the surrounding atoms would seem as reasonable.

When combining the results of this section with the considerations in Sec. 16, it will be concluded that the oxide coating is a semiconductor. This was recently confirmed by measurements of the Hall-effect which have been undertaken by Wright.<sup>5, 6</sup> He found that the sign of the Hall-effect of an oxide coating is that of an

excess conductor\* and that the Hall constant is an exponential function of  $1/T$  as required for semi-conductors by equation (167) or (168). An evaluation of these measurements for determining the number  $n_e$  of excess atoms, however, seems not to be possible at the present state, due to the lack of knowledge of details of the semi-conductor model to be applied to the oxide cathode (cf. Sec. 22).

## 20. The Emission Equation of an Excess Semi-Conductor

The thermal emission of an excess semi-conductor will now be examined theoretically and its emission equation derived. It will then be possible to compare the theoretical results with the experiments, and to find further justification for the semi-conductor model of the oxide cathode as given here. When doing this it will be convenient to deal only with fundamental phenomena which are important for an understanding of the mechanism of the oxide cathode, while phenomena which are of only secondary importance will initially be neglected. Some simplifications will therefore be introduced which will be eliminated later. These simplifications are as follows:

(a) In this chapter we only deal with the fully activated oxide cathode, containing about  $5 \times 10^{-2}$  mol. % excess Ba-atoms which are built into the crystal lattice. Experiments and processes referring to the activation of the cathode are only discussed in this chapter if they are of importance for explaining the mechanism of the fully activated cathode. The real activation process, however, consisting of production and building in of excess Ba-atoms into the crystal lattice, will be discussed in Chapter 6.

(b) It will be assumed that the oxide coating is in an equilibrium, which means that the number of excess barium atoms does not vary with time or space. According to this assumption the electron emission of the oxide cathode occurs in the range below the temperature of "freezing in" (cf. Secs. 15 and 17), and diffusion and ionic conduction which would change the number of excess atoms are negligibly small. This assumption is not fulfilled in practice, as shown in Chapter 6. On the contrary, the difficulties, when working with oxide cathodes, result especially from the existence of diffusion and ionic conduction. But in order to simplify

\* The opposite sign of the Hall-effect was observed under certain conditions, but this was due to impurities, and is consequently of no fundamental importance.

considerations as far as possible, these phenomena may initially be neglected.

(c) It is assumed that the chemical composition of the oxide coating is the same in the whole range between core metal and surface. The influence of interface layers which are sometimes formed at the boundary between core and coating from the components of the two adjoining materials is at first neglected. This influence is important for some phenomena observed with commercial cathodes, but is not of fundamental importance for the mechanism of the oxide cathode (cf. Sec. 32).

(d) It will furthermore be assumed that the oxide coating only consists of barium oxide. The other alkaline earth oxides, the metal oxides in general, and the mixtures of oxides will be discussed in the next chapter. However, as the number of investigations carried out with pure BaO is very small, it will be necessary to use experimental results obtained with [BaSr]O mixtures also in this chapter.

(e) All secondary phenomena resulting from the existence of single, irregularly bounded crystals in the coating will be neglected. This means that the different size and position of the oxide crystals, the pores existing between them, and the roughness of the surface produced by them are neglected, and that the phenomena resulting from this will be discussed in a later section.

(f) It will be finally assumed that the temperature of the cathode is the same over all the coating and that the electrical potential along the cathode does not vary (equipotential cathode).

The energy distribution which the electrons take up in the BaO lattice containing excess Ba must be considered first. This will be done with reference to the NaCl lattice discussed in Sec. 16. There are only two essential differences between NaCl and BaO. The first is the difference in valency: Na is monovalent and Ba bivalent. The other difference results from the fact that the metal ion of NaCl has a lower atomic number and therefore less electrons than the anion Cl, while with BaO it is just the opposite. The barium atom possesses 56 electrons according to Table XVI; oxygen, however, only 8 electrons. The electron configuration of Ba will also be seen from the table mentioned; the configuration of oxygen is:  $2 \times 1s; 2 \times 2s; 4 \times 2p$ .

When the BaO crystal lattice is formed, the two 6s-electrons of barium go into the 2p-shell of oxygen and, together with the electrons already there, make up a completely filled energy band. The position of the highest energy bands in the BaO lattice is given

schematically by Fig. 89. The excess Ba atoms are built into the BaO lattice in the same manner as the excess Na-atoms are built into the NaCl lattice. Hence the energy levels of the electrons of those excess Ba-atoms give interference levels which lie slightly below the corresponding energy bands of the BaO lattice. The interference levels  $\sigma$  of the outer 6s-electrons in particular are located below the empty 6s energy band (conduction band).

The gap between the conduction band and the fully occupied 2p-O band can be estimated from calculations by Wright,<sup>2,3</sup> who computed the energy necessary for lifting an electron from the 2p-band into vacuum. This energy, as will

be seen from the considerations in Sec. 23, is only slightly larger than the energy gap between the 2p-band and the conduction band.

TABLE XX

*Energies  $\chi + \psi$  necessary for lifting an electron from the full 2p-band into vacuum (see figures 89 and 90, values computed by Wright<sup>2</sup>).*

Alkaline earth oxide $\chi + \psi$ (eV)	BaO*	SrO	CaO	MgO
	2.6	3.3	4.8	5.9

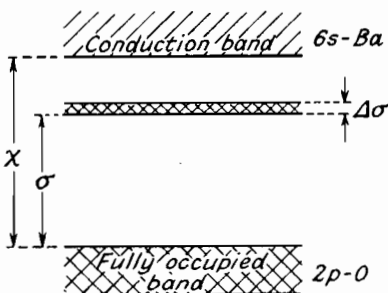


Fig. 89.—Energy Bands of the BaO Lattice with Excess Ba built in.

If the temperature is increased, a part of the 6s-electrons in the impurity levels is excited into the 6s-band previously unoccupied. After having arrived in this band, the electrons may be conducted to the surface of the coating and may be emitted from there into the vacuum. For discussing this emission, the plot of the energy bands in Fig. 89 must be extended towards the surface and the vacuum beyond the surface. It must then be taken into consideration that a potential barrier exists at the surface of the oxide coating in the same manner as with metals. It is, however, not important in this context, whether this potential barrier is only produced by the BaO lattice or whether it is modified by Ba-ions adsorbed at the surface similar to the W-Ba cathode. The potential plot in Fig. 90 is therefore obtained, defining the potential of the electrons in the coating and in the vacuum.

\* Footnote added during proof reading: A recent optical determination by Tyler<sup>1</sup> has given  $\chi = 3.8$  eV.

Two amounts of energy must be supplied to the electrons to enable them to be emitted. These two energies are:

(a) The internal work function  $\phi = \chi - \zeta$  which is necessary to lift the electrons into the conduction band.

(b) The energy  $\psi$  enabling the electrons to overcome the potential barrier at the surface. This energy corresponds to the work function of metals and is now called external work function.

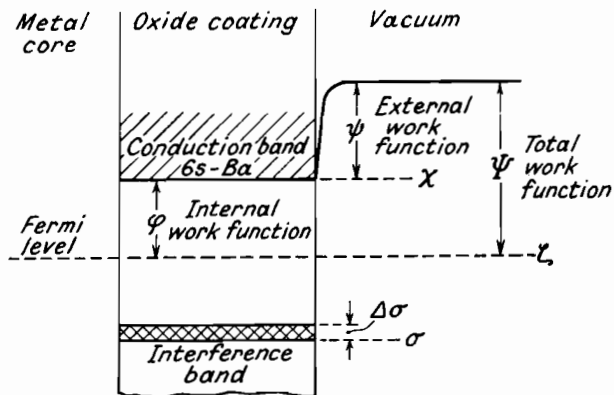


Fig. 90.—Potential of Electrons in and at the Surface of an Oxide Coating.

The total energy to be supplied for the emission of an electron is equal to the sum of the two partial amounts given above and is called total work function  $\Psi$ . Accordingly:

$$\Psi = \phi + \psi \dots \dots \dots \quad (172)$$

The internal work function  $\phi$  in this equation is effective in the interior of the coating and characterizes the share of the interior in the emission. The external work function  $\psi$ , however, is effective at the surface and characterizes the share of the surface.

While a formula for the external work function  $\psi$  cannot be given, the value of the internal work function  $\phi = \chi - \zeta$  can be obtained from the calculations in Sec. 17. It has been shown there that the internal work function, or what is the same, the position of the Fermi-level with reference to the conduction band, depends very much on the special model which is assumed for the semi-conductor. If only one sharp interference level and no additional traps exist equation (143) is valid, while with additional traps present, equation (154), and with an interference band instead of a sharp level, equation (160) must be employed. In this book equation (160) will

mainly be used, implying that a band of interference levels of the width  $\Delta\sigma$  exists (cf. Fig. 90). If condition (143a) is fulfilled the value  $(\chi - \zeta)_{\Delta\sigma=0}$  in (160), indicating the internal work function for zero width of the interference band, can be approximated to by introducing the interference density  $n_{(kT)}$  instead of  $n_\sigma$  into equation (143). It may be repeated here that the interference density  $n_{(kT)}$  indicates the number of excess barium atoms whose interference levels lie in a strip of the width  $kT$  in the interference band (cf. pp. 139, 140). Using the approximate value of  $(\chi - \zeta)_{\Delta\sigma=0}$  from (143), (160) becomes:

$$\phi_{appr} = \frac{1}{2}[\chi - (\sigma + \Delta\sigma)] + 0.99 \times 10^{-4} T \ln \frac{(CT)^{3/2}}{n_{(kT)}} . \quad (173)$$

The deviation between this approximate value and the exact value of  $\phi$  will be seen from Fig. 75 for  $n_{(kT)}$  instead of  $n_\sigma$  and for  $\sigma + \Delta\sigma$  instead of  $\sigma$ .

The fact that the internal work function according to (173) depends on the width  $\Delta\sigma$  of the interference band may be used to explain the increase in emission during the activation of the cathode. As outlined in Sec. 17, the width  $\Delta\sigma$  will increase with increasing number of excess atoms, and both the internal work function according to (173) and the total work function according to (172) will therefore decrease during activation. An increasing emission current is therefore observed.

For deriving the equation of the emission current, the value of the density  $N_x$  of electrons in the conduction band, given, for instance, by (140), must be used. The fraction of  $N_x$  having an energy larger than  $\chi + \psi$  will be enabled to overcome the potential barrier at the surface and will give the required emission current. It must be borne in mind, however, that the energies of the electrons in the conduction band are not distributed according to Fermi as with metals, on account of the fact that the electron density in this band is very small. The density can be estimated from (147), if the number  $n_\sigma$  of excess atoms and the energy  $\chi - \sigma$  are known. Using the value  $n_\sigma = 1 \times 10^{19}$  from (171) and an approximate value  $\chi - \sigma = 0.6$  eV as found by the conductivity measurements (cf. Sec. 22), we obtain  $N_x \approx 10^{18} \text{ cm.}^{-3}$  for the operating temperature  $T = 1000^\circ \text{ K}$ . An application of equation (14) then gives the critical temperature  $T_k \approx 30^\circ$ . As this temperature is exceeded by more than a factor ten during the operation of the cathode, a Maxwell distribution of the electrons will exist in the conduction band.

Contrary to metals the emission equation of the oxide cathode must therefore be derived by using Maxwell's distribution law (20). Apart from this essential difference the calculation can be carried out in the same manner as with metals. First of all the momentum co-ordinates  $p_x$ ,  $p_y$ , and  $p_z$  must be introduced as independent variables into the Maxwell distribution (20) instead of the energy  $E$ . Equation (20) must therefore be multiplied with the ratio of the respective phase volumes.

$$\frac{dp_x dp_y dp_z}{4\pi p^2 dp}$$

By using the values from (6) for  $E$  and  $dE$  and by equating  $N$  to  $N_x$  the relation:

$$N(p) dp_x dp_y dp_z = N_x (2\pi m k T)^{-3/2} e^{-p^2/2m k T} dp_x dp_y dp_z$$

is obtained. This equation is transformed by introducing the value (36) for the energy  $E^{(n)}$ , appropriate to the normal component of velocity (in  $z$ -direction perpendicular to the surface), and by integrating over the tangential momentum components  $p_x$  and  $p_y$ . The number of electrons whose energy is between  $E^{(n)}$  and  $E^{(n)} + dE^{(n)}$  is thus obtained:

$$\bar{N}(E^{(n)}) dE^{(n)} = \frac{N_x}{2(\pi k T)^{1/2} E^{(n)1/2}} e^{-E^{(n)}/k T} dE^{(n)} . . . (174)$$

Furthermore, the number of corresponding electrons striking unit area of the surface per second is derived by multiplication with the velocity component  $v_z = \sqrt{(2E^{(n)}/m)}$ . Then with  $C$  from (41a):

$$N(E^{(n)}) dE^{(n)} = \frac{N_x}{h C^{1/2}} T^{-1/2} e^{-E^{(n)}/k T} dE^{(n)} . . . (175)$$

Of this number all electrons having an energy  $E \geq e\psi$  can be emitted. A suitable integration and a multiplication with the electron charge  $e$  therefore gives the total electron current which is emitted per unit of the surface area:

$$\begin{aligned} j_s &= \frac{e N_x}{h C^{1/2}} T^{-1/2} \int_{e\psi}^{\infty} e^{-E^{(n)}/k T} dE^{(n)} \\ &= N_x \frac{e k}{h C^{1/2}} T^{1/2} e^{-e\psi/k T} . . . . . (176) \end{aligned}$$

If the electron density  $N_x$  were independent of temperature this emission equation would be identical with the old Richardson's  $T^{1/2}$ -law, in which the constant, multiplying the exponential function, also depends on the number  $N$  of electrons.

Actually the electron density  $N_x$  is given by one of the formulæ derived in Sec. 17, either (140), (147), (155), or (161). Whilst formula (140) is universally valid, the other equations refer to one of the respective models to be assumed for the semi-conductor. Using the universal formula (140) with  $\chi - \zeta = \phi$  and  $G=2$ , the result for a surface area of  $S \text{ cm.}^2$  is:

$$I_s = 2e \frac{k}{h} CST^2 e^{-e(\phi+\psi)/kT} \quad . . . . \quad (177)$$

and with (48):

$$I_s = A_0 ST^2 e^{-11610(\phi+\psi)/T} \quad . . . . \quad (177a)$$

The emission equation so obtained for the oxide cathode has the same form as emission equation (47) for metals. The only but essential difference between these two equations is that the external work function  $\psi$ , the only one existing for metals, is replaced in the exponent of (177) by the sum of the internal and external work functions.

The value of the internal work function  $\phi = \chi - \zeta$  in the above equation must be taken from one of the formulæ (143), (154), or (160) calculated in Sec. 17. According to all these formulæ the value of  $\phi$  depends on temperature, and the temperature-dependence of the emission current, given by (177), will be modified by the temperature-dependence pf  $\phi$ . In some cases it will therefore be desirable to introduce the suitable value of  $\phi$  in (177). If equation (160) for  $\phi$  is used, implying the existence of an interference band in the oxide cathode, the result is:

$$I_s = 2e \frac{k}{h} C^{1/4} S n_{(kT)}^{1/2} T^{5/4} e^{-e[\frac{1}{2}(\chi-\sigma)+\psi-\frac{1}{2}\Delta\sigma]/kT} \quad . \quad (178)$$

The constant multiplying the exponential function of this equation will be abbreviated by:

$$\begin{aligned} A_0^{(5/4)} &= 2e \frac{k}{h} C^{1/4} n_{(kT)}^{1/2} \\ &= 2.45 \times 10^{-6} n_{(kT)}^{1/2} \text{ amp./cm.}^2 \text{ degree}^{5/4} \quad . . . . \quad (179) \end{aligned}$$

A similar equation for the case of sharp interference levels instead of an interference band was given by Fowler<sup>1</sup> and Schottky.<sup>1</sup>\*

\* Cf. W. Schottky in C. Ramsauer, *Das freie Elektron in Physik und Technik (The Free Electron in Physics and Technique)*, 1940, p. 48.

If, however,  $\phi$  is taken from equation (154) implying the existence of additional electron traps in the crystal lattice of the oxide coating, the following emission formula is obtained:

$$I_s = \frac{n_o}{n_a} A_0 S T^2 e^{-e(x-\sigma+\psi)/kT} \dots \quad (180)$$

$n_a$  denoting the number of trapping sites ( $n_a \gg N_x$ ).

It may be emphasized that equation (177) is universally valid, while the other two equations (178) and (180) only refer to one of the special models which may be assumed for the semi-conductor "oxide cathode." The universal equation has the further advantage that the total work function which is the essential constant of all emission phenomena occurs in the exponent explicitly. Equation (178) and (180), however, do not contain the work function but values which are identical to the work function only at  $T=0$ . On the other hand, the exponent of the universal equation depends very much on temperature, whilst the exponents of the special equations (178) and (180) are only temperature-dependent if there is a temperature-dependence of the interference energy  $\chi - \sigma$  or of the external work function  $\psi$ .

It may be pointed out that each of the two special formulæ (178) or (180) may be valid for the oxide cathode in a certain state of activation. As the number  $n_o$  of excess atoms is small at low activation states, it may then be comparable with the number  $n_a$  of additional traps, and equation (180) will therefore be valid. If the activation, however, is improved and  $n_o$  increases, the additional traps may be neglected, while the interference levels widen into a band, so giving rise to an emission law as given by (178).

The considerations and calculations leading to the above emission equations are only valid if the number  $n_o$  of excess atoms is not too large. If  $n_o$ , however, exceeds a certain value, the density of the electrons in the conduction band may become so high that there is no longer a Maxwellian distribution. In addition to this, the gap between the conduction and the interference band becomes smaller with increasing  $n_o$ , and equation (161a), which was the main condition for the calculations in Sec. 17, may therefore become invalid. The deviations from the normal emission formula produced by very high values of  $n_o$  have been discussed by Braun and Busch,<sup>1</sup> who considered the case where no additional traps exist in the semi-conductor. They showed that, while equation (177) is valid universally, equation (178) is only valid on two conditions.

Equation (161a) must be fulfilled and in addition to it the following relation must be observed:

$$n_o \ll \frac{(CT)^{3/2}}{0.37} \quad \dots \quad (181)$$

$C$  denoting the constant defined by (41a). For  $T=1000^\circ$  we obtain  $n_o \ll 2 \times 10^{20}$ , a condition which is most likely always to be fulfilled

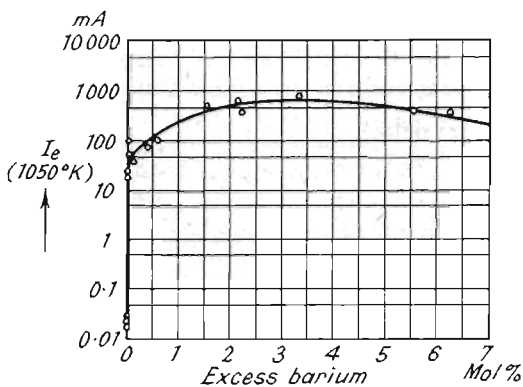


Fig. 91.—Emission Current as a Function of the Quantity of Excess Barium for Large Quantities (Prescott and Morrison).

with oxide cathodes. The only essential condition limiting the application of the emission formulæ is therefore (161a).

Finally an experiment may be mentioned which shows the behaviour of the emission current, as observed if the quantity of excess barium is increased beyond its normal value. Fig. 91, giving the emission currents measured by Prescott and Morrison<sup>1</sup> as a function of the percentage of excess barium, shows that a maximum emission was obtained at about 3%.

Concluding this section it may be pointed out that the work function of an oxide cathode has not a uniform value along the surface of the cathode. Electron images taken from oxide cathodes (cf. Fig. 92) show that different areas of these cathodes emit with different intensities. The conditions are quite similar to those on metal cathodes, the differences in emission being due to differences between the work function

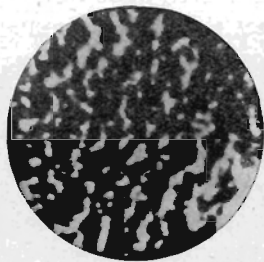


Fig. 92.—Electron Image of an Oxide Cathode (mag.  $\times 30$ ).

of the different areas. The causes for these differences in work function will be discussed later (cf. Sec. 28); it will be sufficient to know in this chapter that on account of these differences all calculations are to be carried out with mean values of the work function. The particular phenomena connected with differences in work function may be discussed as for metal cathodes, and the mean values may be defined in the same manner.

## 21. Application of the Methods of Measuring the Work Function to the Oxide Cathode

### 21.1. Experimental details

It is as important as for metal cathodes to have reliable methods for measuring the work function of oxide cathodes. These methods are to be employed first for comparing the emission of cathodes made in different manners. In addition to this these methods are of importance for proving definitely that the mechanism of the oxide cathode is as described above. According to the results in the previous section the work function, and only the work function, varies during the activation of the cathode, provided this work function has been measured accurately. This behaviour of the work function during the activation can be considered as a criterion for the validity of the concept of emission given in this book.

An important factor in determining the work function is the accurate measurement of the emission current, the details of which have been discussed in Vol. I, Sec. 10. It may be emphasized here that such a measurement of the emission must not vary the composition of the coating, which means the number and distribution of the excess barium atoms. Such a variation of the composition may be produced by phenomena of diffusion and ionic conduction in the coating which always exist to a certain degree. Experimental evidence shows that inaccurate results produced by these phenomena are best avoided when measuring the emission either at low temperatures (lower than 750° K.) or in a very short time by applying short pulses of anode voltage (cf. Vol. I, Sec. 10.1).

When the density of the measured emission current is to be ascertained, a difficulty arises from inadequate knowledge of the emitting surface. This emitting surface may be very different from the macroscopical surface area of the coating due to the considerable roughness normally existing at the surface. The macroscopical surface area or "coating surface"  $S_c$  is defined by the geometric

configuration of the core metal and by the length and thickness of the coating.

The emitting surface  $S_e$ , however, is the total surface contributing to the emission current. The surface so defined also includes those surface elements which have a very high work function and contribute to the total emission of the cathode to a very small degree. On the other hand, surface elements, lying so deep that they are prevented from emitting by a space-charge even under saturated current conditions, will not be included in the emitting surface. The emitting surface according to this definition may be considerably larger than the coating surface  $S_c$  due to the great roughness of the surface. The value  $S_e$  of the emitting surface, which may also depend on the external field strength because of the space-charges in the cavities of the coating, can only be ascertained very roughly.

Wooten and Brown<sup>1</sup> tried to determine the emitting surface by measuring the adsorption of butane and ethylene at oxide cathodes. They obtained for sprayed cathodes an adsorbing surface which was about 30 times larger than the macroscopical surface. However, the adsorbing surface so obtained is likely to be considerably larger than the emitting surface defined above.

Before ascertaining the work function, it must be verified that the emission current to be used is saturated, and this is done by measuring the current as a function of anode voltage. An extrapolation of the saturated current to zero external field is as difficult with oxide cathodes as with atomic film cathodes, the difficulty being due to different reasons. As shown by Morgulis,<sup>2</sup> the Schottky line, representing the relation between saturated current and anode voltage for metals, must be modified when dealing with semiconductors.

Firstly, the fact must be taken into account that the energy levels near the surface of a dielectric or a semi-conductor will be depressed by an applied external field (cf. Fig. 93). Consequently not only the external work function is reduced by an amount  $\Delta\psi$  as with the normal Schottky effect, but an additional reduction  $\Delta\phi$  in internal work function is obtained due to the depression of the conduction

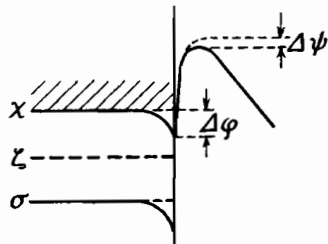


Fig. 93.—Depression of Energy Levels of a Semi-Conductor produced by an External Electrical Field (Morgulis<sup>2</sup>).

band. This additional reduction in work function was calculated by Morgulis and the details may be found in his paper.

Another modification of the normal Schottky line arises from the dielectric properties of the semi-conductor. The electrical charge induced in a dielectric by the image force of an emitted electron is not equal to the charge of the electron but is obtained by multiplying the electronic charge by the factor  $(\epsilon - 1)/(\epsilon + 1)$ ,  $\epsilon$  denoting the dielectric constant. The image force at the surface of a dielectric is therefore derived by introducing the same factor on the right-hand side of equation (25), and this factor will also appear under the square root of equation (71) giving the Schottky line for metals. If a semi-conductor is considered which is somewhere in between a pure dielectric and a metal, the slope of the Schottky line will therefore be modified by a factor whose value is between  $\sqrt{[(\epsilon - 1)/(\epsilon + 1)]}$  and 1. The numerical value of this factor, of course, will not differ very much from 1, as, for instance, for alkaline earth oxides  $\sqrt{[(\epsilon - 1)/(\epsilon + 1)]} \approx 0.9$ .

Checking the formulæ for the relation between saturated current and anode voltage is made difficult by the differences in work function between different areas of the cathode surface and by the roughness of this surface. The influence of the differences in work function is the same as for atomic film cathodes (cf. Sec. 6), while the roughness of the surface makes it impossible to ascertain exact values of the field strength at the surface. For these reasons empirical formulæ have normally been used for extrapolating the saturated current to zero external field.

The following equations have been employed for such an empirical extrapolation in the papers by Heinze,<sup>1</sup> Gill,<sup>1</sup> Wheatcroft,<sup>1</sup> Huber,<sup>1</sup> Sproull,<sup>1</sup> Champeix,<sup>1</sup> and Hung.<sup>1</sup>

$$I_{s1} = I_{s1}^{(0)} e^{k_1(V_A + U_{KA})} \quad \dots \quad \dots \quad \dots \quad \dots \quad \dots \quad (182)$$

$$I_{s2} = I_{s2}^{(0)} e^{k_2 \sqrt{(V_A + U_{KA})}} \text{ (Schottky's } \sqrt{V}\text{-law)} \quad \dots \quad \dots \quad \dots \quad \dots \quad \dots \quad (183)$$

$$I_{s3} = I_{s3}^{(0)} + k_3 \sqrt{(V_A + U_{KA})} \quad \dots \quad \dots \quad \dots \quad \dots \quad \dots \quad (184)$$

$$I_{s4} = I_{s4}^{(0)} (V_A + U_{KA} + 1)^{k_4} \quad \dots \quad \dots \quad \dots \quad \dots \quad \dots \quad (185)$$

The  $k_i$  are independent of  $V_A$ , and may have different values for different cathodes. According to Heinze<sup>1</sup> and Huber<sup>1</sup> the saturated current as a function of anode voltage is best represented by equation (185), this result being valid for both low temperatures (Huber, 550–650° K.) and high temperatures (Heinze, up to 1150° K.) A double logarithmic plot of saturated current against

anode voltage therefore gives a straight line which can be used for extrapolating the saturated current to zero field. Such a plot is shown in Fig. 94 in which  $k_4 \approx 0.3$ . The figure illustrates that little accuracy can be expected if the zero field current is obtained by extrapolation of high currents such as are measured at higher temperatures.

The slope of the straight line so obtained is given by the exponent  $k_4$  and depends on the roughness of the cathode surface, according

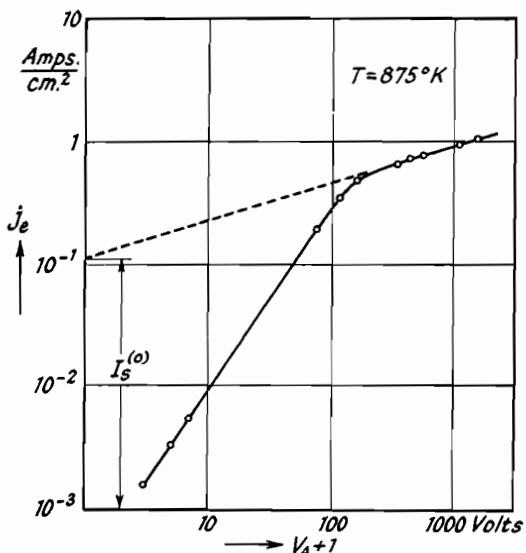


Fig. 94.—Space Charge Current and Saturated Current Characteristic of an Oxide Cathode, obtained by using Anode Voltage Pulses of  $1\mu$  sec. Width.

to unpublished measurements of Krieg. The slope is considerably larger for sprayed cathodes with rough surfaces than for cathodes which are made by electrophoresis, having a very smooth surface. This result can easily be explained as not the anode voltage but the field strength resulting from it will be decisive for the variation of the saturated current with anode voltage, and as the field strength on the average will be higher at the rough surface than at the smooth surface. The exponent  $k_4$ , determining the slope, is independent of temperature in the temperature range in which a D.C. measurement of the saturated current is possible with fully activated cathodes (up to about  $750^\circ$  K.). If the temperature is higher,  $k_4$  normally increases with increasing temperature, but this may be due to

secondary influences, as for instance the heating-up of the coating produced by the emission current.

The individual methods for measuring the work function of oxide cathodes will now be discussed. The discussion in this section will be limited to the measurement of the total work function and will be undertaken in close connection with Chapter 2, dealing with the methods for measuring the work function of metals.

## 21.2. Richardson line

The Richardson method may be used in the same way as for pure metals and atomic film cathodes, but the difficulties which arise are the same as discussed in Sec. 8. Furthermore, it must be taken into account that the diffusion phenomena in the oxide coating which were mentioned above depend on temperature to a high degree. As the temperature must be varied when taking the Richardson line, the composition of the oxide coating may be changed due to the variation of the diffusion with temperature. It may therefore be possible that the individual measured values do not correspond to the same state of the cathode.

Different ways have been tried in order to avoid errors produced by these diffusion phenomena. According to Espe,<sup>1</sup> for example, the cathode is at first heated at the highest temperature necessary for the measurements and at the anode voltage used later on, until a constant emission current is obtained. The emission values for the Richardson line are then measured as quickly as possible (within 3 to 4 minutes), reproducible values being obtained in this manner. But the diffusion processes may produce faulty results in spite of the reproducibility observed, because the diffusion processes may also be reproducible. The optimum conditions are given by a very quick measurement, for instance by the method of Kniepkamp and Nebel.<sup>1</sup> These workers employed the electrical resistance of their directly-heated cathodes as a measure for the temperature and measured the saturated current as a function of the resistance by means of an oscillograph. The time for measuring a Richardson line could so be reduced to  $\frac{1}{2}$  second.

Another question to be discussed here is which of the three emission formulæ (177), (178), and (180) which were derived in Sec. 20, should be used for the Richardson method. In addition to those three formulæ two more equations have been used in practice by the many workers who applied Richardson's method to the oxide cathode. The first of these equations is the old Richardson's

$T^{1/2}$ -law as given by (175), which was frequently employed by the early investigators, whilst the second one was derived by de Boer from his concept of thermal ionization of the excess Ba-atoms (cf. Vol. I, Sec. 1). This latter equation omits the factor  $T^n$  which normally multiplies the exponential function and whose index  $n$  characterizes the main difference between all the different formulæ. According to de Boer: \*

$$I_s = A_0^{(0)} e^{-e\phi/kT} \dots \dots \dots \quad (186)$$

In general, all the emission formulæ can be written as follows:

$$I_s = A_0^{(n)} S_e T^n e^{-e\beta^{(n)}/kT} \dots \dots \dots \quad (187)$$

$n$  denoting the figures 0,  $\frac{1}{2}$ ,  $\frac{5}{4}$ , or 2,  $A_0^{(n)}$  the appropriate emission constant, and  $\beta^{(n)}$  the work function or any other value occurring in the exponent of the respective emission formula. The theoretical value of the emission constants  $A^{(n)}$  may again be indicated by the subscript 0, while this subscript will be omitted if experimental values which more or less differ from the theoretical one are given. As pointed out in Sec. 3, it is not possible to discriminate experimentally between the different emission equations given by (187) for different values of  $n$ .

If formula (187) is used for the Richardson method, we have:

$$\log I_s/T^n = -\frac{5040}{T} \beta^{(n)} + \log A_0^{(n)} S_e \dots \dots \quad (188)$$

Given two values  $I_{s1}$  and  $I_{s2}$  and the appropriate two temperatures  $T_1$  and  $T_2$ , the exponent  $\beta^{(n)}$  is then to be calculated from:

$$\beta^{(n)} = \frac{0.198 \log \frac{I_{s1}/T_1^n}{I_{s2}/T_2^n}}{(1/T_2 - 1/T_1) \times 10^3} \dots \dots \quad (189)$$

Comparing the applicability of the different equations to the Richardson method, equation (178) ( $n=\frac{5}{4}$ ) should be preferred, because the exponent of this equation has from theoretical considerations the smallest temperature-dependence. The exponent of (177) ( $n=2$ ) is certainly much more temperature-dependent due to the temperature-dependence of  $\phi=\chi-\zeta$  as given by (143). Most investigators, however, have preferred this latter equation and a simple formula for converting the emission constant obtained for the one equation into that valid for the other one will therefore

\* J. H. de Boer, *Electron Emission and Adsorption Phenomena*, Cambridge, 1938, p. 340.

be useful. The appropriate formula, which is easily derived from (187) is:

$$\frac{A^{(5/4)}}{A^{(2)}} = T^{3/4} e^{11610(\beta^{(5/4)} - \beta^{(2)})/T} \quad . . . \quad (190)$$

The exponents  $\beta^{(n)}$  obtained from (188) with the same experimental values, by using either  $n=2$  or  $n=\frac{5}{4}$ , are not very different, the difference being approximately 0.05 eV under normal conditions (fully activated cathode). Using this difference:

$$\frac{A^{(5/4)}}{A^{(2)}} \approx 300 \quad . . . . . \quad (191)$$

The fact that the exponents  $\beta^{(n)}$  derived either from (177) for  $n=2$  or from (178) for  $n=\frac{5}{4}$  are not very different from each other may be easily understood.  $\beta^{(2)}$  is equal to the total work function  $\Psi$ , but only the value  $\Psi_0$  at zero temperature can be obtained by means of the Richardson method. Furthermore, it follows from (172) and (173) that

$$\Psi_0 = \frac{1}{2}(\chi - \sigma) + \psi - \frac{1}{2}d\sigma \quad . . . . . \quad (192)$$

provided the terms on the right-hand side of this equation are temperature-independent. On the other hand, the right-hand side of (192) is equal to the exponent  $\beta^{(5/4)}$  of (178), and the difference between  $\beta^{(2)}$  and  $\beta^{(5/4)}$  is therefore only due to the influence of the different indices  $n$  of the temperature  $T$  in (177) ( $n=2$ ) or (178) ( $n=\frac{5}{4}$ ) respectively.

The values measured by the different workers for  $A^{(n)}$  and the mean value  $\bar{\Psi}_0$ , are compiled in Table XXI. The values are valid for fully activated cathodes and for the anode voltage used in the respective measurements, which is normally of the order of 100 volts. The emission equation used for the determination of  $\Psi$  by the worker has been indicated in the table by reference to the respective equation number and by giving the value of  $n$ .

It has been shown in detail in Sec. 8 that an accurate value of the emission constant  $A_0$  cannot be obtained, and it will therefore not be possible to calculate exact values of  $n_{(kT)}$  from the measured emission constants  $A$ . A rough estimate, however, may be given here. The two main influences to be accounted for are the temperature-dependence of  $\bar{\Psi}$  and the inaccurate knowledge of the emitting surface  $S_e$ . If equation (89) is used:

$$A^{(n)} = A_0^{(n)} \frac{S_e}{S_c} e^{-11610d\bar{\Psi}/dT} \quad . . . . . \quad (193)$$

TABLE XXI

Total Work Functions of Oxide Cathodes, measured by the Richardson Method

Composition of oxide coating	Year of measurement	Measured by	$\bar{\Psi}_0$ (eV)	$A$	Emission equation used	$n$
BaO and BaO-SrO.	1920	Arnold <sup>1</sup>	1.55-1.9	—	(176)	$\frac{1}{2}$
BaO-SrO	1924	Davisson and Germer. <sup>1</sup>	1.48-1.65	—	(177)	2
BaO	1924	Spanner <sup>1</sup>	1.85	—	(176)	$\frac{1}{2}$
SrO			2.15	—	(176)	
CaO			2.4	—	(176)	
BaO-SrO	1925	Koller <sup>1</sup>	1.04	$10^{-3}$	(177)	2
BaO	1926	Espe <sup>1</sup>	0.99	$10^{-3}$	(177)	2
SrO			1.27	—	(177)	
CaO			1.77	—	(177)	
Commercial mixture.	1926	Rothe <sup>1</sup>	0.92-1.24	—	(176)	$\frac{1}{2}$
BaO and BaO-SrO.	1927	Detels <sup>1</sup>	1.3	$10^{-3}$	(177)	2
BaO (condensation cathode).	1929	Espe <sup>2</sup>	1.1	$2 \times 10^{-1}$	(177)	2
[BaSr]O	1931	Huxford <sup>1</sup>	1.24	$1.2 \times 10^{-2}$	(177)	2
[BaSr]O	1932	Kniepkamp and Nebel. <sup>1</sup>	0.95-1.1	$10^{-1}$	(177)	2
[BaSr]O	1935	Patai and Frank. <sup>1</sup>	0.71	$7 \times 10^{-2}$	(177)	2
[BaSr]O	1936	Patai and Tomaschek. <sup>2</sup>	1.04-1.24	$1.8 \times 10^{-2}$	(177)	2
[BaSr]O	1938	Prescott and Morrison. <sup>1</sup>	1.37	$-1.6 \times 10^{-1}$	(177)	2
[BaSr]O	1940	Nishibori and Kawamura. <sup>1</sup>	0.98-1.43	—	(177)	
BaO	1943	Fan <sup>1</sup>	1.5	0.1	(177)	2
[BaSr]O	1946	Champeix <sup>1</sup>	1.1	—	(177)	2
Commercial triple carbonates.	1948	Jacobs, Hees, and Crossley. <sup>1</sup>	0.83-1.03	$9.6-28.0 \times 10^3$	(186)	0
[BaSr]O	1949	Wright. <sup>4</sup>	1.2	—	(177)	2
[BaSr]O	1950	Hung. <sup>1</sup>	1.25	—	(178)	$\frac{5}{4}$

For  $n = \frac{5}{4}$  and with the value of  $A_0^{(5/4)}$  taken from (179) therefore:

$$A^{(5/4)} = 2.45 \times 10^{-6} n_{(kT)}^{1/2} \frac{S_e}{S_c} e^{-11610 d\bar{\Psi}/dT} \quad . . . \quad (194)$$

or

$$n_{(kT)} = 1.67 \times 10^{11} (A^{5/4})^2 \left( \frac{S_c}{S_e} \right)^2 e^{2.32 \times 10^4 (d\bar{\Psi}/dT)} \quad . . . \quad (195)$$

The maximum value of  $A^{(2)}$  from Table XXI is  $A^{(2)} \approx 10^{-1}$ . Then with (191)  $A^{(5/4)} = 30$  and  $(A^{(5/4)})^2 \approx 1000$ . If the approximate value  $S_c/S_e \approx 1$  is used,  $n_{(kT)} \approx 10^{17}$  for  $d\bar{\Psi}/dT = 3 \times 10^{-4}$  and  $n_{(kT)} \approx 10^{19}$  for  $d\bar{\Psi}/dT = 5 \times 10^{-4}$  eV/degree. A reasonable agreement with the value  $n_o = 10^{19}$  from (171) is thus obtained if probable values of the temperature coefficient of  $\bar{\Psi}$  are chosen (cf. Sec. 21.6). Nothing more can be expected on account of the inaccurate knowledge of this temperature coefficient and of all the inaccuracies connected with the determination of  $A$ .

Finally the variation of work function  $\bar{\Psi}_0$  and emission constant  $A$  during the activation of the cathode, as obtained from the Richardson measurements, may be discussed. The results given by different authors are quite contradictory. Espe<sup>1</sup> found that the work function does not vary at all and that only the value of  $A$  increases during the activation. According to Detels,<sup>1</sup> Huxford,<sup>1</sup> and Patai and Frank,<sup>1</sup> however, both work function and emission constant vary during the activation. According to Detels, Kniepkamp and Nebel,<sup>1</sup> and Veenemans<sup>1</sup> there is a linear relation between the values of the work function and the emission constant  $A$ , measured at different states of activation. This relation, which may be written:

$$\bar{\Psi}_0 = c_1 \log A + c_2 \quad \dots \quad (196)$$

( $c_1, c_2$  constants), is shown by Fig. 95 giving the measurements of Veenemans. The same relation was found by Liebold<sup>1</sup> for cathodes with different core metals and by Jacobs, Hees, and Crossley<sup>1</sup> during different stages of life of the cathodes.

Formula (196) is very similar to equation (163) obtained for the constant  $a$  and the exponent  $\beta$  of the conductivity formula of semiconductors. As shown in Sec. 22, the conductivity in and the emission from semi-conductors are interconnected, and it seems therefore to be likely that equations (163) and (196) are due to a common cause. As far as the emission is concerned, two possible explanations may be given for the fact that the emission constant  $A$  decreases with decreasing work function  $\bar{\Psi}_0$  according to (196). Firstly, it may be assumed that with improving activation and decreasing work function the interference density  $n_{(kT)}$  decreases too and that therefore  $A$  decreases according to (194). As seen from (194), the same result would be produced by an increase in the temperature coefficient  $d\bar{\Psi}/dT$ . Such an increase in  $d\bar{\Psi}/dT$  with improving activation is in fact to be expected, because the difference

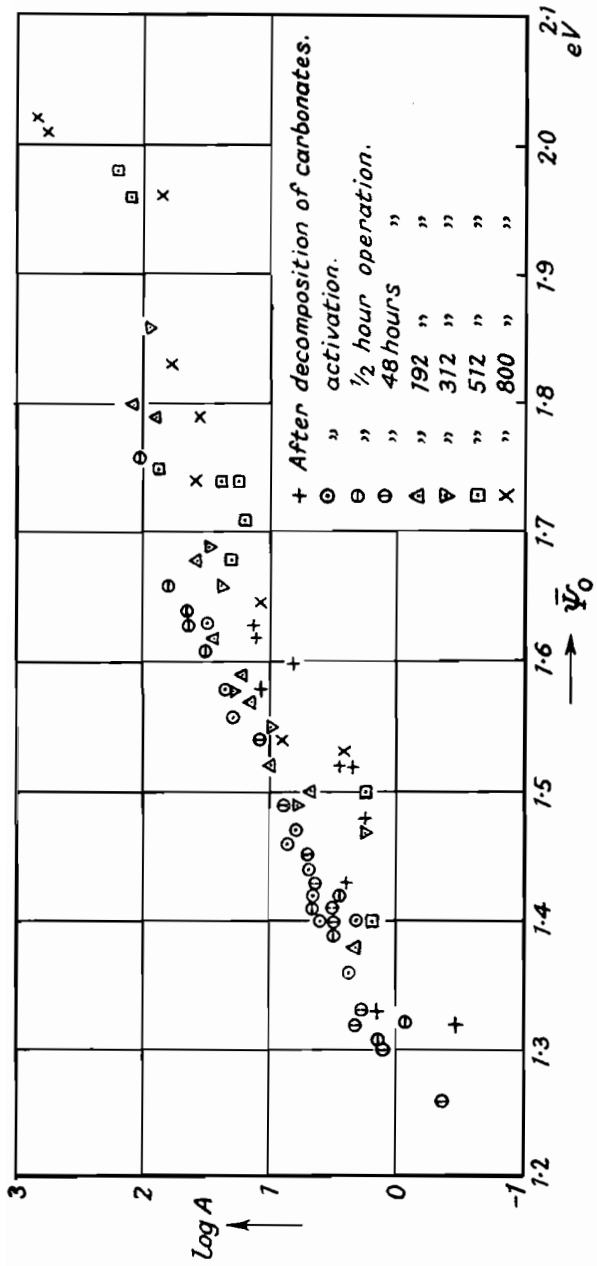


Fig. 95.—Relationship between Emission Constant  $A$  and Work Function  $\bar{\Psi}_0$  of Oxide Cathodes (Veenemans 1).

$\Delta\Psi$  between the maximum and minimum work functions at the cathode surface will increase during activation and because this increase in  $\Delta\Psi$  will give rise to an increasing  $d\bar{\Psi}/dT$  as shown by Fig. 45. An evaluation of equation (196) in detail is not yet possible, as the figures given for the constants  $c_1$  and  $c_2$  by the different authors vary too much.

Veenemans<sup>1</sup> assumed the relation between  $A$  and  $\bar{\Psi}_0$ , shown by Fig. 95, to be a proof that the concept of thermal ionization of Ba-atoms adsorbed at the surface of the oxide coating, as given by de Boer (cf. Vol. I, Sec. 1), would be valid. The above considerations, however, show that within the accuracy of the experimental values the relation between  $A$  and  $\bar{\Psi}_0$  can also be explained by the concept of the mechanism of emission given in this book. Moreover, the correspondence between equation (196) for the emission current and equation (163) for the conductivity of semi-conductors shows the close relationship between these two phenomena which has especially been accounted for in the concept given here. The experimental facts which are against de Boer's assumption will be discussed under (5) in this section.

A fundamental question for deciding between different concepts of the mechanism of emission is, whether the increase in the saturated current during activation is entirely due to a decrease in the work function or not. This question cannot be decided by applying the Richardson method. The variations of  $A$  given by equation (196) only refer to the emission constant  $A^{(5/4)}$  in (178) ( $n = \frac{5}{4}$ ), and the exponent of (178) does not contain the work function at the operating temperature. Although the measured value of  $A$  varies, it is nevertheless possible that the decrease of the total work function  $\Psi$  in the exponent of equation (177) is entirely responsible for the increase of the saturated current during activation. This question can only be decided experimentally by one of the other methods for measuring the work function which give its value at the operating temperature.

### 21.3. Calorimetric measurement

When carrying out the calorimetric measurements described in Sec. 9, the work function is ascertained from the cooling power  $P_{cool}$ . Formulae (92) and (93), which were derived for the cooling power of metals, can be applied to oxide cathodes with only two slight modifications. Firstly the external work function  $\psi$ , being

the only contributor to the cooling power in the case of metals, must be replaced by the total work function, because the internal work function also makes a contribution in the case of oxide cathodes. Secondly it must be taken into account that the emission current, when flowing through the oxide coating, heats the coating (cf. Vol. I, Sec. 12.2) and produces a quantity of heat of amount  $I_e^2 R_C$  per unit time ( $R_C$  resistance of the oxide coating in the direction of the current). The cooling power is thus partly compensated, and the quantity of heat produced must be subtracted from the cooling power when considering the equilibrium of heat in the coating. The final equation for calculating the work function under saturated current conditions therefore is:

$$\bar{\Psi} = \frac{P_{cool}}{I_s} - 1.72 \times 10^{-4} T + I_s R_C \quad . . . \quad (197)$$

The only investigation giving uncontested results by means of the cooling effect is that by Davisson and Germer.<sup>1</sup> They employed the first method discussed in Sec. 9, by directly ascertaining the decrease in temperature after switching on the emission. A work function  $\Psi = 1.61$  eV (after applying the correction term  $1.72 \times 10^{-4} T$  in equation (165)) was obtained for a temperature  $T = 1064^\circ$ . Some other investigations may be quoted here in which either the emission heating of the oxide cathode was not accounted for (Michel and Spanner<sup>1</sup>), or the measurement was carried out in the space-charge range (Rothe,<sup>1</sup> Kroczek and Luebke,<sup>1</sup> and Heinze<sup>1</sup>). The values found in these latter investigations cannot be considered as obtained by means of the cooling effect (cf. Sec. 9).

## 21.4. Photo-electric methods

When the photo-electric methods are used for measuring the thermal work function of the oxide cathode, the special rules for exciting the electrons of a semi-conductor into the conduction band photo-electrically must be taken into account. Two fundamentally different cases can be distinguished. The first case refers to the absolute zero of temperature where the conduction band is empty and the electrons can only be excited from the interference level  $\sigma$  (see Fig. 90). In this case the minimum energy which is necessary for excitation will be equal to the sum of the interference energy  $\chi - (\sigma + \Delta\sigma)$  and the external work function  $\psi$ . If a photo-electric

work function of the oxide coating is defined by relating this work function to the frequency limit  $\nu_0$  in the same way as in equation (102) for metals, we have:

$$\frac{h\nu_0}{e} = \Psi_0^{(ph)} = \chi - (\sigma + \Delta\sigma) + \psi_0 \quad . . . \quad (198)$$

In the second case, when  $T > 0$ , the electrons can be excited from the conduction band; the energy necessary for excitation and the frequency limit therefore become considerably smaller.

The dependence of the photo-emission on frequency has been investigated theoretically by Muto and Yamashita<sup>1, 2</sup> for both ranges of temperature. They found that for  $T=0$  the photo-electric current  $I_{ph}$  can be represented by a straight line in a plot  $I_{ph}$  against  $\nu$ , rising from the frequency limit  $\nu_0$  towards higher frequencies.

TABLE XXII

Photo-electric Work Function  $\Psi^{(ph)}$  of Oxide Cathodes

Type of cathode	Year of measurement	Method	Measured by	Temperature	$\Psi^{(ph)}$ eV
[BaSr]O	1931	?	Huxford <sup>1</sup>	Room temperature. $T=0$	1.32
[BaSr]O	1941	Extrapolation of straight line.	Nishibori, Kawamura and Hirano. <sup>2</sup>	$T=0$	1.66
BaO	1941	Extrapolation of straight line.	Nishibori, Kawamura and Hirano. <sup>2</sup>	$T=0$	1.63
SrO	1941	Extrapolation of straight line.	Nishibori, Kawamura and Hirano. <sup>2</sup>	$T=0$	2.58
[BaSr]O	1949	Fowler	Mahlman <sup>1</sup>	Room temperature.	1.82

If the temperature is raised a temperature-dependent photo-current is obtained for  $\nu < \nu_0$  which passes gradually into the straight line mentioned above. All these considerations are, of course, only valid on the assumption that the photo-emission of the oxide cathode is entirely a semi-conductor phenomenon and that special surface energy states which would influence the photo-current do not exist. This question has not been decided experimentally yet.

Several experimental determinations of the photo-electric work function have been undertaken, and quite different methods have been used. Nishibori, Kawamura and Hirano<sup>2</sup> based their measurements on Muto and Yamashita's calculations and obtained the work function by extrapolating the straight line in a plot  $I_{ph}$  against  $\nu$  to the intersection with the frequency axis. The Fowler method (cf. Sec. 11.1) has also been used, but a theoretical justification for this has not been given. The method of total photo-electric emission has been employed by Suhrmann and Fruehling<sup>1</sup> for BaO and by Suhrmann and Dehmelt<sup>2</sup> for Cs<sub>2</sub>O. However, a theoretical investigation of the application of this method to the oxide cathode has not been given yet and the results obtained in the two above papers will therefore not be discussed further. The other photo-electric work functions which have been measured are compiled in Table XXII.

## 21.5. Contact potential measurements

The laws which were derived for the contact potential between metal electrodes in Sec. 4.1 are only slightly modified if one of the metals is replaced by an oxide cathode. Let us consider the contact potential  $U_{CA}$  between an oxide cathode and a metal anode (cf. the potential plot in Fig. 96). One difference results from the occurrence of the internal work function  $\phi$  which influences the contact potential in the same manner as the external work function, the only one existing for metals. The external work function  $\psi_C$  of the cathode in equation (51) must therefore be replaced by the total work function  $\Psi_C$ , if this equation is applied to an oxide cathode.

Another modification may be necessary with respect to the thermo-voltage correction term to be applied in equation (51). As pointed out on p. 147 the thermo-electric voltage of semiconductors will exceed that of metals by a factor 10 or more. This theoretical conclusion was confirmed for the oxide cathode by measurements of Becker and Sears<sup>2</sup> and Blewett.<sup>2</sup> The latter

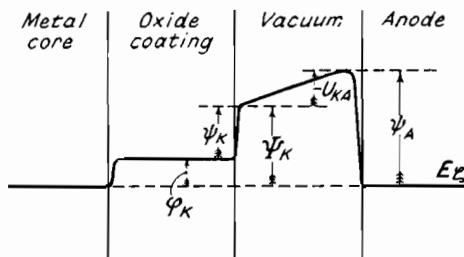


Fig. 95.—Variation of Potential between an Oxide Cathode and a Metal Anode.

The external work function  $\psi_C$  of the cathode in equation (51) must therefore be replaced by the total work function  $\Psi_C$ , if this equation is applied to an oxide cathode.

found a thermo-voltage between  $9 \times 10^{-4}$  and  $3 \times 10^{-3}$  volt/degree. On the other hand, the temperature differences in an oxide coating of normal thickness are so small (about 10 degrees) that the resulting thermo-voltage of about  $10^{-2}$  volt may usually be neglected compared with the contact potential of the order of 1 volt.

Another characteristic of the oxide cathode to be accounted for when measuring contact potentials, is the voltage drop produced across the oxide coating by the emission current. Because of this voltage drop the potential at the cathode surface is not the same as the potential of the core metal determined by the voltmeter. The difference between these two potentials may not be neglected at low cathode temperatures (high resistances) and high emission currents and must be accounted for by a suitable correction.

It has been shown in Sec. 12 that of all contact potential methods the intersection method is the most suitable one, because it gives directly the emissive mean value of the work function. This intersection method is best carried out at low temperatures with small emission currents in order to make the phenomena of ionic conduction and diffusion which change the composition of the coating, negligibly small. The intersection method was employed by Heinze and Wagener,<sup>4</sup> who investigated indirectly heated oxide coatings, consisting of a commercial mixture of the three alkaline earth oxides, on a nickel or platinum core. They especially examined the dependence of the work function on state of activation; the temperature used for these investigations was about  $800^{\circ}\text{K}$ . An example of the results obtained is given by Fig. 97, showing the behaviour of the work function during the activation. It will be seen that the measured mean value  $\bar{\Psi}$  of the work function decreases continuously during the activation.

The saturated currents  $I_s^{(0)}$  obtained by extrapolation to external field zero by means of equation (182), are also plotted in Fig. 97. The values  $I_s^{(0)}$  and the measured mean values of the work function were used for calculating the product  $AS$  of emission constant and surface by means of emission equation (177); this product  $AS$  is plotted in Fig. 97 too. While the saturated current rises from  $3 \times 10^{-9}$  to  $10^{-4}$  amp., the value  $AS$  only varies from 30 to 65. It follows from these and from the other measurements carried out by Heinze and Wagener that the increase of the saturated current during activation is mostly due to a decrease of the mean value of the work function measured by the intersection method.

This decrease in the mean value of the work function observed

during activation may be explained by assuming that the individual work functions  $\Psi$  at the single areas ( $x, y$ ) of the cathode surface decrease too. This would be in line with the mechanism of emission discussed in Sec. 20. On the other hand, however, the results of Heinze and Wagener's experiments, could also justify the concept given by de Boer for the mechanism of emission (cf. Vol. I, Sec. 1). According to de Boer's original concept the work function is given by the ionization voltage  $\Psi'$  of the barium atoms adsorbed at the surface of the coating, and this ionization voltage is a constant which does not vary during activation. The saturated current of

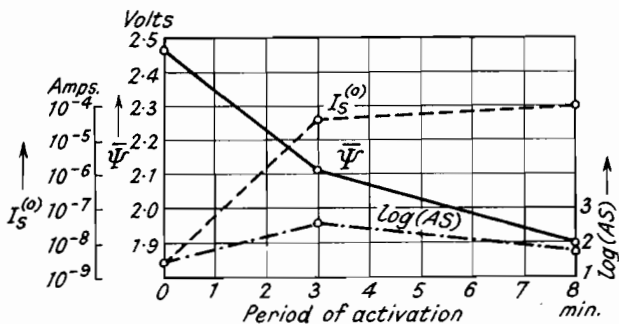


Fig. 97.—Variation of Work Function  $\bar{\Psi}$  and Saturated Current  $I_s^{(0)}$  of an Oxide Cathode during the Activation (Heinze and Wagener<sup>4</sup>).

the cathode is then given by equation (186), in which  $A_0^{(0)}$  is determined by the number of adsorbed Ba-atoms. The increase in emission during activation is explained by an increase in the number of adsorbed atoms and hence of  $A_0^{(0)}$  in (186).

This theory was later supplemented by Veenemans,<sup>1</sup> who assumed different states of adsorption for the Ba-atoms at the surface, each of them characterized by a different value of the ionization voltage  $\Psi'$ . According to this a variation of both  $A_0^{(0)}$  and  $\Psi'$  in (186) would have to be expected.

For deciding between the different concepts of the emission mechanism Heinze and Wagener<sup>2</sup> took electron images of oxide cathodes at different states of activation produced by both heating of the cathode only and drawing of emission current. The saturated current, defining the state of activation of the oxide cathode examined, was measured at about 800° K. in the electron microscope, directly before taking the electron image (cf. Sec. 28). Some of the electron images obtained in this manner are given in Figs. 98 and 99.

As can be seen from these images, the number and position of the emitting centres only varies during the beginning of the activation. A relatively large part of the surface of the coating is occupied by emitting centres during this period, when the saturated current

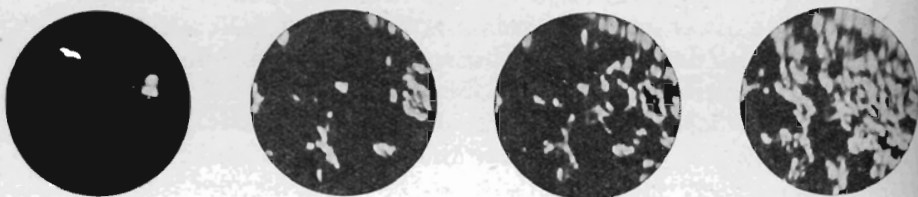


Fig. 98.—Electron Images of an Oxide Cathode, taken at Different Times during the Beginning Period of Activation ( $I_s < 10^{-6}$  amp., mag.  $\times 30$ ).

remains very small ( $< 10^{-6}$  amp.) (cf. Fig. 98). When the activation is continued, the saturated current rising from  $10^{-6}$  to  $2 \times 10^{-2}$  amp., the size and distribution of the emission centres vary very little (cf. Fig. 99). The range of the saturated currents in which the

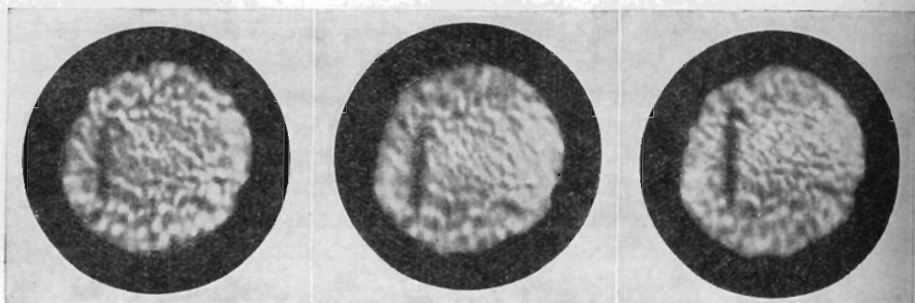


Fig. 99.—Electron Images of an Oxide Cathode taken during Further Activation (mag.  $\times 30$ ): (a)  $I_s = 10^{-6}$  amp.; (b)  $I_s = 2 \times 10^{-3}$  amp.; (c)  $I_s = 2 \times 10^{-2}$  amp. (Heinze and Wagener<sup>2</sup>).

distribution of the emission centres does not vary could be extended to seven powers of 10 in later investigations carried out by means of an electron microscope sealed off the pump (cf. Sec. 28).

This result shows that apart from the period of beginning activation the saturated current increases at all areas ( $x, y$ ) of the cathode surface in the same proportion. In order to account for the concept of de Boer, let us assume for the following that the emission constant  $A_0$  in (187) may depend on the co-ordinates ( $x, y$ ). If two different states of activation denoted by the subscripts 1 and 2

are considered, we have according to the electron microscope images:

$$A_{01}(x, y)e^{-e\Psi_1(x, y)/kT} = KA_{02}(x, y)e^{-e\Psi_2(x, y)/kT} \quad . \quad (199)$$

( $K$  a constant  $> 0$ ). On the other hand, the above result of measuring the work function has shown that the value  $AS = \iint A(x, y)dx dy$  is almost constant during the activation. Hence we have:

$$\iint A_{01}(x, y)dx dy \simeq \iint A_{02}(x, y)dx dy \quad . \quad (200)$$

Let us now assume that  $A_0(x, y)$  increases at some areas of the cathode surface during the activation. This would mean that there are other areas at which  $A_0(x, y)$  decreases because of (200) and at which the work function  $\Psi(x, y)$  increases considerably on account of (194). Such a concept, which would also contradict that of de Boer, seems hardly reasonable. Consequently it can be concluded that the emission constant  $A_0$  is really constant at all areas of the cathode. Then equation (199) gives:

$$\Psi_1(x, y) = \Psi_2(x, y) - \ln K$$

According to this the work function and only the work function decreases uniformly at all areas of the cathode during the activation except at the beginning. This result supports the concept given in Sect. 20 as against de Boer's concept.

The values of the work function measured by Heinze and Wagener<sup>4</sup> for complete activation at 800 °K. were between 1.5 and 2 eV. The deviations between the individual values are due to the fact that the state of best activation was not obtained for all cathodes. More accurate absolute values of the work function were measured by Huber<sup>1</sup> by the same method; he found that fully activated [BaSr]O cathodes have a work function of about 1.4 eV at the operating temperature of 1000° K. (cf. Secs. 25–26).

## 21.6. Temperature-dependence of the work function

The temperature-dependence of the work function of oxide cathodes was measured first by Gysae<sup>1</sup> by the displacement of the characteristic, giving the temperature coefficient of the arithmetic mean value  $\bar{\Psi}$  of the work function according to the considerations in Sec. 12. Gysae found a positive temperature coefficient of about  $1 \times 10^{-3}$  eV/degree for temperatures above 800° K., the values of

different valves differing considerably from each other. In the range below 800° K., however, a widely varying negative temperature coefficient between  $-2$  and  $-15 \times 10^{-3}$  eV/degree was measured. The existence of such a negative coefficient may be doubted, as it gives, for example, at 400° K. a work function of about 3 eV and a saturated current of about  $10^{-31}$  amp./cm.<sup>2</sup> (for  $A_0=120$ ). The saturated current which is really measured with fully activated cathodes at this temperature is about  $10^{-10}$  amp./cm.<sup>2</sup>.

Further evidence of the magnitude of the temperature coefficient can be obtained from the measurements of the work function by Huber,<sup>1</sup> which were carried out by the intersection method. Huber's values, which are valid for the emissive mean value  $\bar{\Psi}$ , are between  $2 \times 10^{-5}$  and  $8.8 \times 10^{-4}$  eV/degree with a mean value of  $3 \times 10^{-4}$  eV/degree; they refer to the temperature range between 600° and 1000° K. Exact values of the temperature coefficient are still to be established. It is not yet possible to decide if the temperature-dependence is only due to taking the mean value of the work function (temperature-dependence of  $\bar{\Psi}$ ) or if an additional temperature-dependence of the individual work functions exists (temperature-dependence of  $\tilde{\Psi}$ , cf. Sec. 12). Another question not yet examined is whether the temperature coefficient of the work function varies with the magnitude of the work function, depending on the state of activation.

Recently Smith<sup>1</sup> has used the measurement of the stopping potential which must be applied for preventing photo-electrons from reaching the anode (cf. 11.2), in order to determine the temperature dependence of the work function of silicon and germanium, these semi-conductors being the anode of his experimental set. An application of this method to the oxide cathode is not known yet.

The temperature-dependence of the work function is normally so large (up to  $10^{-3}$  eV/degree) that it must be taken into account when comparing values of the work function measured at different temperatures. This fact also explains that the work functions, obtained from contact potential measurements at temperatures between 600° and 800° K., are throughout higher than most values obtained by the Richardson method, being valid for  $T=0$  (cf. Table XXI). Since according to equation (89) the temperature coefficient of the work function influences the value measured for the emission constant  $A$  by the Richardson method, the temperature coefficient can be estimated from this value of  $A$ . An approximate value for the work function at higher temperatures can thus be

ascertained from the Richardson values. The most accurate values of the work function obtained by the Richardson method for BaO or [BaSr]O are about 1 eV, while the maximum  $A$ -value is approximately 0.1 (cf. Table XXI). These values together with  $A_0=120$  give a work function of about 1.6 eV at 1000° K. (cf. Fig. 49), which corresponds with the result of the contact potential measurements, if the many errors connected with the Richardson method are accounted for.

After having dealt only with the total work function of the oxide cathode, the question now arises, what are the values of the two components of the total work function, the internal work function  $\phi$  and the external work function  $\psi$ . It will be necessary to discuss these two components separately, the internal work function being considered in connection with the electronic conductivity of the oxide coating. These considerations will also give further proof of the mechanism of the oxide cathode as discussed in this book.

## 22. Electronic Conduction and Internal Work Function of the Oxide Coating

The conductivity of the oxide coating can be measured by the usual methods either by taking a current-voltage characteristic or in a Wheatstone bridge. The application of A.C. is to be preferred in order to avoid electrolysis and polarization voltages. If these normal methods are used, a second electrode in addition to the core metal is needed for applying the measuring voltage. According to Becker and Sears<sup>2</sup> this second electrode may consist of a spirally wound ribbon or wire which is embedded in the coating of a cylindrical cathode (cf. Fig. 100). This method was refined by Fineman and Eisenstein<sup>1</sup> and Danforth and Goldwater,<sup>1</sup> who used two such embedded probes which were arranged concentrically in the coating. The resistance of the coating was measured between these two probes, and it was so possible to exclude the influence of interface layers which may be formed between the core metal and the actual oxide coating (cf. Sec. 32).

When using the above method, a difficulty arises from the fact that the contact resistance between the embedded probe and the loosely built oxide coating is relatively large and that the measurement may be affected by this. Another method was employed by Meyer and Schmidt,<sup>1</sup> who used instead of a normal cathode thin discs of alkaline earth oxide or carbonate which were only some

tenths of a millimeter thick and which were located between two equally formed nickel electrodes. The contact resistance is lowered by this design, but an accurate measurement of the emission which is desirable for comparing conductivity and emission is not possible, because the emission current can only be drawn from the narrow edge of the discs concerned. The employment of thicker specimens of pressed alkaline earth oxides cannot be recommended, as these are very difficult to degas and to activate.

A more accurate measurement of the emission is made possible by the experimental design of Reimann and Murgoci<sup>1</sup> and Reimann

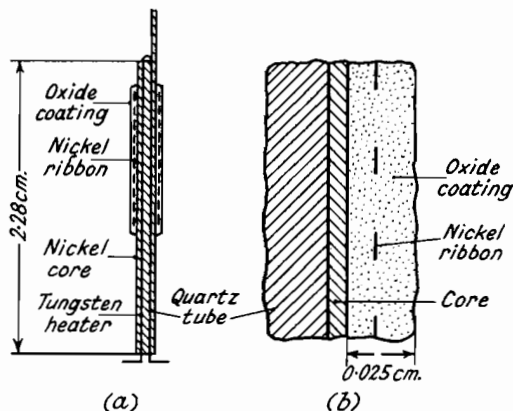


Fig. 100.—Sectional View of an Experimental Cathode for measuring the Conductivity of the Coating: (a) Total View; (b) Enlarged Section (Becker and Sears<sup>2</sup>).

and Treloar.<sup>2</sup> Their cathode consists of two wires of nickel or platinum respectively, which are first coated, then twisted together and coated again after the twisting. The conductivity of the oxide coating is measured between the two core wires as electrodes, the heating current and the current for measuring conductivity being switched on alternately by a special circuit. Eisenstein,<sup>2,3</sup> and Hannay, MacNair and White<sup>1</sup> employed another method by depositing their coating on a ceramic rod. Two platinum contactor wires, previously wound round this rod, supplied the current for the conductivity measurement, while two similar wires were used for measuring the voltage.

Finally, Vink<sup>1</sup> used a combination of two oxide cathodes of the type employed in cathode-ray tubes (cf. Vol. I, Fig. 6), in which the oxide coating is deposited on the end face of a nickel tube. The two

coatings faced each other, and one of them could be moved towards the other along the common axis of the two cathodes. The conductivity could then be measured by bringing the two coatings into contact and using the two nickel cores as electrodes, whilst the emission was measured by separating the cathodes and placing a movable anode in between them.

Other methods for measuring the conductivity are obtained by utilizing the fact that the oxide coating, due to its electrical resistance, is heated up by the emission current. This heating-up of the coating can be counterbalanced by a change in heater power  $\Delta P_H$ , from which the value of the resistance and conductivity can be found. The main difficulty with this method is that the heat equilibrium in the coating (cf. equation (16), Vol. I) is determined not only by the amount of heating-up produced by the emission current, but also by the cooling power  $P_{cool}$ , which depends on the work function of the cathode (cf. Sec. 21.3). The method involves, therefore, the measurement of the work function, but there are two ways to avoid this. The simplest way is to make the heating-up so large that the cooling power can be neglected. This is possible without damaging the coating if pulsed emission currents are taken from the cathode (cf. Vol. I, Fig. 57). Coomes<sup>1</sup> made pulse measurements using two different pulse widths  $w$  and pulse recurrence frequencies  $\nu_r$ . The heating-up, which is different in the two cases, was counterbalanced by an appropriate variation in the heater power  $\Delta P_H$ . Then according to equation (12), Vol. I:

$$\Delta P_H = I_e^2 R_c (w_1 \nu_{r1} - w_2 \nu_{r2}) \dots \quad (201)$$

from which the coating resistance  $R_C$  can be ascertained.

According to Kroczek and Luebke<sup>1</sup> the measurement is undertaken in the space-charge region, in which, as shown in Sec. 9, the cooling power does not depend on the work function. Equation (197) for the cooling power  $P_{cool}$  of the oxide coating has then to be modified as shown in Sec. 9, and the following formula valid in the space-charge region is obtained:

$$P_{cool} = 8.61 \times 10^{-5} T \left( \ln \frac{SA_0 T^2}{I_{sp}} + 2 \right) I_{sp} - R_c I_{sp}^2 \quad . \quad (202)$$

which may be written:

$$\frac{P_{cool}}{I_{sp}} - 8.61 \times 10^{-5} T \left( \ln \frac{SA_0 T^2}{I_{sp}} + 2 \right) = -I_{sp} R_c \quad . \quad (203)$$

If the cooling power  $P_{cool}$  is measured for different space-charge

currents  $I_{sp}$  at a constant temperature  $T$ , the left-hand side of (203) can be calculated and be plotted as a function of  $I_{sp}$ . A straight line is so obtained, the slope of which gives the resistance and the conductivity of the coating.

Another way for measuring the resistance and conductivity of the coating is to determine the potential drop across the coating. Loosjes and Vink<sup>1</sup> used a valve with a movable anode and measured the space-charge characteristic of this valve for different distances between cathode and anode. The anode voltages obtained for constant anode current were then plotted as a function of distance, and the voltage drop in the oxide coating was ascertained by extrapolating this plot to distance zero. In order to ensure a voltage drop which is large enough, high current densities must be applied, which can only be obtained by short time measurements.

Finally Eisenstein<sup>1</sup> gave a method for measuring the voltage drop across the oxide coating by using a diode system with a hole in the anode. The electrons passing through this hole were stopped by a retarding potential applied to an auxiliary electrode. The stopping potential of the auxiliary electrode must then be equal to the potential at the surface of the coating, and the voltage drop across the coating can therefore be determined in this way.

When measuring the conductivity of alkaline earth oxides at or near the operating temperature, another difficulty results from the fact that these oxides are normally not in the range below the temperature of freezing-in, as was assumed before (cf. Secs. 17 and 20). Measuring the conductivity may consequently influence the concentration of the excess barium atoms and therefore the measured value of the conductivity itself. This additional difficulty especially occurs when measuring with D.C.

A further question important for measuring conductivities is that of the validity of Ohm's law. Deviations from Ohm's law were found with the first conductivity measurements of Reimann and Murgoci,<sup>1</sup> who measured at about 1000° K. Becker and Sears,<sup>2</sup> however, showed with the experimental design of Fig. 100 that a linear relation between conduction current and voltage corresponding to Ohm's law is obtained if the experimental conditions are sufficiently good. Their measurements were made with D.C. at 555° K. They observed that the conduction current increased with time and that this increase could be reversed by heating the cathode at higher temperatures. The increasing current is probably produced by an ionic current varying the composition of the coating,

while the restoration of the original state at higher temperatures will be due to a re-establishment of the original composition by diffusion. Whilst the final values of the conduction current gave a slightly bent curve above 1 volt (Fig. 101, curve *b*), the currents at time  $t=0$ , corresponding to the original composition of the coating, gave a straight line in the whole range of voltages (Fig. 101, curve *a*).

In addition to this, Becker and Sears examined the potential distribution in the coating by measuring the voltage which exists between core metal and embedded nickel ribbon, during the flow of emission current. The result showed that the nickel ribbon has a

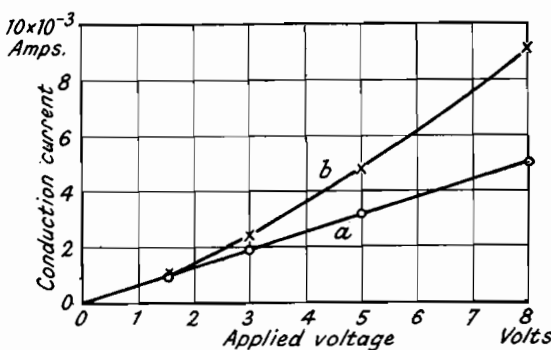


Fig. 101.—Relationship between Conduction Current through the Coating and Applied Voltage (Becker and Sears<sup>2</sup>).

positive potential which varies almost linearly with the emission current, corresponding to the voltage drop at an ohmic resistor.

This linear resistance characteristic, measured by Becker and Sears for low cathode temperatures, was confirmed for higher temperatures ( $750^{\circ}$ – $1350^{\circ}$  K.) by Meyer and Schmidt,<sup>1</sup> Nishibori and Kawamura,<sup>1</sup> Mutter,<sup>1</sup> and Hannay, MacNair, and White,<sup>1</sup> who also measured with D.C. Wright,<sup>1</sup> however, recently found a non-linear relationship between conduction current and voltage. Vink<sup>1</sup> and Loosjes and Vink<sup>3</sup> showed that different shapes of the resistance characteristic may be obtained, depending on the temperature range. They pointed out that the pores of the normal oxide coatings must be taken into account when calculating the conductivity from the measured values. When the measurements are made, as is usual, in vacuum, the electrons traversing the pores from one oxide particle to another shunt the normal current through

the oxide particles themselves. The shunt resistance so obtained may then considerably influence the total resistance characteristic which is measured. Vink's calculations of this shunt resistance show that a curved resistance characteristic is produced by it in the temperature range between 800° and 1000° K., while a linear characteristic is maintained below and above this range. This agrees with Vink's measurements and with those of other authors, who measured in the temperature range 800°–1000° K. and found curved characteristics.

The shunting effect of the pores will certainly depend on the structure of the oxide coating and will decrease with decreasing volume of the pores. Coatings of different structure may therefore show a different behaviour. Hannay, MacNair, and White for instance found that their conductivity values did not vary when they introduced helium of 760 mm. pressure into their experimental valve. They assumed that the pores cannot conduct in such a helium atmosphere and concluded therefore that the pores of their coating did not conduct in vacuum either. This different result may be due to a difference in the coating structures between Vink's and Hannay's cathodes, but on the other hand Hannay's result is not completely conclusive, since the mean free path of thermal electrons in helium of 760 mm. pressure is about  $1 \mu$ ,\* i.e. of the same order as the size of the pores. The experiment should be repeated with higher pressures of helium.

It follows from the above that conductivity measurements should be undertaken with coatings which are very closely packed. Provided this precaution is taken, and provided there are no interface layers between core and coating influencing the conduction properties (cf. Sec. 32), Ohm's law will be valid.

If the relationship between electronic conductivity  $\kappa$  and temperature  $T$  is examined, an exponential law is found corresponding to equation (149) for a semi-conductor. This result, according to which a plot of  $\log \kappa$  against  $1/T$  gives a straight line, was first obtained by Spanner,<sup>1</sup> who examined pressed specimens of pure alkaline earth oxides with D.C. in air (Fig. 102). Such a measurement in air, of course, cannot refer to a composition of the oxides identical with the oxide cathode. The investigation of Reimann and Treloar<sup>2</sup> confirmed the exponential law by measurements in vacuum carried out with D.C. for  $[\text{BaSr}]O$  mixtures. The same result was obtained by Kroczek and Luebke,<sup>1</sup> who used the cooling

\* See J. Townsend, *Electrons in Gases*, London, 1947, p. 52.

effect as described above; by Meyer and Schmidt,<sup>1</sup> who measured thin discs of BaO with A.C. (cf. Fig. 103); by Nishibori and

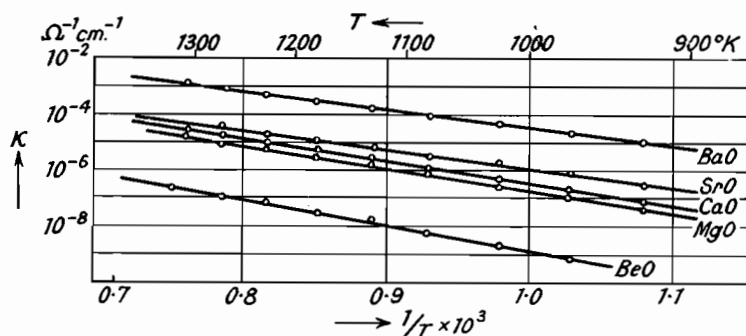


Fig. 102.—Electrical Conductivity of Different Alkaline Earth Oxides as a Function of Temperature (Spanner<sup>1</sup>).

Kawamura<sup>1</sup> and by Wright,<sup>1</sup> who used [BaSr]O cathodes with embedded nickel ribbon and D.C.

These measurements, which give single straight lines in the

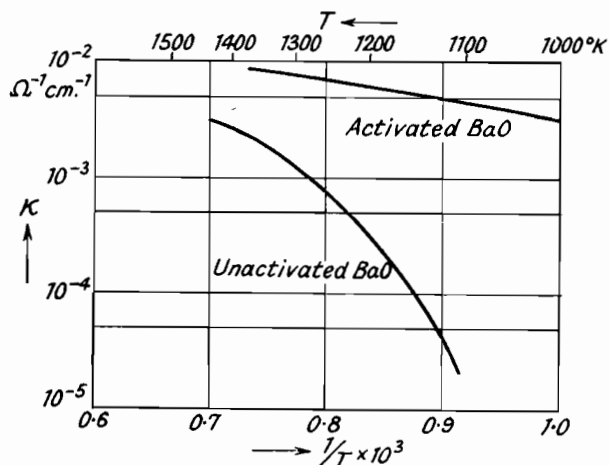


Fig. 103.—Electrical Conductivity of BaO as a Function of Temperature for Different States of Activation (High-Temperature Range) (Meyer and Schmidt<sup>1</sup>).

logarithmic plot for the fully activated cathode, were undertaken in a relatively small temperature range. If this range is extended, two or more lines with different slopes representing two or more different exponential functions are obtained as found by Becker,<sup>3</sup> Vink,<sup>1</sup> and

Loosjes and Vink<sup>3</sup> (cf. Fig. 104). As pointed out by Loosjes and Vink, the differences in slope can be explained by accounting for the shunt resistance of the pores conducting electrons in vacuum (cf. page 197). This shunt resistance increases the slope of the line representing  $\log \kappa$  or  $\log R$  against  $1/T$  in the range between 800° and 1000° K., if coatings with normal pore volumes are used. In

the range below 800° K., however, where the shunt resistance is too high, the normal slope appropriate to the conductivity of the alkaline earth oxide will always be obtained.

The exponents  $\beta$  which have been obtained by different workers, using the conductivity formula (162) have been compiled in Table XXIII, together with the temperature range and the methods used for the conductivity measurement.

A reference to the emission of the cathodes investigated has not been given because only very few of the authors give accurate emission values which are determined by one of the standard methods (cf. Vol. I, 10). The values of  $\beta$

Fig. 104.—Electrical Conductance of a  $[\text{BaSr}]O$  Coating as a Function of Temperature for Different States of Activation (Range of Medium and Low Temperatures) (Vink<sup>1</sup>).

given in the table always refer to the highest activation state investigated by the respective worker. It should be pointed out that the emission obtained in some of the investigations is rather low and certainly not the optimum one.

As will be seen from the above considerations, the derivation of an accurate value of the internal work function from the experimental data will hardly be possible. First of all the values of  $\beta$  in the medium-temperature range, which are all rather high, cannot be used due to the probable influence of the pores. Furthermore, it was pointed out in Secs. 17 and 20 that the particular formula

to be used for deriving the internal work function from the exponent  $\beta$  or from the interference energy  $\chi - \sigma$  depends on details of the mechanism of the semi-conductor which are not known so far. Finally, account must be taken of the fact that all measurements are undertaken at different temperatures in the same way as when ascertaining the total work function by the Richardson method (cf. Sec. 21.2). It is therefore possible again that the composition of the coating is varied during the measurement due to the phenomena of diffusion and ionic conduction which depend on temperature.

TABLE XXIII

\* Exponents  $\beta$  in the Conductivity Formula (162) for the Activated Oxide Coating

Type of cathode	Year of measure- ment	Method	Author	$\beta$ in eV in the temperature range		
				$T < 800^\circ$	$T = 800^\circ$ $- 1000^\circ$	$T > 1000^\circ$
BaO-SrO	1931	Two coated wires twisted together.	Reimann and Treloar. <sup>2</sup>	—	1.0	—
BaO-SrO	1931	Embedded probe.	Becker <sup>3</sup>	0.53	1.49	—
BaO	1932	Discs	Meyer and Schmidt. <sup>1</sup>	—	—	0.3
? [BaSr]O	1935 1940	?	Clausing * Nishibori and Kawamura. <sup>1</sup>	— —	— 1.0	0.27
[BaSr]O	1947	Embedded probe.	Wright <sup>1</sup>	—	0.57	—
[BaSr]O	1948	Two cathodes brought in contact.	Vink <sup>1</sup>	0.09-0.18	0.65-1.6	—
[BaSr]O	1948	Ceramic base.	Eisenstein <sup>2</sup>	—	—	0.26-0.35
?	1949	Embedded probe.	Mahlman <sup>1</sup>	—	1.2	—
[BaSr]O	1949	Embedded probe.	Danforth and Goldwater. <sup>1</sup>	—	—	0.44
[BaSr]O	1949	Ceramic base.	Hannay, MacNair and White. <sup>1</sup>	—	1.1	0.3-0.45

\* P. Clausing, quoted in J. H. de Boer, *Electron Emission and Adsorption Phenomena*, 1935, p. 361.

If the values of  $\beta$  measured in the range  $800^{\circ}\text{--}1000^{\circ}\text{K}$ . are excluded, the mean value of  $\beta$  from Table XXIII is  $0.3\text{ eV}$ . If equation (161) is used this value is equal to half the distance between interference and conduction band, which is  $\frac{1}{2}(\chi - (\sigma + \Delta\sigma))$ . As seen from equation (173), the average internal work function at  $T=0$  then has the same value  $\phi_0 = 0.3\text{ eV}$ .

The value of  $\phi$  found in such experiments has recently been used for some theoretical considerations, for instance by combining it with values obtained for  $n_\sigma$ , the number of excess Ba-atoms (cf. Rittner, du Pré, and Hütner<sup>1</sup> and Loosjes and Vink<sup>2</sup>). Such an undertaking, however, seems to be rather premature on account of the inaccuracy of the known values of  $\phi$  as pointed out above.

The relationship between conductivity and emission was also first recognized by Spanner,<sup>1</sup> who found that the conductivity of the different alkaline earth oxides BaO, SrO, CaO, MgO, and BaO (cf. Fig. 102) decreases in the same sequence as the emission which was measured too. Furthermore, Reimann and collaborators,<sup>1, 2</sup> observed that conductivity and emission current increase or decrease together, if the cathode is activated or poisoned. The variations in conductivity produced were about 1000 times. A similar result, represented by Figs. 103 and 104, was obtained by Meyer and Schmidt<sup>1</sup> and Vink.<sup>1</sup> Finally Albrecht<sup>1</sup> and more recently Hannay, MacNair, and White<sup>1</sup> found that conductivity  $\kappa$  and saturated current  $I_s$  vary proportionately. This proportionality is observed with rising emission during the activation. It is also observed with falling emission due to poisoning, provided this poisoning takes place homogeneously in the entire interior of the coating.

As with other semi-conductors, the slope of the line representing conductivity or resistance (the value of  $\beta$ ) decreases with improving activation. This is best seen from the set of curves in Fig. 104. As outlined in Sects. 17 and 20, this decrease may be explained by the assumption that the width  $\Delta\sigma$  of the interference band increases with improving activation. The internal work function then decreases according to (173), so giving rise to the observed increase in emission. Exact values for the variation of the internal work function during activation cannot be given yet due to the above-mentioned difficulties of determining an exact value of the internal work function itself.

The temperature-dependence of the internal work function will best be seen from Fig. 75, in which the parameter  $n_\sigma$  has to be

replaced by the interference density  $n_{(kT)}$ . For full activation equation (173) may be used, giving:

$$\frac{d\phi}{dT} = \frac{1}{2} \frac{d[\chi - (\sigma + \Delta\sigma)]}{dT} + 9.9 \times 10^{-5} \log \frac{(CT)^{\frac{1}{2}}}{n_{(kT)}} + 6.5 \times 10^{-5} . \quad (204)$$

Provided the first term on the right-hand side is zero, we obtain for  $T=1000^\circ$  K. and  $n_{(kT)}=10^{18}/\text{cm.}^3$  (cf. page 182)  $\frac{d\phi}{dT}=2.5 \times 10^{-4}$  eV/degree, a value which corresponds with the temperature coefficient of the total work function found experimentally (cf. Sec. 21.6).

Exact values for the mobility  $u$  of the electrons in the coating cannot be given yet because there are too few measurements of the Hall-effect. Also an estimation of  $u$  from equation (169), using the values of the conductivity  $\kappa$  and of the number  $N_x$  of electrons in the conduction band, seems to be premature before a more accurate value of the internal work function  $\phi$  is known, as this greatly influences the number  $N_x$ .

### 23. The Potential Barrier at the Surface of the Oxide Cathode (External Work Function)

The value  $\psi_0$  of the external work function at absolute zero can be obtained by means of equation (172), taking the difference between total work function  $\Psi_0$  and internal work function  $\phi_0$ . As  $\Psi_0=1.0$  eV and  $\phi_0 \approx 0.3$  eV,  $\psi_0 \approx 0.7$  eV.

A further possibility for estimating the value of the external work function is obtained by combining equations (172) and (173) for the total and the internal work functions with equation (198) for the photo-electric work function.

For  $T=0$ , it follows,

$$\Psi_0 = \phi_0 + \psi_0 = \frac{1}{2} [\chi - (\sigma + \Delta\sigma)] + \psi_0 . . . . . \quad (205)$$

By combining with (198):

$$\psi_0 = 2\Psi_0 - \Psi_0^{(ph)} . . . . . \quad (206)$$

As pointed out on page 186 the validity of equation (198) and therefore of (206) depends on the non-existence of surface levels on the surface of the oxide coating. If  $\Psi_0=1.0$  and  $\Psi_0^{(ph)}=1.6$  from Table XXII is used, an external work function of 0.4 eV is derived.

There is a possibility for directly determining the external work function obtained, if emission equation (176) is divided by equation (135) for the conductivity. Then with (41a):

$$\left. \begin{aligned} j_s/\kappa &= \frac{1}{e\sqrt{\pi}} \sqrt{\frac{2mk}{\pi}} 10^{-7} \frac{\bar{v}}{l} T^{1/2} e^{-e\psi/kT} \\ &= 1.76 \times 10^{-10} \frac{\bar{v}}{l} T^{1/2} e^{-e\psi/kT} \end{aligned} \right\} \dots \quad (207)$$

Accordingly the ratio between saturated current and conductivity only depends on external work function, temperature, and mean free path. If the logarithm of this ratio is plotted as a function of  $1/T$ , a straight line will be obtained according to (207), and the external work function can be ascertained from the slope of this line. In a similar manner, Nishibori and Kawamura<sup>1</sup> derived the value 0.3 eV for the external work function.

According to these results the value of the external work function at  $T=0$  is between 0.3 and 0.7 eV. The considerable spread between these values must be explained by the lack of accurate measurements and by the fact that values which are not measured for the same cathode must be used for the calculation. Certainly the external work function of the oxide cathode is considerably lower than the lowest value measured for metals ( $\psi_{cs}=1.9$  eV).

In principle it is possible to calculate the external work function from the series limit of the ultra-violet absorption spectra, by using a method given by Mott and Gurney.\* These authors obtained values for the external work function of different alkali halides which were between 0.4 and 0.7 eV. This method, however, cannot be applied to alkaline earth oxides at the present time, as the necessary optical measurements have not been carried out yet. On the other hand, the values given above for the alkali halides show that the low external work function seems to be a general property of ionic crystals (cf. Wright<sup>2, 3</sup>).

The question now arises, whether the external work function varies during the activation in addition to the internal work function. This question can also be answered by means of equation (207). According to the measurements of Albright<sup>1</sup> and Hannay<sup>1</sup> and collaborators mentioned on page 202, conductivity and saturated current change proportionately and therefore give a constant value for the left-hand side of (207) during the activation. Consequently

\* N. F. Mott, R. W. Gurney, *Electronic Processes in Ionic Crystals*, Oxford, 1940, p. 95.

the external work function on the right-hand side of (207) also remains constant during the activation. The same result was obtained by direct measurements of the external work function by Nishibori and Kawamura.<sup>1</sup> It follows therefore that the increase of emission current during the activation is almost exclusively due to the decrease in internal work function discussed in the previous section.

The constancy of the external work function during the activation leads to the conclusion that the composition of the surface of the coating will also remain unchanged during the activation. The original assumption of Koller<sup>1</sup> and Becker<sup>1</sup> that a dipole layer of barium ions is set up at the surface during the activation can therefore be maintained no longer. A reasonable assumption will be that the structure of the surface is an extension of the structure of

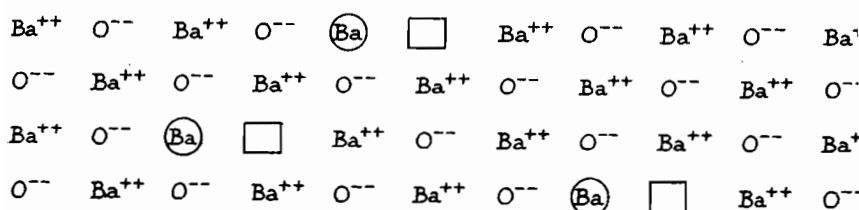


Fig. 105.—Composition of the Surface of a Barium Oxide Coating.

vacancies existing in the interior of the coating. The conditions then existing will be seen from Fig. 105 showing a section through the surface of a fully activated oxide coating in an (001) direction. The number of excess Ba-atoms in the atom layer at the surface then is  $s_o = n_o^{2/3} \approx 5 \times 10^{12} \text{ cm.}^{-2}$  if  $n_o$  is taken from (171). This number, if compared with a total of  $2/d_{\text{Ba}0^2} = 6.5 \times 10^{14} \text{ Ba-ions per cm.}^2$  in the surface layer, is relatively small, and it is evident that such a small number will not greatly influence the value of the external work function.

These considerations are only valid if the equilibrium of the activated coating is not disturbed by external interference. Such an interference can be produced by evaporating barium on the surface of the cathode, as in the experiments of Becker<sup>1</sup> discussed in Sec. 17.3, or by accumulating oxygen by an increased oxygen pressure in front of the cathode. In the first case the number of excess barium atoms at the surface is increased and the external work function decreased, while in the second case the opposite

effect is obtained and the cathode is poisoned (cf. Vol. I, Sec. 12.5). When such an interference exists a proportionality of emission and conductivity can of course no longer be expected. For instance, as observed by Hannay and collaborators, the emission can be lowered by several powers of ten by poisoning at a low temperature, whilst the conductivity measured simultaneously remains almost unchanged. On the other hand if such external interferences can be neglected, the number of excess barium atoms will take its equilibrium value and the external work function will then be determined by properties of the interior of the BaO crystal lattice.

Summarizing the results of this chapter, the fundamental emission phenomenon of the oxide cathode in equilibrium can be explained by assuming the oxide coating to be a semi-conductor and considering only the properties of the interior.\* Processes at the surface of the coating which may interfere with this equilibrium seem to be only of secondary importance for the mechanism of emission. These processes, of course, are of considerable importance for the practical use of the cathode and they will therefore be dealt with in detail in the following two chapters.

It may finally be mentioned that Uehara and Takahari<sup>1</sup> associated a two-dimensional lattice with the surface atoms or ions of the oxide coating and tried to introduce special energy bands in this lattice in order to derive the emission equation. In our opinion, however, the influence exerted on the work function by barium atoms at the surface can only be dealt with after having at first considered the crystal lattice in the interior.

## 24. Allied Phenomena

Concluding this chapter, some additional phenomena will be discussed which are observed with the oxide cathode and which are connected with its thermal emission. These phenomena are photoelectric emission, secondary emission, and luminescence.

\* Moore and Allison<sup>1</sup> have recently observed that the emission from thin films of stoichiometrically pure alkaline earth oxides (thickness equal to a few molecule layers) is of the same magnitude as the emission from oxide cathodes of normal thickness. We cannot, however, agree with their conclusion that this interesting observation contradicts the existing theory of the oxide cathode. The emission obtained from thin films is only an emission of the metal carrier which is modified by the existence of the film. There is no direct relationship with the oxide cathode which fundamentally consists of a large number of atom or molecule layers forming an ionic solid.

## 24.1. Photo-electric emission

The photo-electric emission of oxide cathodes was partly dealt with when the methods for measuring the total work function were discussed (cf. Sec. 21.4). In this section some special investigations carried out by Koppius,<sup>1</sup> Newbury,<sup>1</sup> Berger,<sup>1</sup> Newbury and Lemery,<sup>2</sup> and Ramadanoff<sup>1</sup> will first be quoted. These authors observed that the photo-electric emission of the oxide cathode increases considerably when passing from room temperature to operating temperature. This phenomenon is easily explained since the electrons, lifted into the conduction band by temperature excitation, can be emitted from the conduction band into vacuum by an amount of photo-energy smaller than for  $T=0$ . Consequently the number of emitted electrons will increase to the same degree (cf. Sec. 21.4).

Another observation was made by Debiesse and Champeix<sup>1</sup> who illuminated a cold oxide cathode with intermittent light. They found that the photo-electric emission obtained in this way from an unactivated cathode was considerably higher than the emission obtained from the same cathode after activation. Unfortunately the states of activation to which these observations refer have not been defined in any way, for instance by giving the appropriate thermal emission currents.

The velocity distribution of photo-electrons emerging from an oxide cathode will now be discussed. These electrons do not show a distribution over a wide range of velocities as do the photo-electrons emerging from a metal cathode (cf. Fig. 55). Pjatnitzki and Timofeew<sup>1</sup> examined a caesium oxide cathode, irradiated by infra-red light, and observed that nearly all the emitted electrons leave this cathode with the maximum velocity resulting from equation (105). This observation shows that the photo-electrons emitted from caesium oxide and from similar oxide cathodes originate from a sharp energy level and not from an energy band.

On the other hand electrons which are emitted thermally from an oxide cathode show a velocity distribution which is Maxwellian according to Demski,<sup>1</sup> Heinze and Hass,<sup>3</sup> Fan<sup>1</sup> and Hung.<sup>1</sup> The velocity distributions of photo-electrons and thermal electrons originating from oxide cathodes are therefore completely different which is quite contrary to the respective phenomena observed with metals. This suggests that the two emission processes discussed—photo-electric and thermal emission from the oxide cathode—are due to completely different fundamental processes. This must be

taken into account when transferring to the thermal emission case concepts which were formed for photo-electric emission.

## 24.2. Secondary emission

Secondary emission from a material is the emission of electrons which are produced by bombarding this material with electrons coming from another source. The secondary emission of unactivated alkaline earth oxides ( $\text{BaO}$ ,  $\text{SrO}$ ,  $\text{CaO}$ ) was examined at room temperature by Geyer<sup>1</sup>; the value 2 was found for the ratio between secondary electron current  $I_{\text{sec}}$  and primary electron current  $I_{\text{pr}}$  (secondary emission coefficient). Further investigations were carried out at both different states of activation and different

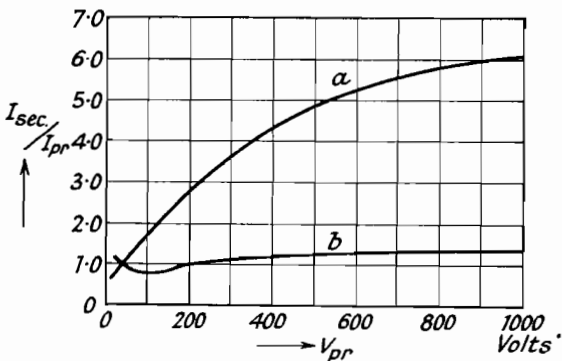


Fig. 106.—Coefficient of Secondary Emission ( $I_{\text{sec}}/I_{\text{pr}}$ ) of an Oxide Cathode as a Function of Primary Voltage  $V_{\text{pr}}$ : (a) activated, (b) poisoned (Bruining and de Boer<sup>1</sup>).

temperatures of the cathode. The result of an investigation at different states of activation, undertaken by Bruining and de Boer<sup>1</sup> for  $[\text{BaSr}] \text{O}$  cathodes, is shown in Fig. 106, giving the coefficient  $I_{\text{sec}}/I_{\text{pr}}$  as a function of the acceleration voltage  $V_{\text{pr}}$  of the primary electrons. The curve indicated by (a) is valid for the activated cathode, while curve (b) was obtained for a cathode poisoned by oxygen. A considerable difference between the secondary emission of the activated and the poisoned (unactivated) cathode can be seen from the figure. The coefficient  $I_{\text{sec}}/I_{\text{pr}}$  at high primary voltages is about 6 for the activated cathode, but only 1 for the unactivated cathode. This increase of the coefficient during activation was confirmed by Pomerantz.<sup>1</sup>

Definite values of the temperature-dependence of secondary emission cannot be given yet, since there is considerable disagreement

between the different workers. Morgulis and Nagorski<sup>1</sup> and Pomerantz<sup>1, 2, 3</sup> observed a very strong dependence on temperature which obeyed an exponential function of  $1/T$ . This was confirmed by Timofeew and Aranowitsch<sup>1</sup> when examining thin layers of barium oxide obtained by evaporation of barium metal and subsequent oxidation. These results, however, were contested by Johnson,<sup>1, 2, 3</sup> who measured a slight decrease of the coefficient  $I_{sec}/I_{pr}$  with increasing temperature up to 800° K., while in the range above this temperature a so-called enhanced emission was found which increases with temperature as does the normal thermal emission. After switching off the primary emission, this enhanced emission continued to flow and only decreased slowly. Finally Jones<sup>1</sup> measured a secondary emission coefficient which was nearly independent of temperature.

The physical cause of the phenomena described above will not be dealt with in detail, as the theoretical investigation of secondary electron emission has not yet given definite results even in the simpler case of metals.

### 24.3. Luminescence

Luminescence is the emission of light which occurs if a material is irradiated with primary light or X-rays, or bombarded by electrons or ions. Crystals showing this luminescence may be obtained by building a small quantity of a metal, called an activator, into the pure crystal lattice. A luminescent material, consisting of such activated crystals, is called a phosphor, of which zinc sulphide, activated by copper, is an example. The frequency of the luminescence of such a phosphor is determined by both the basic material of the phosphor and the activator. The phenomenon of luminescence produced by activation was explained by Riehl and Schön<sup>1</sup> using the concept of energy bands. It was assumed that the luminescence originates from the electrons in the interference levels of the activating atoms which are built into the crystal lattice of the phosphor.\*

In the normal case discussed so far, the activating metal is different from the metal component of the crystal lattice to be activated. The other case, however, in which activator and metal component of the crystal lattice are identical is also known. Schleede<sup>1</sup> and Seitz,<sup>1</sup> for example, describe zinc sulphide which is activated by building in excess zinc atoms. Such a phosphor is

\* For details see G. F. J. Garlick, *Luminescent Materials*, Oxford, 1949.

called self-activated, while the normal case discussed above is called foreign-activated.

As the configurations of a self-activated phosphor and of an oxide-coated cathode are similar, it seems to be likely that the oxide cathode may act as a phosphor too. The phosphorescence of foreign-activated alkaline earth oxides has been known for a long time by the fundamental experiments of Lenard. A phosphorescence of pure alkaline earth oxides which can only be explained by self-activation was observed by Ewles,<sup>1</sup> who examined especially CaO, exciting the luminescence by both electrons and ultra-violet light. These experiments show that there is a certain connection between luminescence and thermal emission, but the connection would appear more definite if it could be shown by further experiments that alkaline earth oxides which do not emit electrons are not luminescent and that thermal emission and luminescence rise together during the activation.

Finally an observation by Huber<sup>1</sup> may be mentioned, according to which oxide cathodes containing CaO gleam when emission current is drawn from them. The gleaming phenomenon was observed with emission currents of more than  $10^{-6}$  amp./cm.<sup>2</sup> and anode voltages of more than 20 volts; the phenomenon increased with increasing current and voltage. The wavelength of the emitted radiation was between 5400 and 6600 Å. The gleaming phenomenon was also found with cathodes made of very pure CaCO<sub>3</sub> and with a very pure nickel core. Presumably this phenomenon is also connected with the building of excess Ca-atoms into the CaO crystal lattice.

#### REFERENCES

- |                     |  |
|---------------------|--|
| ALBRICHT, W.        | (1) <i>Physica</i> 11 (1931), 146.   |
| ARNOLD, H. D.       | (1) <i>Physic. Rev.</i> 16 (1920), 70.   |
| BACHMANN, C. H.     | (1) and CARNAHAN, C. W., <i>Proc. I.R.E.</i> 26 (1938), 529.   |
| BARTON, H. A.       | (1) <i>Physic. Rev.</i> 26 (1925), 360.  |
| BECKER, J. A.       | (1) <i>Physic. Rev.</i> 34 (1929), 1323.<br>(2) and SEARS, R. W., <i>ibid.</i> 38 (1931), 2193.<br>(3) <i>Trans. Electrochem. Soc.</i> 59 (1931), 207. |
| BERDENNIKOWA, T. P. | (1) <i>Physik. Z. Sow.-Union</i> 2 (1932), 77.   |
| BERGER, C.          | (1) <i>Physic. Rev.</i> 34 (1929), 1566.   |
| BLEWETT, J. P.      | (1) and JONES, E. I., <i>Physic. Rev.</i> 50 (1936), 464.<br>(2) <i>J. Appl. Phys.</i> 10 (1939), 668.   |
| BRAUN, A.           | (1) and BUSCH, G., <i>Helv. Physica Acta</i> 20 (1947), 33.  |
| BROADWAY, L. F.     | (1) and PEARCE, A. F., <i>Proc. Phys. Soc.</i> 51 (1939), 335.   |

# ACTIVATED OXIDE COATING IN EQUILIBRIUM

- BRUINING, H. (1) and DE BOER, J. H., *Physica* 6 (1939), 823.
- CHAMPEIX, R. (1) *Ann. Radioélectricité* 1 (1946), 208.
- COOMES, E. H. (1) *J. Appl. Phys.* 17 (1946), 647.
- CORK, I. (1) and GERHARD, G. L., *Amer. Mineralogist* 16 (1931), 71.
- DANFORTH, W. E. (1) and GOLDWATER, D. L., *J. Appl. Phys.* 20 (1949), 163.
- DAVISSON, C. (1) and GERMER, L. H., *Physic. Rev.* 24 (1924), 666.
- DEBIESSE, J. (1) and CHAMPEIX, R., *Le Vide* 4 (1949), 545.
- DEMSKI, A. (1) *Physik. Z.* 30 (1929), 291.
- DETELS, F. (1) *Jb. d. drahtl. Telegr. u. Teleph.* 30 (1927), 10, 52.
- EISENSTEIN, A. (1) *Physic. Rev.* 71 (1947), 473.  
(2) *Advances in Electronics*, New York, 1948, pp. 1-64.  
(3) *J. Appl. Phys.* 20 (1949), 776.
- ESPE, W. (1) *Wiss. Veröff. Siemens-Werken* 5 (III) (1927) 29, 46,  
(2) *Z. techn. Physik* 10 (1929), 489.
- EWLES, I. (1) *Proc. Roy. Soc. (A)* 167 (1938), 34.
- FAIVRE, R. (1) and MAUGUIN, Ch., *C. R.* 222 (1947), 227.  
(2) and CHAUDRON, G., *C. R.* 226 (1948), 249.  
(3) *ibid.* 226 (1948), 903.
- FAN, H. Y. (1) *J. Appl. Phys.* 14 (1943), 552.
- FINEMAN, A. (1) and EISENSTEIN, A., *J. Appl. Phys.* 17 (1946), 663.
- FOWLER, R. H. (1) *Proc. Roy. Soc. (A)* 140 (1933), 505.
- FRITZ, H., (1) *Mikrochem.* 11 (1935), 191.
- GEHRTS, A. (1) *Z. techn. Physik* 11 (1930), 246.
- GEYER, K. H. (1) *Ann. Phys.* 42 (1942), 241.
- GILL, E. W. B. (1) *Philos. Mag.* 24 (1937), 1093.
- GYSAE, B. (1) Thesis, Technical University Berlin (1938).
- HANNAY, N. B. (1) McNAIR, D., and WHITE, A. H., *J. Appl. Phys.* 20 (1949), 669.
- HEINZE, W. (1) *Ann. Phys.* 16 (1933), 41.  
(2) and WAGENER, S., *Z. techn. Physik* 17 (1936), 645.  
(3) and HASS, W., *ibid.* 19 (1938), 166.  
(4) and WAGENER, S., *Z. Physik* 110 (1938), 164.
- HUBER, H. (1) Thesis, University Berlin (1941).  
(2) and WAGENER, S., *Z. techn. Physik* 23 (1942), 1.
- HUNG, C. S. (1) *J. Appl. Phys.* 21 (1950), 37.
- HUXFORD, W. S. (1) *Physic. Rev.* 38 (1931), 379.
- ISENSEE, H. (1) *Z. physik. Chem.*, Abt. B. 35 (1937), 309.
- JACOBS, H. (1) HEES, G., and CROSSLEY, W. P., *Proc. I.R.E.* 36 (1948), 1109.
- JENKINS, R. O. (1) and NEWTON, R. H. C., *Nature*, 163 (1949) 572.  
(2) and NEWTON, R. H. C., *J. Sci. Instr.* 26 (1949), 172.
- JOHNSON, J. B. (1) *Physic. Rev.* 66 (1944), 352.  
(2) *ibid.* 69 (1946), 693.  
(3) *ibid.* 73 (1948), 1058.
- JONES, T. J. (1) *Nature* 161 (1948), 846.
- JOST, W. (1) and NEHLEP, G., *Z. physik. Chem. (B)* 32 (1936), 1.

# THE OXIDE-COATED CATHODE

- KALLWEIT, H. (1) *Z. Naturforschg.* 4a (1949), 140.  
 KNIEPKAMP, H. (1) and NEBEL, C., *Wiss. Veröff. Siemens-Werken* 11  
     (II) (1932), 75.  
 KOLLER, L. R. (1) *Physic. Rev.* 25 (1925), 671.  
 KOPPIUS, O. (1) *Physic. Rev.* 18 (1921), 443.  
 KROCZEK, J. (1) and LUEBKE, E., *Wiss. Veröff. Siemens-Werken* 9  
     (II) (1930), 253.  
 LIEBOLD, W. (1) Thesis, University Berlin (1941).  
 LOOSJES, R. (1) and VINK, H. J., *Philips Res. Rep.* 2 (1947), 190.  
     (2) and VINK, H. J., *J. Appl. Phys.* 20 (1949), 884.  
     (3) *Phil. Res. Rep.* 4 (1949), 449.  
 MAHLMAN, G. W. (1) *J. Appl. Phys.* 20 (1949), 197.  
 MEYER, W. (1) and SCHMIDT, A., *Z. techn. Physik* 13 (1932), 137.  
 MICHEL, G. (1) and SPANNER, H. J., *Z. Physik* 35 (1926), 395.  
 MOORE, G. E. (1) and ALLISON, H. W., *Physic. Rev.* 77 (1950), 246.  
 MORGULIS, N. D. (1) and NAGORSKI, A., *Techn. Physics, U.S.S.R.* 5  
     (1938), 844.  
     (2) *Journ. of Phys., U.S.S.R.* 11 (1947), 67.  
 MUTO, T. (1) and YAMASHITA, J., *J. Phys. Soc. Japan* 2 (1947),  
     187.  
     (2) *ibid.* 2 (1947), 190.  
 MUTTER, W. E. (1) *Physic. Rev.* 72 (1947), 531.  
 NEWBERY, K. (1) *Physic. Rev.* 34 (1929), 1418.  
     (2) and LEMERY, F., *J. Opt. Soc. America* 21 (1932),  
     276.  
 NISHIBORI, E. (1) and KAWAMURA, H., *Proc. Physico-Math. Soc. Japan* III 22, (1940), 378.  
     (2) KAWAMURA, H., and HIRANO, K., *ibid.* 23 (1941),  
     37.  
 PATAI, E. (1) and FRANK, G., *Z. techn. Physik* 16 (1935), 254.  
     (2) and TOMASCHEK, A. Z., *Kolloid-Z.* 74 (1936), 253.  
 PJATNITZKI, A. I. (1) and TIMOFEEW, P. W., *Z. Sow.-Union* 9 (1936), 187.  
 POMERANTZ, M. A. (1) *Physic. Rev.* 70 (1946), 33.  
     (2) *Journ. Franklin Inst.* 241 (1946), 415.  
     (3) *ibid.* 242 (1946), 41.  
 PRESCOTT, C. H. (1) and MORRISON, J., *J. Amer. Chem. Soc.* 60 (1938),  
     3047.  
 RAMADANOFF, D. (1) *Physic. Rev.* 37 (1931), 884.  
 REIMANN, A. L. (1) and MURGOCI, R., *Philos. Mag.* 9 (1930), 440.  
     (2) and TRELOAR, L. R. G., *ibid.* 12 (1931), 1073.  
 RIEHL, N. (1) and SCHÖN, M., *Z. Physik* 114 (1939), 682.  
 RITTNER, E. S. (1) DU PRÉ, F. K., and HUTNER, R. A., *Physic. Rev.*  
     76 (1949), 996.  
 ROTHE, H. (1) *Z. Physik* 36 (1926), 737.  
 SCHAEFER, H. (1) and WALCHER, W., *Z. Physik* 121 (1943), 679.  
 SCHLEEDE, A. (1) *Angew. Chemie* 50 (1937), 908.  
 SCHOTTKY, W. (1) *Naturwiss.* 23 (1935), 115.  
     (2) *Z. physik. Chem. (B)* 29 (1935), 335.

## ACTIVATED OXIDE COATING IN EQUILIBRIUM

- SCHRIEL, M. (1) *Z. anorg. allg. Chem.* 231 (1937), 313.  
 SEITZ, F. (1) *J. Chem. Phys.* 6 (1938), 454.  
 SLOANE, R. H. (1) and WATT, C. S., *Proc. Phys. Soc.* 61 (1948), 217.  
 SMITH, A. H. (1) *Physic. Rev.* 75 (1949), 953.  
 SPANNER, H. J. (1) *Ann. Phys.* 75 (1924), 609.  
 SPROULL, R. L. (1) *Physic. Rev.* 67 (1945), 166.  
 SUHRMANN, R. (1) and FRUEHLING, G., *Naturwiss.* 26 (1938), 108.  
 (2) and DEHMELT, F. W., *Z. Physik* 118 (1942), 677.  
 TIMOFEEW, P. W. (1) and ARANOWITSCH, R. M., *J. Techn. Physics* 10 (1940), 32.  
 TYLER, W. W. (1) *Physic Rev.* 76 (1949), 1887.  
 UEHARA, Y. (1) and TAKAHARI, M., *Bull. Chem. Soc. Japan* 15 (1940), 15.  
 VEENEMANS, C. F. (1) *Nederl. Tijdsch. Naturkunde* 10 (1943), 1.  
 VINK, H. J. (1) Thesis, Leiden, 1948.  
 WEHNELT, A. (1) *S.-B. physik.-med. Soz. Erlangen* 95 (1903), 115.  
 WHEATCROFT, E. L. E. (1) *Philos. Mag.* 29 (1940), 16.  
 WOOTEN, L. A. (1) and BROWN, C. J., *Amer. Chem. Soc.* 65 (1943), 113.  
 WRIGHT, D. A. (1) *Proc. Roy. Soc. London (A)* 190 (1947), 394.  
 (2) *Proc. Phys. Soc.* 60 (1948), 13.  
 (3) *ibid.* 60 (1948), 22.  
 (4) *ibid.* 62 (1949), 188.  
 (5) *Nature*, 164 (1949), 714.  
 (6) *Brit. Journ. Appl. Phys.*, 1 (1950), 150.  
 ZIMENS, K. E. (1) *Z. physik. Chem. Abt. B* 37 (1937), 231, 241.

## CHAPTER 5

### OXIDE COATINGS OF DIFFERENT COMPOSITION

After having considered the mechanism and the emission constants of the oxide cathode, we shall now eliminate step by step the simplifying suppositions made at the beginning. At first the supposition is eliminated according to which the oxide coating only consists of barium oxide. Cathodes will be considered in the following which consist of one or several of the other alkaline earth or of normal metal oxides. In this context we shall distinguish between the "pure oxide cathode," the coating of which contains only one alkaline earth oxide, and the "composite oxide cathode," being composed of several oxides or of oxides and other components. The different possibilities for these compositions are discussed below.

#### 25. Emission from Pure Metal Oxides

As the mechanism of the emission of pure oxides will be always the same, we may restrict our considerations to comparing the magnitude of the emission from single oxides. For this comparison it will be as desirable as with metals that the work function, the characteristic constant of emission, can be given.

According to the discussions in Sec. 21 the intersection method is most suitable for an exact measurement of the work function at or near the operating temperature. This method, however, requires considerable experimental equipment, especially if it must be applied to a series of cathodes, in order to obtain the work function with the necessary exactness. It is therefore useful to know that according to Huber<sup>1</sup> the work function may also be derived directly from an emission measurement with sufficient accuracy.

Huber measured the work function of different alkaline earth oxides ( $\text{BaO}$ ,  $\text{SrO}$ ,  $\text{CaO}$ ) and of mixtures of these oxides by means of the intersection method at the two temperatures  $640^\circ$  and  $770^\circ$  K. The saturated current measured at the same temperatures was extrapolated to zero external field by means of equation (182) (the deviation against the extrapolation by means of the more suitable

equation (185) is small). The logarithms of the saturated currents  $I_s^{(0)}$ , obtained in this manner, were plotted as a function of the work functions  $\bar{\Psi}^{(0)}$  measured before. The result was a linear relation:

$$\log I_s^{(0)} = C_1 \bar{\Psi}^{(0)} + C_2 \quad . . . . \quad (208)$$

If emission equation (177a) is used, the relation between  $I_s^{(0)}$  and  $\bar{\Psi}^{(0)}$  is:

$$\log I_s^{(0)} = -\frac{5040}{T} \bar{\Psi}^{(0)} + \log A_0 T^2 \quad . . . . \quad (209)$$

It was shown that the constants  $C_1$  and  $C_2$  in (208) which were obtained from the experiments correspond with the theoretical values in (209) within the experimental errors. It follows from this that the emission constant  $A$  of the oxide cathodes examined by Huber may be equated to the theoretical value  $A_0=120$  in (177a) within the experimental errors. The variations around this theoretical value, which were between 11 and 195, were, of course, rather high. This result once more confirms the validity of emission equation (177a).

One sees from the above result that the total work function  $\Psi$  of the oxide cathode can be obtained in a simple way by measuring the saturated current at a definite temperature and by calculating  $\Psi$  from emission equation (177a) for  $A_0=120$ . This calculation can be simplified more by replacing it by a graphical method using the plot of Fig. 12. The existence of this simpler method, however, does not affect the importance of the intersection method, as this method is the basis for the reliability of the simple method.

The work functions of the three most important alkaline earth oxides were measured by Huber<sup>1</sup> in the way described above. The carbonates used for making these oxides had a grain size between 5 and 15  $\mu$ . An organic binder was employed for depositing  $\text{BaCO}_3$  and  $\text{SrCO}_3$ , while  $\text{CaCO}_3$  was used as water paste. The core metal of the cathodes consisted of commercial nickel with a small percentage of Mg. The coatings were obtained by spraying, the final thickness after decomposition being between 40 and 60  $\mu$ . The cathodes were activated up to the maximum emission by heating and drawing emission current at the optimum activation temperature ascertained before (cf. Vol. I, Sec. 8). The measured values of the work function which are mean values of about 10 cathodes are compiled in Table XXIV. The saturated currents used for these values were directly measured at  $640^\circ$  and  $770^\circ$  K.,

while the saturated current at 1050° K. was ascertained by the extrapolation method of Hinsch<sup>1</sup> (cf. Vol. I, Sec. 10.3).

Table XXIV ought to be completed by the value of the work function of radium oxide. This value is likely to be relatively small too. The making of such a RaO cathode in the usual manner, however, will be difficult, as it can be concluded from the behaviour of the other alkaline earth metals that the dissociation pressure of  $\text{RaCO}_3$  is small (cf. Vol. I, Fig. 29) and the vapour pressure of RaO is high (cf. Fig. 83). For this reason and on account of the rarity of radium no measurements with this oxide appear to have been made.

TABLE XXIV

*Work Functions of Alkaline Earth Oxides (Huber<sup>1</sup>)*

Alkaline earth oxide	$T=640^\circ \text{K.}$	$T=770^\circ \text{K.}$	$T=1050^\circ \text{K.}$
BaO	1.57	1.65	1.66
SrO	2.03	2.07	2.12
CaO	—	2.37	—

Only a few measurements have been undertaken for other metal oxides, and reliable measurements of the work function are only found for thorium. The saturated currents measured for the respective oxides are compiled in Table XXV. The work functions, with the exception of that of thoria, have been calculated from the Richardson equation in order to facilitate comparison. As will be seen from the table, the values obtained by different authors differ considerably. This may be explained by the fact that attention has not been paid to the state of activation of the oxides examined in the earlier investigations. It is therefore possible that one author examined a rather unactivated oxide and another author a fully activated one. Apart from this the differences can be explained by impurities which may not only decrease but also increase the emission of the pure oxides, as shown when discussing the foreign-activated oxide cathodes (Sec. 27.2).

Furthermore, the table shows that the oxides of alkali metals (caesium) emit even better than those of the alkaline earth metals. This fact confirms the view expressed before in this book, that the properties of the oxide cathode are not restricted to alkaline earth oxides but extend to quite a number of other metal oxides. One main characteristic of these metal oxides is that it must be possible

to make them excess semi-conductors by a suitable activation treatment. Another condition is that the ionic conductivity of the oxide concerned is so low that this oxide is not dissociated during the operation of the cathode.

TABLE XXV

*Saturated Currents and Work Functions of different Metal Oxides*

Oxide	Year of measurement	Measured by	Saturated current		Work function		A
			at $T =$	amp./cm. <sup>2</sup>	eV	Method of measurement	
Cs <sub>2</sub> O	1929	Koller <sup>1</sup>	400° K.	$5.7 \times 10^{-6}$	0.99	calculated	—
	1931	Campbell <sup>1</sup>		$1.0 \times 10^{-4}$	0.89	„	—
	1940	Goerlich <sup>1</sup>		$4.0 \times 10^{-7}$	1.08	„	—
	1942	Suhrmann and Dehmelt. <sup>1</sup>		$3.0 \times 10^{-8}$	1.17	„	—
MgO	1924	Spanner <sup>1</sup>	1400° K.	$2.0 \times 10^{-3}$	3.1	calculated	—
	1939	A. Schmidt (unpublished).		$3.1 \times 10^{-8}$	4.4	„	—
BeO	1924	Spanner <sup>1</sup>		$5.0 \times 10^{-6}$	3.8	„	—
	1939	A. Schmidt (unpublished).		$2.0 \times 10^{-9}$	4.7	„	—
Y <sub>2</sub> O <sub>3</sub> Sc <sub>2</sub> O <sub>3</sub> Al <sub>2</sub> O <sub>3</sub> B <sub>2</sub> O <sub>3</sub>	1924	Spanner <sup>1</sup>	1400° K.	$2.5 \times 10^{-4}$	3.3	calculated	—
		“		$5.0 \times 10^{-6}$	3.8	„	—
		“		$4.0 \times 10^{-8}$	4.7	„	—
		“		$2.0 \times 10^{-9}$	4.7	„	—
ThO <sub>2</sub>	1924	Spanner <sup>1</sup>	1400° K.	$2.5 \times 10^{-6}$	3.9	calculated	—
	1945	Weinreich <sup>1</sup>		$1.2 \times 10^{-2}$	2.57		7.9
	1947	Wright <sup>1</sup>	1900° K.	2.5	2.54	„	2.5
	1948	Hanley <sup>1</sup>	1900° K.	1.15	2.67	„	5.6
ZrO <sub>2</sub> TiO <sub>2</sub> SiO <sub>2</sub>	1924	Spanner <sup>1</sup>	1400° K.	$1.2 \times 10^{-7}$	4.2	calculated	—
		“		$2.0 \times 10^{-9}$	4.7		—
		“		$2.0 \times 10^{-10}$	5.0	„	—

Finally, it may be pointed out that the work function of the activated metal oxides varies within the individual groups of the periodical system, and when passing from one of these groups to another one, in exactly the same manner as with pure metals. This fact, which will be seen by comparing Tables V, XXIV, and XXV, indicates a connection between the work functions of the activated oxides and of the pure metals.

The especially good emission of caesium oxide, as seen from Table

XXV, cannot be utilized in practice, as  $\text{Cs}_2\text{O}$  evaporates and dissociates in vacuum at temperatures above  $450^\circ$  to  $500^\circ$  K. An adequate emission density can therefore not be obtained with  $\text{Cs}_2\text{O}$ .

## 26. Emission from Mixed Oxide Coatings

### 26.1. Mixtures of alkaline earth oxides

After having discussed the emission phenomena of the individual metal oxides we proceed to the mixtures of these oxides and start with the mixtures of alkaline earth oxides which are most important for technical applications. As the emission phenomena of these mixtures are closely related to their crystallographical properties we must consider these properties first.

(a) *Crystallographical properties.* The crystallographical properties of mixtures of alkaline earth oxides can be obtained by taking X-ray patterns. The oxide mixtures are best prepared for these investigations by using the same methods as for the preparation of normal cathodes. As the composition of the oxides is easily influenced by oxygen or water vapour, the X-ray photos must either be taken in a vacuum camera or the oxide coating must be protected against those influences in a suitable manner. According to Benjamin and Rooksby<sup>1, 2</sup> this can be done by designing the experimental valve with a thin stem tube made of Lindemann glass. The cathode in this valve, after being processed, is set free by burning out the lead wires and is moved into the stem tube, which is subsequently sealed off and brought into the X-ray camera. Another possibility is to take the cathode out of the experimental valve in an inert atmosphere and either to dip it into paraffin oil (Burgers<sup>1</sup>) or to coat it with a protective lacquer (Huber and Wagener<sup>2</sup>).

The investigation of the mixtures of the two most important oxides,  $\text{BaO}$  and  $\text{SrO}$ , shows that these oxides, provided they are made in a suitable manner, form a continuous series of mixed crystals (cf. Vol. I, Sec. 4, Benjamin and Rooksby,<sup>1, 2</sup> Burgers,<sup>1</sup> Huber and Wagener<sup>2</sup>). The lattice constant of the mixed crystals  $[\text{BaSr}] \text{O}$  varies linearly with the composition of the crystals given in mol. % (cf. Fig. 107).\*

According to Huber and Wagener,<sup>2</sup>  $\text{SrO}$  and  $\text{CaO}$  also form a continuous series of mixed crystals with a linear variation of the lattice constant. The behaviour of the system  $\text{BaO}-\text{CaO}$ , however,

\* Mixed crystals are characterized by square brackets, mechanical mixtures by a short dash in between the components ( $\text{BaO}-\text{SrO}$ ).

is the opposite, as no mixed crystals could be observed after heating the mixture for two hours at the high temperature of 1400° K. The reason for this opposite behaviour is the large difference between the lattice constants of the two components of this system ( $d_{\text{BaO}} = 5.52 \text{ \AA}$ . compared with  $d_{\text{CaO}} = 4.80 \text{ \AA}$ ). As is well known, formation of mixed crystals is prevented by such a large difference in the lattice constants.

Of the remaining two alkaline earth oxides MgO was examined in mixtures with BaO, SrO, or CaO by Wartenberg and Prophet<sup>1</sup> and no formation of mixed crystals was found in these systems. This result was confirmed by Herrmann<sup>1</sup> for mixtures between MgO and [BaSr]O. The missing formation of mixed crystals in

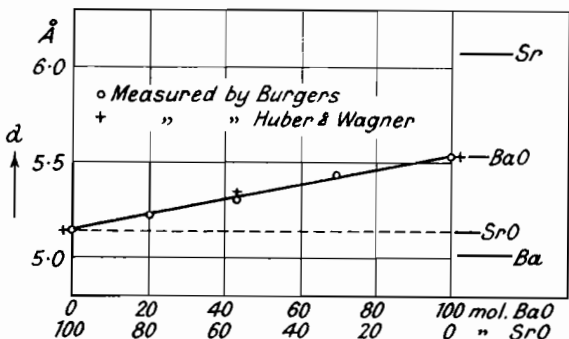


Fig. 107.—Lattice Constant  $d$  of Mixed Crystals [BaSr]O as a function of Composition (Burgers,<sup>1</sup> Huber and Wagener<sup>2</sup>).

these systems can also be explained by the large differences between the lattice constants ( $d_{\text{MgO}} = 4.20 \text{ \AA}$ .). The last alkaline earth oxide, BeO, has a hexagonal crystal structure, contrary to the other oxides which crystallize in the face-centred cubic system. A formation of normal mixed crystals between BeO and the other alkaline earth oxides is therefore not to be expected.

(b) *Emission phenomena.* The connection between the crystallographical and the emission properties of oxide mixtures was first described by Benjamin and Rooksby.<sup>1, 2</sup> They found that the emission current of a mechanical mixture of BaO and SrO is equal to the sum of the emission currents of the two components of the mixture. An oxide coating consisting of the corresponding mixed crystals, however, gives a larger emission current than is obtained by adding the shares of BaO and SrO. Accordingly a mixed crystal [BaSr]O gives a larger emission current than a pure BaO or a pure SrO crystal with the same surface and at the same

temperature. This fact was confirmed by further observations of Benjamin and Rooksby, showing that the emission current of a mechanical mixture BaO-SrO increases if this mixture is transformed

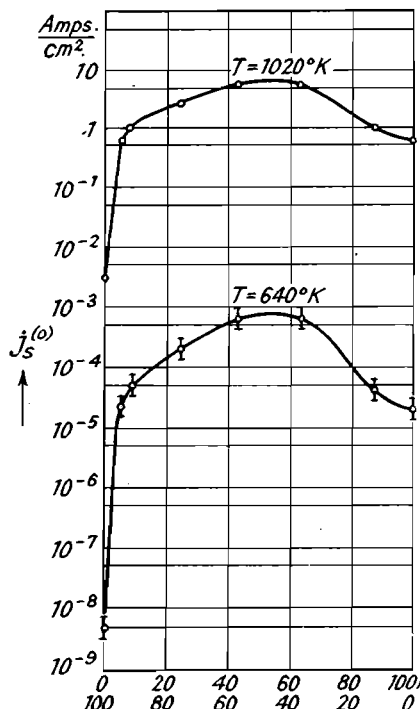
into mixed crystals by heating at about 1200° K. (cf. Vol. I, Sec. 7).

If the saturated current of oxide cathodes, consisting of mixed crystals [BaSr]O of different compositions, is plotted against the composition expressed in mol. %, a curve is obtained showing a maximum at approximately equal amounts of BaO and SrO. Fig. 108 shows this curve according to the most recent measurements made by Huber.<sup>1\*</sup> The mixtures used for these measurements were made of alkaline earth carbonates precipitated together (cf. Vol. I, Sec. 4); the experimental conditions were the same as for the examinations of pure alkaline earth oxides described in the preceding paragraph. The saturated currents shown in

Fig. 108.—Density  $j_s$  of the Saturated Current of an Oxide Cathode, consisting of Mixed Crystals [BaSr]O, as a Function of Composition (Huber<sup>1</sup>).

Fig. 108 were measured at 640° K. and extrapolated to external field zero by equation (182). The values given for 1020° K. were obtained by extrapolation according to the method of Hinsch.<sup>1</sup> As can be seen from the figure, the saturated current increases rapidly when giving small additions of BaO to the pure SrO, the increase amounting to two powers of 10 for 5% BaO (at 1020° K.). If the amount of BaO is increased further, a more gradual increase in emission of about one power of 10 is obtained, until a flat maximum is reached at a composition of 50 : 50 mol. %. Eventually the saturated current falls again by one power of 10 down to the pure BaO.

\* Pulsed emission measurements which were recently undertaken by Widell and Hellar<sup>1</sup> gave the emission maximum at 70% SrO.



Huber<sup>1</sup> also examined the systems [SrCa]O and BaO-CaO; the results are shown by Figs. 109 and 110 for  $T=770^\circ$  and  $640^\circ$  K.

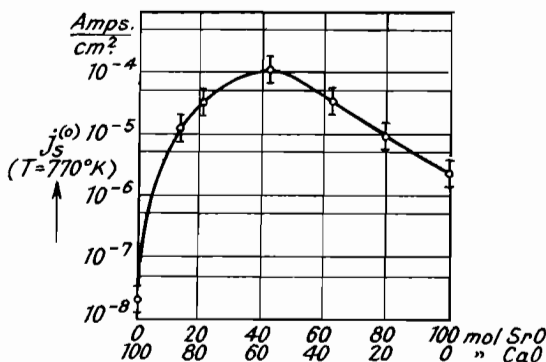


Fig. 109.—Density  $j_s$  of the Saturated Current of an Oxide Cathode, consisting of Mixed Crystals [SrCa]O, as a Function of Composition (Huber<sup>1</sup>).

respectively. The curve for [SrCa]O is similar to that for [BaSr]O discussed above, while the curve for BaO-CaO is slightly different.

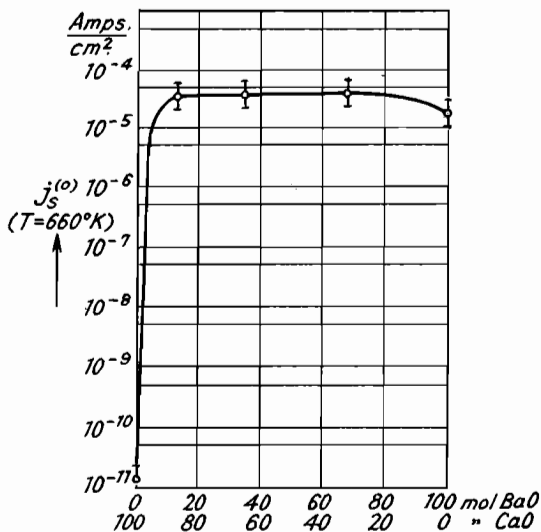


Fig. 110.—Density  $j_s$  of the Saturated Current of an Oxide Cathode, consisting of a BaO-CaO Mixture, as a Function of Composition (Huber<sup>1</sup>).

This latter curve shows a very steep rise of about  $10^6$  on the pure CaO side, then runs exactly horizontally over a wide range of

concentrations (between 10 and 70 mol. % BaO) and eventually falls very slightly when approaching the pure BaO.

The mixtures with the other two alkaline earth oxides MgO and BeO were examined by Herrmann.<sup>1</sup> Different percentages of these oxides were added to a commercial emission paste, consisting of mixed crystals [BaSr]O. The saturated currents of the cathodes sprayed with these emission pastes were measured at low temperatures (about 600° K.). The result for the mixture MgO+[BaSr]O is shown by Fig. 111, according to which the logarithm of the saturated current decreases linearly with increasing molecular concentration of MgO.

In the system BeO+[BaSr]O, however, a large decrease in emission was measured by Herrmann if only some tenths per cent. of BeO were added.

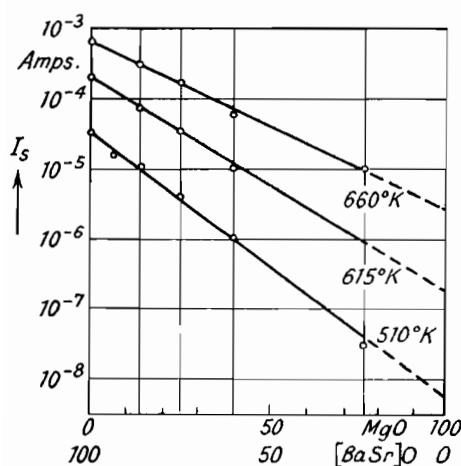
If the completely different BeO is disregarded, the results of the measurements of emission of binary mixtures of alkaline earth oxides can be summarized as follows:

(1) If the mixtures concerned consist of mixed crystals, the emission current is increased considerably by adding the less emitting oxide to the better emitting one, a maximum being reached at about 50 : 50 mol. %. On increasing the percentage of the less emitting oxide still more, the emission current falls at first slowly and eventually rapidly until the value of the pure, less emitting oxide is reached.

Fig. 111.—Saturated Current of Oxide Cathodes, made of Mixtures of [BaSr]O and MgO, as a Function of Composition (Herrmann<sup>1</sup>).

(2) If, however, the mixtures concerned do not form any mixed crystals, there will be either no maximum of emission, as, for instance, for mixtures with MgO, or the maximum obtained is very flat and only slightly higher than the emission value of the better emitting component itself (BaO-CaO).

According to the concept of the mechanism of the oxide cathode given above, the differences in emission between the differently composed mixtures of oxides can be explained by appropriate



differences in the work function. This conclusion is supported by the experimental results of Huber,<sup>1</sup> who found that the emission constant  $A$  of such mixed oxide cathodes, determined as shown on page 215, is independent of composition and is equal to the theoretical value  $A_0=120$  within the experimental errors. A different result given by Nishibori, Kawamura, and Hirano<sup>1</sup> does not seriously conflict with the above conclusion, as their results were obtained by combining photo-electric and thermionic measurements, which were not carried out with the same cathodes.

The total work functions of the three most important mixtures of

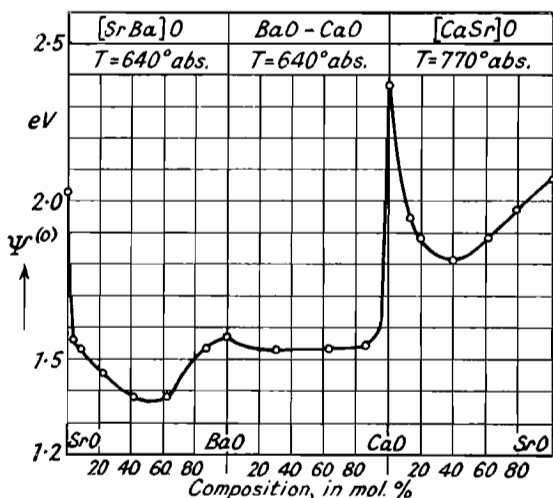


Fig. 112.—Work Function  $\Psi$  as a Function of Composition of Mixtures of Alkaline Earth Oxides (Huber<sup>1</sup>).

oxides were calculated from the saturated currents for  $A_0=120$  and plotted in Fig. 112 as a function of composition. The commercially used mixture [BaSr]O of equal gravimetric proportions has an average work function of 1.4 eV at a temperature of 1000° K. For converting this value to other temperatures the measurements indicate that a temperature coefficient of about  $3 \times 10^{-4}$  volt/degree should be used.

(c) *Constitution of the surface.* Before discussing the physical causes for the emission phenomena of mixtures of alkaline earth oxides, we must consider the surface of these mixed oxide coatings in more detail. The suitable method for examining the surface is the electron diffraction, which gives only the structure of the

uppermost atom layers, because the depth of penetration of electron beams is much smaller than that of X-rays.

The first investigations employing electron diffraction for oxide cathodes were carried out by Gärtner<sup>1</sup> and Darbyshire<sup>1</sup> with [BaSr]O cathodes consisting of mixed crystals in equal gravimetric proportions. The diffraction patterns showed the structure of pure SrO. According to this result the composition of the surface of such an oxide coating is different from the composition of the interior. While in the interior of the coating there are Ba- and Sr-ions at a distance corresponding to the lattice constant of the mixed crystals

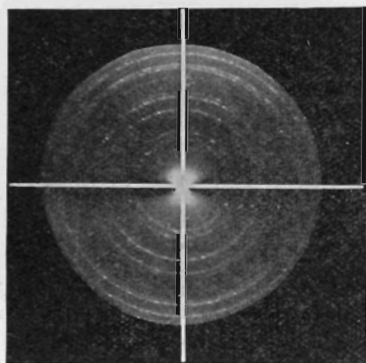


Fig. 113.—Electron Diffraction Patterns of an Oxide Cathode coated by SrO on the One Side and by [BaSr]O on the Other Side (Huber and Wagener<sup>2</sup>).

cathode is heated to high temperatures for a longer time, BaO also evaporates from the interior of the coating, so producing a considerable decrease of the emission current as discussed in Vol. I, Sec. 7.

Further investigations by electron diffraction were undertaken by Huber and Wagener,<sup>2</sup> who used cathodes made of colloidal alkaline earth carbonates prepared by the method of Buzagh<sup>1</sup> and deposited by cataphoresis. In this manner a very smooth cathode surface was obtained which was especially favourable for producing good electron diffraction patterns.

When examining [BaSr]O mixtures with a higher percentage of BaO the lattice constant at the surface remained equal to that of SrO up to a percentage of 90 mol. % BaO. This result is demonstrated by Fig. 113, showing two electron diffraction patterns of

[BaSr]O, only Sr-ions exist at the surface and the distance between these ions is given by the lattice constant of pure SrO. Obviously the absence of Ba-ions in the surface layer will be due to the large rate of evaporation of BaO (cf. Vol. I, Sec. 12.1), which produces a preferred evaporation of BaO from the surface when the cathode is heated to high temperatures during the decomposition of the carbonates and during the activation process. During the normal manufacture this preferred evaporation is limited to the uppermost part of the coating, while if the

the two sides of an oxide cathode, the one side being coated with pure SrO and the other side with a [BaSr]O mixture. One sees that the diffraction rings of the two patterns are parts of complete circles, so showing that the two surface layers producing the diffraction rings have the same lattice constant.

The SrO crystal lattice at the surface, proved by these experiments, is formed during the decomposition of the carbonate into the oxide. Diffraction patterns which were obtained during the different stages of decomposition showed that the SrO lattice at the surface already existed at the lowest temperatures at which the first diffraction rings could be observed (about 1200° K.).

The thickness of the SrO layer at the surface can be estimated from the fact that the electron diffraction patterns only showed the diffraction rings of that layer, while on the X-ray patterns only the diffraction rings of the mixed crystals were seen. If the coefficient of absorption for the electron beam is used, it can be calculated that the thickness of the SrO surface layer is between 300 and 2000 atom layers. Considering a total thickness of the coating of about 50  $\mu$  corresponding to  $2 \times 10^5$  atom layers, the SrO layer on top amounts to about 0.5% of the total oxide coating on the average.

The results obtained with the other two systems, BaO-CaO and [CaSr]O, completely correspond with the result found for [BaSr]O. The more readily evaporable oxide always evaporates from the atom layers at the surface, whilst the oxide which evaporates less easily remains. Consequently there is only a layer of CaO left at the surface of the BaO-CaO cathodes, when the decomposition has been completed. With the third system, [SrCa]O, however, there is a peculiarity resulting from the lower rate of evaporation of SrO compared with CaO. When these cathodes have been decomposed at the appropriate temperature of 1300° K., mixed crystals [SrCa]O are observed at the surface. These mixed crystals are converted into pure CaO crystals by evaporation of SrO if the higher temperature of 1450° K. is applied which is needed for the activation. Not only the final state but also the process of evaporation can be observed in this case due to the lower rate of evaporation of SrO.

Summarizing the results of the electron diffraction experiments, we can state that the atom layers near the surface of fully activated mixtures are normally different from those existing in the interior of the coating. The atom layers concerned form a crystal lattice of only one, the less readily evaporable alkaline earth oxide.

When mixed oxide cathodes are operated at high temperatures

during life, the evaporation of BaO will extend to deeper parts of the coating, and it then can be detected by X-ray patterns by means of the broadening of the diffraction lines. Eisenstein<sup>1</sup> calculated the percentage of remaining SrO from this broadening of the lines for different times of operation (cf. Fig. 114). It is quite clear that the emission of the cathode will be considerably influenced by such a strong evaporation of BaO.

The crystal lattice near the surface will contain excess alkaline earth atoms as well as the interior of the coating, but these excess

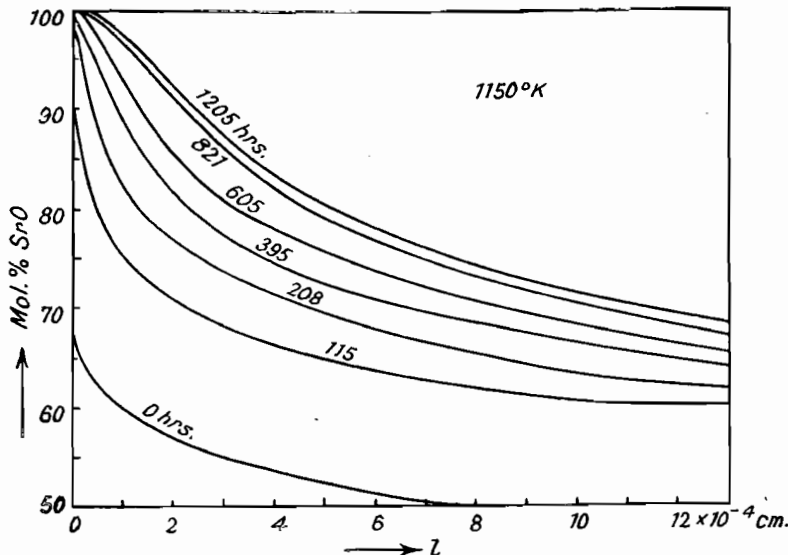


Fig. 114.—Percentage of Strontium Oxide in a [BaSr]O Cathode as a Function of Distance  $l$  from the Surface (Eisenstein<sup>1</sup>) (operating time as parameter).

atoms in the surface layer will not necessarily be identical with the metal ions of the crystal lattice there. For reasons to be explained later, we may assume that both Sr and Ba excess atoms exist in the SrO layer on top of the surface (cf. Sec. 27.3). The structure of the surface of a [BaSr]O coating will therefore be as shown in Fig. 115. The surface of the other two systems of oxides will be composed correspondingly.

The number of excess Ba-atoms in the SrO layer at the surface is, however, so small compared with the number of Sr-ions that those excess atoms will hardly influence the intensity of the lines of the electron diffraction patterns. This corresponds with the result of Huber and Wagener,<sup>2</sup> who, when comparing patterns of [BaSr]O

and pure SrO cathodes, did not find any essential difference in the ratio of the intensities of the diffraction lines.

After having obtained information concerning the structure of mixed oxide cathodes we shall now reconsider the total work function of these cathodes and the components of this total work function, the internal and external work functions. Considering the [BaSr]O system, for instance, there are two co-existing activating atoms Sr and Ba, and it will be proved later, when the foreign-activated cathodes are considered (cf. Sec. 27.2), that of those atoms barium has the deciding influence on the work function. The internal work function of [BaSr]O will therefore mainly be determined by Ba as activator in the lattice of the mixed crystals [BaSr]O.

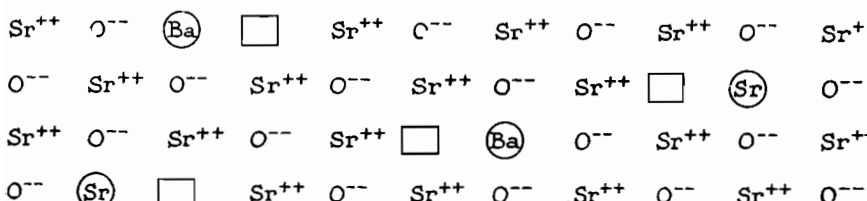


Fig. 115.—Configuration of Ions and Atoms at the Surface of a [BaSr]O Cathode.

We denote this internal work function by a symbol  $\phi_{[\text{BaSr}]O}^{\text{Ba}}$ , the subscript [BaSr]O indicating the basic material and the superscript indicating the activator. The external work function of these cathodes is determined by SrO as basic material and again by Ba as activator and will therefore be denoted by the symbol  $\psi_{\text{SrO}}^{\text{Ba}}$ . Using these symbols, the total work function of the [BaSr]O cathode is:

$$\Psi_{[\text{BaSr}]O} = \phi_{[\text{BaSr}]O}^{\text{Ba}} + \psi_{\text{SrO}}^{\text{Ba}} \dots \dots \quad (210)$$

In the same manner the total work function of the pure BaO cathode is obtained as:

$$\Psi_{\text{BaO}} = \phi_{\text{BaO}}^{\text{Ba}} + \psi_{\text{BaO}}^{\text{Ba}} \dots \dots \quad (211)$$

and the total work function of the pure SrO cathode as:

$$\Psi_{\text{SrO}} = \phi_{\text{SrO}}^{\text{Sr}} + \psi_{\text{SrO}}^{\text{Sr}} \dots \dots \quad (212)$$

Corresponding symbols and equations may also be introduced and established for the other types of cathodes. The further problem will be to reduce the variations of the total work function of mixed cathodes shown by Fig. 111 to corresponding variations of the appropriate internal or external work functions. Only after having done this, the physical cause for the differences in emission

between mixed oxides of different compositions may be found. We shall return to this subject later.

## 26.2. Mixtures with other metal oxides

The emission properties of mixtures between alkaline earth oxides and other metal oxides have been examined by Herrmann.<sup>1</sup> These experiments were undertaken with commercial valves in the same manner as the examination of mixtures with MgO and BeO discussed above, but the measurement of the saturated current was replaced by measuring an underheating characteristic (cf. Vol. I, Sec. 10.4). Only white metal oxides were taken for the additions in order to avoid influencing the radiant emissivity of the coating by these additions. The metal oxides examined were as follows:

2nd column of the periodic table: ZnO

3rd      „      „      „      „      Al<sub>2</sub>O<sub>3</sub>, La<sub>2</sub>O<sub>3</sub>

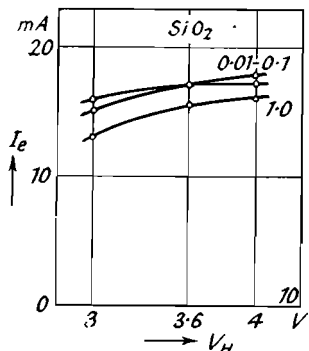
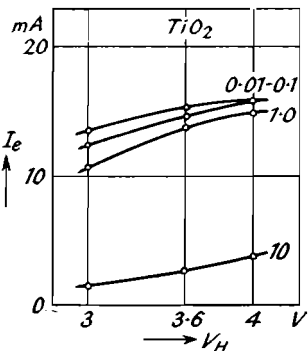
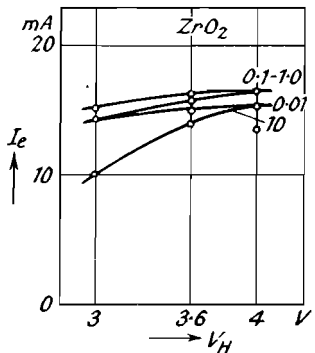
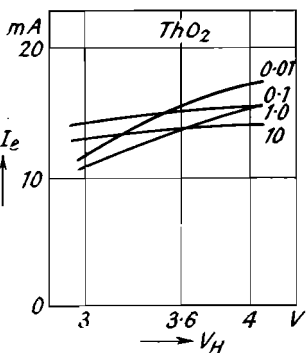
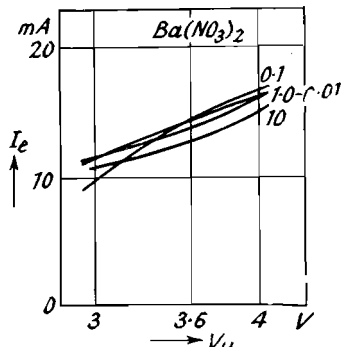
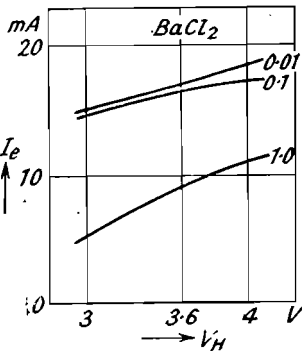
4th      „      „      „      „      SiO<sub>2</sub>, TiO<sub>2</sub>, ZrO<sub>2</sub>, ThO<sub>2</sub>, SnO<sub>2</sub>

5th      „      „      „      „      Ta<sub>2</sub>O<sub>5</sub>

6th      „      „      „      „      WO<sub>3</sub>

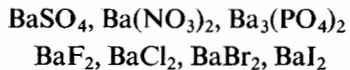
When discussing the results obtained for the different mixtures, Herrmann distinguished between metal oxides which form chemical compounds (salts) with the alkaline earth oxides, and metal oxides which do not form such compounds. The oxides forming compounds decreased the emission very much. It was therefore assumed that the alkaline earth oxide, emitting the electrons, is more or less consumed by the formation of these compounds, which are, for instance, the silicate (Ba<sub>2</sub>SiO<sub>4</sub>), the titanate (Ba<sub>2</sub>TiO<sub>4</sub>), the tungstate (BaWO<sub>4</sub>), etc. The effect of these metal oxides was the stronger the more acidic the oxide concerned. As an example the underheating characteristics for additions of SiO<sub>2</sub>, TiO<sub>2</sub>, and ZrO<sub>2</sub> are given in Figs. 116–118 (the amount of the additions, given in percentage by weight, has been written beside the curves). Contrary to these oxides, thoria which does not readily form compounds with the alkaline earth oxides, decreased the emission only slightly (cf. Fig. 119).

Furthermore, the effect of adding barium salts to the alkaline earth oxides was examined. This effect may be of importance because the salts concerned or the products of their dissociation will always exist in the oxide coating in certain quantities due to the

Fig. 116.—Addition of  $\text{SiO}_2$ .Fig. 117.—Addition of  $\text{TiO}_2$ .Fig. 118.—Addition of  $\text{ZrO}_2$ .Fig. 119.—Addition of  $\text{ThO}_2$ .Fig. 120.—Addition of  $\text{Ba}(\text{NO}_3)_2$ .Fig. 121.—Addition of  $\text{BaCl}_2$ .

Figs. 116-121. Underheating Characteristics of Oxide Cathodes with Additions of Different Magnitude (additions in %) (Herrmann<sup>1</sup>).

manufacture of the emission paste. The following additions were investigated:



Only a small poisoning effect was observed with  $\text{BaSO}_4$ ,  $\text{Ba}(\text{NO}_3)_2$ , and  $\text{Ba}_3(\text{PO}_4)_2$  (cf. Fig. 120); the halides, however, as for instance  $\text{BaCl}_2$ , have a severe poisoning action (cf. Fig. 121).

## 27. Multilayer Cathodes and Foreign-Activated Cathodes

### 27.1. Multilayer cathodes

When examining the mixed oxide cathodes it was found that several hundred atom layers at the surface of these cathodes are different from the majority of the atom layers. It is apparent that such oxide coatings may be made artificially, for example, by depositing on an oxide coating of pure  $\text{BaO}$  of the usual thickness a thin layer of another alkaline earth oxide. These cathodes will be called "multilayer cathodes." They were examined by Huber,<sup>1</sup> who sprayed a thin layer of  $\text{SrCO}_3$  or  $\text{CaCO}_3$  on top of a coating of  $\text{BaCO}_3$ . The ratio between the thicknesses of the layer on top and of the total coating was 1 : 8. This ratio was considerably larger than with normal mixed crystal cathodes because smaller ratios are difficult to be obtained by spraying. The values measured with those multilayer cathodes, however, will be near the values valid for cathodes with the right ratio of thicknesses. The saturated currents measured at  $T=750^\circ\text{ K}$ . with the cathodes concerned are set out in Table XXVI, the saturated current of pure  $\text{BaO}$  being given for comparison.

TABLE XXVI  
*Emission of Multilayer Cathodes*

Type of cathode	$I_s (T \approx 750^\circ\text{ K.})$ (amp.)
$\text{BaO}$	$1.2 \times 10^{-3}$
$\text{SrO}$ on $\text{BaO}$	$1.3 \times 10^{-2}$
$\text{CaO}$ on $\text{BaO}$	$2.4 \times 10^{-3}$

The fact that the emission current of a  $\text{BaO}$  cathode is increased by a  $\text{SrO}$  surface layer by about a factor ten shows the importance of the surface layer for the emission. The differences in emission between the two types of cathodes can be explained by assuming

that the different surface layers have different external work functions. The internal work function, however, will be almost the same with both cathodes because the interior of the SrO surface layer on top of the multilayer cathode may be neglected on account of the relatively small thickness of this layer.

Corresponding to the symbols introduced in the preceding section, the external work function of the multilayer cathode "SrO on BaO" will be denoted by  $\psi_{\text{SrO}}^{\text{Ba}}$  while the internal work function is the same as with pure BaO. Consequently the total work function of the multilayer cathode is:

$$\Psi_{\text{SrO}}^{\text{BaO}} = \phi_{\text{BaO}}^{\text{Ba}} + \psi_{\text{SrO}}^{\text{Ba}} \dots \dots \quad (213)$$

This relation differs from equation (210) for the mixed cathode [BaSr]O only in the internal work function and from equation (211) for the pure BaO cathode only in the external work function. If therefore the respective total work functions are determined from the saturated currents of the multilayer cathode, the mixed cathode, and the pure BaO cathode, it will be possible to ascertain from the differences of those total work functions the differences between the internal and external work functions of mixed cathode and pure BaO cathode. The calculation gives a value of 0.05 eV for the difference between the internal work functions and a value of 0.15 eV for that of the external work functions. It is seen from this that the better emission of the [BaSr]O cathode compared with the pure BaO cathode is mainly due to the smaller external work function resulting from the development of the SrO surface layer activated by Ba.

In addition to the multilayer cathodes mentioned above, some other cathodes were examined by Herrmann.<sup>1</sup> They consisted of a [BaSr]O coating of  $70 \mu$  thickness on top of which one of the metal oxides quoted in Sec. 26 ( $\text{ThO}_2$ , etc.) was sprayed in a thickness of about 5 to  $10 \mu$ . A large decrease of the emission current, as compared with normal [BaSr]O cathodes, was always observed with these cathodes. It follows therefore that the external work function of such metal oxide layers activated by Ba is considerably larger than the external work function of the normal alkaline earth oxide layer activated by Ba.

## 27.2. Foreign-activated cathodes

Further evidence of the emission phenomena of mixed cathodes will be obtained by considering another type, the "foreign-activated

cathode." The activating metal of these cathodes is no longer identical with one constituent of the alkaline earth oxides forming the basic material, but a metal foreign to these oxides is built in as an activator. The first evidence that such a foreign activation may produce a good emitter resulted from the measurements of Herrmann<sup>1</sup> with the system  $MgO + [BaSr]O$ , described in the preceding section. These measurements showed (cf. Fig. 111) that a relatively large emission current is obtained if the  $MgO$ -content is as high as 80%. It was concluded from this that a cathode with 100%  $MgO$ , foreign-activated by barium, would probably give a relatively high emission current, considerably higher than the very low emission of pure self-activated  $MgO$  (cf. Table XXV). In the meantime this conclusion has been confirmed by measurements of the authors. Some more foreign-activated cathodes were examined by Huber,<sup>1</sup> barium as an activator being built into oxide coatings of  $SrO$  or  $CaO$ . The barium was produced by a Ba-getter, being arranged in such a manner that the barium could evaporate on to the  $SrO$  cathode, which was heated to 1300° K. simultaneously. The measurement of the emission showed that the saturated current of such a  $SrO$  cathode activated by Ba is about three powers of 10 larger than the saturated current of a pure  $SrO$  cathode. Table XXVII shows details of the emission values.

TABLE XXVII  
*Emission of Foreign-Activated Oxide Cathodes*

Type of cathode	$I_s$ ( $T \approx 750^\circ$ K.) (amp.)
Self-activated	$BaO$ , activated by Ba
	$SrO$ "    "    Sr
	$CaO$ "    "    Ca
Foreign-activated	$SrO$ "    "    Ba
	$CaO$ "    "    Ba

In these experiments a large quantity of barium was evaporated from the getter in the valve on the cathode to be examined. If a normal oxide cathode containing  $BaO$  is used as a source of barium instead of the getter and if this auxiliary cathode is arranged opposite to the cathode to be examined (measuring cathode), the barium can be evaporated on to this measuring cathode in small controllable quantities. It is then possible to measure the saturated current of the measuring cathode during the evaporation of barium.

The measuring cathode was kept at room temperature during the evaporation, but the temperature was increased for short periods to a value of  $750^{\circ}$  K. necessary for the emission measurement. The experiments, carried out by Huber with SrO cathodes, at first showed a steep rise of the saturated current and subsequently, after passing through a flat maximum, a slow decrease of the emission.

The variation of the emission obtained in this manner is represented by Fig. 122 and is similar to the curve obtained by Becker<sup>1</sup> when evaporating barium on a [BaSr]O cathode (Fig. 86). The fundamental process will certainly be a similar one in both experiments. In both cases the barium impinging upon the surface is

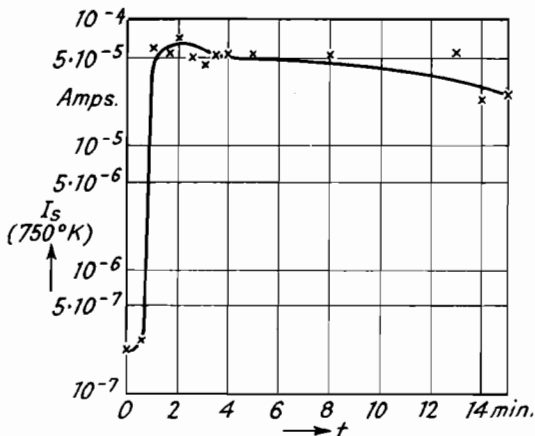


Fig. 122.—Variation of the Saturated Current of a SrO Cathode, when Evaporating Barium on the Surface (Huber<sup>1</sup>).

accumulated there, and the external work function is decreased and the emission current increased in this manner. After a certain time of evaporation the surface is occupied by an optimum number of Ba-atoms or ions. The emission current therefore reaches a maximum and subsequently falls, when the optimum state of occupation by Ba has been surpassed and when the conditions on the cathode surface approach those of a metallic Ba surface. The only difference between the experiments of Becker with [BaSr]O cathodes and those of Huber with SrO cathodes is that the surface of the [BaSr]O cathode is partially occupied by Ba already in the beginning, while the evaporation on a SrO cathode can be started with a surface which is completely free of barium. During this evaporation the external work function is changed from the value  $\psi_{\text{SrO}}^{\text{Sr}}$

belonging to a self-activated SrO surface to the value  $\psi_{\text{SrO}}^{\text{Ba}}$  belonging to a SrO surface foreign-activated by Ba.

The internal work function cannot be changed in the experiments described above, as the barium impinging upon the surface cannot diffuse into the interior of the oxide coating when the cathode is cold. If, however, the measuring cathode is heated, the barium at the surface will traverse into the interior of the coating and will influence the internal work function there. Such experiments, carried out by Huber,<sup>1</sup> at first showed that the saturated current decreased to the value of the pure SrO when the measuring cathode was heated up to 1000° K. Evidently the quantity of barium necessary for the activation of the surface is so small that this quantity, after having diffused into the interior, can only produce a variation of the internal work function which is unmeasurably small. If, however, considerably more barium than is necessary for observing the maximum of emission was evaporated on to the measuring cathode, an increase of the saturated current was measured after the heating at 1000°. Then the final value of the current was almost equal to the value obtained before by evaporation of the barium from the getter. The barium supply at the surface produced by this large evaporation seems to be sufficient to change the internal work function considerably, if the barium is brought into the interior and built into the vacancies of the SrO crystal lattice. In this case the internal work function varies again from the value  $\phi_{\text{SrO}}^{\text{Sr}}$  of the pure self-activated SrO coating to the value  $\phi_{\text{SrO}}^{\text{Ba}}$  of a coating foreign-activated by Ba.

According to these considerations we have to distinguish between two types of foreign-activated cathodes. Considering the one type, only the external work function is influenced by the foreign activation, while with the other type both the external and the internal work functions are varied. The first of these two types of cathodes is only stable at low temperatures, at which a measurable diffusion does not occur. At high temperatures this first type changes into the second stable type. The total work function of the first type may be denoted by  $\Psi_{\text{SrO}}^{\text{Ba}}$  the total work function of the second type by  $\Psi_{\text{SrO}}^{\text{Ba}}$ . Then with the usual symbols:

$$\Psi_{\text{SrO}}^{\text{Ba}} = \phi_{\text{SrO}}^{\text{Sr}} + \psi_{\text{SrO}}^{\text{Ba}} \quad \dots \quad (214)$$

$$\Psi_{\text{SrO}}^{\text{Ba}} = \phi_{\text{SrO}}^{\text{Ba}} + \psi_{\text{SrO}}^{\text{Ba}} \quad \dots \quad (215)$$

These equations differ from equation (210) for the [BaSr]O mixed

cathode in the internal work function only. They may be used therefore together with (210) for ascertaining the difference between the internal work functions of the mixed cathode  $[BaSr]O$  on the one hand, and the self-activated  $SrO$  cathode and the foreign-activated  $SrO$  cathode on the other hand. Finally, equation (214) differs from equation (212) for the total work function of the pure  $SrO$  cathode in the external work function only. Therefore the difference between the external work functions  $\psi_{SrO}^{Sr}$  and  $\psi_{SrO}^{Ba}$  may be obtained by means of (212) and (214).

Similar considerations and experiments may be carried out for cathodes containing  $CaO$  and for those activated by  $Sr$  and  $Ca$ . It will always be necessary to distinguish between the basic material, one of the alkaline earth oxides or a mixture of these, and the activator. If the activator is identical with one of the metallic constituents of the basic material, the cathode is self-activated, if not, it will be foreign-activated.

The phenomena observed with foreign-activated cathodes and described above give a good confirmation of our concept of the mechanism of the oxide cathode. It will be difficult to explain them by means of other concepts, which do not pay sufficient attention to the interior of the oxide coating.

### 27.3. Conclusions for the composite cathodes

If the total work functions of all composite cathodes discussed above are measured it will be possible to ascertain the differences between the corresponding internal and external work functions by using equations (210)–(215). In particular it will be possible to calculate the differences between internal and external work functions of different pure alkaline earth oxides and between these pure oxides and the mixed oxides. For obtaining the absolute values the knowledge of one absolute value of the internal work function and of one absolute value of the external work function will then be sufficient. As the absolute values of the internal work function measured so far show a considerable spread we shall be satisfied here with only giving the differences and not the absolute values. Those differences will be seen from Fig. 123, in which all internal and external work functions are related to the smallest appropriate value as datum level.

When discussing the differences seen from Fig. 123 attention must be paid to the fact that the measurements with foreign-activated and multilayer cathodes have so far only been undertaken with a few

valves. A very good accuracy can therefore not be expected. Furthermore, the multilayer cathodes used for the experiments should be made with a thinner surface layer which is more similar to the surface layer of the mixed oxide cathodes. This could possibly be achieved by preparing these layers by an evaporation method. Finally there is some doubt whether the cathodes which are foreign-activated only at the surface have really been in a state of equilibrium, because these cathodes are stable only at low temperatures.

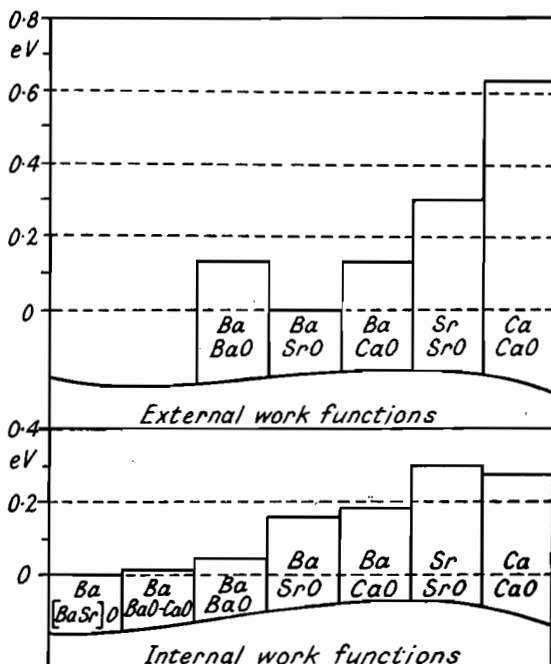


Fig. 123.—Differences between Internal and External Work Functions of differently composed Oxide Cathodes according to Huber.<sup>1</sup>

It seems to be possible that the conditions at the surface of such a cathode are different from the conditions at the surface of a cathode which is foreign-activated in the interior too. The relatively large difference which was calculated between the external work functions of self-activated CaO and of CaO foreign-activated by Ba may possibly be due to such an influence.

Independently of this fact the diagram of Fig. 123 shows again that the increase in emission obtained when changing from pure BaO to the mixed [BaSr]O is due mostly to the decrease of the

external work function ( $\psi_{\text{BaO}}^{\text{Ba}} \rightarrow \psi_{\text{SrO}}^{\text{Ba}}$ ) and only to a small degree to the decreasing internal work function ( $\phi_{\text{BaO}}^{\text{Ba}} \rightarrow \phi_{[\text{BaSr}]O}^{\text{Ba}}$ ).

We may now return to the question, if the assumption of Ba excess atoms built into a SrO crystal lattice, as for instance with the foreign-activated SrO cathode, is justified. The number of such excess Ba-atoms lying beside vacancies in the lattice of the Sr-ions (cf. Fig. 115) will only be considerable if the energy for building-in these excess atoms is smaller than or equal to the energy necessary for building-in excess Sr-atoms. The corresponding energies can be easily calculated for the two cases, if the process of building-in is considered in detail. First of all a vacancy must be formed in the lattice of the oxygen ions by removal of such an ion, the necessary energy which was calculated in Sec. 13 being the same for both cases. Then the metal atom (either Ba or Sr) which may exist in an appropriate vapour outside the crystal must be ionized, and both metal and oxygen ion must be deposited on the surface of the crystal. The energy to be supplied for this process is equal to the difference of ionization voltage  $\xi$  and lattice energy. Only the ionization voltages are different in the two cases, while the lattice energy remains nearly the same, because the Ba-ion is built in with the same lattice constant as the Sr-ion. The respective metal ion deposited will then diffuse into its position beside the vacancy, and finally it must be transformed into an atom by taking up the two electrons obtained from the ionization before. The energy set free during this last process is equal to twice the total work function of the cathode formed. In this way the difference between the total energies to be supplied in the two cases is obtained as:

$$\xi_{\text{Ba}^{++}} - \xi_{\text{Sr}^{++}} - 2(\psi_{\text{SrO}}^{\text{Ba}} - \psi_{\text{SrO}}^{\text{Sr}})$$

The difference of the ionization voltages is equal to 0.9 eV according to Table XVI, while the difference between the total work functions, which may be taken from Fig. 123, is 0.45 eV. The total difference above therefore becomes approximately zero, which means that the building-in of Ba excess atoms is as likely as the building-in of Sr-atoms within the limits of our calculation.

In order to give a final explanation of the emission phenomena of composite oxide cathodes, the differences in work function shown by Fig. 123 must be explained by the properties of the atoms bringing about those different work functions. Considering the influence of the activating metal for constant basic material, the relation between work function and ionization potential of

the atoms of the activator is evident. Both the internal and the external work function increase with increasing ionization potential; for example:  $\psi_{\text{SrO}}^{\text{Ba}} > \psi_{\text{SrO}}^{\text{Ba}}$ ,  $\phi_{\text{SrO}}^{\text{Sr}} > \phi_{\text{SrO}}^{\text{Ba}}$ . The variation of the work functions due to varying the basic material with constant activator is less clear. The two following relations will be seen from Fig. 123:

$$\begin{aligned}\psi_{\text{BaO}}^{\text{Ba}} &> \psi_{\text{SrO}}^{\text{Ba}} < \psi_{\text{CaO}}^{\text{Ba}} \\ \phi_{\text{BaO}}^{\text{Ba}} &> \phi_{[\text{BaSr}]O}^{\text{Ba}} < \phi_{\text{SrO}}^{\text{Ba}} \simeq \phi_{\text{CaO}}^{\text{Ba}}\end{aligned}$$

A theoretical explanation of these relations has not been given yet.

Concluding this section, we may point out that the smaller internal work function of a [BaSr]O cathode compared with pure BaO must be connected with a corresponding higher conductivity. Exact investigations of the conductivity of mixed crystals have not been made so far. An indication that such an influence exists can be deduced from measurements of Spanner.<sup>1</sup> He found that both the emission and the conductivity of CaO were increased by adding certain quantities of BaO or SrO.

## 28. The Influence of Heterogeneity in the Composition of the Oxide Coating on the Emission

It has been tacitly assumed during most of the previous considerations that both the interior and the surface of the oxide coating are homogeneous. However, we know from discussing the manufacture of the oxide coating (cf. Vol. I, Sec. 5) that the interior of the commercially employed coatings contains a large number of relatively large pores in between the individual oxide crystals. Moreover, we know that most of the commercial oxide cathodes do not possess a smooth surface, but that the cathode surface, due to the irregular shape and configuration of the individual crystals, normally is extremely rough. The emission phenomena produced by this heterogeneity could be neglected before because they are less important for the mechanism of the oxide cathode. After having discussed this mechanism in detail, however, it will be necessary to consider the influence of this heterogeneity.

The heterogeneous composition of the oxide coating has the result that the coating surface does not emit with equal intensity at all areas and that the emission current is limited to a number of emission centres (patches), while in between these centres there are areas emitting considerably less than those centres. The size and

configuration of these emission centres can be examined by means of the emission electron microscope (cf. Fig. 92). When undertaking such an examination, it is important to use cathodes which have the same high emission values as commercial cathodes. By not paying attention to this condition phenomena may be produced which may be useful for checking an electron microscope, but which do not normally occur with the high-vacuum cathodes used in commercial valves.

When investigating commercial oxide cathodes Heinze and Wagener<sup>1, 2</sup> used an electron microscope in which the emission

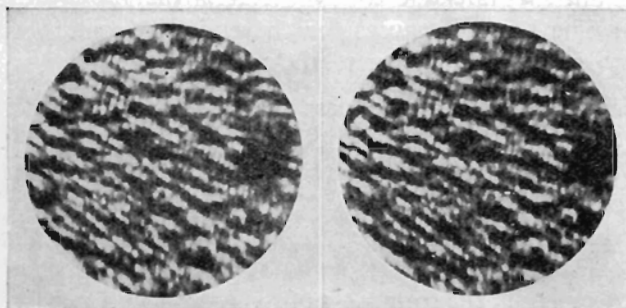


Fig. 124.—Electron Images of an Oxide Cathode taken before and after Poisoning with Oxygen (mag.  $\times 30$ ) (Heinze and Wagener<sup>2</sup>).

current of the oxide cathode examined could be measured and in which micro-photographs of the cathode surface could be taken. In addition to this another microscope was used which could be sealed from the pump before starting the measurements. The emission values of the best activated commercial cathodes were reached and the behaviour of the cathode during life could be examined in this microscope. The temperature of the cathodes, when taking the electron images, was between  $800^\circ$  and  $1000^\circ$  K.

It was found by this investigation that the size and distribution of the emission centres do not vary—

- (a) during the activation of the cathode (cf. Fig. 99);
- (b) during life;
- (c) when poisoning the cathode with oxygen (cf. Fig. 124);
- (d) when transforming the alkaline earth oxide back into the corresponding carbonate and decomposing this carbonate again;
- (e) when varying the temperature of the cathode.

The invariability of size and distribution of the emission centres as seen from this result shows the great difference between the oxide cathode on the one side and an atomic film cathode, for instance the tungsten-thorium cathode, on the other side. The high variability of the emission centres of such a cathode was shown in Sec. 6 (cf. Fig. 38). This different behaviour is another proof that the emission of the oxide cathode, unlike that of the atomic film cathodes, is not only due to qualities of the surface, but that in fact the interior of the oxide coating has the decisive influence.

According to these results the emission centres are not formed at random, but they are due to some special qualities of the oxide coating. The possible causes for the emission centres were discussed by Heinze and Wagener<sup>2</sup> they are:

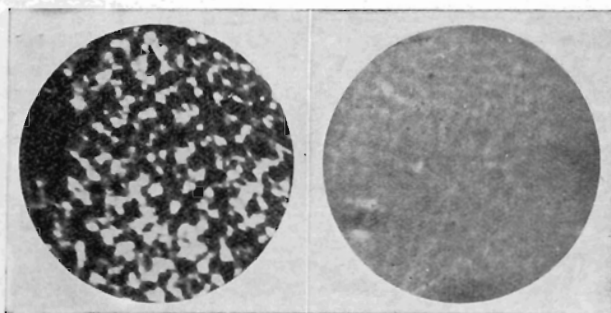
- (a) differences in the thickness of the oxide coating between different areas of the cathodes;
- (b) variations in the size and configuration of the pores in the coating;
- (c) possible variations in the ratio between the two alkaline earth oxides BaO and SrO;
- (d) differences in the roughness of the coating surface;
- (e) the different orientation of the emitting surface areas with reference to the crystal system of the appropriate alkaline earth oxide crystals.

According to Heinze and Wagener, only the last two of the possible causes are of importance. Their existence was proved in the following way.

The individual elements of the surface will have different curvatures due to the roughness of the surface. These differences in curvature produce differences in the field strength at those surface elements and consequently differences in emission current on account of the relationship between saturated current and field strength. Emission centres may be produced in this manner. The existence of this influence was proved by examining oxide coatings with different roughness obtained by different methods of manufacture. As described in Vol. I, Sec. 5, a rough coating surface was obtained by spraying and a smooth surface by depositing the alkaline earth carbonates by means of electrophoresis. The electron images obtained with these coatings (cf. Fig. 125) show clearly defined emission centres on the surface of the rough cathode, while the differences in emission between individual points of the surface of

the smooth cathode are only very small. The clearly defined emission centres will therefore be due to the greater roughness of the sprayed cathode.

Differences in the external work function between individual areas of the surface must be considered in addition to the roughness. The external work function of an alkaline earth oxide crystal will depend on the orientation of the emitting crystal plane in the same manner as with metals. Considering the surface of an oxide coating, the crystal planes there, as belonging to different crystals, will normally have different orientation and will therefore emit electron currents of different intensity. Emission centres may also be produced in this manner. This assumption was confirmed by



(a) Made by Spraying      (b) Made by Electrophoresis

Fig. 125.—Electron Images of Oxide coatings deposited in Different Ways (mag.  $\times 30$ ) (Heinze and Wagener<sup>2</sup>).

Heinze and Wagener<sup>2</sup> and Benjamin, Huck, and Jenkins<sup>4</sup> by examining cathodes with different crystal size. The electron images of these cathodes show that the size of and the distance between the emission centres decrease with decreasing crystal size in the same manner as the emitting crystal planes (cf. Fig. 126). It can be concluded from this that the orientation of the crystal planes also influences the formation of the emission centres. A further proof of this was obtained by taking electron images of a number of small BaO crystals which were arranged at random on a nickel ribbon. The emission currents emitted from the upper planes of these crystals were of different intensities due to the different orientation of those planes.

According to the above the emission centres at the surface of an oxide cathode are produced by two contributory factors, namely the roughness of the surface and the orientation of the emitting crystal

planes. One of these two factors which is determined by the size of the oxide crystals and the degree of roughness will predominate in general.

While the above investigations were undertaken with an electron microscope of a relatively small amplification (30 times), Brueche<sup>1</sup> and Mecklenburg<sup>1</sup> obtained electron images of oxide cathodes with considerably higher magnification, up to 50,000 times (corresponding to a resolution of about  $50 \text{ m}\mu$ ). Knowledge of the emission properties of the oxide cathode, however, cannot be obtained yet from these first investigations. An electron microscope in which the variation of the emission current along the surface can be measured has been described by Jacob.<sup>1</sup>

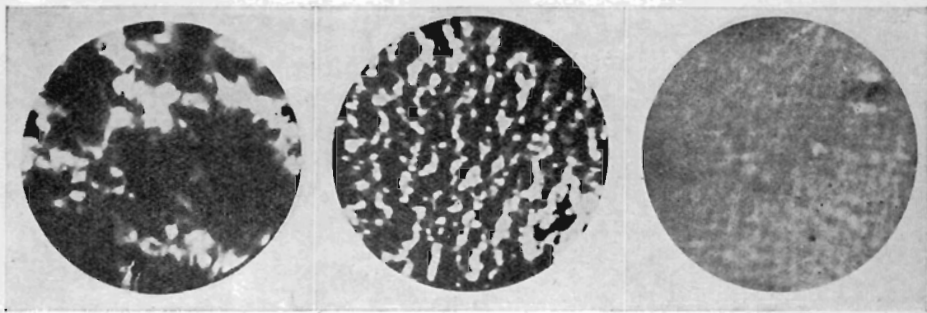


Fig. 126.—Electron Images of Oxide Coatings of Different Crystal Size (mag.  $\times 30$ ) (Heinze and Wagener<sup>2</sup>).

Quantitative values of the variation in work function along the cathode surface can be obtained from measurements of either the retarding field current or the saturated current by comparing the relationship between current and voltage found experimentally with the theoretical formulæ (cf. Sec. 6). Such an investigation of the retarding field current was undertaken by Hung<sup>1</sup> who found deviations between the experimental and the theoretical (Maxwell) characteristics at retarding voltages which were smaller than 0.2 volt. From these deviations he calculated the maximum variation in work function as 0.15 eV. The saturated current measured for different accelerating fields was used by Hung and Mahlman.<sup>1</sup> The latter employed the photo-electric emission and calculated the surface field by using equation (79). From the values obtained for this surface field he concluded that the emission centres have a size of  $3 \times 10^{-4} \text{ cm}$ . and that the differences in work function along the

surface are 0.2 eV. The size of the emission centres obtained in this way nearly corresponds with the normal particle size of the coating.

As the roughness, the first of the causes responsible for the difference in work functions, depends on the method of manufacturing the oxide coating (cf. Vol. I, Fig. 19), coatings prepared in different manners may give differences in emission which are only due to the different roughness of the surfaces of those coatings. Two influences must be distinguished in this context, the influence of the emitting surface itself which varies together with the roughness, and the influence of the field strength which is also changed by the roughness. The variation of the emitting surface produces an equal variation of the saturated current extrapolated to zero field. As can be seen from Fig. 127, the extrapolated saturated current of an oxide coating prepared with an organic binder is about twice as large as the saturated current of a coating prepared with water paste. This difference in emission is due to the greater roughness of the coating prepared with binder (cf. Vol. I, Sec. 5). In addition to this the saturated current flowing at higher anode voltages is increased by the influence of the field strength, which draws higher values from the rougher surface (cf. Sec. 21.1).

The second cause responsible for the differences in work function, the orientation of the emitting crystal planes, causes the emission current to increase with decreasing size of the crystals employed for preparing the oxide coating. This increase in emission results from the increasing emitting surface as seen from Fig. 126, and was confirmed by measurements of Benjamin, Huck, and Jenkins<sup>4</sup> for crystal sizes larger than 1 to 5  $\mu$  (cf. Vol. I, Table IV). If, however, crystals are examined which are smaller than this value, especially colloidal crystals, the emission current decreases with decreasing crystal size according to measurements of Benjamin,<sup>3, 4</sup> and collaborators, and of Buzagh.<sup>1</sup>

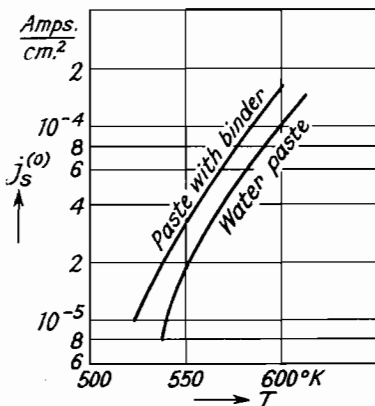


Fig. 127.—Saturated Currents of Oxide Coatings prepared with and without Organic Binder as a Function of Temperature (Liebold<sup>1</sup>).

Up to the present the knowledge of the relationship between the heterogeneity of the oxide coating and the value of the emission current is mostly based on experience gained during the commercial manufacture of oxide cathodes; a thorough investigation has yet to be undertaken.

### REFERENCES

- BECKER, J. A. (1) *Physic. Rev.* 34 (1929), 1323.  
 BENJAMIN, M. (1) and ROOKSBY, H. P., *Philos. Mag.* 15 (1933), 810.  
     (2) *ibid.* 61 (1933), 519.  
     (3) COSGROVE, C. W., and WARREN, G. W., *J. Instn. Electr. Engr.* 80 (1937), 401.  
     (4) HUCK, R. J., and JENKINS, R. O., *Proc. Physic. Soc.* 50 (1938), 345.
- BRÜCHE, E. (1) *Kolloid-Z.* 100 (1942), 192.  
 BURGERS, W. G. (1) *Z. Physik* 80 (1933), 352.  
 BUZAGH, A. V. (1) *Kolloid-Z.* 77 (1936), 172.  
 CAMPBELL, N. R. (1) *Philos. Mag.* 12 (1931), 173.  
 DARBYSHIRE, J. A. (1) *Proc. Phys. Soc.* 50 (1938), 635.  
 EISENSTEIN, A. (1) *J. Appl. Phys.* 17 (1946), 434, 654.  
 GÄRTNER, H. (1) *Philos. Mag.* 19 (1935), 82.  
 GORLICH, P. (1) *Z. Physik* 116 (1940), 704.  
 HANLEY, T. E. (1) *J. Appl. Phys.* 19 (1948), 583.  
 HEINZE, W. (1) and WAGENER, S., *Z. techn. Physik* 17 (1936), 645.  
     (2) *ibid.* 20 (1939), 16.  
 HERRMANN, G. (1) *Techn. Wiss. Abh. Osram* 5 (1943), 311.  
 HINSCH, W. (1) *Z. techn. Physik* 12 (1931), 528.  
 HUBER, H. (1) Thesis, University Berlin, 1941.  
     (2) and WAGENER, S., *Z. techn. Physik* 23 (1942), 1.  
 HUNG, C. S. (1) *J. Appl. Phys.* 21 (1950), 37.  
 JACOB, L. (1) *J. Sci. Instr.* 26 (1949), 262.  
 KOLLER, L. R. (1) *Physic. Rev.* 33 (1929), 1082.  
 LIEBOLD, W. (1) Thesis, University Berlin, 1941.  
 MAHLMAN, G. W. (1) *J. Appl. Phys.* 20 (1949), 197.  
 MECKLENBURG, W. (1) *Z. Physik* 120 (1942), 47.  
 NISHIBORI, E. (1) KAWAMURA, H., and HIRANO, K., *Proc. Physico-Math. Soc. Japan* III 23 (1941), 37.  
 SPANNER, H. J. (1) *Ann. Phys.* 75 (1924), 609.  
 SUHRMANN, R. (1) and DEHMELT, F. W., *Z. Physik* 118 (1942), 677.  
 WARTENBERG, H. v. (1) and PROPHET, E., *Z. anorg. allg. Chem.* 208 (1932), 369  
 WEINREICH, M. O. (1) *Revue générale de l'Electricité* 14 (1945), 243.  
 WIDELL, E. J. (1) and HELLAR, R. A., *J. Appl. Phys.* 21 (1950), 1115.  
 WRIGHT, D. A. (1) *Nature* 160 (1947), 129.

## CHAPTER 6

# VARIATIONS IN THE EQUILIBRIUM OF THE OXIDE COATING

The considerations of the previous chapters referred to the fully activated oxide coating which was assumed to be in a state of equilibrium with an invariable number of excess barium atoms. We shall now proceed to the discussion of phenomena which are produced by variations of this equilibrium. The processes to be discussed first in this context are those which establish the equilibrium of the fully activated oxide coating during the activation.

### 29. The Activation

When discussing the technique of the activation process in Vol. I, Sec. 8, it has been pointed out that a distinction must be made between an activation by reduction, consisting of a pure temperature treatment of the cathode, and an activation which is undertaken by drawing an emission current from the cathode. This classification will be maintained here and activation by reduction will be discussed first. The historical development of the ideas underlying the activation process will be described as an introduction.

Originally it was assumed that the excess barium was formed by the thermal dissociation of barium oxide. This theory, however, was refuted by Dushman and Villars,<sup>1</sup> who calculated that the dissociation pressure of BaO at 1000° K. is smaller than  $10^{-40}$  kg./cm.<sup>2</sup>. No dissociation is therefore possible with the pressures between  $10^{-6}$  and  $10^{-10}$  kg./cm.<sup>2</sup> normally existing in valves. Later it was concluded from investigations on combined cathodes that activation by drawing current, which is the only possible method with this type of cathode, would be the only possible type of activation in general (Espe,<sup>1</sup> Berdennikowa<sup>1</sup>). When uncombined cathodes came more and more into use it was, however, recognized that with these cathodes activation by reduction is by far the more important process. The first investigation showing that activation is possible without drawing current was that by Lowry,<sup>1</sup> who

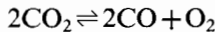
examined a  $[BaSr]O$  coating, prepared by means of a water paste and deposited on a Ni-Co-Fe-Ti alloy (Konel). This work was followed by that of Benjamin,<sup>2</sup> Maddock,<sup>1</sup> and others mentioned below.

### 29.1. Activation by reduction

The agent reducing the barium oxide to excess barium is not known *ab initio*. The different possibilities existing for these agents are:

(a) The carbon which arises during the decomposition of the carbonates as a product of the dissociation of the binder in the emission paste (cf. Vol. I, Sec. 7).

(b) The carbon monoxide present during the carbonate decomposition. This carbon monoxide may have two possible sources, the first being the dissociation of the carbon dioxide formed during decomposition, as given by the equilibrium:



The second possible source is a reaction between carbon dioxide and the carbon existing in the coating according to (a). Such a reaction is determined by the equation:



which was discussed in Vol. I, Sec. 7.

(c) The core metal or impurities and other metals alloyed to the core metal.

The first possibility, namely reduction by carbon, was checked by Huber,<sup>1</sup> who examined cathodes of pure BaO deposited on a core of commercial nickel. A number of these cathodes were prepared with a paste containing a nitrocellulose binder, while the cathodes of the remainder were kept free from carbon by using a water paste. The experiment showed that both the variation of the saturated current during the activation (Vol. I, Fig. 34) and the optimum activation temperature, as defined in Vol. I, Sec. 8, were the same for the two types of cathodes. Only the final value of the saturated current obtained during the activation showed a difference, being twice as high for the cathodes prepared with binder as for those made with water paste. This difference was explained by the fact that cathodes prepared with a binder have a higher emitting surface (cf. Fig. 127) than those made with water paste. It can therefore be concluded that the carbon in the coating formed during the

decomposition is not of much importance for the process of activation by reduction.

Considering the second possibility, the assumption that carbon monoxide is formed by one of the above equilibria, is justified. A detailed calculation based on the equilibrium quoted first, shows that about 0.1% of the carbon dioxide decomposes into carbon monoxide, if a temperature of 1350° K. and a total pressure of 0.1 mm. is assumed.\* Furthermore, the formation of carbon monoxide due to the second reaction quoted above has been shown to be possible in Vol. I, Sec. 7.

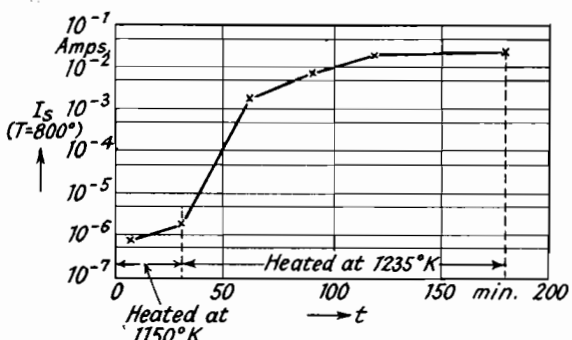
For examining the reducing effect of carbon monoxide Huber<sup>1</sup> prepared cathodes with a coating of barium peroxide ( $BaO_2$ ) instead of the normal barium carbonate. The  $BaO_2$  was decomposed into  $BaO$  at a temperature of 1300° K., and the existence of CO could so be avoided when processing the cathode. The subsequent activation showed that the saturated current measured at 750° K. for the cathodes prepared from  $BaO_2$  was only between  $10^{-8}$  and  $10^{-7}$  amp., whilst the saturated current of cathodes prepared from carbonates was  $5 \times 10^{-4}$  amp. It may be concluded from this result that the carbon monoxide present during the decomposition of normal cathodes plays an important part in activation by reduction. As this CO is not present in the sealed-off valve in which the final activation takes place, it may be assumed that a barium supply is formed during the decomposition by the reducing action of the CO and that this barium supply is utilized for producing the excess barium in the coating during the final activation.

The low saturated current of the cathodes prepared from  $BaO_2$  increased considerably when the activation temperature was raised from 1300° K., as applied previously, to between 1400° and 1450° K. Finally the same value was reached as was obtained at the lower temperature with cathodes made with  $BaCO_3$ . The stronger reduction occurring at the higher temperature according to this result can be explained by the third possibility, reduction by the core metal, which will be discussed now.

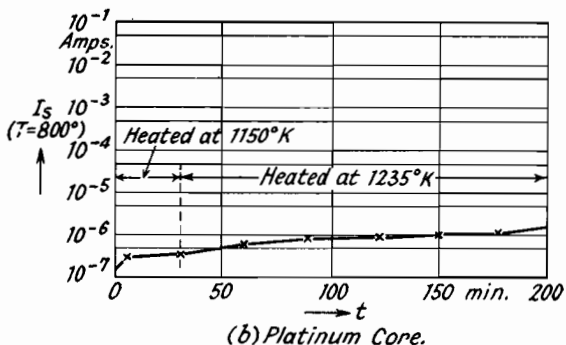
Herrmann<sup>1</sup> and Heinze and Wagener<sup>1</sup> compared the reducing effect of nickel with that of platinum using carbonate cathodes. The reducing action of the carbon monoxide could be eliminated by exposing the decomposed cathodes to an atmosphere of oxygen (between 5 and 10 mm. for some hours). The excess

\* Cf. H. Ulich, *Kurzes Lehrbuch der physikalischen Chemie (Short Textbook of Physical Chemistry)*, 1942, p. 124.

barium produced during the decomposition was so removed by reoxidation. Herrmann's experiment showed that cathodes with nickel cores, after being activated at  $1500^{\circ}$  K., gave an emission current which was 50 to 100 times higher than the current obtained from cathodes with platinum cores activated in the same way. Only an activation by drawing current could raise the emission



(a) Nickel Core.



(b) Platinum Core.

Fig. 128.—Variation of the Saturated Current during the Activation by Reduction of a Cathode previously poisoned by Oxygen (Heinze and Wagener<sup>1</sup>).

current of the cathodes with platinum cores to the same value as those with nickel cores. A similar result was found by Heinze and Wagener, who undertook the activation at  $1235^{\circ}$  K. and who measured the variation of the saturated current at a temperature of  $800^{\circ}$  K. during this activation. When activating by reduction, the saturated current of the cathodes with nickel cores rose to  $2 \times 10^{-2}$  amp. (cf. Fig. 128a), while with platinum a value of only  $10^{-6}$  amp. was reached (Fig. 128b). If the latter cathodes, however, were

activated by drawing current (cf. Fig. 129), a saturated current of  $1.5 \times 10^{-3}$  was obtained, which was nearly of the same magnitude as the value measured for nickel. The reducing effect of nickel on barium oxide was also shown directly by Blewett.<sup>2</sup>

The reducing action can be produced not only by the core metal itself but also by impurities of the core metal or by small percentages of other metals which are alloyed to it. This was recognized by Benjamin,<sup>2</sup> who examined directly heated cathodes, the core metal of which contained small additions of other metals. These cathodes were activated at  $1250^{\circ}\text{K}$ . and their emission current was measured at  $1020^{\circ}\text{K}$ . during the activation. The result

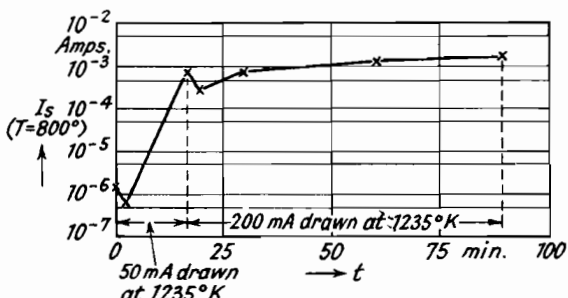


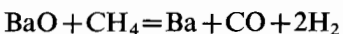
Fig. 129.—Variation of the Saturated Current during the Activation by Drawing Current of a Cathode with Platinum Core previously poisoned with Oxygen (Heinze and Wagener<sup>1</sup>).

obtained by Benjamin is shown in Fig. 130, from which the type and quantity of the additions will be seen. The activation was improved by additions of Al, Ti, and Mg to pure nickel, whilst it was inhibited by additions of Mn and Fe.

From the above we can conclude that the core metal assists in the activation by reduction and that the reducing effect depends on the type of core metal and on the impurities and additions to the core metal. The cause for the differences between individual core metals, such as between nickel and platinum, and between different additions, such as Al and Fe, will be discussed later, when the effect of the reduction on the fully activated cathode is considered (cf. Sec. 32).

An entirely different method of activation which so far is mainly useful for experimental work was employed by Prescott and Morrison and Hannay, MacNair, and White. These authors used methane gas which was introduced into the experimental valve up to a pressure of  $10^{-2}$  mm. Hg. The activation then was obtained by

heating the cathode at 1200 to 1300° K. for about 5 to 10 minutes. At this temperature barium oxide is reduced by methane according to the equation



and excess barium is so produced. The method is for instance useful for experimental coatings which are deposited on a ceramic base and which cannot be activated by the reducing effect of the core metal.

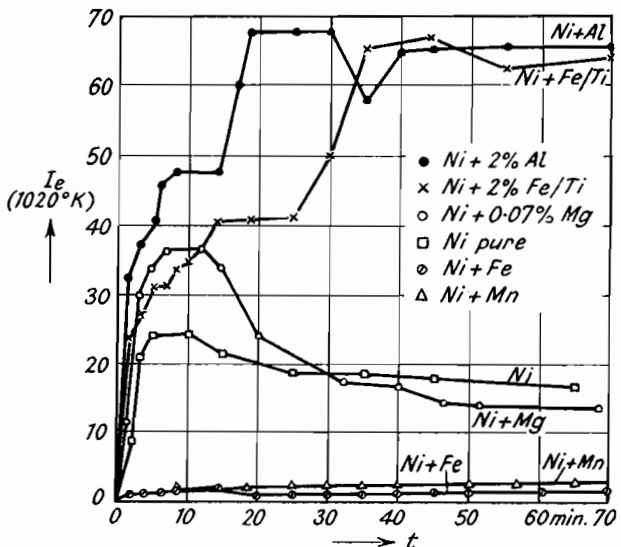


Fig. 130.—Variation of the Emission Current during the Activation by Reduction of Cathodes with Nickel Cores alloyed with Different Materials in Small Quantities (Benjamin<sup>2</sup>).

The dependence of the reduction on the type of alkaline earth oxides employed was examined by Huber,<sup>1</sup> who used cathodes prepared from carbonates of different composition and who measured the optimum activation temperature  $T_{opt}$  defined in Vol. I, Sec. 8. Figs. 131 and 132 show this optimum activation temperature plotted against the composition of the [BaSr]O and BaO-CaO mixtures employed. It is seen that, when adding SrO or CaO to pure BaO, the optimum activation temperature rises at first slowly and then more and more rapidly. The optimum activation temperatures of the pure alkaline earth oxides increase in the sequence BaO, SrO, CaO, which is to be expected because the heats of formation of these oxides increase in the same order.

So far only the formation of the excess barium has been considered, but two other processes are also of importance in the

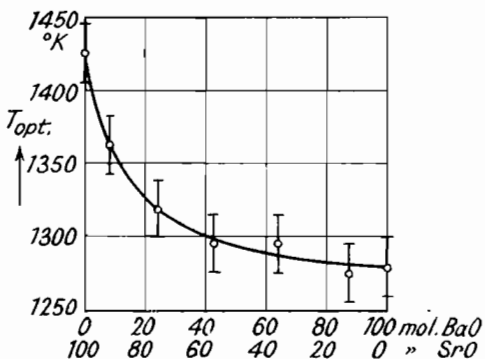


Fig. 131.—Optimum Activation Temperature  $T_{opt}$  as a Function of the Composition of a [BaSr]O Mixture (Huber<sup>1</sup>).

activation. They are firstly the diffusion of the excess barium into the crystal lattice of barium oxide, into which the barium must be

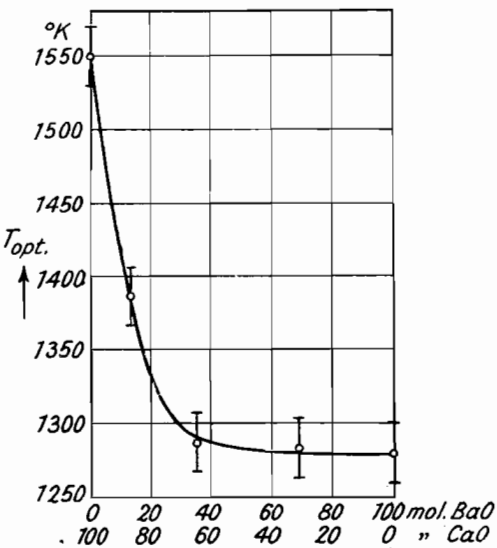


Fig. 132.—Optimum Activation Temperature  $T_{opt}$  as a Function of the Composition of a BaO-CaO Mixture (Huber<sup>1</sup>).

built, and secondly the evaporation of this barium from the surface of the oxide coating into the vacuum. In order to have a clear picture of how these three processes act together or against one

another, it will be assumed that only the reduction by the core metal is effective. This may be realized in practice by poisoning the cathode with oxygen after decomposition. At the beginning of the activation some oxygen ions of the barium oxide at the boundary between coating and core metal will react either with the core metal itself or with impurities or additions to this metal. In this way some vacancies at the sites of oxygen ions and some associated barium atoms are formed in the crystal lattice of the barium oxide near the core metal.

Two further processes will now be possible. The vacancies concerned may be filled by oxygen ions moving from adjoining parts of the oxide coating, or the excess barium atoms may diffuse into the interior of the coating over the vacancies in the lattice of the barium ions. In both cases the ratio between vacancies at oxygen ion sites and vacancies at barium ion sites is increased in the interior of the coating, and excess barium atoms are produced there. During the further activation the formation of vacancies at oxygen sites or, what is the same thing, of excess barium atoms, is continued in the same way. When the excess barium atoms arrive at the surface of the coating, a new process, the evaporation of the Ba-atoms at the surface, will occur, acting against the increase of excess barium in the interior. The three processes quoted, reduction of barium oxide to excess barium, diffusion of excess barium into the coating, and evaporation of excess barium from the surface, will finally establish an equilibrium with a definite number and distribution of the excess barium atoms in the coating. This equilibrium, of course, together with the three processes discussed will depend on temperature to a high degree.

## 29.2. Activation by drawing current

The activation by drawing current is only important for producing excess barium if there is no possibility of reducing the barium oxide, as, for instance, with the combined cathodes in which all reducing agents are oxidized during the combining process. In this latter case the excess barium must be produced by an electrolytical dissociation of the barium oxide into barium and oxygen. The anode voltage is then applied to the valve containing the cathode and an emission current is drawn which gradually increases with the quantity of barium produced, the barium oxide being dissociated by the ionic component of the total emission current flowing through the coating.

The first detailed investigations of activation by drawing current were undertaken by Espe<sup>1</sup> with combined cathodes, his results being shown by Fig. 133. It will be seen that an increase in temperature or in anode voltage produces an increase of the measured emission current which will be due to an increased formation of excess barium. The oxygen which is set free by the dissociation of the BaO was detected by Rothe<sup>1</sup> by measuring the pressure during the activation. Further works in which the evolution of oxygen has been proved by direct chemical analysis have been quoted in Sec. 19.

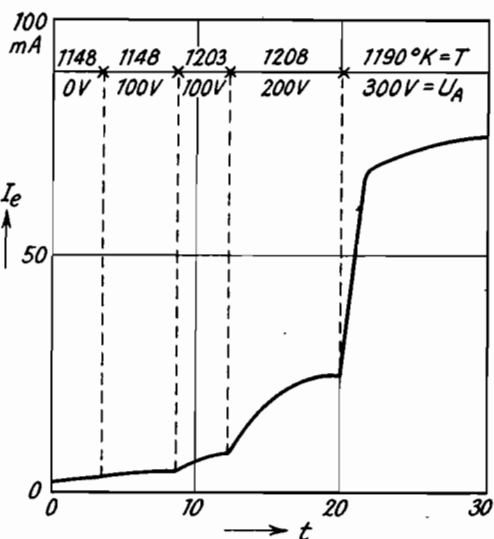


Fig. 133.—Variation of the Emission Current  $I_e$  during an Activation by Drawing Current from a Combined BaO Cathode (Espe<sup>1</sup>).

The processes occurring during activation by drawing current will be the following: At first some oxygen ions at the surface of the coating will be removed from the crystal lattice of the barium oxide. The vacancies arising at the site of oxygen ions near the surface in this way, will then be filled by oxygen ions coming from the interior and moving with the ionic current. Vacancies at the site of oxygen ions are produced in this manner in the interior of the coating. This process is repeated many times during the activation, and the number of vacancies at oxygen ion sites in the interior will therefore increase more and more until an equilibrium is reached which is controlled by the temperature of the cathode and the magnitude of the emission current or of its ionic component.

If the activation by drawing current is applied to uncombined cathodes with nickel core and normal thickness, no higher current is obtained than may be reached by an activation by reduction. This was proved by Herrmann<sup>1</sup> and Heinze and Wagener.<sup>1</sup> The latter authors also showed that the fall in emission which is observed at the beginning of the activation by drawing current (cf. Vol. I, Figs. 36 and 37) is only due to gases set free by the electron bombardment of the anode. There is no connection between this initial fall in emission and the mechanism of the oxide cathode, as was sometimes assumed by earlier investigators.

### 29.3. Activation by electron and ion bombardment

As shown for instance by Becker,<sup>1</sup> the oxide cathode can also be activated by bombarding it with electrons (cf. Sec. 19.3). If the cathode is unactivated, the electrons accumulating at the surface of the coating will induce the oxygen ions to move to the core metal. The ionic current so produced will act in the same way as that flowing during activation by drawing emission current, and the cathode will therefore be activated. This type of activation is important for the oxide coating produced on the grids of a valve by evaporation of barium oxide (cf. Vol. I, Sec. 8).

Activation of the oxide cathode by bombarding positive ions (e.g. A-ions) has been observed by Koller,<sup>1</sup> Benjamin and Rooksby,<sup>1</sup> and Herrmann and Krieg.<sup>2</sup> This phenomenon may be explained by the same process as the activation by electron bombardment. Furthermore, it is possible that small quantities of foreign material which are adsorbed or deposited at the cathode surface are removed by the sputtering effect produced by the ion bombardment, and activation may be obtained in this way.

## 30. Experimental Details of Variations in the Equilibrium of the Fully Activated Oxide Coating

We shall now return to the fully activated cathode and drop the supposition made in Sec. 20 that the oxide coating is in equilibrium and that the number of excess barium atoms is invariable with time and space. Actually the number of excess atoms may be altered by such phenomena as diffusion and ionic conduction in the coating, which will be discussed below.

A variation in the number and distribution of the excess barium atoms will produce a variation of the saturated current of the

cathode. Such a variation may, for instance, be observed if an oxide cathode is operated at a definite temperature  $T$  and a definite anode voltage  $V_A$  (possibly  $V_A=0$  for a certain time), and if either the temperature or the anode voltage is suddenly altered. In many cases the saturated current does not immediately take up the final value appropriate to the new temperature or voltage, but gradually approaches this final value during a certain time. The details of this phenomenon, which was named "time changes" by Becker<sup>1</sup> and which makes the measurement of the saturated current and of the work function difficult (cf. Sec. 21.2), will be discussed now.

### 30.1. Influence of variations in temperature

Davisson and Germer,<sup>1</sup> who examined combined [BaSr]O cathodes, observed that the emission current falls after an increase

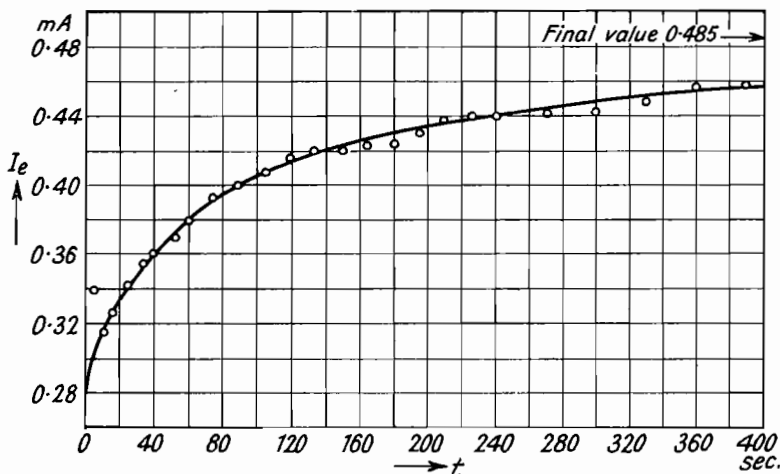


Fig. 134.—Variation of the Emission Current  $I_e$  after decreasing the Cathode Temperature (Davisson and Germer<sup>1</sup>).

in temperature, while it rises after a decrease (cf. Fig. 134). The time which elapses before the final emission value is reached increases with decreasing temperature from some seconds up to 15 minutes.

A similar phenomenon was observed by Maddock<sup>1</sup> using uncombined [BaSr]O cathodes. Contrary to Davisson and Germer, Maddock undertook a short time measurement of the emission current (measuring time = 1/100 sec.); the measured emission value was converted from the measuring temperature to a standard

temperature of  $1075^{\circ}\text{K}$ . If the cathodes were heated without applying anode voltage, the emission current, measured intermittently, fell at high temperatures and rose at low temperatures. As the emission current in these experiments only flowed during the very short measuring time, the variation in emission, as observed by Davisson and Germer and by Maddock, cannot be produced by the flow of the current alone.

### 30.2. Influence of variations in anode voltage

The influence of anode voltage was examined by Espe,<sup>1</sup> who, when heating a combined cathode without anode voltage, observed

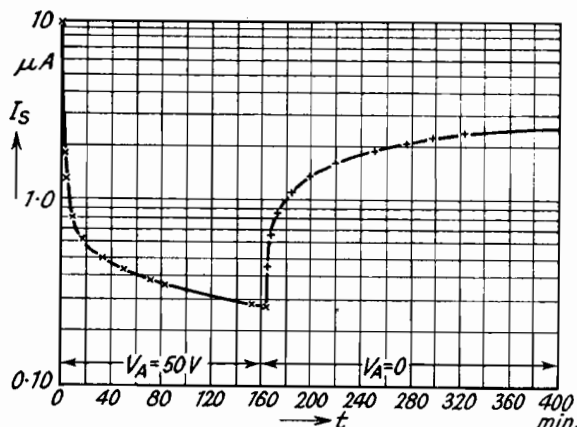


Fig. 135.—Fall and Rise of the Saturated Current  $I_s$ , when operating the Cathode with and without Anode Voltage (Becker<sup>1</sup>).

that the emission current measured after this heating was smaller than the current measured previously. This result is opposed by observations of Becker<sup>1</sup> and Becker and Sears,<sup>2</sup> who operated combined cathodes at a temperature of  $715^{\circ}\text{K}$ . and measured their saturated current at  $475^{\circ}\text{K}$ . When switching on the anode voltage the saturated current fell to a minimum reached after a certain time (left-hand side of Fig. 135), whilst the current rose again if the cathode was subsequently heated without anode voltage (right-hand side of Fig. 135).

The same result as that found by Becker was obtained by Kniepkamp and Nebel,<sup>1</sup> who also used combined cathodes, and by Blewett<sup>4</sup> with uncombined cathodes. According to Kniepkamp and Nebel the rate of the decay of emission, observed after switching

on the anode voltage, increases with increasing anode voltage. According to Blewett, however, such a dependence on anode voltage does not exist in the saturation range, while in the space-charge range a fall in anode current was observed which became more marked with increasing current. Blewett also examined the influence of cathode temperature and found that the rate of decay in emission increases with the temperature of the cathode.

According to experiments undertaken by the authors such a decay in emission, however, cannot always be observed after

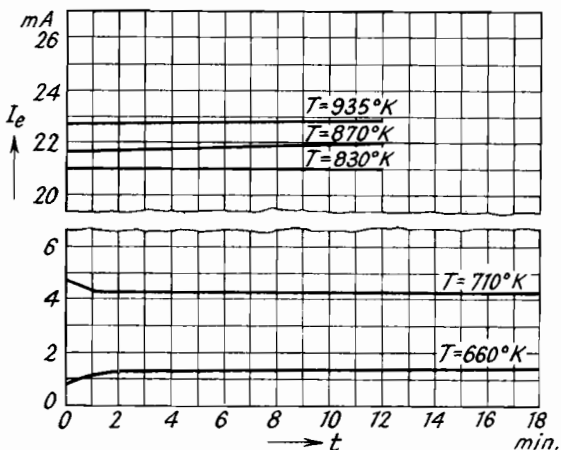


Fig. 136.—Variation of the Emission Current  $I_e$  of a well activated Cathode after switching on the Anode Voltage.

switching on the anode voltage. The triodes used in these experiments were made of materials selected and processed according to the lines given in Vol. I, Chapter 2. When these triodes were measured, a noticeable decay in emission after switching on the anode voltage could not be observed either in the saturation range (cf. Fig. 136 for  $T=660^\circ$  and  $710^\circ$  K.) or in the space-charge range ( $T=830^\circ$ – $935^\circ$  K.).

On the other hand Sproull<sup>1</sup> found that the decay in emission current may be easily reproducible. This was shown by examining short pulses of emission current which were obtained by applying to the valve concerned pulsed anode voltages of a width between 100 and 2000  $\mu$ -sec. The emission current so obtained from [BaSr]O and [BaSrCa]O cathodes was of the order of some amps. initially, but fell to between  $\frac{1}{3}$  and  $\frac{1}{5}$  of the initial value during the time of the pulse. In the time between two consecutive pulses, which was

between 0.5 and 50  $\mu$ -sec., the emission current recovered to its original value and, when the next pulse was applied, the same decay in emission was observed as previously. The time before the stable final value was reached increased with decreasing temperature and was 20  $\mu$ -sec. at 1200° K. and 500  $\mu$ -sec. at 900° K. (cf. Fig. 137).

The same phenomenon of a decay in emission current during a very short time has been described by Riethmüller,<sup>1</sup> Ptitsin,<sup>1</sup> and Danforth and Ramsay.<sup>1</sup> Riethmüller, however, points out that

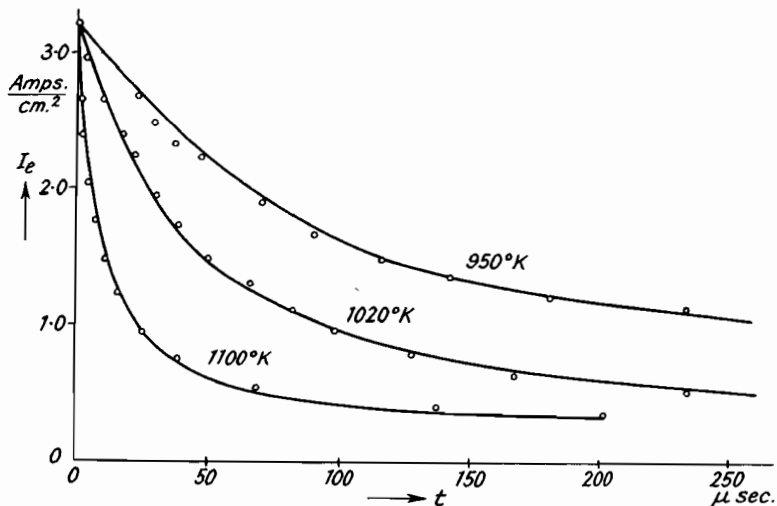


Fig. 137.—Variation of the Emission Current obtained by applying a pulsed Anode Voltage (Sproull<sup>1</sup>).

only a part of the cathodes examined by him showed this phenomenon. Wright,<sup>1</sup> who also investigated the decay phenomena, could not find a decay in emission within the pulse width of 35  $\mu$ -sec. used in his measurements. He observed such a decay when measuring the emission with D.C. voltages instead of the pulsed voltages. Due to this decay the D.C. emission values were considerably lower than the pulsed values (cf. Table XXIX).

In a further publication Wright<sup>2</sup> showed that these differences between pulsed and D.C. emission disappeared if the anodes of his experimental diodes were carefully prepared and outgassed. In one of the experimental designs used by him two anodes were employed, one of them facing the cathode as usually and the other alongside it. The first anode was used for the activation of the

cathode, while the second, which remained free from evaporation products originating from the cathode, could be used for the measurement of the emission by deflecting the electrons with a magnet. In this arrangement pulsed and D.C. emission remained equal even during longer periods.

Finally Feaster<sup>1</sup> who used 10  $\mu$ -sec. pulses, found no decay in emission provided the anodes of his experimental valves were adequately cleaned. He could produce such a decay by contaminating his anodes with small quantities of sodium chloride or sodium fluoride.

### 30.3. The processes producing the variations in equilibrium

As can be seen from the foregoing discussion the observed phenomena are partly contradictory. In order to explain these phenomena use has been made of all possible processes, such as diffusion, ionic conduction, evaporation of excess barium, destruction of the oxide coating by ion bombardment, orientation of dipoles at the cathode surface due to an electrical field, etc. Some of these explanations are closely connected with earlier ideas of the mechanism of the emission. The explanation of the time changes is made difficult by the fact that sufficient details of the experimental conditions have not always been given. Not only should the cathode temperature, the anode voltage, and the pressure in the valve be included in these details, but the composition of the materials used for the oxide coating, the core metal, and the anode must also be given (cf. Sec. 18). The definition of the state of activation of the cathode is also of importance because, as found by the authors, the observed phenomena decrease with improving activation.

If an anode material is used which is insufficiently cleaned or degassed, the emission current—after switching on the anode voltage—may fall, due to these deficiencies. The electrons, bombarding the anode, may set free gases which impair the emission of the cathode. Furthermore, thin layers of metal compounds existing on the anode surface may be decomposed by the bombarding electrons and the products of this decomposition, such as oxygen or other gases, may also produce a decrease in emission. Such a decomposition of metal oxides by bombarding electrons was observed by Wagner,<sup>1</sup> Headrick and Lederer,<sup>1</sup> and Jacobs.<sup>1</sup> The latter author examined CuO, FeO, MoO<sub>3</sub>, NiO, Ta<sub>2</sub>O<sub>5</sub>, ZrO<sub>2</sub>, and WO<sub>2</sub> and found that the dissociation occurs above a critical voltage at which the energy of the electrons is equal to the heat of formation

of the oxide concerned. The existence of such a critical voltage was confirmed by Metson,<sup>3</sup> who dissociated by electron bombardment the barium compounds formed on the control grid of commercial valves. A dissociation produced by electron bombardment was also observed with BaCl<sub>2</sub> by Hamaker, Bruining, and Aten.<sup>1</sup>

When examining the time changes it must also be remembered that the temperature of the oxide coating may either increase or decrease after switching on the anode voltage. An increase will be caused if the heating-up of the oxide coating due to its electrical resistance predominates, and a decrease if the cooling effect prevails. Finally, if the space-charge current is examined, it should be realized that this current is greatly influenced by variations in the work function of the anode and the grids. Owing to these two influences, variations in the emission current may be obtained which are not due to variations of the saturated current or of the work function of the cathode.

All these considerations show that, using the existing experimental results, it will hardly be possible to obtain a complete and clear picture of the processes producing the observed time changes. First of all it will be necessary to use our knowledge of the emission mechanism of the oxide cathode for compiling all the processes which may take part in producing the time changes and the variations of the equilibrium of the oxide coating in general. When this is done it will be possible to estimate the magnitude of the processes concerned and to compare their effectiveness.

The individual processes will be compiled and discussed by using Fig. 138. This figure gives a schematical cross section through the fully activated oxide coating showing the atoms or ions of coating and core metal, and the vacancies in the crystal lattice of the oxygen ions, producing the excess of barium atoms. One sees from the figure that the following processes must be taken into account:

A. Processes occurring at the boundaries of the oxide coating, namely:

- (1) Processes at the oxide-coating-vacuum boundary where a distinction must be made between—
  - (a) evaporation of excess Ba-atoms from the surface;
  - (b) emission of ions from the surface; and
  - (c) chemical reactions at the surface occurring between the excess barium and residual gases (poisoning of the cathode).

(2) Processes at the oxide-coating–core-metal boundary; chiefly chemical reactions with barium oxide.

B. Processes occurring in the interior of the oxide coating by which the number of vacancies and excess barium atoms in the coating is altered, namely:

- (1) Ionic conduction, and
- (2) Diffusion.

The processes quoted above will be discussed in the same sequence in the following sections. All considerations will refer to normal

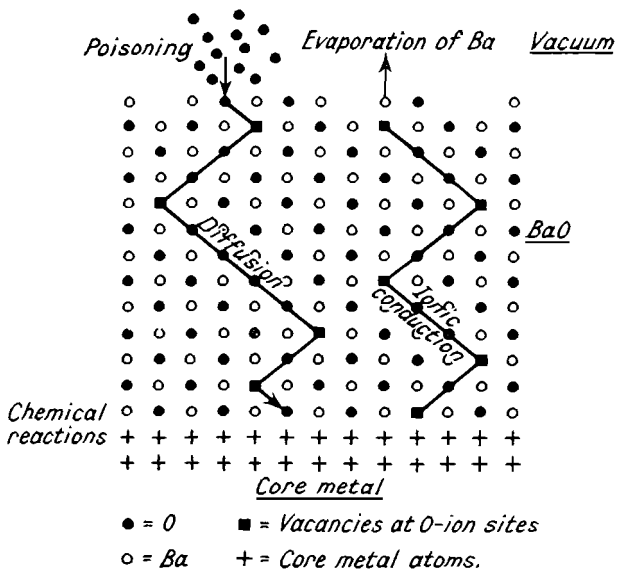


Fig. 138.—Cross Section through a fully activated Oxide Coating.

operating conditions of the cathode; phenomena produced by overloading (e.g. sputtering, cf. Vol. I, Sec. 12.3) will not be considered. For the sake of simplicity cathodes consisting of pure barium oxide will be considered, but as there are only few experiments undertaken with pure BaO, it will be necessary to use the results of experiments made with the normal [BaSr]O mixtures.

### 31. Processes at the Surface of the Oxide Coating

#### 31.1. Evaporation of excess barium

Evidence of the evaporation of excess barium from the oxide coating may be obtained from an experiment by Becker,<sup>1</sup> carried

out with combined cathodes. In this experiment, which has been described in Sec. 19.1, the excess barium was evaporated on to a tungsten ribbon, and an emission maximum of this tungsten ribbon, as shown by Fig. 84, was observed during the evaporation. The relative density of barium atoms or ions on tungsten, appropriate to the emission maximum, is  $\theta_m = 0.29$ , as given in Sec. 5.3. It may be assumed that a monatomic layer of Ba-ions on tungsten possesses the same lattice constant as the crystal lattice of metallic barium,  $d = 5.02 \text{ \AA}$ . Using this value, the number of Ba-atoms or ions which evaporate on to unit area of the tungsten ribbon until the emission maximum is reached can be estimated as:

$$S_m = \frac{\theta_m}{d^2} = \frac{0.29}{5.02^2 \times 10^{-16}} = 11.6 \times 10^{13} \frac{\text{atoms} + \text{ions}}{\text{cm.}^2}$$

From this value the total number of barium atoms evaporating per unit time and area can be calculated, using the dimensions of the valve assembly.

The values obtained in this way from Becker's measurements are at

1200° K.	1400° K.
$5 \times 10^{14}$	$6 \times 10^{16}$
0.1	14

Ba-atoms/cm.<sup>2</sup> hour       $\mu\text{g./cm.}^2$  hour

The values have been converted into  $\mu\text{g.}$  by using the conversion factor  $1 \mu\text{g.} = 4.4 \times 10^{15}$  Ba-atoms. It must be emphasized that the above values refer to combined cathodes in which there are no reducing agents supplying excess barium and making it available for evaporation. Higher values are to be expected for modern cathodes possessing such reducing agents. This has been confirmed by Kawamura<sup>1</sup> who used Becker's method and found an evaporation of  $7.5 \mu\text{g./cm.}^2$  hour at 1200° K. (for [BaSr]O).

An important point to be taken into account during such experiments is a proper discrimination between metallic barium and evaporated barium oxide which will also activate the tungsten wire to a certain extent. A chemical analysis of the metallic barium which excludes the oxide is therefore to be preferred. Such an analysis was undertaken by Jenkins and Newton,<sup>1,2</sup> who used Berdennikowa's method (cf. Sec. 19.1). The quantity of metallic barium evaporated to the anode of experimental diodes during an activation treatment of 1 hour at 1225° K. was  $4 \mu\text{g./cm.}^2$  (for a core containing 0.12 % Mg, cf. Table XXX).

The quantities quoted above for the evaporated barium cannot readily be used for an estimate of the loss of excess barium in the coating during operation. It must be borne in mind that, while barium metal evaporates from the coating, new metal may be provided by reduction. The loss of excess barium is therefore determined only by the balance between the two processes evaporation and reduction, and the investigation of the reduction process becomes of major importance in this context (cf. Sec. 32).

### 31.2. Emission of ions

Only the emission of negative ions from the surface of the oxide coating, giving detrimental effects in cathode-ray and television tubes (cf. Vol. I, Sec. 12.4), has been observed and examined so far. The design of the mass spectrometers used for these examinations may be seen from the appropriate papers (Blewett and Jones,<sup>1</sup> Bachmann and Carnahan,<sup>1</sup> Broadway and Pearce,<sup>1</sup> Schaefer and Walcher,<sup>1</sup> Sloane and Watt<sup>1</sup>). One of the main difficulties of such examinations is that ions emitted from places other than the cathode are also detected by the mass spectrometer. The ions observed can also be due to a collision between gas atoms and electrons in the space in front of the cathode or to atoms and molecules adsorbed at the cathode surface which are bombarded by ions of a different kind. The first source of error is especially to be expected in mass spectrometers operated at the pump, as the vacuum in these is normally not extremely good.

The ions emitted from the cathode which were observed by Sloane and Watt in a sealed-off spectrometer were mainly Cl<sup>-</sup>, O<sup>-</sup>, and H<sup>-</sup>. Using an electron current of about 30 mA, these authors measured the following ion currents:

$$\begin{aligned} \text{Cl}^- & 1.85 \times 10^{-11} \text{ amp.} \\ \text{O}^- & 1.5 \times 10^{-13} \text{ amp.} \\ \text{H}^- & 2.5 \times 10^{-13} \text{ amp.} \end{aligned}$$

After operating the valve for a longer time the current of the chlorine ions fell to  $2 \times 10^{-13}$  amp. and that of the oxygen ions to less than  $10^{-14}$  amp. Further ions, emitted from the cathode with less intensity, were C<sup>-</sup>, CH<sup>-</sup>, F<sup>-</sup>, CN<sup>-</sup>, O<sub>2</sub><sup>-</sup>, Br<sup>-</sup>. The absolute intensities of the ion currents cannot be derived from the intensities given above, as an unknown but essential fraction of the ions gets lost on the way from the ion source to the Faraday cage collecting the ions.

### 31.3. Poisoning of the cathode

Chemical processes on or in the oxide coating, producing an increase in work function and a decrease in emission, are called poisoning. Only poisoning reactions at the oxide-coating-vacuum boundary will be discussed in this section.

Poisoning at the boundary with the vacuum is produced by residual gases which either remain in the valve when it is sealed off, or which are given off during operation from components of the valve which were insufficiently degassed or cleaned. Such a residual gas will poison the cathode if it attacks chemically either the excess barium or the alkaline earth oxide of the coating and changes these into some other chemical compound. The poisoning phenomena to be observed will depend on the composition of the residual gas, on its pressure, on the temperature of the cathode and on the voltages applied to the valve.

The composition of the gas has been analyzed to a certain degree by Jacobs and Wolk.<sup>2</sup> The gases found as given off during the decomposition of the cathode and during degassing the electrodes were mainly H<sub>2</sub>, CO<sub>2</sub>, CO and to a smaller extent H<sub>2</sub>O, O<sub>2</sub>, and N<sub>2</sub>.

It has been pointed out in Vol. I, Sec. 12.5, that all gases are detrimental to the cathode at pressures above 10<sup>-3</sup> mm. In this case the oxide coating is destroyed by the impact of ions, either by sputtering or by an increased evaporation due to an increase in temperature. These processes are more of a mechanical nature and depend on the resistibility and the thermal properties of the coating; they are of importance only for the cathodes in gas-discharge tubes and lamps (cf. Sec. 16). It is not yet possible to draw a definite line between the conditions responsible for destruction of the oxide coating by ion bombardment and the conditions causing an activation by ion bombardment as discussed in Sec. 29.3.

If low pressures are considered ( $\leq 10^{-3}$  mm.), which are of chief interest in the case of high-vacuum cathodes, oxygen has the strongest poisoning effect, because oxygen ions may fill the vacancies at oxygen sites in the coating and may so remove the excess barium in this simple way. For this reason poisoning by oxygen will be discussed first, separately from poisoning by other gases.

(a) *Poisoning by oxygen.* The poisoning effect of oxygen has been observed by Koller,<sup>1</sup> Reimann and Murgoci,<sup>1</sup> and Benjamin and Rooksby<sup>1</sup> at pressures of about 10<sup>-3</sup> mm., but without giving quantitative values. Heinze and Wagener<sup>2</sup> pointed to an important feature by distinguishing between a transient and a permanent

poisoning by oxygen. The first type of poisoning is observed at low oxygen pressures and medium to high cathode temperatures. In this case, after removing the poisoning oxygen molecules, the emission current rises again without any special treatment being given to the cathode. The phenomenon was investigated in detail by Metson,<sup>2</sup> and Fig. 139 shows an example taken from his paper.

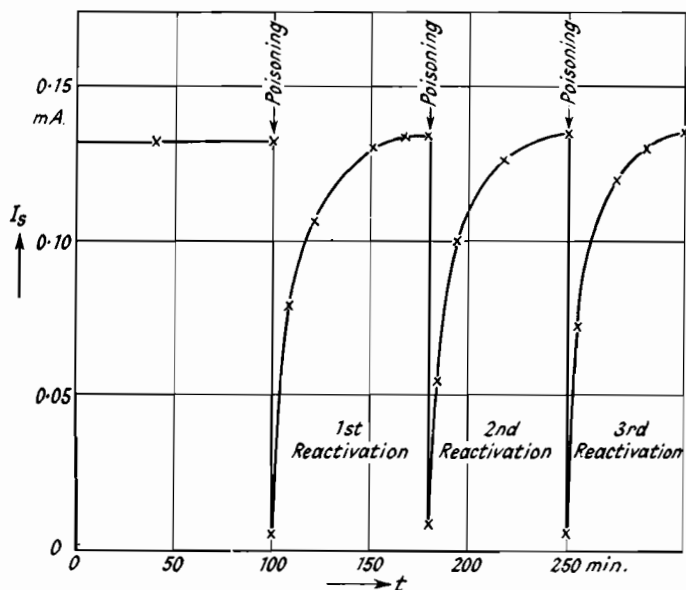


Fig. 139.—Variation of the Saturated Current during the Reactivation after Poisoning by Oxygen (Metson<sup>2</sup>).

The cathode concerned was poisoned at a temperature of  $1050^{\circ}$  K. and was left at this temperature when the evolution of oxygen producing the poisoning was stopped. The saturated current of the cathode was measured intermediately at a temperature of about  $750^{\circ}$  K. ( $V_A = 4$  volt). One sees from the figure that, after poisoning, the saturated current rises very quickly initially, then more gradually, and finally reaches the same value as measured before poisoning. The poisoning, therefore, is only transient.

If the second type of poisoning, however, is observed which occurs at higher pressures or very low temperatures, the poisoning effect remains after pumping off the oxygen. The emission current keeps the low value which was reached during the poisoning, and the poisoning is permanent. In this case the original state of the

cathode can only be restored by a new activation undertaken at higher temperatures. The explanation of these phenomena will be discussed below.

Quantitative details of oxygen poisoning were given in a paper by Herrmann and Krieg,<sup>2</sup> who examined  $[BaSr]O$  deposited in a thickness between 60 and 70  $\mu$  on nickel sleeves with 0.07% Mg. The cathodes were activated to an optimum and were then exposed to oxygen at different temperatures and pressures. The emission current was measured before and during the poisoning with an anode voltage of 10 volts. As this voltage is lower than the ionization voltage of the usual gases the observed phenomena were so confined to non-ionized gases.

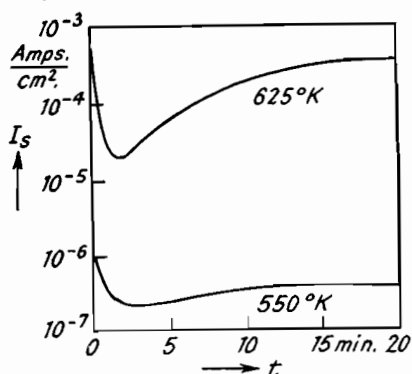


Fig. 140.—Variation of the Saturated Current during Poisoning by Oxygen (Initial Pressure  $3 \times 10^{-5}$  mm.) (Herrmann and Krieg<sup>2</sup>).

Fig. 140 shows the fall of the saturated current during poisoning measured for two different cathode temperatures ( $625^\circ$  and  $550^\circ$  K.) and with an initial pressure of  $3 \times 10^{-5}$  mm. It will be noted that the saturated current at the higher temperature, after falling for a short time, rises again considerably. The poisoning at these particular values of pres-

sure and temperature is only transient. A continuous measurement of the pressure shows that the oxygen which is initially present in the valve is consumed during the poisoning and that only a final pressure of less than  $10^{-6}$  mm. remains after 20 minutes. When sufficient oxygen has been consumed reactivation evidently occurs, and a minimum of the emission current and a subsequent rise is obtained in this way. At the lower temperature, however, neither can a decrease in pressure be detected nor an appreciable reactivation be observed.

As the consumption of oxygen by the poisoned cathode renders the observations more difficult, especially at high temperatures, the oxygen pressure in some later experiments was kept constant during poisoning, by adding further oxygen. Fig. 141 shows two poisoning curves obtained in this way for a pressure of  $1.4 \times 10^{-3}$  mm. and for two different temperatures ( $1048^\circ$  and  $1005^\circ$  K.). One sees from

this figure that the poisoning effect is increased by lowering the temperature of the cathode. If, after reaching a constant value of the emission current, the oxygen is pumped off, reactivation is observed in this case also (cf. the curve for 1005° K.).

In order to represent the numerous experimental results in a clear manner the work functions of the cathodes concerned were calculated from the saturated currents, measured after 10 minutes' exposure to oxygen (assuming  $A = A_0 = 120$ ). These work functions were associated with the appropriate temperature  $T$  of the cathode and with the pressure  $p_0$  measured when starting poisoning. They

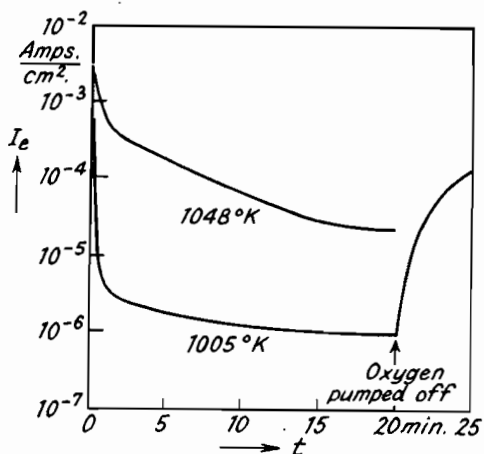


Fig. 141.—Variation of the Emission Current during Poisoning at a Constant Oxygen Pressure of  $1.4 \times 10^{-3}$  mm. (Herrmann and Krieg).

were then used for drawing lines of equal work function in a pressure-temperature diagram, as shown in Fig. 142 ( $p_0$  against  $1/T$ ). The respective curves give the values of pressure and temperature at which the poisoning effect, as measured by the work function, is of equal strength. All the lines shown refer to experiments during which the decrease in pressure produced by the poisoning was not compensated by adding oxygen. As the fall in oxygen pressure during poisoning will depend on the volume of the experimental vessel the curves of the diagram in Fig. 142, strictly speaking, are only valid for the volume of 970 cm.<sup>3</sup> used in the experiments. The values plotted in the diagram are always mean values obtained for several cathodes. The large increase of the poisoning effect with decreasing temperature is again seen from the diagram.

We now return to the phenomenon of reactivation mentioned several times before. The term reactivation in this context will only be used if the emission state of the cathode, existing before poisoning, is restored at or below the operating temperature of the cathode. Activation obtained by increasing the cathode temperature above the operating temperature will be called new activation.

As pointed out above, reactivation occurs more rapidly and efficiently, the higher the cathode temperature and the lower the

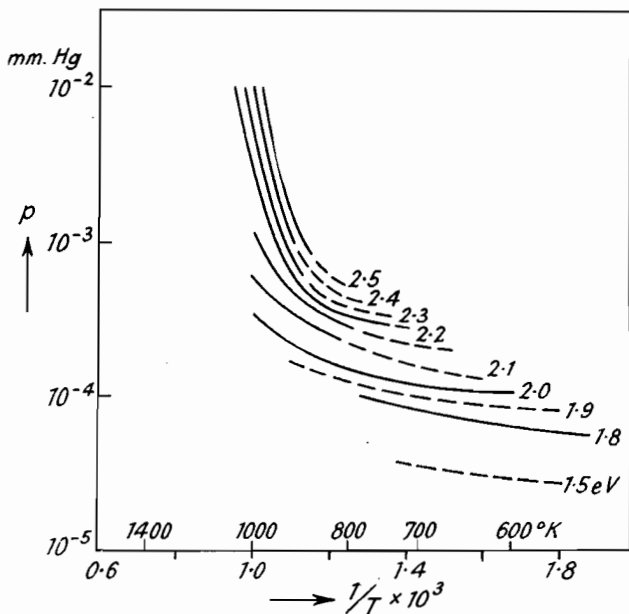


Fig. 142.—Pressure-Temperature Diagram showing Curves of Equal Work Function for Poisoning by Oxygen after 10 Minutes Exposure (Herrmann and Krieg).

oxygen pressure during the preceding poisoning. Quantitative values for the dependence on temperature, pressure, and time, however, have not been given yet. Poisoning and reactivation may be repeated many times under suitable conditions (cf. Fig. 139).

For explaining reactivation, the mechanism of oxygen poisoning must be discussed in more detail. The poisoning effect of oxygen will be due to oxygen ions which are first adsorbed at the surface of the oxide coating. The work function of the coating will be increased by such an adsorption in the same way as the work function of metals (cf. Sec. 5.5). If the reactivation, represented by the curve for  $T=1005^{\circ}\text{K}$ . in Fig. 141, is considered again, the

quantity of oxygen taken up by the oxide coating during the preceding poisoning may be estimated from the data given by the investigators. The initial oxygen pressure of  $1.4 \times 10^{-3}$  mm. was reduced during poisoning by more than one power of ten, until new oxygen was introduced. Using these values and the known volume of the experimental vessel ( $970 \text{ cm.}^3$ ), the quantity of oxygen taken up is calculated as  $1.4 \times 10^{-3} \times 6 \times 10^{23} \times 0.97/22.4 \times 760 = 5 \times 10^{16}$  molecules or  $10^{17}$  atoms. This number may be compared with the total number of vacancies which are at the sites of oxygen ions in the coating. For a coating weight of  $5 \text{ mg./cm.}^2$  the latter number is  $0.005 n_o/\delta$  which is about  $10^{16}$ .

It follows from this that the number of poisoning oxygen atoms which are taken up by an oxide coating during a transient poisoning may be larger than the number of vacancies and of excess Ba-atoms in the coating. Bearing in mind this and the fact that reactivation can be repeated many times, two conclusions can be drawn. Firstly, reactivation cannot be explained by assuming that all the poisoning oxygen ions are permanently bound by a certain fraction of the excess barium atoms or by a barium supply near the core of the cathode. Secondly, it will be necessary to conclude that some of the poisoning ions move into the vacancies of the coating and occupy these.

The activated oxide coating, which has a given number of vacancies, thus shows a considerable stability against exposure to oxygen, provided the temperature exceeds a certain value. This stable activated state may be disturbed by oxygen molecules impinging upon the coating surface, a certain number of vacancies then being occupied by additional oxygen ions. If, however, the oxygen pressure has not been too high and the oxygen atmosphere is removed, the additional oxygen ions leave the oxide coating, and a state of the coating similar to the original one is reached again.

The fact that the additional oxygen ions easily leave the vacancies occupied by them can be explained in a simple way by assuming that these additional ions are somehow different from the oxygen ions forming the normal crystal lattice. Such a difference may be due to the fact that two types of negative oxygen ions are known, the doubly charged ion  $O^{--}$  and the singly charged  $O^-$ . The  $O^{--}$  ion is only stable when a constituent of a crystal lattice, while it is unstable when free. It dissociates into an oxygen atom and two electrons by giving off energy, which means its electron affinity is negative ( $\xi_{O^{--}}^* = -7.3 \text{ eV}$ ). The singly charged  $O^-$  ion, however,

is always stable, as energy must be supplied for its dissociation into the atom; its electron affinity is positive ( $\xi_{O_2}^* = +3.8$  eV). Assuming that some of the oxygen molecules impinging upon the cathode are transformed into  $O^-$  ions, these  $O^-$  ions may occupy the vacancies of the BaO lattice and may increase the work function of the cathode in this way. A subsequent conversion of these  $O^-$  ions into  $O^{--}$  ions is not very likely, as a considerable energy of  $7.3 + 3.8 = 11.1$  eV will be necessary for this. When the exposure to oxygen is stopped, the  $O^-$  ions, being foreign to the BaO lattice, will leave the vacancies and will return to the vacuum. The fact that a poisoned cathode may be reactivated so easily could be explained in this way.

If the energy balance for the formation of  $O^-$  ions from oxygen molecules at the surface of the oxide coating is considered, it will be seen that such a formation is certainly possible. The energies necessary for this formation are the dissociation energy of the oxygen molecule (5.1 eV) and the energy needed for the emission from the oxide coating of the two electrons necessary for forming the two  $O^-$  ions (work function). A total energy of  $5.1 + 2 \times 1.4 = 7.9$  eV is therefore required. On the other hand, twice the electron affinity of  $O^-$  and twice the adsorption energy  $\Phi_{O^-}$  of the  $O^-$  ions is gained, in all an energy of  $7.6 + 2\Phi_{O^-}$  eV. The adsorption energy can be calculated from equation (72). This energy would amount to 1.8 eV for a distance  $z_i = 2$  Å, but as this distance is certainly too large, the actual adsorption energy will be still higher. One sees from this that the energy which is gained is certainly larger than the energy which is needed during the formation of  $O^-$  ions from  $O_2$  molecules. Such a formation is therefore possible. On the other hand, the formation of  $O^{--}$  ions is unlikely, as a large energy must be supplied on account of the high negative electron affinity of  $O^{--}$ .

The conclusion that  $O^-$  ions are formed at the surface of the oxide cathode is confirmed by the investigations with mass spectrometers quoted under point 2 of this section. Furthermore, Arnot,<sup>1, 2</sup> showed, also by means of a mass spectrometer, that  $O^-$  ions may be formed from oxygen molecules which are positively ionized. These latter experiments were not undertaken with an oxide cathode, but with a metal cathode.

If the oxygen poisoning is more extensive, the poisoning ions may move from the vacancies near the surface to those in the interior of the coating. Consequently the diffusion of oxygen ions from the surface into the interior will then play an important part, but this phenomenon will be discussed later (Sec. 33.2).

Considering the above results, one might assume that poisoning by oxygen is exclusively transient at the pressures normally existing and that the cathode therefore will never be impaired permanently. Such a conclusion, however, would be premature, especially if cathodes are considered which are operated with higher anode voltages and which are therefore exposed to ionized oxygen molecules, e.g.  $O_2^+$ . Such ionized molecules have an ionization voltage of approximately 12 eV which would be set free during a conversion into negative oxygen ions and which could therefore be used for producing an  $O^{--}$  ion. Even if the number of  $O^{--}$  ions produced

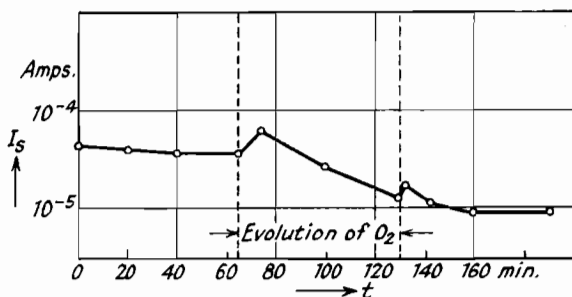


Fig. 143.—Variation of the Saturated Current of an Oxide Cathode when setting free Small Quantities of Oxygen from a Second Cathode with Iron Core (Liebold<sup>1</sup>).

in this manner were small, it could nevertheless have a noticeable effect on the emission of the cathode over long periods (permanent poisoning, cf. Sec. 34).

Finally a phenomenon may be mentioned which is observed when an oxide cathode is exposed to very low oxygen pressure at low temperatures. As measured by Liebold<sup>1</sup> and by the authors the emission current then rises at first. The current reaches a maximum which is between 20% and 100% higher than the initial value, and subsequently falls as with normal poisoning. Fig. 143 shows an example of this. For explaining the initial rise in emission it may be assumed that during this time a favourable arrangement of oxygen and barium ions, producing an especially small work function, is established at the surface. The phenomenon may be analogous to similar observations made with W-Cs and W-Ba cathodes (cf. Sec. 5.6).

(b) *Poisoning by other gases.* The poisoning by carbon dioxide, carbon monoxide, and by some hydrocarbons was also examined by Herrmann and Krieg<sup>2</sup> by the same method as described above for

oxygen. The results obtained for  $\text{CO}_2$  and CO are plotted in Figs. 144 and 145, in the same way as for oxygen in Fig. 142, by curves representing a poisoning effect of equal strength. While the poisoning effect of oxygen (Fig. 142) increases continuously with decreasing temperature, the poisoning effect of  $\text{CO}_2$  and CO is

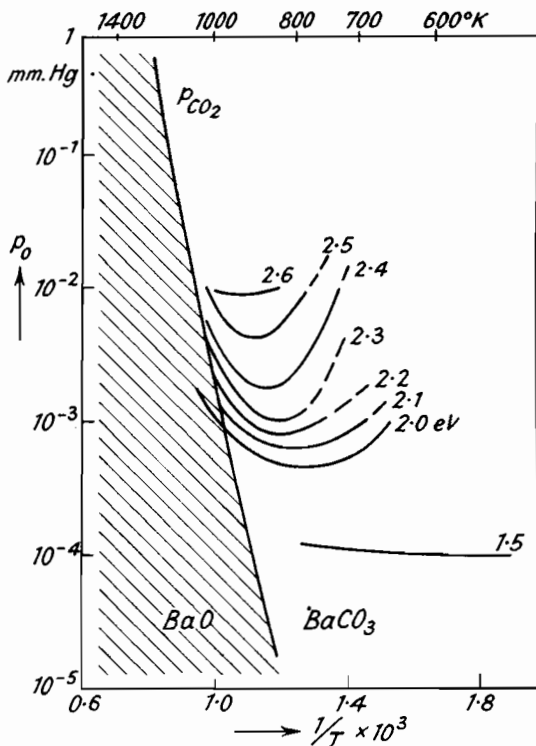


Fig. 144.—Pressure-Temperature Diagram showing Curves of Equal Work Function for Poisoning by Carbon Dioxide after 10 Minutes Exposure. The Dashed Line represents the Dissociation Pressure of  $\text{BaCO}_3$  (Herrmann and Krieg<sup>2)</sup>.

strongest at a certain temperature and decreases towards both low and high temperatures. The equilibrium curves representing the pressures and temperatures at which  $\text{CO}_2$  or CO are in equilibrium with BaO are also plotted in the respective figures. One sees from Fig. 145 that the poisoning by CO preferably occurs in the region on the right-hand side of the equilibrium curve in which a reaction between CO and BaO, forming  $\text{BaCO}_3$ , is possible. The poisoning effect of CO is therefore explained by the formation of barium

carbonate. If  $\text{CO}_2$ , however, is considered (Fig. 144) poisoning is also observed on the left-hand side of the equilibrium curve. This was explained by a direct reaction between the carbon dioxide and the excess barium metal.

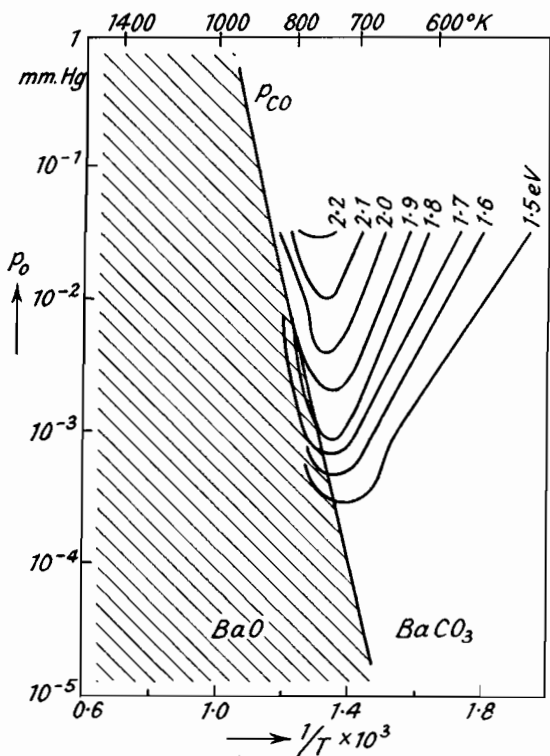


Fig. 145.—Pressure-Temperature Diagram showing Curves of Equal Work Function for Poisoning by Carbon Monoxide after 10 Minutes Exposure. The Dashed Line represents the Equilibrium between  $\text{BaO}$  and  $\text{CO}$  (Herrmann and Krieg<sup>2</sup>).

Of the hydrocarbons, methane, propane, and benzene were examined. The result is seen from the plot in Fig. 146 showing curves of equal poisoning for a work function of 2.0 eV. The curves for the gases discussed before have also been plotted in this figure for comparison. Furthermore, a second curve for oxygen is given referring to the experiments undertaken with a constant oxygen pressure during poisoning.

Herrmann and Krieg found that the poisoning effect of the hydrocarbons increases in the same sequence and shows the same

dependence on temperature as the tendency of these gases to dissociate as calculated by thermodynamical methods. It was observed that, when poisoning an oxide cathode with such hydrocarbons, the gas pressure in the experimental vessel always

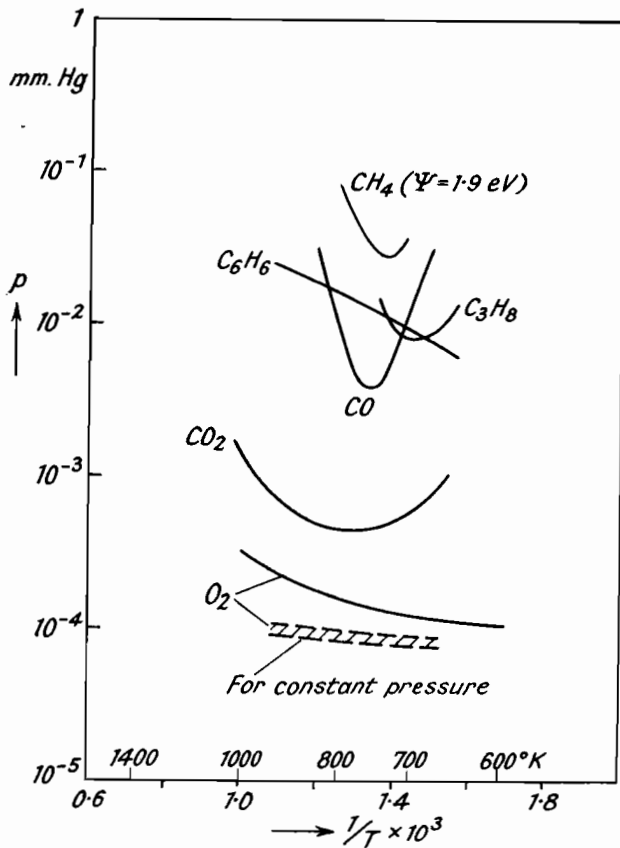


Fig. 146.—Pressure-Temperature Diagram showing Curves of Equal Work Function ( $\Psi=2.0\text{ eV}$ ) for Poisoning by Different Gases after 10 Minutes Exposure. The Dashed Curves refer to Poisoning by Oxygen with Constant Pressure. (Herrmann and Krieg<sup>2</sup>).

increases. From this it was concluded that the poisoning is produced by a dissociation of the hydrocarbons occurring at the surface of the cathode and by the carbon deposited there during such a dissociation. The poisoning due to methane and carbon monoxide is only observed under the pressure and temperature conditions seen from Fig. 146. There is no contradiction between this poisoning

effect and the activating effect of the respective gases which is observed at much higher temperatures (cf. Sec. 29.1).

The variation of the gas pressure during poisoning was measured not only for the hydrocarbons but also for the other gases examined. As seen from Fig. 147, the behaviour of individual gases is completely different. While with oxygen, for instance, the pressure

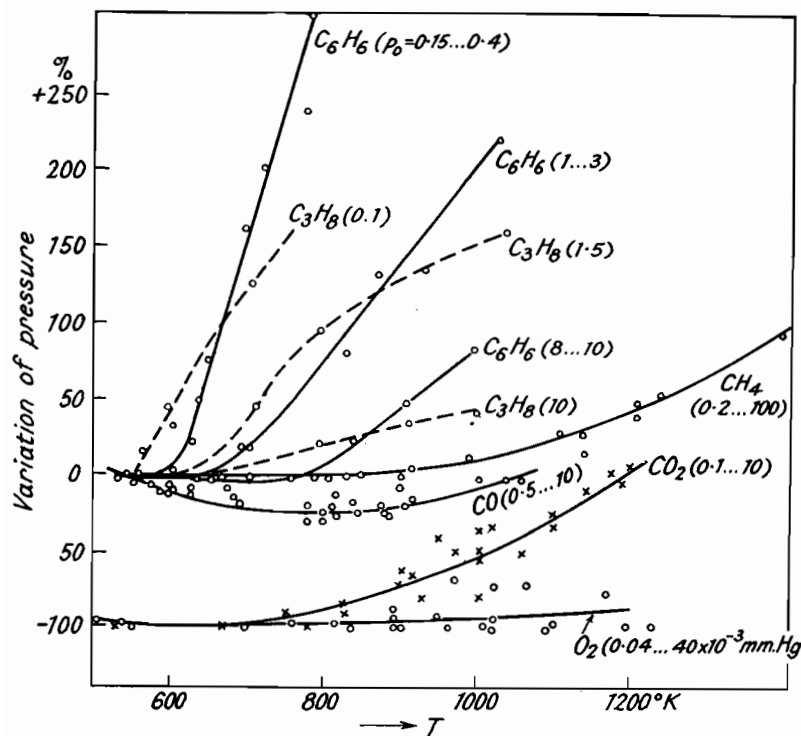


Fig. 147.—Variation of Gas Pressure during 10 Minutes Poisoning of an Oxide Cathode by Different Gases as a Function of the Temperature of the Cathode (Herrmann and Krieg<sup>2</sup>).

always decreases by nearly 100% for all temperatures, the variation of pressure is temperature-dependent with carbon monoxide and carbon dioxide. An analysis of the observed variations of pressure confirms that the poisoning is caused by the reactions mentioned above and that mere adsorption processes only play an inferior part in the poisoning phenomena.

Finally, Herrmann and Krieg studied the question whether the poisoning effect of the gases examined may be increased by

ionization. Carbon dioxide and methane were examined (with  $V_A = 50$  volt); an increased poisoning effect due to ionization could only be found with  $\text{CH}_4$ .

Other gases examined are water vapour, which poisons as much as oxygen according to Koller<sup>1</sup> and Jacobs and Wolk,<sup>2</sup> and chlorine, the poisoning effect of which was observed by Hamaker, Bruining, and Aten.<sup>1</sup> The latter authors found that chlorine poisoning can be produced by hydrochloric acid given off from the glass walls of the valve.

The influence of sulphurous gases on the emission has been examined by the authors. It was found that the emission of cathodes which are exposed to gases such as  $\text{SO}_2$ ,  $\text{SO}_3$ ,  $\text{H}_2\text{S}$  during storing, deteriorates. Due to the effect of these gases a deleterious surface layer of barium sulphide ( $\text{BaS}$ ) is formed which could be detected by Huber and Wagener<sup>2</sup> by means of electron diffraction. The most effective of the above gases is  $\text{SO}_3$  which showed a strong detrimental effect on the emission, while the results obtained with the other gases were not reproducible. They depended on humidity and temperature in a way not yet sufficiently investigated. Some of the experimental results have been described in a paper by Stahl.<sup>1</sup>

Rare gases (He, Ar, Kr) and hydrogen do not produce poisoning according to Koller and to Herrmann and Krieg. If these gases are ionized by applying an anode voltage of 100 volt and drawing a current between 10 and 20 mA/cm.<sup>2</sup>, no decrease in emission is observed during several hundred hours of operation, although a large part of the oxide coating is sputtered away during this time. One sees from this again that the surface area has not such an overriding importance for emission from the oxide cathode as it has for atomic-film cathodes.

## 32. Processes at the Interface between Oxide Coating and Core Metal

Early workers were of the opinion that the core material had no influence on the emission. This was based on the experiments of Deininger,<sup>1</sup> who examined the emission of various core metals coated with CaO. He found no difference in emission, but his result may be due to the poor state of vacuum technique at that time, pressures of about  $10^{-3}$  mm. being used. The first indication that the core metal does influence the emission was obtained from the experiments of Beese<sup>1</sup> and Lowry.<sup>1</sup> The former examined

[BaSr]O coatings on a nickel core to which 0·15% barium was alloyed. He found that these cathodes had a better life than those made with a pure nickel core. Lowry observed that [BaSr]O cathodes with a konel core (cf. Vol. I, Table II) gave a considerably higher emission current than those with a platinum-iridium core if the two types of cathodes were processed in exactly the same way. Lowry's results are plotted in Fig. 148, showing the emission current as a function of cathode temperature for different anode voltages.

Further proof for the influence of the core material on emission was given by Benjamin,<sup>2</sup> when investigating the activation by reduction discussed in Sec. 29. He found that his reducing additions (Al, Mg, Ti, Th) not only speeded up the activation, but also

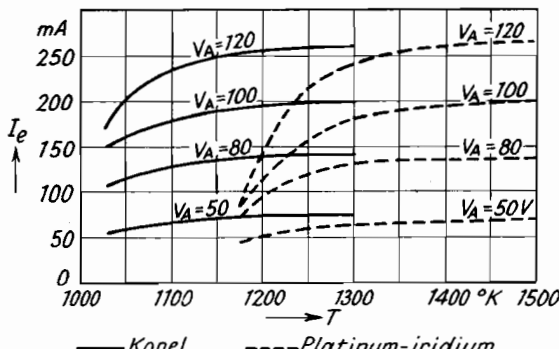


Fig. 148.—Emission Current of Oxide Cathodes with Platinum-Iridium Core or with Konel Core as a Function of Temperature (Lowry<sup>1</sup>).

influenced the final value of the emission reached during the activation. The cathodes containing reducing additions in the core metal always gave higher emission currents than those with a pure nickel core, even after an additional activation by drawing current.

Liebold<sup>1</sup> investigated eleven different metals as core of an oxide coating consisting of a commercial mixture of the three main alkaline earth oxides. The coatings concerned were first activated by reduction at the optimum activation temperature previously determined (cf. Vol. I, Sec. 8). Subsequently activation by drawing current was carried out at a slightly lower temperature in order to ensure that the maximum possible emission current was obtained with every core metal. After activation the saturated current of the cathodes was determined for a range of temperatures in which the current density was between  $1 \times 10^{-5}$  and  $3 \times 10^{-4}$  amp./cm.<sup>2</sup>.

The total work functions of the cathodes were then calculated from the saturated currents extrapolated to zero field by using emission equation (177). It may be questioned if such a calculation is justified without checking the results by means of measurements of the work function by the contact potential method (cf. Sec. 25). But the values calculated will nevertheless give an idea of the influence of the core metal on the emission, and they will therefore be quoted here as given by the investigator (cf. Table XXVIII).

The considerable differences between the work functions calculated for the different types of cathodes may be due to the fact

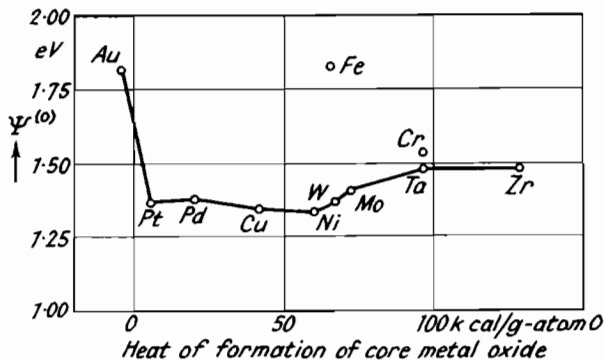
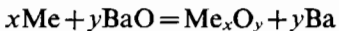


Fig. 149.—Relation between Work Function  $\Psi^{(0)}$  and Heat of Formation of the Core Metal Oxide, for Cathodes with Different Core Metals (Liebold<sup>1</sup>) (the Work Functions shown are calculated from the Emission Equation).

that the reduction at the interface is different and hence produces different quantities of excess barium. The reduction of BaO occurs according to the chemical equation:



The rate of reduction and therefore the quantity of excess barium produced is mainly determined by the heat of formation of the core metal oxide. Consequently there may be a relation between the heat of formation of the core metal oxide on the one hand and the emission current or the work function on the other. In order to check this relation Liebold tried to analyse the oxides formed during the reduction by microscope and chemical examination. The oxides which are assumed to be formed are given in Table XXVIII, together with their heats of formation.

A plot of the calculated values of the work function as a function of the heats of formation is shown in Fig. 149. The left-hand side

of this plot, up to nickel as core metal, shows the expected dependence; the work function in this region decreases with increasing heat of formation. This may be explained by the increasing amount of excess barium due to the increasing heat of formation. Beyond nickel, however, the plot runs quite contrary to expectations; the work function increases in spite of the further increase in the heat of formation. Apart from this, the values measured for chromium and especially for iron do not fit at all into the curve defined by the other values.

In this region, as pointed out by Liebold, the reducing action of the core metal is inhibited by the formation of core metal oxides. These oxides are stable if both their vapour pressures and their dissociation pressures are smaller than the oxygen pressure of the order of  $10^{-6}$  mm. normally existing in the valves. If the vapour pressure, however, is higher than this value, the core metal oxide will evaporate soon after its formation, while if the dissociation pressure is too high, it will dissociate and produce oxygen. The evaporation can be neglected, as it could not be observed with any of the core metal oxides concerned. The quantity of the core metal oxide produced therefore depends on the heat of formation of this oxide and on the dissociation pressure, the value of which has also been given in Table XXVIII. The larger the heat of formation

TABLE XXVIII

*Work Functions of Oxide Cathodes with Different Core Metals; Heat of Formation and Dissociation Pressure of the Core Metal Oxides (Liebold<sup>1</sup>)*

(The work functions quoted are calculated from the emission equation.)

Core metal	Work function (eV)	Metal oxide assumed to be formed during the reduction of BaO	Heat of formation of this oxide (k. cal./g.-atom O)	Dissociation pressure at 1225° K. (mm. Hg)
Au	1.81	Au <sub>2</sub> O <sub>3</sub>	-4.1	>760
Pt	1.37	PtO	5 *	>760
Pd	1.37	PdO	20.4	>200
Cu	1.34	Cu <sub>2</sub> O	41	$3 \times 10^{-4}$
Ni	1.32	NiO	58.4	$3 \times 10^{-6}$
Fe	1.83	Fe <sub>2</sub> O <sub>3</sub>	65.1	$8 \times 10^{-5}$ – $3 \times 10^{-3}$
W	1.36	WO <sub>2</sub>	65.7	$10^{-11}$
Mo	1.40	MoO <sub>2</sub>	71.4	†
Cr	1.54	Cr <sub>2</sub> O <sub>3</sub>	96.3	$<10^{-19}$
Ta	1.48	Ta <sub>2</sub> O <sub>5</sub>	97	†
Zr	1.48	ZrO <sub>2</sub>	129	†

\* Estimated.

† A dissociation could not be observed with these oxides after heating them in high vacuum for some days.

compared with the dissociation pressure the more core metal oxide can be formed and the more readily can an interface layer consisting of the oxide concerned be produced between the coating and the core metal.

As will be seen from Table XXVIII, the dissociation pressures of the core metal oxides up to nickel oxide are larger than the pressure limit of  $10^{-6}$  mm., and consequently these oxides cannot be stable. Corresponding with this, no interface layer produced by the oxides could be found for the cathodes made with the respective core metals. The oxides concerned dissociate completely, as their heat of formation is too small compared with the high dissociation pressure. Consequently these metals can act as reducing agents without detriment, and the work function therefore will decrease with increasing heat of formation.

The phenomena observed with tungsten and the core metals plotted on the right-hand side of this metal are quite different. The heats of formation of the oxides of these metals are large, while their dissociation pressures are very small. Consequently the core metal oxides between oxide coating and core metal can be produced without difficulty and in a quantity that increases with increasing heat of formation of the metal oxide. The chemical and microscopical examination carried out by Liebold showed that the oxides concerned react with the alkaline earth oxide and form interface layers of alkaline earth tungstates, molybdates, chromites, and similar compounds. As found by Rooksby and Stewart<sup>2</sup> by means of X-ray patterns, the interface layer in cathodes with tungsten cores consists of  $M_3WO_6$  where M stands for any one of the alkaline earth metals. These interface layers, when growing between the boundary of the oxide coating and the core metal, make a reduction of the barium oxide to excess barium more and more difficult. Furthermore, the excess barium is directly bound by the core metal oxide and the work function therefore increases as the interface layer gets thicker, i.e. with increasing heat of formation of the core metal oxide. This is in agreement with the experimental results.

In this manner the observed relationship between work function and core metal can be explained by the two processes reduction and formation of interface layers acting against one another. The deviation of the values measured for the cathodes with iron cores which is seen from Fig. 149, was also explained by Liebold. The interface layer of these cathodes, consisting of alkaline earth

ferrites, dissociates and gives off an especially large quantity of oxygen which could be measured. This large quantity of oxygen cannot immediately be absorbed by the getter of the valve, and therefore the oxide coating is heavily poisoned and the work function considerably increased in agreement with Fig. 149.

In addition to the two main influences discussed above, namely reduction and formation of interface layers, there exist some secondary influences, for instance the formation of an alloy between gold and barium, explaining the high work function of the cathodes with gold core. The detrimental effect of gold as a core metal has been confirmed by Rothstein.<sup>1</sup>

The especially favourable effect of nickel as a core metal, as seen from Fig. 149, can be explained in the following way. The heat of formation of nickel oxide (58.4 k.cal./g.-atom O) has the proper value for ensuring a sufficient reduction of the barium oxide to excess barium without producing a noticeable interface layer at the dissociation pressure of nickel oxide ( $3 \times 10^{-6}$  mm.). On the other hand, the heat of formation and dissociation pressure are such that the oxygen produced by the dissociation of the nickel oxide may be absorbed by the getter of the valve without poisoning the oxide coating. Another factor in favour of nickel as a core metal—as opposed to platinum, for example—is its low solubility for the excess barium of the coating.

The reduction occurring at the core metal–oxide coating boundary is best utilized by following the example of Benjamin<sup>2</sup> and adding small quantities of reducing metals to nickel. The added percentage can then be chosen in such a way that the thickness of the interface layer is kept below an admissible value. Such cathodes with additions to the core metal were examined in detail by Wright.<sup>2</sup> The result of this investigation obtained for [BaSr]O coatings of 10 mg./cm.<sup>2</sup> weight has been compiled in Table XXIX.

The second and third column of this table give for the cathodes concerned the saturated currents which were determined by both a D.C. and a pulsed measurement. It is seen that additions of Mg, Al, and Ti increase the direct emission current, provided the percentage of the addition is not too high. The pulsed values, however, are only increased by an addition of Ti under certain conditions which are not exactly known. The reason for the different behaviour of D.C. and pulsed values will be discussed below. The fact that the D.C. values are always considerably lower than the pulsed values is due to the decay phenomena discussed in Sec. 30.

TABLE XXIX

*Properties of Cathodes, containing additions in the Core Metal (Wright<sup>2</sup>)*

Core Material	I <sub>s</sub> at 1015° K.		Interface layer		Heat of formation of the oxide formed during reduction
	D.C. measurement	Pulsed measurement	Composition	Thickness	
Pure Ni	A/cm. <sup>2</sup>	A/cm. <sup>2</sup>	—	μ	k.cal./g.-atom O
"Grade A" Ni (0.12% Mg).	0.3	8	MgO, Ba <sub>2</sub> SiO <sub>4</sub>	—	58.4
Ni+0.1% Al	0.9	6	BaAl <sub>2</sub> O <sub>4</sub>	1	146*
Ni+0.4% Al	0.6	7	BaAl <sub>2</sub> O <sub>4</sub>	0.5	127
Ni+0.25% Ti	0.2	0.5	Ba <sub>2</sub> TiO <sub>4</sub>	5	127
Ni+0.4% Si	0.3-3.0	6-12	Ba <sub>2</sub> SiO <sub>4</sub>	10	109
Pure Pt	0.07	1.5	Ba <sub>2</sub> SiO <sub>4</sub>	10	102
	0.2	1	Barium platinate.	up to 10	5

\* f. MgO

Columns four and five of the table give the composition of the interface layers according to X-ray examinations by Rooksby,<sup>1,3</sup> and the thickness of these interface layers. A comparison between the two cathodes with different additions of Al definitely shows the detrimental influence of the formation of strong interface layers. A further measurement of the thickness of interface layers was undertaken by Eisenstein.<sup>1</sup> He investigated cathodes with a nickel core containing 5% Si and found by means of X-ray patterns that the thickness of the interface layer obtained was between 5 and 10 μ.

The details of the process of reduction at the boundary between core and coating need further study. Direct examinations of the reactions in question have been undertaken by Schrieh<sup>1</sup> and Blewett.<sup>3</sup> Schrieh found that BaO is reduced to metallic barium by the metals Al, Ce, Cr, Si, Th, Ti, Zr at temperatures between 1000° and 1600° K. while Blewett observed that Ti and Th have the greatest reducing effect. However, it must be borne in mind that the conditions existing in the oxide cathode are different from those with normal chemical reactions, because the BaO of the oxide coating is not intermixed with the reducing metal. On the contrary, the reaction between BaO and the reducing metal only takes place at the boundary between coating and core. Another difference arises from the

fact that the reactions occurring in the oxide cathode have not given a 100% yield. A very small quantity of metal produced by the reduction (0.1% or less) will be adequate for obtaining a full activated oxide coating.

An experimental investigation of the reduction process, under the conditions actually existing in the coating, has been undertaken by Jenkins and Newton.<sup>1,2</sup> They examined different oxide cathode in diodes and determined chemically the quantity of metallic barium which evaporated on the anode of these diodes during the activation of the cathodes (for the method of analysis see Sec 19.1). Table XXX gives the measured quantities of evaporated barium together with the emission currents of the cathodes concerned. The heat of formation of the oxide of the reducing component which is effective in the respective core metals has also been given. It is seen that the quantity of evaporated barium increases with the reducing effect of the core metal and with the emission current produced. This result shows again that a higher reductior by the core metal makes the cathode more emissive by producing larger quantities of metallic barium.

TABLE XXX

*Quantity of Metallic Barium evaporated from Cathodes with different Core Metal (Jenkins and Newton)*

Core metal	Pt	Pure Ni	Ni+0.2% Si	Ni+0.12% Mg
Heat of formation of the oxide formed during reduction.	5	58.4	102	146 k.cal/g.-atom O
Barium evaporated I, at $T=825^\circ\text{K}$ .	0.62 0.2	1.03 0.3	1.64 4.7	3.4 $\mu\text{g.}$ 7.3 mA

The theory of the reduction at the interface coating-core metal is not very much advanced yet. Kroll<sup>1</sup> pointed out that the existence of secondary reactions must be taken into account. When examining the reduction of CaO by Al he found that not only the metal Ca but also a metallic compound CaAl<sub>3</sub> is formed during this process. Furthermore the heats of formation which were calculated for standard conditions (see Tables XXVIII, XXIX and XXX) are not an accurate measure of the rate of reduction occurring at the interface. Instead of employing these heats of formation, the variation of the free energy computed for the reactions concerned and for the temperatures actually existing, should

be used. The exact values of most of the free energies required are not sufficiently known as yet, but an approximate computation for some of the reactions in question has recently been undertaken by White.<sup>1</sup> If the variation of the free energy is known, the equilibrium constant of the reaction concerned and the pressure of the barium vapour produced by the reaction can be computed, using the known thermodynamical methods. The amount of excess barium produced by different reactions can be compared in this way. The above-mentioned calculations by White, for instance, show that magnesium is a most powerful reducing agent for obtaining the excess barium.

Concluding this section the interface layers which are formed during the reduction process will be considered in more detail, because these interface layers are important for various phenomena observed. The interface layers do not only impair the emissivity of the cathode as pointed out above; they are also detrimental because their electrical resistance can be much higher than that of the actual oxide coating. This was shown by Fineman and Eisenstein<sup>1</sup> who examined cathodes the core metal of which contained 5% silicon or was plated with chromium. They measured the electrical resistance of the interface layers of these cathodes by means of a probe wire embedded in the layer and found that this resistance was 10 times higher than the resistance of the oxide coating itself. These measurements were refined by Eisenstein<sup>6</sup> who measured the conductivity of  $\text{Ba}_2\text{SiO}_4$  layers which were deposited on ceramic rods (cf. p 194). The resistance of such layers was 10 times higher than that of an activated oxide coating at  $1250^\circ \text{ K}$ . and 10,000 times higher at  $1000^\circ \text{ K}$ . If a cathode with such an interface layer has to supply a high emission current, a considerable voltage drop will arise across the layer.

Furthermore, it must be taken into account that the core-metal-interface-layer-oxide-coating system acts like a rectifier. Such rectifiers, consisting of a metal, a semi-conductor, and a layer of high resistance in between (blocking layer), were discussed theoretically by Mott.<sup>1</sup> He showed that the electrons in such a system preferably pass in the direction from semi-conductor to metal. Mutter<sup>1</sup> showed that the same applies to oxide cathodes having an interface layer. He used cathodes the core metal of which contained 5% Si and measured the resistance of both the interface layer and the coating by means of embedded probe wires (cf.

Sec. 22). The volt-amp. characteristics obtained in these measurements are shown in Fig. 150. While the coating gives the linear characteristic of an Ohmic resistor, the characteristic of the interface layer is asymmetric and curved as it is typical for a rectifier. The resistance for electrons passing from the core across the interface to the coating (positive voltages in Fig. 150) is 3 to 5 times higher than for electrons passing in the opposite direction.

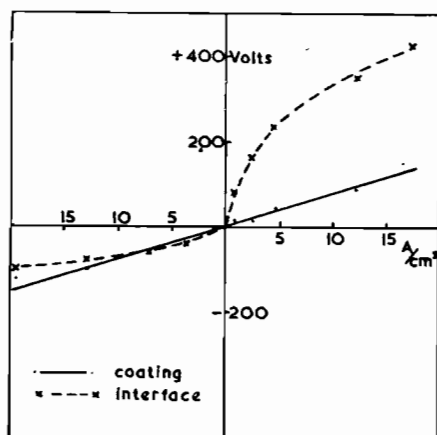


Fig. 150.—Voltage-current characteristic of a  $[BaSr]O$  coating on  $Ni + 5\%$  Si-core metal, and of the interface layer between coating and core ( $T=1135^\circ K$ , curves obtained by 5  $\mu$  sec. pulses) (Mutter<sup>1</sup>).

As the blocking layer at the core-metal-coating boundary renders the passage of electrons from core metal to coating more difficult, the drawing of high emission currents may be greatly inhibited by this layer (cf. Coomes<sup>1</sup>). If a cathode has to supply high peak currents, it therefore becomes more important to avoid the formation of the interface layer and the reduction producing this layer, while it will be less important in this case that an optimum excess of barium is produced in the coating by such a reduction.

When using pure nickel or a nickel having only a low content of reducing agents, the interface layer and the rectifying effect will be negligibly small. The theory of rectifiers shows that, if no interface layers exist at the boundary between metal and semi-conductor, a rectifier effect is only obtained if the number of impurities or defects in the semi-conductor is smaller than  $10^{17} \text{ cm.}^{-3}$  (Schottky<sup>2</sup>). Such a rectifier effect will therefore not occur in an activated cathode,

as the number of excess atoms in such a cathode is higher than the above value. This conclusion was confirmed by Mutter,<sup>1</sup> who, when extending his resistance measurements mentioned above to cathodes with pure nickel core, could not detect a rectifier effect. Only after operating the cathodes for 130 hours a small difference between the resistances measured in the two directions of current was observed. A similar result was obtained by Loosjes and Vink<sup>1</sup> who used a nickel with a total of only 0.1% impurities and could not detect a layer of high resistance at the boundary with the core nickel.\*

The formation of the interface layers will also depend on the manner of preparing the cathode. If the normal method of preparation from carbonates is used, the formation of an interface layer will start during the decomposition of the carbonate because the oxygen resulting from the dissociation of the carbon dioxide will oxidize the core metal and will so give rise to an interface layer. A special case is given by the combined cathodes used in the early years. The interface layer of these cathodes was formed during the combining process which was part of their preparation.

### 33. Processes in the Interior of the Oxide Coating

If the discussion is confined to cathodes with nickel cores the results of the two preceding sections may be summarized as follows.

The processes which are effective at the oxide-coating-vacuum boundary reduce the quantity of excess barium in the coating. If the temperature is not too high (lower than 1100° K.) the main process to be expected here is poisoning by different gases, while a second process, the evaporation of excess barium, will be important at higher temperatures. If, however, the coating-core-metal boundary is considered, the processes occurring there have exactly the opposite effect, provided the formation of interface layers may be neglected (pure nickel). If the temperature is high enough, new excess barium is continuously formed by reduction, or, at lower temperatures, excess barium may be transferred into the coating from a barium supply existing at the boundary.

These two processes, acting against each other, are connected by

\* Loosjes and Vink<sup>1</sup> detected a layer of high resistance near the surface of their coatings. Further information should be awaited before an explanation of this result which was obtained with rather thick coatings ( $d_c > 200 \mu$ ) is attempted (cf. Loosjes and Vink<sup>2</sup>).

the processes in the interior of the coating. These are diffusior and ionic conduction, which were discussed in general in Secs. 14 and 15 and whose application to the oxide cathode will be dealt with now.

### 33.1. Ionic conduction

The existence of an ionic conduction in the fully activated oxide coating could be concluded from observations of polarization voltages which have been reported by several authors (Reimann and Murgoci,<sup>1</sup> Becker,<sup>1</sup> Meyer and Schmidt,<sup>1</sup> Wright<sup>1</sup>). The measured voltages were between 0.1 and 0.5 volts. It should,

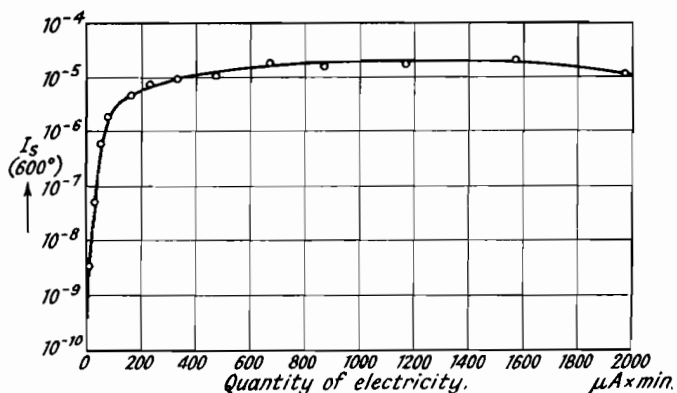


Fig. 151.—Variation of the Saturated Current of a SrO Cathode during Bombardment by Electrons (Becker<sup>1</sup>).

however, be borne in mind that thermo-electric voltages which are produced by the temperature differences in the coating (cf. page 187) can easily be mistaken for polarization voltages. Until these polarization voltages have been investigated in more detail, final conclusions should therefore not be drawn from the above-mentioned observations.

On the other hand there are some experiments in which the existence of an ionic current in the coating has been shown directly. Becker<sup>1</sup> for instance estimated the magnitude of the ionic current from measurements with an SrO cathode. The cathode concerned was bombarded with electrons in the same way as described for a [BaSr]O cathode in Sec. 19.3. An increase of the saturated current up to a maximum was again observed during the bombardment (cf. Fig. 151). This increase in emission may be explained

by assuming that the ionic current, accompanying the electron current, transfers oxygen ions in the direction from surface to core. In this way the quantity of excess strontium at the surface is increased and the external work function decreased. The maximum in emission will then correspond to an optimum density of excess strontium at the surface. Becker assumed that the optimum density is given by a monatomic layer and compared the quantity of strontium in such a monatomic layer with the electrical charge necessary for producing the maximum of emission. In this way he found that the ionic current was  $1/200$  of the total current. The value so obtained is certainly too high in view of the fact that the optimum density of excess strontium at the surface will be less than a monatomic layer.

A further estimate of the ionic conductivity was given by Berdennikowa<sup>1</sup> for cathodes consisting of BaO, SrO, and CaO (at  $T=1275^\circ\text{ K}.$ ). When determining the amount of excess barium in these cathodes (cf. Sec. 19.1), it was found that an electrical charge of 1 coulomb produced  $0.05\ \mu\text{g.}$  additional barium in the coating. Using the Faraday-number, an ionic conductivity of about  $0.005\%$  is calculated from this value.

Isensee<sup>1</sup> determined the ionic conductivity by a direct chemical analysis of the number of oxygen ions evaporating from the cathode (cf. Sec. 19.2). He also used cathodes consisting of BaO, SrO, and CaO which were deposited on a platinum core and which were measured at a temperature of  $1225^\circ\text{ K}.$  When starting the activation of the cathode, the amount of oxygen measured was  $0.15\ \mu\text{g./coulomb}$  and this amount decreased to  $10^{-3}\ \mu\text{g./coulomb}$  during activation. According to this the ionic conductivity decreases from  $0.2\%$  to  $10^{-3}\%$ . This value agrees with the results obtained by Jenkins and Newton,<sup>1, 2</sup> who measured  $10^{-3}\%$  at  $1215^\circ\text{ K.}$  and  $5 \times 10^{-3}\%$  at  $1265^\circ\text{ K.}$  The result obtained by Isensee for pure BaO-cathodes, however, was different. The amount of oxygen detected in this case was constant during activation, the value measured being  $0.05\ \mu\text{g./coulomb}$  (ionic conductivity  $\approx 0.05\%$ ).

If pure BaO is considered, the ionic conductivity  $\kappa_i$  can be calculated using the value of the electronic conductivity  $\kappa_e = 7.0 \times 10^{-3}\ \Omega^{-1}\text{ cm.}^{-1}$  given by Meyer and Schmidt for  $T=1225^\circ\text{ K}.$  With the above value  $\kappa_i/\kappa_e = 5 \times 10^{-4}$  an ionic conductivity  $\kappa_i \approx 4 \times 10^{-6}\ \Omega^{-1}\text{ cm.}^{-1}$  is obtained. This value may be introduced into equation (124) for determining the ionic mobility  $u_i$ .

With  $\vartheta=2$  and with the total number of oxygen ions per unit volume:

$$n = \frac{L\delta_{\text{BaO}}}{m_{\text{BaO}}} = 2.35 \times 10^{22} \text{ ions/cm.}^3$$

the ionic mobility  $u_i \approx 5 \times 10^{-10} \text{ cm.}^2 \text{ sec.}^{-1} \text{ volt}^{-1}$  is derived.

Only very rough values can be obtained in this way, because the quantities of oxygen detected are very near to the limit of sensitivity of the methods used. For further determinations of the ionic conductivity the application of the mass spectrometer as described in Sec. 31.2 would seem to be useful.

Finally the question will be discussed as to which of the two types of ions existing in the oxide coating,  $\text{Ba}^{++}$  or  $\text{O}^{--}$ , is the main carrier of the ionic current. The mobilities of the two constituent ions are not known. It must be borne in mind, however, that the number of vacancies at oxygen ion sites is considerably larger than those at barium sites. As pointed out by Schottky,<sup>1</sup> the number of oxygen ions producing ionic conduction by moving over the appropriate vacancies is therefore likely to predominate, even if the mobility of these oxygen ions were smaller than that of the barium ions. It will be assumed therefore that ionic conduction and consequently diffusion are mainly produced by the movement of oxygen ions.

At first such an assumption seems to be contradictory to the results of the theory of tarnishing reactions (cf. Sec. 14), where the metal ions are found to move through the lattice of the tarnishing oxide layers.\* The oxide layers, however, for which these reactions have so far been studied, are either defect semi-conductors (vacancies at metal ion sites) or, if excess semi-conductors, they are produced by interstitial atoms and not by vacancies. The conditions are likely to be different in excess semi-conductors, such as the oxide coating, which are produced by vacancies at oxygen ion sites.

### 33.2. Diffusion

Diffusion in the oxide coating will exist if there are differences in the concentration of the excess Ba-atoms in the coating. These differences can be equalized by a movement of the vacancies in the oxygen lattice as described in Sec. 14. The oxygen ions will then move over the vacancies from regions in the coating with more

\* Cf. N. F. Mott and R. W. Gurney, *Electronic Processes in Ionic Crystals*, Oxford, 1940, p. 249.

oxygen ions (less Ba excess) to regions having less oxygen ions (more Ba excess).

The assumption that oxygen ions are the main carriers of diffusion in the coating is supported by the experiments showing that oxide cathodes can alternatively be poisoned by oxygen and be reactivated many times (cf. Sec. 31.3). This phenomenon was explained by assuming the poisoning oxygen ions to diffuse into the coating during poisoning and to diffuse out of it during reactivation. It would be difficult to explain this by a diffusion of barium ions, because in such a case the excess barium in the coating would soon be consumed during the repeated process of poisoning.

It may appear that the assumption of oxygen ions as carriers of diffusion is contradictory to the experiments of Becker and Sears<sup>1,2</sup> discussed in Sec. 19.3. The variation of the emission current during heating of the cathode as seen from Figs. 86 and 87 was explained by a diffusion of excess barium atoms into the interior of the coating. These experiments, however, can also be explained by a diffusion of oxygen ions from the interior to the surface. Such oxygen ions arriving at the surface will compensate barium atoms existing in excess at the surface and will make them a constituent of the BaO crystal lattice. Simultaneously the number of vacancies at oxygen ion sites in the interior will increase. Additional barium atoms will therefore be formed in the interior, obtaining their electrons from the new barium ions formed at the surface. Finally the concentration of the barium atoms and ions will be the same as it would be due to a direct diffusion of barium atoms from the surface to the interior.

There is one experiment, however, which cannot be explained by the assumption of diffusing oxygen ions, namely the activation of strontium oxide by barium evaporated on its surface as described in Sec. 27.2. The experiment showed that the barium atoms or ions traverse into the interior of the strontium oxide and produce an activation there when the temperature is raised to 1000° K. This may be explained by assuming that the barium ions concerned diffuse over the small number of residual vacancies existing at strontium ion sites of the SrO lattice.

The diffusion coefficient of an alkaline earth oxide coating has not been determined yet by a direct method. It is only possible to calculate this coefficient from the above value of the ionic mobility by using equation (126). In this way  $D \approx 2.5 \times 10^{-11} \text{ cm.}^2 \text{ sec.}^{-1}$  is obtained for  $T = 1225^\circ \text{ K.}$

### 34. The Combination of the Various Processes and their Influence on Emission and Life

An attempt will now be made to examine how the individual processes discussed above work together. For such an examination it will be necessary to know the relations between the number of excess barium atoms in the interior or on the surface and the internal or external work function respectively. The second relation between surface atoms and external work function can be obtained from an early experiment by Becker,<sup>1</sup> the same as was used by him for estimating the ionic conductivity of the oxide coating (cf. Sec. 33).

The rise of the saturated current during this experiment, produced by an electron bombardment of the oxide coating (at  $T=600^{\circ}\text{K}.$ ), is shown by Fig. 151. If the final period of bombardment is disregarded, the logarithm of the saturated current varies proportionately with the electrical charge sent into the coating. On the other hand, the quantity of oxygen ions removed from the surface of the coating is also proportional to the electrical charge. Let  $s$  denote the number of oxygen ions per unit area of the surface atom layer and  $s_{tot}$  the number of such ions in an atom layer without vacancies. Then we have:

$$\ln j_s = k_1 b(s_{tot} - s) + k_2 \dots \dots \dots \quad (216)$$

$b$  and  $k$  being constants.

This equation may be transformed by introducing the values  $j_{opt}$  and  $s_{opt}$  which refer to an optimum density of excess barium (or strontium) atoms at the surface producing the maximum emission current. If the current emitted from a surface layer without excess barium (no vacancies) is denoted by  $j_{tot}$ , it follows from (216):

$$\begin{aligned} \ln j_{opt} &= k_1(s_{tot} - s_{opt}) + k_2 \\ \ln j_{tot} &= k_2 \end{aligned} \quad \dots \dots \dots \quad (217)$$

By introducing the abbreviation:

$$F = \ln(j_{opt}/j_{tot}) \dots \dots \dots \quad (218)$$

the following relation is finally obtained from (216) and (217):

$$\ln(j_s/j_{tot}) = K \frac{s_{tot} - s}{s_{tot} - s_{opt}} \dots \dots \dots \quad (219)$$

This relation between the saturated current  $j$  and the density  $s$  of oxygen ions at the surface can be used for giving an explanation

for the decay of the saturated current observed after switching on the anode voltage (cf. Sec. 30). Sproull<sup>1</sup> and Wagener<sup>1</sup> tried to explain this decay by a combination of ionic conduction and diffusion. Wagener pointed out that the ionic current accompanying the electron current in the coating will move oxygen ions towards the surface of the coating and will so decrease the number of excess barium atoms at the surface and increase the work function there. The movement of the oxygen ions towards the surface then corresponds to a movement of vacancies at oxygen ion sites towards the core metal. Such a movement of vacant anion sites directed towards the cathode is also observed with alkali halides when an electrical field is applied. The well-known migration of *F*-centres in alkali halides is produced in this way.\*

Due to the movement of the oxygen ions in the oxide coating a concentration gradient is produced between the ions at the surface and those in the interior. This gradient will be opposed by a diffusion of oxygen ions towards the interior. The two phenomena act against one another, and after a certain time they produce a new equilibrium in the coating, the work function being higher, giving a lower emission current.

Let  $s$  now denote the number of oxygen ions per unit area of an atom layer in general. The number of oxygen ions which are conducted towards the surface per unit time is then given by:

$$\frac{ds_i}{dt} = \frac{\kappa_i}{2e\kappa_e} j \quad \dots \quad \dots \quad \dots \quad \dots \quad (220)$$

Furthermore, the number of ions moving back per unit time due to diffusion is obtained from (118) as:

$$\frac{ds_o}{dt} = -\frac{D}{\Delta} \frac{s - s_0}{d/2} \quad \dots \quad \dots \quad \dots \quad \dots \quad (221)$$

where  $s_0$  denotes the number of ions at time  $t=0$ ,  $d$  the lattice constant of BaO and  $\Delta$  the thickness of the layer in which ionic conduction and diffusion take place. By taking the sum of the two equations, the total number of moving ions is obtained, giving the differential equation:

$$\frac{ds}{dt} = \frac{\kappa_i}{2e\kappa_e} j - \frac{2D}{\Delta d} (s - s_0) \quad \dots \quad \dots \quad \dots \quad \dots \quad (222)$$

\* N. F. Mott and R. W. Gurney, *Electronic Processes in Ionic Crystals*, Oxford, 1940, p. 140.

By using (219), this differential equation can be transformed in such a way that the emission current  $j$  is obtained as the only variable. Sproull gave a solution of this differential equation and obtained a very good agreement between this solution and the curve measured for the fall in emission.

By using this solution the ionic conductivity of the coating can be calculated from the values measured for the emission current  $j$  as a function of time. The value of the ionic conductivity obtained in this way is of the same order as those given in Sec. 33 (cf. Wagener<sup>1</sup>).

It follows from this that theoretically the decay in emission can be explained by a combination of ionic conduction and diffusion. However, the experimental evidence discussed in section 30, especially that obtained by Wright<sup>3</sup> and Feaster,<sup>1</sup> seems to show that most of the decay phenomena observed are due to external influences, mainly to the poisoning effect of gases originating from other electrodes. The question, whether there is any decay which is an inherent phenomenon of the oxide coating itself, remains to be decided.

Further evidence of the processes in the interior of the coating will be obtained, if not only the decay in emission is examined, but also the rise observed after switching off the anode voltage or after poisoning the cathode by some other means (cf. Fig. 135). This rise is only determined by the diffusion and the formulæ therefore become simpler. The differential equation valid in this case is derived in analogy with (222). Thus:

$$\frac{ds_D}{dt} = -\frac{2D}{\Delta d}(s - s_{equ}) \quad \dots \quad (223)$$

where  $s_{equ}$  denotes the equilibrium value obtained when diffusion has ended. The variable  $s$  in this equation is replaced by using (219). The solution of the differential equation derived in this manner is:

$$\ln(j/j_{equ}) = \ln(j_0/j_{equ}) e^{-(2D/\Delta d)t} \quad \dots \quad (224)$$

where  $j_0$  now denotes the current flowing when the rise in emission begins.

The rise in emission current, following the decay, was used by Blewett<sup>4</sup> for determining the activation energy  $E_r$  in equation (121) giving the temperature-dependence of diffusion. According to (224) the emission current  $j$  is a function of the product  $Dt$ . Combining this result with (121) therefore gives:

$$j_e = f(e^{-E_r/kT} \times t) \quad \dots \quad (225)$$

According to this equation it would be possible to superimpose different curves  $f(T, t)$ , representing the rise in emission for different temperatures, by multiplying the time scale by a suitable factor  $\beta$  which would depend on the temperature  $T$ . A plot of  $\log \beta$  against  $1/T$  would then give a straight line from the slope of which the energy  $E_r$  could be ascertained. Blewett found that it was in fact possible to superimpose the individual curves and to obtain the straight line  $\log \beta = f(1/T)$ , but with a considerable spread. The value of  $\Gamma$  determined from the straight line was 0.7 eV (for  $T=800^\circ - 1100^\circ$  K.).

The processes considered are also of considerable importance for the life of the oxide cathode. At first one would assume that of these processes the ionic conduction is decisive for the life, as such a conduction will gradually dissociate the oxide coating. The time  $t_d$  which would be necessary for a complete dissociation of the coating is obtained from the relation:

$$\frac{\kappa_i}{\kappa_e} j_e t_d = \frac{2 \times 96500 d_c \delta}{M} \quad \dots \quad (226)$$

$d_c$  denoting the thickness of the oxide coating. According to this:

$$t_d \approx 2 \frac{d_c}{j_e \kappa_i / \kappa_e} \text{ hours} \quad \dots \quad (227)$$

Using the value  $\kappa_i/\kappa_e = 10^{-5}$ , measured by Isensee,  $d_c = 5 \times 10^{-3}$  cm., and  $j_e = 10$  mA/cm.<sup>2</sup>, a time  $t_d = 100,000$  hours is obtained. The minimum life derived in this way is much higher than the life normally demanded of an oxide cathode.

If the usual life of an oxide cathode of some thousand hours is considered, poisoning and diffusion will be of much more importance than ionic conduction (cf. Vol. I, Sec. 13). This is shown by some experiments of the authors, who aged cathodes in commercial triodes at different temperatures and different anode and grid voltages. If the normal heater voltage was applied ( $T \approx 1000^\circ$  K.), a fall of the emission current could not be observed during a life of several hundred hours. A different result, however, shown by Fig. 152, was obtained at a lower cathode temperature ( $T \approx 800^\circ$  K.). The emission currents plotted in Fig. 152 as a function of life were all measured under the same conditions with a grid voltage  $V_G = 0$ . The individual curves of the figure refer to different anode and grid voltages which were applied to the valves concerned during the ageing process, but not during the measurement. The values of

these anode and grid voltages as shown by the figure influenced the result considerably. No fall of the measured emission current was observed with low voltages ( $V_A = V_G = 0$  or  $V_A = V_G = 5$  volts), while when applying an anode voltage of  $V_A = 220$  volts, the emission current fell from 26 mA to 12 mA within 50 hours. This fall was independent of the value of the grid voltage (0 or  $-3.5$  volts)

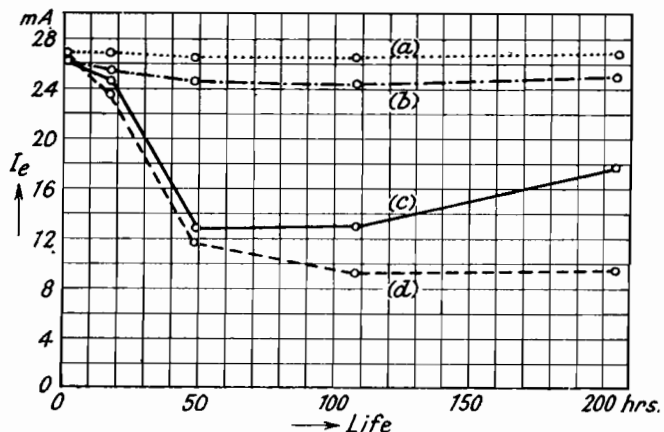


Fig. 152.—Variation of the Emission Current  $I_e$  during Life at a Cathode Temperature of  $800^\circ$  K.

Voltages applied during life:

- (a) .....  $V_A = 0$  volt;  $V_G = 0$  volt.
- (b) — · —  $5$  volts;  $5$  volts.
- (c) — — —  $220$  volts;  $0$  volts.
- (d) - - - -  $220$  volts;  $-3.5$  volts.

and therefore independent of the value of the emission current flowing during the ageing process. The fall in emission during life as obtained in these experiments is therefore not produced by the emission current and by an ionic conduction accompanying this current. This will also be seen from curves (b) and (d) in Fig. 150, which show a different life obtained with different anode and grid voltages, although the emission current flowing during life was the same in these two cases.

The influence of anode voltage on life was investigated in detail by Metson and Holmes,<sup>1</sup> who examined two batches of pentodes of a similar design. When operating these pentodes under normal conditions ( $V_A = 200$  volts), the life of the first batch was  $>40,000$  hours, while the second batch had a life of only  $<3000$  hours. Two points of significance were found. Firstly, the second batch

of valves showed no appreciable deterioration over a period of 6000 hours when a low voltage of 2 volts was connected to anode and grids instead of the normal 200. Secondly, the vacuum of these valves, as detected by measuring the reverse grid current, was considerably worse than that of the valves of the first group, which had a long life under normal conditions.

The influence of the emission density on the life of an oxide cathode was further examined by Wagener.<sup>2</sup> When investigating diodes ( $V_A = 15$  volts) he found no appreciable difference in life between operation with 10 and 45 mA/cm.<sup>2</sup> within 10,000 hours and also no difference between 10 and 230 mA/cm.<sup>2</sup> within 3000 hours. These results were obtained for two different cathode temperatures 900° and 1075° K.

Summarizing all these results, three factors seem to be decisive in determining the life of an oxide cathode—the vacuum in the valve, the magnitude of the voltages applied to the electrodes, and the temperature of the cathode. The first two factors are interconnected, because an increasing anode voltage is normally connected with an increasing load and therefore with an increasing evolution of gas from the anode. For this reason it is difficult to show definitely that the magnitude of the anode voltage influences the life directly. Metson and Holmes tentatively concluded from their experiments that the emission deterioration during life is produced by bombarding ions which are formed from residual gases in the valve if the anode voltage is sufficiently high.

The influence of the third factor, the temperature, also depends on the vacuum conditions in the valve. The effect of residual gases, such as oxygen, can be compensated more easily at high temperatures, since at these temperatures the oxygen ions will diffuse towards the core more readily and will be made harmless by reacting with the barium supply there. If the temperature is lowered, the diffusion decreases according to equation (121) and finally freezes in. The compensation of residual gases by the barium near the core is therefore made more and more difficult with decreasing temperature and the poisoning effect of these gases will increase correspondingly. Under good vacuum conditions, however—or with low anode voltages—the lowering of the temperature will have rather a beneficial effect, since secondary phenomena, e.g. evaporation, decrease with falling temperature. In agreement with this Wagener,<sup>2</sup> when working with low anode voltages, obtained a slight improvement in life by lowering the cathode temperature from 1075° to 900° K.

The considerations dealt with in this chapter have only been given in general terms. A more detailed examination will be possible if further measurements of the fundamental processes, as for instance diffusion and ionic conduction, are made. Finally a phenomenon will be discussed which is not directly connected with the investigations considered so far, namely the fluctuations which are observed with an oxide cathode at low frequencies.

### REFERENCES

- |                     |  |
|---------------------|--|
| ARNOT, F. L.        | (1) and MILLIGAN, J. C., <i>Proc. Roy. Soc. (A)</i> 156 (1936), 538.<br>(2) <i>Proc. Roy. Soc. (A)</i> 158 (1937), 137.  |
| BACHMANN, C. H.     | (1) and CARNAHAN, C. W., <i>Proc. I.R.E.</i> 26 (1938), 529.   |
| BECKER, J. A.       | (1) <i>Physic. Rev.</i> 34 (1929), 1323.<br>(2) and SEARS, R. W., <i>ibid.</i> 38 (1931), 2193.  |
| BEESE, N. C.        | (1) <i>Physic. Rev.</i> 36 (1930), 1309.   |
| BENJAMIN, M.        | (1) and ROOKSBY, H. P., <i>Philos. Mag.</i> 15 (1933), 810.<br>(2) <i>Philos. Mag.</i> 20 (1935), 1.   |
| BERDENNIKOWA, T. P. | (1) <i>Physik. Z. Sow. Union</i> 2 (1932), 77.   |
| BLEWETT, J. P.      | (1) and JONES, E. I., <i>Physic. Rev.</i> 50 (1936), 464.<br>(2) <i>Physic. Rev.</i> 53 (1938), 935.<br>(3) <i>J. Appl. Phys.</i> 10 (1939), 668.<br>(4) <i>Physic. Rev.</i> 55 (1939), 713. |
| BROADWAY, L. F.     | (1) and PEARCE, A. F., <i>Proc. Phys. Soc.</i> 51 (1939), 335.   |
| COOMES, E. H.       | (1) <i>J. Appl. Phys.</i> 17 (1946), 647.  |
| DANFORTH, W. E.     | (1) and RAMSAY, W. E., <i>Physic. Rev.</i> 73 (1948), 1244.  |
| DAVISSON, C.        | (1) and GERMER, L. H., <i>Physic. Rev.</i> 24 (1924), 666.   |
| DEININGER, F.       | (1) <i>Ann. Phys.</i> 25 (1908), 285.  |
| DUSHMAN, S.         | (1) and VILLARS, D. S., <i>Rev. mod. Phys.</i> 2 (1930), 433.  |
| EISENSTEIN, A.      | (1) <i>Physic. Rev.</i> 72 (1947), 531.<br>(2) <i>J. Appl. Phys.</i> 20 (1949), 776.   |
| ESPE, W.            | (1) <i>Wiss. Veröff. Siemens-Werken</i> 5 (III) (1927), 29, 46.  |
| FEASTER, G. R.      | (1) <i>J. Appl. Phys.</i> 20 (1949), 415.  |
| FINEMAN, A.         | (1) and EISENSTEIN, A., <i>J. Appl. Phys.</i> 17 (1946), 663.  |
| HAMAVER, H. C.      | (1) BRUINING, H., and ATEN, A. H. W., <i>Philips Res. Rep.</i> 2 (1947), 171.  |
| HEADRICK, I. B.     | (1) and LEDERER, E. A., <i>Physic. Rev.</i> 50 (1936), 1094.   |
| HEINZE, W.          | (1) and WAGENER, S., <i>Z. techn. Physik</i> 17 (1936), 645.<br>(2) <i>ibid.</i> 20 (1939), 16.  |
| HERRMANN, G.        | (1) <i>Z. physik. Chem. Abt. B</i> 35 (1937), 298.<br>(2) and KRIEG, O., <i>Ann. Phys.</i> 4 (1949), 441.  |
| HUBER, H.           | (1) Thesis, University Berlin, 1941.<br>(2) and WAGENER, S., <i>Z. techn. Physik</i> 23 (1942), 1.   |
| ISENSEE, H.         | (1) <i>Z. physik. Chem. Abt. B</i> 35 (1937), 309.   |

## THE OXIDE-COATED CATHODE

- JACOBS, H. (1) *J. Appl. Phys.* 17 (1946), 596.  
 (2) and WOLK, B., *Proc. I.R.E.* 37 (1949), 1247.
- JENKINS, R. O. (1) and NEWTON, R. H. C., *Nature* 163 (1949), 572.  
 (2) and NEWTON, R. H. C., *J. Sci. Instr.* 26 (1949), 172.
- KAWAMURA, H. (1) *Journ. Phys. Soc. Japan* 1 (1946), 8.
- KNIEPKAMP H. (1) and NEBEL, C., *Wiss. Veröff. Siemens-Werken* 11  
 (II) (1932), 75.
- KOLLER, L. R. (1) *Physic. Rev.* 25 (1925), 671.
- KROLL, W. (1) *Z. anorg. allg. Chem.* 219 (1934), 301.
- LIEBOLD, W. (1) Thesis, University Berlin, 1941.
- LOOSJES, R. (1) and VINK, H. J., *Le Vide* 5 (1950), 73.  
 (2) and VINK, H. J., *J. Appl. Phys.* 21 (1950), 350.
- LOWRY, E. F. (1) *Physic. Rev.* 35 (1930), 1367.
- MADDOCK, A. I. (1) *Philos. Mag.* 19 (1935), 422.
- METSON, G. H. (1) and HOLMES, M. F., *Nature* 163 (1949), 61.  
 (2) *Nature* 164 (1949), 540.  
 (3) *Proc. Phys. Soc.* 62 (1949), 589.
- MEYER, W. (1) and SCHMIDT, A., *Z. techn. Physik* 13 (1932), 137.
- MOTT, N. F. (1) *Proc. Roy. Soc. (A)* 171 (1939), 27.
- MUTTER, W. E. (1) *Physic. Rev.* 72 (1947), 531.
- PTITSIN, S. B. (1) *Journ. Techn. Physics* 17 (1947), 965.
- REIMANN, A. L. (1) and MURGOCI, R., *Philos. Mag.* 9 (1930), 440.
- RIETHMUELLER, J. (1) *Annales Radioélectricité* 2 (1947), 329.
- ROOKSBY, H. P. (1) *J. Roy. Soc. Arts* 88 (1940), 308.  
 (2) and STEWART, E. G., *Nature*, 157 (1946), 548.  
 (3) *Nature*, 159 (1947), 609.
- ROTHE, H. (1) *Z. Physik* 36 (1926), 737.
- ROTHSTEIN, J. (1) *Physic. Rev.* 69 (1946), 693.
- SCHAFFER, H. (1) and WALCHER, W., *Z. Physik* 121 (1943), 679.
- SCHOTTKY, W. (1) *Z. physik. Chem. B* 29 (1935), 335.  
 (2) *Z. Physik* 118 (1942), 539.
- SCHRIEL, M. (1) Thesis, Technical University, Berlin, 1930.
- SLOANE, R. H. (1) and WATT, C. S., *Proc. Phys. Soc.* 61 (1948), 217.
- SPROULL, R. L. (1) *Physic. Rev.* 67 (1945), 166.
- STAHL, A. H. (1) *Schweiz. Arch. angew. Wiss. Techn.* 14 (1948), 337.
- WAGENER, S. (1) *Proc. phys. Soc.* 61 (1948), 521.  
 (2) *Nature* 164 (1949), 357.
- WAGNER, E. R. (1) *Trans. Electrochem. Soc.* 59 (1931), 223.
- WHITE, A. H. (1) *J. Appl. Phys.* 20 (1949), 856.
- WRIGHT, D. A. (1) *Proc. Roy. Soc. London (A)* 190 (1947), 394.  
 (2) *ibid.* 62 (1949), 188.  
 (3) *ibid.* 62 (1949), 398.

## APPENDIX

### FLUCTUATIONS OF THE EMISSION CURRENT OF THE OXIDE CATHODE (FLICKER EFFECT)

An emission current which seems to be constant when measured by a D.C. method, in fact fluctuates to a very small extent, and these fluctuations can be detected as appropriate alternating currents. The most elementary of these fluctuations which occurs with all types of cathodes, including pure metals, is called the shot effect. This fluctuation is due to the fact that the emission current is produced by individual electrons which, when passing from cathode to anode, give corresponding current pulses. As the number of emitted electrons and therefore the current pulses are distributed according to the laws of statistics, the emission current composed of these pulses will fluctuate correspondingly. The direct current formed by the emitted electrons is therefore superimposed by alternating currents of small amplitude which can be measured in the resonant circuits connected to the valve. When operating the valve these small alternating currents, which are called shot currents, produce a noise limiting the amplification of faint A.C. signals.

The shot current can be calculated by expanding the current pulse connected with the passage of an electron into a Fourier series, and by adding the terms of this series lying in a certain band width. When examining the saturated current Schottky<sup>1</sup> derived the following formula for the mean shot current within a band of width  $\Delta\nu$

$$\overline{I_{sh}} = \sqrt{(2eI_s\Delta\nu)} = 5.64 \times 10^{-10} \sqrt{(I_s\Delta\nu)} \text{ amp. . . (228)}$$

According to this the shot current is independent of the frequency, but depends on the saturated current and the band width. Equation (228) has been confirmed experimentally at high frequencies. If the emission current is not saturated but limited by space-charge, the shot current is smaller than obtained from (228) owing to the interaction between the electrons.\*

If atomic film cathodes and oxide cathodes are examined at low frequencies (below 10 kc/sec.) fluctuations of the emission current

\* For details see K. R. Spangenberg; *Vacuum Tubes*, New York, 1948.

are observed which are considerably larger than the shot current given by (228). These fluctuations, known as the flicker effect, were discovered by Johnson<sup>1</sup> and investigated in detail by Kozanowski and Williams<sup>1</sup> and Graffunder.<sup>1</sup> Fig. 153 shows some results obtained by Graffunder for different oxide cathodes, when drawing a saturated current of 2 mA. The ratio between the mean

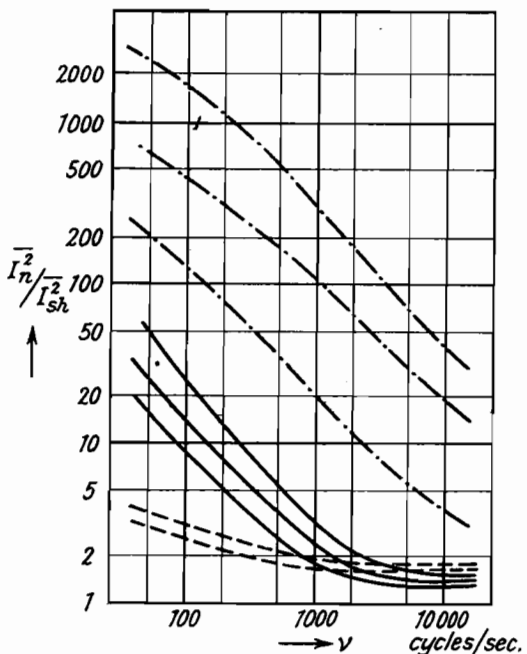


Fig. 153.—Ratio between Mean Square of Noise Current  $\bar{I}_n^2$  and Mean Square of Shot Current  $\bar{I}_{sh}^2$  of Oxide Cathodes as a Function of Frequency  $\nu$  (Graffunder<sup>1</sup>).

- indirectly heated cathodes.
- - - - directly heated cathodes made from carbonates.
- directly heated cathodes made by the condensation method.

square  $\bar{I}_n^2$  of the total noise current and the mean square of the shot current  $\bar{I}_{sh}^2$  calculated from (228) has been plotted in this figure as a function of frequency  $\nu$ . The figure shows that the noise current increases considerably with decreasing frequency, the increase being approximately proportional to  $1/\nu$  for all valves examined.

The intensity of the flicker effect is different for different types of cathodes. It increases in the sequence: indirectly heated cathodes (dashed curves), directly heated cathodes made by the condensation

method (full curves), directly heated cathodes made from carbonates (dash and dot curves). These differences in intensity can be explained by the fact that different temperatures are needed for obtaining from the different cathodes the saturated current of 2 mA used for the measurement. This temperature was lowest with the indirectly heated cathodes and highest with the directly heated carbonate cathodes. According to this the flicker effect would increase with increasing temperature.

The variation of the flicker effect with the magnitude of the saturated current is shown by Fig. 154, giving the mean square of

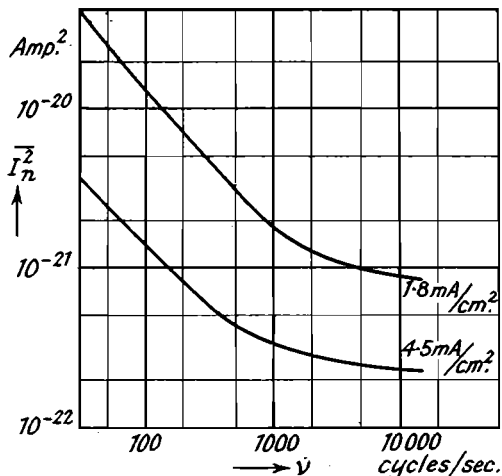


Fig. 154.—Mean Square of Noise Current as a Function of Frequency for Different Densities of the Saturated Current (Graffunder<sup>1</sup>).

the noise current as a function of frequency. If the flicker effect is examined in the space-charge region it becomes smaller than in the region of the saturated current in the same way as does the shot effect.

For explaining the flicker effect Johnson assumed that the fluctuations of the emission current are produced by appropriate fluctuations of the work function of the cathodes examined. If atomic film cathodes are considered these latter fluctuations may be due to variations in the number of foreign atoms adsorbed at the surface of the cathodes concerned. By transferring this concept to the oxide cathode Schottky<sup>2</sup> gave a theory of the flicker effect. If the variation of the flicker effect with frequency is considered, this theory, however, gives an increase proportional to  $1/\nu^2$ , while

an increase with  $1/\nu$  is obtained by the experiments. More recently Macfarlane<sup>1</sup> gave another theory by combining the fluctuations of the emission with the ionic current accompanying the emission current. As shown in Sec. 34, when dealing with the decay of emission, this ionic current produces a concentration gradient of the excess barium near the surface and a diffusion opposing this gradient. The elementary processes, such as arrival of individual ions at the surface or disappearance of these ions from there, may then be used for explaining the fluctuations of the emission current. By using the differential equation (222) Macfarlane obtained the following formula for the mean square of the noise current as a function of frequency:

$$\bar{I_n^2} = \frac{Bj^{n+1}}{\nu^n} \quad \dots \quad \dots \quad \dots \quad \dots \quad \dots \quad (229)$$

$n$  representing all values between 1 and 2, depending on the selection of the constants to be employed.

Besides the normal flicker effect discussed so far, there is an anomalous flicker effect which is produced by gas ions impinging upon the cathode surface and which can consequently be observed with pure metal cathodes too. As this phenomenon is not typical of the oxide cathode, we shall not deal with it here.

#### REFERENCES

- |                   |   |
|-------------------|---|
| GRAFFUNDER, W.    | (1) <i>Telefunken-Röhre</i> 15 (1939), 41.                                      |
| JOHNSON, J. B.    | (1) <i>Physic. Rev.</i> 26 (1925), 71.  |
| KOZANOWSKI, H. N. | (1) and WILLIAMS, N. H., <i>Physic. Rev.</i> 36 (1930), 1314.                   |
| MACFARLANE, G.    | (1) <i>Proc. Phys. Soc.</i> 59 (1947), 366.                                     |
| SCHOTTKY, W.      | (1) <i>Ann. Phys.</i> 57 (1918), 541.<br>(2) <i>Physic. Rev.</i> 28 (1926), 74. |

## BIBLIOGRAPHY

### I. Thermal Emission in general and Oxide Cathodes

- (1) RICHARDSON, O. W. *Emission of Electricity from Hot Bodies.* (London, 1921.)
- (2) BLOCH, E. *Les Phénomènes Thermioniques.* (Paris, 1923.)
- (3) WEHNELT, A. Die Oxydkathode und ihre praktischen Anwendungen. [The oxide-coated cathode and its practical applications.] *Erg. exakt. Naturwiss.* 4 (1925), 86.
- (4) SIMON, H. Herstellung der Glühelektroden. [Manufacture of hot electrodes.] *Handb. d. Exp. Phys.* XIII/2. (Leipzig, 1928).
- (5) SCHOTTKY, W., and ROTHE, H. Physik der Glühelektroden. [Physics of hot electrodes.] *Handb. d. Exp. Phys.* XIII/2. (Leipzig, 1928.)
- (6) HODGSON, B., HARLEY, L. S., and PRATT, O. S. The Development of the Oxide-Coated Filaments. *J. Inst. electr. Engr.* 67 (1929), 762.
- (7) DUSHMAN, S. Thermionic Emission. *Rev. mod. Phys.* 2 (1930), 381.
- (8) LANGMUIR, I., and COMPTON, K. T. Electrical Discharges in Gases. *Rev. mod. Phys.* 2 (1930), 123; 3 (1931), 191.
- (9) GEHRTS, A. Oxydkathoden. *Naturwiss.* 20 (1932), 732.
- (10) REIMANN, A. L. *Thermionic Emission.* (London, 1934.)
- (11) SUHRMANN, R. Elektronenemission metallischer Leiter. [Electron emission of metallic conductors.] Contribution to Mueller-Pouillet, *Lehrb. d. Physik*, Vol. IV/4, Chapter 3. (Braunschweig, 1934.)
- (12) BECKER, J. A. Thermionic Electron Emission and Adsorption. *Rev. mod. Phys.* 7 (1935), 95.
- (13) RUKOP, H., SCHOTTKY, W., and SUHRMANN, R. *Die Physik* 3 (1935), 133.
- (14) DE BOER, J. H. *Electron Emission and Adsorption Phenomena.* (Cambridge, 1935.)
- (15) JONES, T. J. *Thermionic Emission.* (London, 1936.)
- (16) BLEWETT, J. P. The Properties of Oxide-Coated Cathodes. *J. Appl. Phys.* 10 (1939), 668, 831. Oxide-coated Cathodes Literature. *J. appl. Phys.* 17 (1946), 643.
- (17) WEINREICH, O. Les Cathodes à Oxydes, leur Développement expérimental, théorique et technique. [Oxide-coated Cathodes, their experimental, theoretical and commercial development.] *Revue Générale de l'Electricité* 56 (1947), 75.
- (18) BIGUENET, CH. *Les Cathodes Chaudes.* Editions de la Revue d'Optique. (Paris, 1947.)
- (19) FRIEDENSTEIN, H., MARTIN, S. L., and MUNDAY, G. L. The Mechanism of the Thermionic Emission from Oxide-coated Cathodes. *Reports on Progress in Physics* 11 (1948), 298.
- (20) EISENSTEIN, A. Contribution to Vol. I of *Advances in Electronics.* (New York, 1948.)
- (21) HERRING, C., and NICHOLS, M. H. Thermionic Emission. *Rev. mod. Phys.* 21 (1949), 185.

## BIBLIOGRAPHY

### II. Conduction of Electricity and Diffusion

- (1) TUBANDT, C. Leitfähigkeit und Überführungszahlen in festen Elektrolyten. [Conductivities and Transport Numbers of Solid Electrolytes.] *Handb. d. Exp. Phys.* XII/1, p. 381. (Leipzig, 1932.)
- (2) JOST, W. Elektrische Leitfähigkeit nichtmetallischer Kristalle. [Electrical conductivity of non-metallic crystals.] Contribution to Mueller-Pouillet, *Lehrb. d. Physik*, IV/4, p. 631. (Braunschweig, 1934.)
- (3) JOST, W. Diffusion und chemische Reaktion in festen Stoffen. [Diffusion and chemical reaction in solids.] (Dresden, Leipzig, 1937.)
- (4) MOTT, N. F., and GURNEY, R. W. *Electronic Processes in Ionic Crystals*. (Oxford, 1940.)
- (5) BARRER, R. M. *Diffusion in and through Solids*. (Cambridge, 1941.)
- (6) BUSCH, G. Elektronenleitung in Nichtmetallen. [Electronic Conduction in Non-metals.] *Zeitschr. f. angew. Math. u. Physik*, 1 (1950), 3/81.

# INDEX TO AUTHORS

- ADAM, H., 43  
Adams, M. I., 41  
Ahearn, A. I., 64, 76, 99  
Albright, W., 202, 204  
Allison, H. W., 206  
Anderson, P. A., 72, 97  
Apker, L., 100, 135  
Aranowitsch, R. M. 209  
Arizumi, T., 77, 87  
Arnold, H. D., 181  
Arnot, F. L., 270  
Aten, A. H. W., 260, 276
- BACHMANN, C. H., 159, 263  
Band, W., 13  
Bardeen, D., 17  
Bartelink, E. H. B., 17  
Barton, H. A., 159  
Bassoe, E., 98  
Becker, J. A., 34, 52, 53, 55, 59, 61, 64, 73, 103, 156, 159, 161, 187, 193, 196, 199, 201, 205, 254, 256, 261, 287, 290, 291  
Beese, N. C., 276  
Benjamin, M., 218, 241, 243, 246, 249, 254, 264, 277, 281  
Berdennikowa, T. P., 157, 245, 288  
Berger, C., 207  
Bethe, H., 18  
Blewett, J. P., 159, 187, 249, 256, 263, 282, 293  
Bley, H., 36  
Bloch, F., 130  
Blochinzew, D., 17  
Blodgett, K. B., 41  
de Boer, J. H., 48, 53, 55, 56, 179, 189, 208  
Bosworth, R. C. L., 100, 103  
Bowie, M., 100  
Brattain, W. H., 55, 73, 103  
Braun, A., 99, 172  
du Bridge, L. A., 76, 78, 92, 97, 104  
Broadway, L. F., 159, 263  
Brown, C., 175  
Brueche, E., 21, 58, 242  
Bruining, H., 208, 260, 276  
Burgers, W. G., 218  
Busch, G., 99, 135, 139, 143, 144, 172  
Buzagh, A. v., 224, 243
- CAMPBELL, N. R., 217  
Cardwell, A. B., 99, 104  
Carnahan, C. W., 159, 263  
Cashman, R. J., 98  
Champeix, R., 176, 181, 207
- Clausing, P., 158, 201  
Compton, K. T., 37  
Coomes, E. H., 195, 285  
Cork, I., 155  
Crossley, W. P., 181, 182
- DAHLSTROM, R. K., 96  
Danforth, W. E., 193, 201, 258  
Darbyshire, I. A., 224  
Davisson, C., 18, 33, 79, 181, 185, 255  
Debiesse, J., 207  
Dehmelt, F. W., 187, 217  
Deininger, F., 276  
Demski, A., 71, 207  
Deponte, R., 98, 102  
Detels, F., 36, 159, 181, 182  
Dickey, J., 100, 135  
Dixon, E. H., 100  
Djatlowizkaja, B. I., 64  
Dushman, S., 25, 103, 245
- EICHBORN, L. v., 94  
Eisenstein, A., 193, 194, 196, 201, 282, 284  
Epstein, P. S., 38  
Espe, W., 178, 181, 182, 245, 253, 256  
Ewald, I. W., 103  
Ewles, I., 210
- FAIVRE, R., 156  
Fan, H. Y., 181, 207  
Farnsworth, H. E., 84, 93  
Feaster, G. R., 259, 293  
Ferris, W. R., 40  
Fineman, A., 193, 284  
Fisher, E., 122  
Fiske, M. D., 99  
Fleming, G. M., 100  
Foote, F., 124  
Fowler, R. H., 92, 98, 104, 171  
Fox, W., 100  
Frank, G., 181, 182  
Freitag, H., 76, 99  
Friederich, E., 122  
Fritsch, O., 141  
Fritz, H., 158  
Fruehling, G., 187  
Fry, Th. C., 38
- GALLAGHER, CH. J., 103  
Gärtner, H., 224  
Gehrtz, A., 157  
Gerhard, G. L., 155  
Gericke, H., 82

# INDEX TO AUTHORS

- Germer, L. H., 18, 32, 71, 79, 84, 181,  
     185, 255  
 Geyer, K. H., 208  
 Gill, E. W. B., 176  
 Gisolf, J. H., 144  
 Glasoe, N., 84  
 Glockler, G., 99  
 Goerlich, P., 217  
 Goldwater, D. L., 193, 201  
 Goss, W., 95  
 Graffunder, W., 300  
 Grover, H., 76, 99  
 Gurney, R. W., 126, 138, 144, 204  
 Guth, E., 46  
 Gysae, B., 30, 42, 65, 67, 77, 88, 102, 191  
 HAEFER, R., 95, 97, 103  
 Hamaker, H. C., 260, 276  
 Hanley, T. E., 217  
 Hannay, N. B., 194, 197, 201, 204, 206,  
     249  
 Harris, 58, 103  
 Hartmann, W., 143  
 Hass, W., 207  
 Headrick, L. B., 259  
 Hees, G., 181, 182  
 Heinze, W., 66, 80, 85, 87, 176, 185, 188,  
     189, 207, 239, 241, 247, 254, 264  
 Hellmann, H., 17  
 Henderson, J. E., 95, 96, 100  
 Henry, D. E., 98  
 Herring, C., 18, 79, 94  
 Herrmann, G., 219, 222, 228, 231, 247,  
     254, 266, 271, 276  
 Herzfeld, K. F., 18  
 Hevesy, G. v., 117  
 Hinsch, W., 216, 220  
 Hirano, K., 186, 223  
 Hole, W. L., 100  
 Holmes, M. F., 295  
 Huber, H., 155, 176, 191, 192, 210, 214,  
     218, 220, 223, 224, 230, 232, 236,  
     246, 250, 276  
 Huck, R. J., 241, 243  
 Hung, C. S., 176, 181, 207, 242  
 Hutner, R. A., 202  
 Huxford, W. S., 181, 182, 186  
 ISENSEE, H., 159, 288, 294  
 Ivey, H. F., 99  
 JACOB, L., 242  
 Jacobs, H., 181, 182, 259, 264, 276  
 Jamison, N. C., 98  
 Jenkins, R. O., 158, 241, 243, 262, 283,  
     288  
 Jentzsch, F., 80  
 Jette, E. R., 124  
 Johnson, H. C., 76, 100  
 Johnson, J. B., 300  
 Johnson, R. P., 77  
 Jones, E. J., 159, 263  
 Jones, T. J., 209  
 Jost, W., 118, 164  
 Jupnik, H., 99  
 KALLWEIT, H., 155  
 Kawamura, H., 181, 186, 197, 201, 204,  
     223, 262  
 King, A., 65, 77, 93, 102  
 Kingdon, K. H., 50, 56, 97, 103  
 Kleen, W., 34, 40  
 Kluge, W., 72  
 Kniepkamp, H., 178, 181, 182, 256  
 Koller, L. R., 181, 205, 217, 254, 264,  
     276  
 Koppius, O., 207  
 Kossatotschkin, W., 17  
 Kozanowski, H. N., 300  
 Krieg, O., 177, 254, 266, 271, 276  
 Kroczek, J., 185, 195, 198  
 Kroll, W., 283  
 Krueger, F., 76, 99, 101, 104  
 LABHART, H., 135  
 Langmuir, D. B., 102  
 Langmuir, I., 37, 38, 41, 50, 53, 54, 56,  
     78, 97, 103  
 Laue, M. v., 25  
 Lederer, E. A., 259  
 Lehfeld, W., 119  
 Lemery, F., 207  
 Liebmann, G., 39  
 Liebold, W., 182, 243, 271, 277  
 Linford, L. B., 62  
 Littleton, M. J., 111  
 Loosjes, R., 196, 197, 200, 286  
 Lowry, E. F., 245, 276  
 Luebke, E., 185, 195, 198  
 MACCOLL, L. A., 25  
 Macfarlane, G., 301  
 MacNair, D., 194, 197, 201, 249  
 Maddock, A. I., 246, 255  
 Mahl, H., 58  
 Mahlman, G. W., 186, 201, 242  
 Mann, M. M., 97  
 Martin, S. T., 20  
 Maurer, R. J., 97  
 Mayer, H., 97, 103  
 Mecklenburg, W., 242  
 Mendenhall, C. E., 21  
 Metson, G. H., 260, 265, 295  
 Meyer, W., 122, 131, 141, 143, 145, 193,  
     197, 201, 287  
 Meyerhof, W. E., 84  
 Michel, G., 185  
 Miller, P. H., 84, 136, 146  
 Moeglich, F., 131, 144  
 Moeller, G. H., 36  
 Moench, G., 88

# INDEX TO AUTHORS

- Moore, G. E., 59, 206  
 Morgulis, N. D., 64, 175, 209  
 Morrison, J., 158, 173, 181, 249  
 Mott, N. F., 111, 126, 138, 144, 204, 284  
 Mott-Smith, H. M., 46  
 Mrowka, B., 17, 21  
 Mueller, E. W., 21  
 Mueller, W., 61  
 Mullin, C. I., 46  
 Murgoci, R., 194, 196, 264, 287  
 Muto, T., 186  
 Mutter, W. E., 197, 284  
  
 NAGORSKI, A., 209  
 Nebel, C., 178, 181, 182, 256  
 Nehlep, G., 164  
 Neldel, H., 143  
 Newbury, K., 207  
 Newton, R. H. C., 158, 262, 283, 288  
 Nichols, M. H., 18, 21, 94  
 Nijboer, B. R. A., 138, 144  
 Nishibori, E., 181, 186, 197, 201, 204,  
     223  
 Nordheim, L. W., 25, 77  
 Nottingham, W. B., 46, 64, 100, 102  
  
 OATLEY, C. W., 72, 89, 99, 103  
  
 PAGE, L., 41  
 Patai, E., 181, 182  
 Pearce, A. F., 159, 263  
 Peierls, R., 130, 146  
 Phipps, T. E., 46, 76, 100  
 Pietrzik, J., 98  
 Pjatnitzki, A. I., 207  
 Pohl, R. W., 125  
 Pomerantz, M. A., 208  
 Potter, I. G., 101, 104  
 du Pré, F. K., 202  
 Prescott, C. H., 158, 173, 181, 249  
 Prophet, E., 219  
 Ptitsin, S. B., 258  
 Putley, E. H., 135  
  
 RAMADANOFF, D., 207  
 Ramsay, W. E., 258  
 Recknagel, A., 17, 77  
 Reimann, A. L., 18, 76, 99, 102, 103,  
     104, 194, 196, 198, 201, 264, 287  
 Reinhold, H., 118  
 Rentschler, H. C., 98  
 Reynolds, I. A., 76, 99  
 Richardson, O. W., 25, 78  
 Riehl, N., 209  
 Riethmueller, J., 258  
 Rittner, E. S., 202  
 Roehr, W. W., 76, 92, 99, 104  
 Rooksby, H. P., 218, 254, 264, 280, 282  
 Rothe, H., 34, 80, 84, 181, 185, 253  
 Rothstein, J., 281  
 Ryde, 58, 103,
- SANO, S., 86  
 Sausville, J. W., 99  
 Schaefer, H., 159, 263  
 Schallmanach, A., 98, 104  
 Schleede, A., 209  
 Schmidt, A., 193, 197, 201, 217, 287  
 Schoen, M., 209  
 Schottky, W., 15, 22, 25, 32, 36, 38, 45,  
     73, 109, 111, 135, 164, 171, 285, 289,  
     299, 301  
 Schriehl, M., 163, 282  
 Sears, R. W., 161, 187, 193, 196, 290  
 Seely, S., 18, 101  
 Seifert, R. L. E., 46, 76, 100  
 Seith, W., 117, 118  
 Seitz, F., 209  
 Shifrin, K., 135  
 Shockley, W., 122  
 Simpson, J. H., 126  
 Slater, J. C., 122  
 Sloane, R. H., 159, 263  
 Smith, A. H., 192  
 Smith, K. D., 98  
 Smoluchowski, R., 21  
 Sommerfeld, A., 25  
 Sordahl, L. C., 99  
 Spanner, H. J., 181, 185, 198, 202, 217,  
     238  
 Sproull, R. L., 176, 257, 292  
 Stabenow, G., 99, 101, 104  
 Stahl, A. H., 276  
 Stewart, E. G., 280  
 Steyskal, H., 72  
 Stranski, I. N., 21, 53, 98  
 Suhrmann, R., 21, 53, 94, 102, 104, 187,  
     217  
 Sun Nien Tai, 13  
  
 TAFT, E., 100, 135  
 Takahari, M., 206  
 Tamm, I., 17  
 Taylor, J. B., 51, 53, 97, 103  
 Tibbs, S. R., 126  
 Timofeev, P. W., 207, 209  
 Tomaschek, A. Z., 181  
 Tonks, L., 77  
 Treloar, L. R. G., 194, 198, 201  
 Tubandt, C., 118  
 Turnbull, O., 46  
  
 UEHARA, Y., 206  
  
 VAN VELZER, H. L., 78, 100  
 Veenemans, C. F., 53, 182, 189  
 Vervey, E. J. W., 55  
 Vick, F. A., 76, 100  
 Villars, D. S., 245  
 Vink, H. J., 194, 196, 197, 199, 201,  
     286  
 de Voe, Ch. F., 21

## INDEX TO AUTHORS

- WAGENER, S., 30, 42, 65, 66, 67, 77, 85,  
88, 102, 155, 188, 189, 218, 224, 239,  
241, 247, 254, 264, 276, 292, 296  
Wagner, C., 79, 109, 118  
Wagner, E. R., 259  
Wahlin, H. B., 76, 99  
Walcher, W., 159, 263  
Warner, A. H., 100  
Wartenberg, H. v., 219  
Watermann, A. T., 101, 104  
Watt, C. S., 159, 263  
Wehnelt, A., 36, 80, 152  
Weinreich, M. O., 217  
Weise, E., 122, 127  
Wheatcroft, E. L. E., 176  
White, A. H., 194, 197, 201, 249, 284  
Whitney, L., 76, 78, 100  
Wigner, E., 17, 18, 73  
Williams, N. H., 300  
Wilson, A. H., 129  
Wilson, H. A., 25, 78  
Winch, R. P., 84, 93  
Wohlfahrt, E. P., 13  
Wolk, B., 264, 276  
Wooten, L. A., 175  
Wright, D. A., 164, 167, 181, 197, 198,  
201, 204, 217, 258, 281, 287, 293  
Wright, R. W., 76, 99  
**YAMASHITA, J.**, 186  
**ZIMENS, K. E.**, 155  
Zisman, W. H., 84  
Zwikker, C., 102

# SUBJECT INDEX

- ACTIVATION, 52, 58, 245  
by drawing current, 252  
by reduction, 246  
curves of caesium and tungsten, 52  
energy, 117, 133, 294  
of oxide cathodes, 245
- Adsorption  
by van der Waal's forces, 48  
of barium, 53  
of caesium, 50  
of dipoles, 48  
of ions, 47  
of oxygen, 55  
of several foreign materials, 56  
of thorium, 54
- Alkaline-earth metals, physical constants of, 153
- Alkaline-earth oxides, physical constants of, 154
- Atomic film cathodes, 50
- Atomic volume, 12
- BARIUM, ADSORPTION OF, 53**
- Barium atoms,  
evaporation of, 261, 283  
excess of, 156, 163, 173, 237
- Boltzmann statistics, 6
- CÆSIUM,**  
activation curves of, on tungsten, 52  
adsorption of, 50  
evaporation of, 51, 52  
oxide cathode, 217  
vapour pressure of, 50
- Cathodes,  
atomic film, 50  
combined, 245, 286  
composite, 214, 235  
foreign-activated, 231  
mixed oxide, 218  
multi-layer, 230
- Cells in phase space, 7
- Characteristics of a diode, 28
- Combined cathodes, 245, 286
- Concentration differences, 14
- Conduction band, 127, 131, 167
- Conductivity,  
electronic, of chemical compounds, 121  
„ of metals, 4, 129  
„ of oxide cathodes, 199
- formula of semi-conductors, 131
- ionic, 117, 288
- measurement of, 193
- Contact potential,  
definition of, 29, 187  
intersection method, 84, 188  
measurement of, 82
- Cooling effect,  
in saturation range, 78  
in space-charge range, 81  
measurement of, 79, 184
- Cooling power, 79, 185, 195
- Core metal, 248, 276  
oxide, 278  
„ heat of formation, 278, 282, 283
- Coulombs force, 108
- Critical temperature, 10, 169
- DEFECT SEMI-CONDUCTORS, 128**
- Defects of crystal lattices, 124
- Dielectric constant, 126, 144, 154, 176
- Diffraction coefficient of electron waves, 18
- Diffusion, 113  
coefficient of, 115, 290  
in oxide cathodes, 289
- Displacement of characteristic, 87
- Dissociation pressure,  
of alkaline-earth oxides, 245  
of core-metal oxides, 279
- ELECTROLYSIS OF OXIDE COATING, 252**
- Electron  
bombardment, 161, 254  
configuration, 3, 108, 153, 166  
diffraction, 116, 224  
images, 58, 173, 239  
microscope, 58, 239  
volt, 2
- Electronic  
conduction, 121  
conductivity of oxide coating, 199
- Electrons,  
free, 8  
kinetic energy of, 24  
transmissivity of surface for, 24
- Emission  
centres, 238, 242  
constant, 25  
„ measurement of, 76, 78, 179, 181  
dependence on heterogeneity of oxide coating, 238
- equation of oxide cathodes, 171  
„ of semi-conductors, 165  
„ Richardson's, 25

## SUBJECT INDEX

- Emission—continued**  
 mechanism of oxide cathode, 165, 184,  
 189, 206, 235, 276  
 patches, 58, 238, 242
- Energy**  
 bands, 4, 121  
 distribution of electrons in a metal, 6  
 distribution of electrons in a semi-conductor, 131  
 level, 1  
 of disorder, 111
- Evaporation**  
 of barium on to the oxide coating, 161, 205, 232, 290  
 of excess barium, 261, 283
- Excess barium atoms**, 163, 182, 205
- Excess semi-conductors**, 127
- Exchange forces**, 109
- FARADAY'S LAW**, 117
- Fermi-Dirac statistics**, 6
- Fermi level**, 8, 131, 138, 139, 146, 147, 168
- Fermi's distribution function**, 7
- Fermi's distribution law**, 9
- Field emission**, 47, 94
- Film cathodes**, 50
- Flicker effect**, 300
- Foreign-activated cathodes**, 210, 231
- Foreign materials**, adsorption of, 47
- Free path, mean**, 130, 144
- Frenkel defects**, 109
- Frequency limit**, 90, 186
- GALVANI POTENTIAL**, 29
- HALL EFFECT**, 145, 164
- Heats of formation**, 153, 154, 278, 282, 283
- Heisenberg's uncertainty principle**, 7
- Heterogeneous composition of oxide coating**, 238
- Hydrocarbons**, dissociation of, 274
- IMAGE FORCE**, 15
- Impurity level**, 126
- Insulators**, 122
- Interface layers**, 166, 193, 280, 284
- Interference**  
 energy, 136  
 band, 139, 168  
 level, 126, 131, 167
- Intersection method**, 84, 188
- Interstitials of crystal lattices**, 109
- Intrinsic semi-conductors**, 127
- Ion bombardment**, 254
- Ionic**  
 conduction, 117, 287  
 conductivity of oxide cathodes, 288  
 mobility, 117
- Ions, emission of**, 263
- LATTICE DEFECTS**, 109
- Lattice energy**, 109, 154
- Life of cathodes**, 294
- Limiting energy of Fermi statistics**, 6, 8, 12, 133, 138
- Luminescence**, 209
- MAGNETIC METHOD** (for measurement of contact potential), 89
- Mass spectrometer**, 263
- Maxwell's distribution law**, 11
- Maxwell's velocity distribution of electrons**, 27, 32, 207
- Mixed crystals of alkaline-earth oxides**, 218
- Mixed-oxide cathodes**, 218  
 crystallographic properties, 218  
 saturated current of, 220  
 surface of, 223  
 work function of, 223
- Mobility**  
 of electrons, 129, 203  
 of ions, 117  
 of lattice defects, 113
- NOISE**, 299
- OHM'S LAW**, 196
- Orientation of surface to crystal lattice**, 20, 241
- Oxidation semi-conductors**, 128
- Oxygen**,  
 evolution during activation, 159, 253  
 increase in work function due to, 55, 267  
 ions, conduction of, 289  
 „ diffusion of, 289  
 „ poisoning by, 205, 264
- PATCHES OF EMISSION**, 58, 238, 242
- Pauli principle**, 3
- Phase space**, 6
- Photo-electric**  
 emission, 89  
 line, 93, 187  
 stopping potential, 93, 135, 192
- Photo-emission of oxide cathodes**, 185, 207
- Photons**, 89
- Poisoning**, 264  
 by carbon dioxide, 272  
 by carbon monoxide, 272  
 by chlorine, 276  
 by hydrocarbons, 273  
 by oxygen, 55, 205, 264  
 by sulphur, 276  
 by water vapour, 276  
 permanent, 264  
 transient, 264
- Poisson's equation**, 36

## SUBJECT INDEX

- Polarization**  
 constant, 48, 153  
 voltage, 118, 287
- Potential barrier,**  
 at the surface of a metal, 14, 47  
 due to space charge, 35
- Potential box, 14**
- Pulsed operation of cathodes, 177, 285**
- QUANTUM NUMBER,**  
 azimuthal, 1  
 principal, 1
- RE-ACTIVATION, 265, 268**
- Reduction,**  
 activation by, 246  
 by additions in the core metal, 249, 281  
 by carbon, 246  
 by carbon monoxide, 247  
 by methane, 249  
 by the core metal, 247, 278  
 dependence on type of alkaline-earth oxide, 250  
 semi-conductors, 127
- Retarding field current, 31**
- Richardson line, method of, 72, 178**
- Roughness of oxide coating, 238, 240**
- SATURATED CURRENT,**  
 definition, 27  
 dependence on anode voltage (field strength), 44, 176  
 time changes of, 255
- Schottky defects, 110**
- Schottky line, 45, 175**
- Secondary electron emission, 208**
- Self-activated cathodes, 210**
- Semi-conductors,**  
 defect, 128  
 emission equation of, 170  
 excess, 127
- Shot effect, 299**
- Single crystals, work function of, 20**
- Space charge, 35**  
 barrier, 35  
 current, 36  
 density, 37
- Stoichiometric excess, 123**
- Surface,**  
 emitting, 175  
 fields, 60
- Surface—continued**  
 of oxide coating, 175  
 oxide, 55
- TEMPERATURE OF FREEZING IN, 120, 131, 165, 196**
- Thermo-electric voltage, 30, 147, 187**
- Transmissivity, coefficient of, for electrons, 24**
- VACANCIES, FORMATION OF, 110, 163**
- Valency, 117, 122**
- Van der Waal's forces, 48**
- Vapour pressure**  
 of alkaline-earth metals, 154  
 of alkaline-earth oxides, 155
- Velocity distribution of electrons, 27, 90, 207**
- WORK FUNCTION,**  
 arithmetic mean value, 65  
 calculation of, 17  
 calorimetric measurement of, 78, 184  
 decrease due to caesium-adsorption, 50  
 decrease due to dipole layers, 49  
 definition of, 15  
 dependence on external field, 19  
 dependence on orientation in crystal lattice, 20, 241  
 dependence on state of activation, 188  
 differences along the surface, 65, 242  
 emissive mean value, 65  
 external, 168, 203, 227, 235  
 influence of oxygen on, 55, 267, 271  
 internal, 133, 138, 139, 168, 200, 227, 235  
 mean value of, 65, 174  
 measured values, 76, 97, 101, 103, 181, 186, 191, 203, 216, 217, 223, 236  
 measurement of, 70, 174  
 of atomic film cathodes, 103  
 of foreign-activated cathodes, 233  
 of multi-layer cathodes, 231  
 of pure metals, 97, 101  
 photo-electric, 186, 203  
 temperature-dependence, 101, 104, 191, 223  
 total, of oxide cathodes, 168, 181, 191, 223
- X-RAY PATTERNS, 218**
- ZISMAN METHOD, 84**